Design Development and Control of a Compact Autonomous Underwater Vehicle

Thesis Submitted in the partial fulfillment of the requirement

for the degree of

Doctor of Philosophy

by

Avilash Sahoo

Roll No. 166103029

Department of Mechanical Engineering
Indian Institute of Technology Guwahati
Guwahati-781039, Assam, India

January, 2022

Indian Institute of Technology Guwahati
Guwahati, Assam, India

Department of Mechanical Engineering

DECLARATION

I declare that this thesis titled "Design Development and Control of a Compact Autonomous Underwater Vehicle", submitted by me is a presentation of my original research work done under the guidance of Dr. Santosha K. Dwivedy, Professor, Department of Mechanical Engineering, Indian Institute of Technology Guwahati and Dr. P. S. Robi, Professor, Department of Mechanical Engineering, Indian Institute of Technology Guwahati. This work has not been submitted elsewhere for the award of any degree, diploma, associateship, fellowship, titles in this institute or any other university or institute of higher learning.

Avilash Sahoo

January 2022
Place: IIT Guwahati.

Avilash Sahoo
Department of Mechanical Engineering,
Indian Institute of Technology Guwahati,
Assam - 781039, India.

Indian Institute of Technology Guwahati
Guwahati, Assam, India

Department of Mechanical Engineering

CERTIFICATE

This is to certify that this thesis titled "Design Development and Control of a Compact Autonomous Underwater Vehicle," submitted by "Avilash Sahoo," in partial fulfilment of the requirements for the award of the degree of Doctor of Philosophy, to the Indian Institute of Technology Guwahati, Assam, India, is a record of the *bonafide* research work carried out by him under our guidance and supervision at the Department of Mechanical Engineering, Indian Institute of Technology Guwahati, Assam, India. To the best of our knowledge, no part of the work reported in this thesis has been presented for the award of any degree, diploma, associateship, fellowship, titles in this institute or any other university or institute of higher learning.

January 2022
Place: IIT Guwahati.

Dr. Santosha K. Dwivedy
Professor
Email: dwivedy@iitg.ac.in
Phone: +91-361-258 2670

Dr. P. S. Robi
Professor
Email: psr@iitg.ac.in
Phone: +91-361-258 2668

ACKNOWLEDGEMENT

First and foremost, I would like to express my wholehearted and sincere gratitude to my advisors Prof. Santosh K. Dwivedy and Prof. P. S. Robi, for their kind support, guidance, encouragement, compassion and patience through out this journey. Their encouraging words and energetic enthusiasm have always motivated me. Their vast knowledge and profound intellect have helped me to understand the intricacies of the subject. I am grateful to them for all the discussions, the knowledge they imparted and the academic freedom that has given to me.

I am grateful to my doctoral committee chairman, Prof. K. S. R. K. Murthy, for his critical assessment during the entire period of progress. I extend my sincere thanks to my doctoral committee members Prof. S. N. Joshi and Prof. H. B. Nemade for their helpful suggestions.

I extend my sincere thanks to prof. Pankaj Biswas for his advice and knowledge. I am grateful to Prof. Subashisa Dutta and Prof. Rishikesh Bharati for their encouragement, support and the opportunity of deploying the developed system in the field. I am thankful to Mr. Monoranjan Duarah for his help and support during the entire period. I am grateful to workshop staffs for their help during development of the system.

I am grateful to all the discussions with my lab-mates and friends from different streams and background. I sincerely thankful to my co-researchers Mr. Anshul Garg, Mr. Sibananda Mohanty, Mr. Bhaben Kalita, Mr. Jyotindra Narayan and Mr. Rajesh Ranjan for the intellectual discussions, word of encouragement and support. I am thankful to my friends and colleagues Dr. Nur Alom, Dr. Rubi Chakraborty, Mr. Suman Kumar, Smt. Ramyani Chakraborty, Mr. Supratim Koushik and Mr. Sambit Majumder for their knowledge from their field of expertise, constant encouragement and support.

I want to express my immense gratitude and heartfelt thanks to my parents, Smt. Pramila Ku. Sahoo and Dr. Sarat Chandra Sahoo for their support, encouragement and kind blessings. I would like to thank my younger brother Mr. Abinash Sahoo, my elder sister Dr. Sharmistha Sahoo and her better half Dr. Ajinkya Kamat for fruitful discussions, great support and encouragement. I am grateful to all my family and friends for their blessings and support.

I would like to thank all the workers, managers and administrators, of the institute for their constant effort for efficient running of the institute. I sincerely thank all whose grace helped me move forward.

January 2022

Avilash Sahoo

Avilash Sahoo,
IIT Guwahati.

ABSTRACT

Unmanned Underwater Vehicles (UUVs) are robotic devices used for various underwater applications. UUVs have gained popularity in scientific community because of their potential applications ranging from military and research establishments to marine industries. Most of these devices are expensive, bulky and developed for deep ocean applications. To extend the benefits of this technology to small-scale industries and general public, affordable compact AUVs are need of the hour. Here the design and development of an affordable compact underwater robot is presented. After identifying the design requirements, the robot model is designed using 3D modeling software SOLIDWORKS^{TM}. MATLAB Optimization Toolbox^{TM} is used for the estimation of optimal position of internal components. Shape optimization with ANSYS FLUENT^{TM} is carried out for drag coefficient minimization. The designed model has been analyzed using Finite Element Analysis to ensure its structural integrity in the underwater environment. Here stress analysis is used to show that the UUV with glass fiber composite body can withstand the underwater pressure at 100m depth with 1.8 factor of safety. Computational Fluid Dynamics (CFD) study is used to estimate the drag and lift coefficients, and the maximum velocity of the robot. The validated design is used to manufacture the UUV body using glass fiber composite. The developed robot is neutrally buoyant and has a three-part modular structure. This robot has 4 Degrees of Freedom (DOF) and uses three thrusters for propulsion. It has a closed-frame watertight enclosure, which houses different essential components such as battery, depth and temperature sensors, camera, Raspberry pi computer, Pixhawk controller and thrusters. During operation, the robot is connected to the computer on the ground using tethered connect for transmission of live underwater footage, sensor data, and control signal. Detailed cost analysis of the developed robot is also presented. The robot was successfully tested in a swimming pool, nearby river, and lakes, and the results are discussed.

AUVs have to navigate complex underwater environments autonomously based on its algorithms. Accurate kinematic and dynamic model of an AUV, guidance, control and localization technique are vital components in navigation, which helps an AUV to follow the defined path. This thesis presents development of a trajectory tracking controller for the developed AUV. First, kinematic and dynamic model of the underwater robot are developed. Using detailed

CAD model of the AUV, inertia and buoyancy parameters are estimated. Hydrodynamic damping parameters are estimated using simulations carried out with CFD software package ANSYS Fluent^{TM}. 3D added mass coefficients are estimated numerically using strip theory. The developed AUV model is validated with experimental results. A 3D guidance system is developed to follow the generated path by way-point technique using Line-of-Sight (LOS) strategy. An Inertia navigation system is used to estimate the position and orientation of the AUV to be use in feedback loop of a closed loop controller. Initially, Close loop PD controller was developed which resulted in a constant steady state error due to under actuation. Then a classic PID controller is developed which eliminated the steady state error and successfully simulated for multi way-point path. PID controller gain has to be tuned for individual path, thus an adaptive Fuzzy-PID controller is designed to handle variation in the path. This controller is compared with the PID controller and results are discussed. A robust Neuro-Fuzzy controller is developed to handle dynamic environmental forces and unknown system behavior. Here a neural network model of the system is fitted with the experimental data and the fitted model is used with the PID system to adapt to different working environments. A comparative simulation of both the controllers under external disturbance force is carried out to showcase the robustness of the controllers. Objective of this work is to develop an robust non-linear adaptive control strategy for the navigation of the newly developed AUV on a predefined path. Such affordable compact systems can bring significant benefit to the small-scale marine industries, can create new opportunities, and help monitor and preserve underwater ecosystems.

Key Words: Autonomous Underwater Vehicles (AUVs); Inertial Navigation; Kalman Filter; Dynamic Model; FUZZY-PID Controller; Neuro-FUZZY Controller; Guidance System; Line-Of-Sight(LOS).

Contents

List of Figures

List of Tables

Abbreviations

AUV	Autonomous Underwater Vehicle
C.B	Centre of Buoyancy
C.G	Centre of Gravity
CAD	Computer Aided Design
CFD	Computational Fluid Dynamics
DVL	Doppler velocity log
EnKF	Ensemble Kalman Filter
EKF	Extended Kalman Filter
FEM	Finite Element Method
FKF	Fuzzy Kalman Filter
FRP	Fiber Reinforced Plastic
FVM	Finite Volume Method
GPS	Global Positioning System
IMU	Inertial Measurement Unit
INS	Inertial Navigation System
KF	Kalman Filter
Li-Po	Lithium Polymer

LOS	Line-of-Sight
NLO	Non Linear Observer
PWM	Pulse Width Modulation
ROV	Remotely Operated Underwater Vehicle
SLAM	Simultaneous Localization And Mapping
UKF	Unscented Kalman Filter
USBL	Ultra Short Base Line
UUV	Unmanned Underwater Vehicle

Symbols

A_f	Reference area (m^2)
B	Buoyancy force vector
c_d	Drag coefficient of drag
c_m	Moment coefficient
C	Coriolis and Centripetal matrix
D	Damping matrix
e	Position and orientation error
f_b	Buoyancy vector (N)
f_g	Gravitational vector (N)
$g(\eta)$	Gravitational and buoyancy matrix
H	Observation matrix
h_1	Height of the structure at front end
h_2	Height of the structure at tail end
I_b	Inertia tensor
J	Jacobian
k_d	Derivative control gain
k_i	Integral control gain

k_p	Proportional control gain
L	Thruster configuration vector (m)
M_{RB}	Rigid body Inertia matrix
M_A	Added mass matrix
m	Mass (Kg)
p	Roll rate (rad/s)
Q_k	State noise covariance matrix
q	Pitch rate (rad/s)
R_k	Measurement noise covariance matrix
r	Yaw rate (rad/s)
r_a	Radius of acceptance (m)
r_g	C.G Position in B-frame (m)
r_b	C.B Position in B-frame (m)
T	Actuator thrust (N)
t	Time (s)
U	Control input vector (N)
u	Surge (m/s)
v	Sway (m/s)
W	Gravitational force vector
w	Heave (m/s)
x	Position along X axis (m)
y	Position along Y axis (m)
z	Position along Z axis (m)

Greek symbols

η	Position and orientation in N-frame
θ	Pitch (rad)
ν	Linear and angular velocity in B-frame
ρ	Density of the flow medium (Kg/m^3)
τ	Body-fixed forces and moments
ϕ	Roll (rad)
ψ	Yaw (rad)
∇	Displaced fluid volume (m^3)

Chapter 1

INTRODUCTION

1.1 Introduction

Most of the earth's surface is covered with water in form of oceans, rivers and lakes, many of which remain unexplored till date. These environments contain some of the most natural resource rich habitats. These habitats directly or indirectly affect humans. Deployment of underwater robotic vehicles can help to study these environments to ensure their safety against environmental pollution and use the available natural resources for human development.

Manned underwater vehicles have humans on board which increase the risk as well as operational cost, so underwater unmanned systems are getting very popular. These systems can be used in greater depth and extremely harsh conditions. "Autonomous underwater vehicle (AUV)" and "Remotely operated underwater vehicle (ROV)" are two categories of unmanned underwater robotic systems. ROVs are controlled from the surface, generally by a wired connection. These can do a variety of tasks, but the wired connection limits its maneuverability as well as accessibility to remote locations. AUVs navigate autonomously relying on its navigation algorithm and surrounding information. Once deployed, they collect data and come back to the surface after completion of the predefined task. As AUVs are not connected to the ground they have high maneuverability, can travel to remote locations, narrow complex pathways, involve no human fatigue and operation cost is very less. Underwater wireless communication has its limitations so AUVs have seen an increase in interest from underwater research community. It has always been a challenge to make a robotic device to explore these hostile territories. With advancements in AUV research, materials, manufacturing techniques, sensors, computational

power and battery technology, autonomous decision making underwater robots have become more reliable and practical. A reliable, fully autonomous decision making robotic system is the objective of current AUV research.

The first AUV "SPURV" (The Self Propelled Underwater Research Vehicle) was developed by Stan Murphy and Bob Francois in 1957 in the Applied Physics Laboratory at the University of Washington [1]. "SPURV" operated at 2 to 2.5 m/s up to a depth of 3,600 m [2]. In 1970s few AUVs were developed in MIT and also in Soviet Union [1]. These early underwater robots were bulky, expensive and inefficient. AUVs have come a long way since then. The modern day AUVs can have six degrees of freedom, can travel faster than 20 m/s, accurately detect obstacles and map ocean floors. These are getting compact, less expensive, yet sophisticated and accessible to the general population for exploration, fishing, and entertainment etc.. These systems have yet to go a long way in terms of autonomy till fully autonomous robotic systems help us explore and protect these deep and hazardous habitats.

AUVs have a large number of applications in the hazardous underwater environments. Still, AUVs have to overcome some limitations to have large-scale adoption. Some of the key challenges are low price, underwater wireless communication, long lasting batteries, use of smart materials, compact on-board computers with high computational power for better decision making, on-board energy generation and its efficient use.

1.2 Applications

AUVs are becoming very popular for underwater exploration in commercial, military and industrial applications. Over the years a large number of AUVs have been developed for various application. Table 1.1 lists the potential applications along with AUVs used for these purposes.

With the help of different sensors, these vehicles can collect variety of useful scientific information like temperature, depth, pH level, chemical composition, turbidity etc. These information can help in environmental monitoring and scientific study. Cameras can be used to take pictures of the environment to study underwater ecosystems, different aquatic animals and underwater ground structure ([3, 4, 12, 13, 17]). With multiple cameras and sonars, 3D mapping and reconstruction of the sea floor can be done which can be used in site selection

Table 1.1: Applications of AUVs

Military	Surveillance	REMUS-6000 [3];AUV-150 [4]
	Anti-submarine warfare	Bluefin21, Echo Ranger, Gavia Defence, SOG Seagliders, Eagle Ray [5]
	Mine countermeasures	Bluefin21, 2016 [6]; [7]
	Inspection of wreckage	U-CAT [8]
	Payload delivery to ocean floor	GIRONA 500 I-AUV ([9])
	Search and rescue	Bluefin21, 2016 [6]
	Air crash investigation	GIRONA 500 I-AUV [10, 11]
Scientific	Ocean exploration and bathymetric study	Theseus AUV [12, 13]; REMUS-6000 [3]; AUV-150 [4]; AE2000A [14]
	Mapping of ocean floor	Autosub 6000 [15]; AUV-150 [4]; D. Allan B [16]; Bluefin21, 2016 [6]
	Marine biology studies	Maya AUV [17]; SoFi [18]
	Geological Survey	Tri-TON 2 [19]
	Archaeological survey	MARTA, A-Size [8]
	Environmental monitoring	Maya AUV [17]; REMUS-6000 [3], Folaga [20]
Industry	Track oil-spill and gas leakage	SOTAB [21]
	Repair and maintenance	SAUVIM [22], Folaga [20], SeaCat [23]
	Track and repair underwater cables	AE1000 [24]
	Underwater structure inspection	SeaCat [23]
Other	Underwater video footage collection	Maya AUV [17]
	Fishing	
	Entertainment and Tourism	

for constructions like tidal energy plant, ports; claim the maritime borders with continental shelf data ([4, 14, 15, 16]). Allotta et al. [8] presented AUVs "MARTA" and "A-Size" used for 3D mapping of underwater archaeological cites and a turtle inspired bio-mimetic AUV "U-CAT" used for ship wreckage penetration and survey. AUVs are being used for inspection of cracks and damages in underwater structure [23], track and discover ore [19], oil, natural gas reserves. Underwater vehicles can be used to track oil leakages from oil mines, gas leakage from under-sea gas pipelines to protect the underwater ecosystem and avoid pollution [21]. Intervention-AUVs with autonomous manipulator systems are being used for various intervention tasks such as self docking, search and retrieve objects [11], payload delivery to ocean floor, pipeline and cable deployment etc. Such I-AUVs can be used for black-box search and retrieval during air crash investigations. Various co-operative tasks such as pipeline ([9]) and cable deployment, transportation of long and heavy payload to ocean floor can be carried out by fleet of AUVs and I-AUVs. Some bio-mimetic underwater robot like a snake and fish robots and other AUVs are being used for inspection and surveillance [4]. Bio-mimetic robots [18] are being developed with soft flexible materials to create life like motion. Such AUVs can be used for closed-up observation aquatic life without disturbance. Apart from these scientific and

commercial applications AUVs are being extensively used for military purpose. Bio-mimetic as well as other AUVs can be used for surveillance and reconnaissance. Using sonar AUVs can be used for mine countermeasures without engendering the human life. Other applications may include anti-submarine warfare, search and rescue and site inspection etc. Generally, these robotic vehicles are used in oceanographic applications. Underwater robots are also being used to study underwater environments in rivers and lakes and carry out surveys. In recent years AUVs have gained much more popularity because of its potential applications in the fields of scientific research, military and industries. AUVs have been initially developed by military and research establishments for specific applications. Later multi-purpose as well as application specific industrial AUVs have been developed. "REMUS-6000"(Fig. 1.1(a)) developed by Kongsberg Maritime [3] is such a multi-purpose industrial AUV. REMUS-6000 weighs 862 kg with maximum depth range of 6 km and travel velocity upto 2.3 m/s. The AUV houses acoustic modem for communication, side-scan sonar for bathymetric data collection and acoustic underwater positioning and navigation system with IMU(Inertial Measurement Unit) and DVL (Doppler Velocity Log) sonar for navigation. This AUV can be used for fisheries research, habitat mapping, under ice exploration, marine archaeology, deep sea ecology, seabed investigation, deep sea mining, mine countermeasures, surveillance and reconnaissance etc. "Bluefin-21" (Fig. 1.1(b)) developed by General Dynamics Mission Systems [6] is another multi-purpose industrial AUV rated for 4.5 km depth. This AUV can be used for oceanographic study, mine countermeasures, anti-submarine warfare and underwater exploration etc. Maintenance and repair of underwater gas and oil pipelines is a major potential industrial application for AUVs. An AUV (Fig. 1.1(d)) with robotic arm for pipeline inspection is under development by Kawasaki Subsea (UK) Limited [25]. Table 1.2 presents some examples of AUVs being used in the field for various applications encountered during this literature survey. More examples of such AUVs used for different applications can be found in the AUV database AUVAC [5].

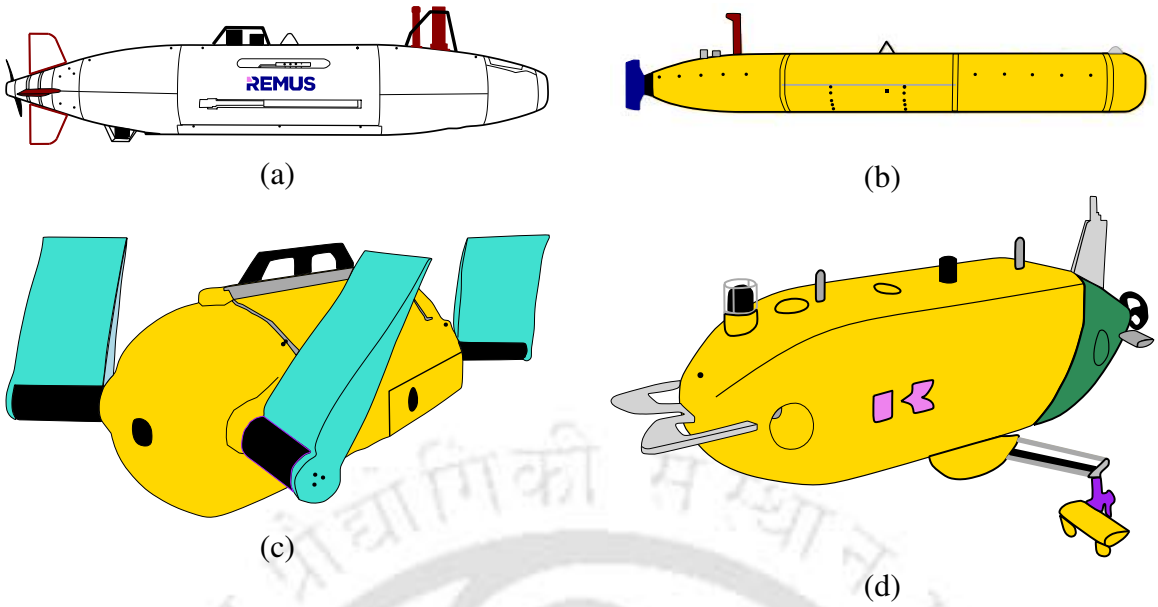

Figure 1.1: (a)"REMUS-6000"([3]) (b)"Bluefin-21" ([6]) (c)"U-CAT" ([8]) (d) Kawasaki AUV ([25])

Table 1.2: AUVS Used in different field applications

AUV Name	Developed In	Applications	Dimensions	Working Depth
AE1000 [24]	Japan	Inspection of underwater telecommunication cables	2.3m x 2.8m x 0.7m	1000m
Maya AUV [17]	NIO, Goa, India	Oceanography study	1.742m, dia 0.234m	200m
Theseus AUV [12, 13]	Canada	Under-ice bathymetric surveys	10.7m, dia 127cm	2000m
Autosub 6000 [15]	AUVAC, USA	Scientific survey and mapping	5.5m x 0.9m x 0.9m	6000m
REMUS-6000 [3]	Kongsberg Maritime, Norway	oceanography study, Monitoring, surveillance and reconnaissance etc.	3.96m, dia 71cm	6000m
AUV-150 [4]	CMERI, India	oceanography study, mapping, surveillance and reconnaissance etc.	4.85m, dia 0.5m	150m
D. Allan B [16]	MBARI, USA	Seafloor mapping	5.18m, dia 54cm	6000m
SOTAB [21]	Osaka university, Japan	Track oil leakage from oil mines	3m, dia 27 cm	200m
AE2000A [14]	Japan	Under-ice survey	3m x 0.7m x 0.7m	2000m
Tri-TON 2 [19]	University of Tokyo, Japan	Estimate ore reserves in underwater hydrothermal deposits	1.4m x 0.7m x 1.4m	2000m
SeaCat [23]	Germany	Autonomous inspection of underwater structures	2.5m x 0.58m x 0.67m	600m
Bluefin21 [6]	General Dynamics, USA	Search and explore, Oceanography, Mine countermeasures	5m, dia 53cm	4500m

1.3 Background and Motivation

Autonomous Underwater Vehicles (AUVs) are robotic devices capable of navigating underwater independently without human intervention using on-board sensors for understanding the surroundings, propulsion system for navigation and an on-board computer for decision making. AUVs can help us explore and study the unexplored underwater environments to ensure their safety and to use the available natural resources for development of human beings. Such autonomous underwater robotic systems are need of the hour for exploration and environmen-

tal safety of the vast and deep oceans and shallow water bodies. AUV technologies have seen significant development in the last decade. Still in developing countries majority of underwater robotic systems are being developed by military establishments and marine research institutes. Few examples of such robotic systems are Maya AUV [17] by NIO, Goa, India, AUV-150 [4] by CMERI, India, Theseus AUV [12, 13], Autosub 6000 by AUVAC, USA [15], KAIKO Mk-IV by JAMSTEC [26], MBARI's Ventana, Tiburon and DocRicketts [27, 28], SUB-fighter 30K ROV by Sperre AS [29]. These underwater systems are bulky and expensive as they are designed to operate at higher depth. These vehicles are more than 2 m long and can travel up to 2000 m depth [30]. Underwater robotic systems can also bring significant benefits to the small-scale marine industries, educational institutes, disaster management groups, environmental protection groups and recreation industries etc. But till date underwater robots are not available in the public domain for adoption for such applications. High cost and size of the available underwater robots are some of the major challenges against wider adoption. Thus, there is a requirement of affordable, compact, and shallow water robots. Furthermore affordable compact AUVs are not available for autonomous monitoring, survey and search etc. Now a days availability of low-cost high-precision sensors, compact one-board computers such as Raspberry pi, high-density batteries encouraged the development of low-cost compact AUVs. With development of robust control algorithms, navigation and localization with MEMS sensors coupled with numerical techniques and using artificial intelligence affordable compact AUVs can become reality. Such systems will create new opportunities for small-scale industries and research establishments towards sustainable development of underwater ecosystem. To develop a low-cost compact AUV with robust controller, a detailed literature review has been carried out which is presented in the next chapter. Objectives of the work have been selected after the literature review which is presented in the next section.

1.4 Objective of the Present Work

Objectives of this work is to develop an affordable compact UUV with a robust trajectory tracking controller. To achieve the main objective different works to be carried out are summarized below:

- Identify system requirement and design a compact close-frame UUV.
- Develop a fully functional affordable compact UUV, which can be deployed as a ROV as well as an AUV.
- Develop the AUV with required sensors and hardware, software and communication infrastructure to implement the control strategy and navigation algorithm.
- Develop kinematic and dynamic model of the AUV along with system parameter estimation.
- Experimental validation of estimated system parameters.
- Design a simulated environment for simulation of the AUV using the developed kinematic and dynamic model.
- Develop a 3D way-point guidance system for AUV to follow a predefined path.
- Implement the modified KF coupled with the IMU, GPS and dynamic model for development of a robust state estimator and simulate the algorithm for validation.
- Development of PD and PID closed loop controller for autonomous navigation of the AUV to understand the basics of the contol system design for an AUV.
- Development of adaptive Fuzzy-PID and Neuro-Fuzzy controllers to address variable environmental forces.

1.5 Organization of the thesis

Content of this thesis is presented in seven chapters in following manner.

Chapter 1 introduces the topic of AUVs, ROVs and presented their various applications. Objective of the present work and thesis organization is also stated in this chapter.

Chapter 2 presents a detailed literature review highlighting different aspects of AUVs and their usefulness. Summary of the literature review with potential scope of the work is also presented in this chapter.

Chapter 3 discusses design process of the compact UUV and design validation with numerical

simulation. Manufacturing of the system along with sensor integration, software and communication infrastructure is presented and field test result of the developed system is discussed.

Chapter 4 presents the development of kinematic and dynamic model of the AUV. To complete the mathematical model, system parameter estimation is carried out using CAD modeling, physical measurements, and CFD simulations. Comparative study of the system model prediction and field test results are also discussed.

Chapter 5 discusses a 3D guidance system, inertial navigation system, development of simulation environment and classic control system such as PD and PID design for the AUV. Multiple simulation for 2D and 3D way-point trajectories has been carried out and comparison of the two controllers are also presented.

Adaptive Fuzzy-PID controller design and simulations are presented in the chapter 6. Comparative study of the adaptive and classical controller is also presented. Experimental data has been used for development of the Neuro-fuzzy model to improve the robustness of the controller.

The general and specific conclusions are presented in Chapter 7. Also the scope of future work has been discussed in this chapter.

Chapter 2

LITERATURE REVIEW

2.1 Introduction

A detailed review of the prior literature has been carried out to develop a deep understanding of unmanned underwater vehicles. This will help towards development of an affordable compact underwater system and its autonomous control in dynamic underwater environments. This system in hands of individuals and small-scale industries will create new opportunities and bring the benefit of this technology to the masses. The different aspect of the underwater robotic systems considered under the study are presented in the following sections. AUV structure design is presented in section 2. Study on different propulsion techniques are presented in section 3. kinematics and dynamics modeling of different AUVs are discussed in section 4. Section 5 presents different path planning and control systems used in underwater systems. Navigation and localization techniques are presented in section 6. Summary of the literature study is presented in section 7.

2.2 AUV Structure

The body structure of AUV is an important element as it safely houses all the mechanical and the electronic components in a watertight enclosure. The shape of the AUV also affects the dynamics of motion because of the fluid-structure interaction with surrounding water. Inspired from submarines, AUVs are generally torpedo shaped. The first AUV "SPURV" Widditsch [2] was torpedo shaped. AUV presented by Jun et al. [31], Shome and Das [4], Ferguson [12],

Hiller et al. [32], Hyakudome [33], 'STARFISH' by Hong et al. [34], 'Maya' by Desa et al. [17], 'SPARUS II' by Carreras et al. [35], 'FOLAGA' by Alvarez et al. [20] and 'MARTA' by Allotta et al. [36] are some examples of torpedo-shaped AUVs. Depending on different requirement AUVs have adopted various shapes. Fittery et al. [37] developed an egg-shaped AUV called 'Omni-Egg" at MIT. He et al. [38], Yue et al. [39], Ma et al. [40], Li et al. [41] and Wan et al. [42] presented spherical AUVs. These AUVs are highly maneuverable and can easily travel in complex pathways and access remote locations which are otherwise difficult to access. Apart from these simple structures, nowadays AUVs are being developed in complex shapes with hydrofoil profiles to increase efficiency and reduce drag. P-SURO AUV Li et al. [43], AUV presented by Alam et al. [44] are some such AUVs. All these AUVs with different body shapes use a watertight close-frame structure. AUVs operating at low speed often use open frame structures as the drag force at flow speed is less. Girona 500 AUV Wirth et al. [45] and AUV presented by Hung and Na [46] are some open-frame AUVs.

Apart from these artificial structures, AUVs have taken inspiration from the nature and mimicked aquatic animals. In addition to exploration and other underwater applications these bio-mimetic AUVs can seamlessly integrate to the marine environment to study and understand the aquatic life without disturbing them. Fish robots are most popular among the bio-mimetic AUVs. Yang et al. [47], Parameswaran and Selvin [48], Shriyam et al. [49], Kadiyam and Mohan [50], Santhakumar and Asokan [51], Chowdhury et al. [52], Chowdhury et al. [53], Chowdhury et al. [54], Ashar et al. [55], Vo et al. [56], Choi and Lee [57], Listak et al. [58], Yu et al. [59] and Jung et al. [60] developed fish robots. Figure 2.1 presents the robotic fish developed by Yang et al. [47].

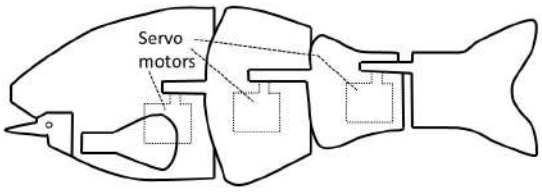

Figure 2.1: Robotic Fish "Ichthus" [47]

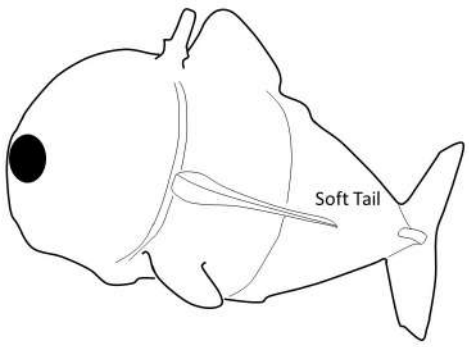

Figure 2.2: Soft Robotic Fish "Sofi" [18]

AUVs have also been developed which mimic other aquatic animals such as snake, turtle, beetle and crab etc. Zhao et al. [61] presented turtle-like robots with four mechanical flippers inspired from soft-shell turtles. Allotta et al. [8] presented a turtle-like robot 'U-CAT', developed for shipwreck penetration. Kim and Lee [62] presented a six-legged underwater robot CALEB 10(D.BeeBot) inspired by beetles which can walk as well as swim. Jun et al. [63, 64] also presented a six-legged seabed walking robot 'CR200' inspired by crabs. Kang et al. [65], Nguyen et al. [66] presented underwater glider inspired by manta ray. Recently soft Bio-mimetic AUVs have been used for closeup exploration of aquatic-life without disturbing the natural habitats. For example Ming et al. [67] developed a soft snake robot and recently a soft robotic fish (SoFi) was designed and developed by Katzschmann et al. [18](fig. 2.2).

AUVs nowadays are adapting modular design in the body structure. The whole AUV is a combination of different modules such as propulsion, sensor modules which can be easily and quickly replaced in case of a failure as well as can be interchanged with different modules according to the mission requirements. Such modular AUVs are highly versatile and incur less maintenance cost. 'AUV-150' Shome and Das [4], 'MAYA' National Institute Of Oceanography(NIO) [68], 'STARFISH' Hong et al. [34], 'Bluefin21' General Dynamics Mission Systems [6], 'SPARUS II' Carreras et al. [35], 'FOLAGA' Alvarez et al. [20], 'MARTA' Allotta et al. [36] and AUVs presented in Alam et al. [44] and Hiller et al. [32] are examples of some modular AUVs.

During motion, AUV experiences drag and lift forces because of the friction between the body and surrounding water, which affect the dynamics of AUV. Body structure greatly affects these forces. Fluid-structure interaction study of the AUV with the surrounding water is essential to predict the drag and lift. Minimizing these forces using different numerical and optimization technique, increases the efficiency of the AUVs. Drag and lift estimation also help in developing an accurate dynamic model for navigation and control. Alam et al. [44] used non-dominated sorting genetic algorithm (NAGA), population-based optimization algorithm and in-feasibility driven evolutionary algorithm (IDEA) to optimize the hull structure of a torpedo-shaped AUV for minimum drag and clash-free component placement. Sun et al. [69] presented an underwater glider with a blended wing-body structure. The glider structure

is shape-optimized for maximum gliding range considering the internal space as proportional function to energy reserve. Elsayed et al. [70] presented an elliptical submersible pressure hull designed with multi-objective optimization to minimize buoyancy and maximize buckling load capacity to reach a depth of 6000m. ANSYS^{TM} FEM analysis is carried out to verify the design. Nguyen et al. [66] presented a shape optimized underwater glider inspired by manta ray using CFD analysis to have least fluid resistance. Mitra et al. [71] presented experimental and numerical study on effect of free stream turbulence on hydrodynamic parameters of AUV hull structure. Here results from the experiments, carried out at three different depths are used to validate the estimations predicted by a Reynolds stress model. In this study it was observed that, the presence of free stream turbulence decreases skin friction, drag and lift coefficients. Such studies can help towards development of more efficient AUV structures. A popular Computational Fluid Dynamics (CFD) software ANSYS FLUENT^{TM} is being used for the hydrodynamic study of the AUVs. Allotta et al. [72] presented design and development of a low-cost 5-DOF AUV "Tifone". shape of the AUV is optimized for maximum efficiency with ANSYS CFX^{TM} finite element modeling. Alam et al. [44], He et al. [38], Yue et al. [39] and Ma et al. [40] used ANSYS FLUENT^{TM} to study the hydrodynamic behavior of their AUVs. Liou [73], Listak et al. [58] and Wu [74] adapted theoretical and experimental method for hydrodynamic study.

AUVs experience hydrostatic pressure due to water head and hydrodynamic pressure due to their movement. AUV body can deform or get damaged due to excess pressure, which increases with depth. Researchers are using 'Finite Element Method'(FEM) for stress and buckling analysis of the hull structure which helps in selection of proper material, thickness of the wall as well as set the operational depth limit of the AUVs. Stevenson et al. [75] presented mechanical design and development of a deep water AUV "AUTOSUB-1" considering the buckling failure. Shome and Das [4] and Jun et al. [64] used FEM for stress estimation of the AUV bodies. Błachut and Smith [76] presented numerical and experimental study of buckling of a multi-segment pressure hull subjected to uniform hydrostatic pressure. Rahim et al. [77] presented the design of a pressure hull for a underwater pole inspection robot. Finite element stress and buckling analysis was carried out to determine the wall thickness of the structure. Allotta

et al. [72] used FEM for buckling verification of the central cylindrical structure at 700m water depth and experimentally verified upto 300m depth. Li et al. [41] presented stress analysis of the frame holding the servo motor and water-jet propellers. Complex hydrofoil structures are difficult to manufacture and costly with traditional materials and techniques. Composite materials can be used in such cases for ease of manufacturing and strength and other properties comparable and sometimes better than traditional materials. Kang et al. [65] presented an underwater glider made of carbon fiber composite with similar strength but 40% less weight compared to high tensile aluminum. Here stress and buckling analysis is used to show that the glider can withstand the underwater pressure at 200m depth with 1.8 factor of safety. Next section presents different propulsion methods used by AUVs for navigation.

2.3 Propulsion Techniques

AUVs depend on its propulsion system to travel in the underwater environment. Bio-mimetic AUVs mimic propulsion technique as well as body structure of aquatic animals. These AUVs travel in water using undulatory propulsion. In this technique pressure difference is created in water by moving some part of their body in a wave-like pattern. Most of these AUVs use electric motors for this purpose. Yang et al. [47], Parameswaran and Selvin [48], Ashar et al. [55], Vo et al. [56], Choi and Lee [57], Yu et al. [59], Zhao et al. [61] and Jung et al. [60] used servo and DC motors for moving their body parts for propulsion. Instead of rigid body parts, soft flexible parts are being used to have more life-like motion in case of these bio-mimetic AUVs. Katzschmann et al. [18] presented a Soft Robotic Fish (SoFi) with a hydraulically driven flexible soft elastomer tail and servo driven hard fins. Smart materials have also been used to create such wave-like motions for propulsion. Kadiyam et al. [78] uses threee oscillatory fins for propulsion. Ming et al. [67] have presented a soft snake underwater robot made of piezo-electric fibre composite, which mimics undulatory propulsion of a sea snake. These vehicles are energy efficient, quiet and flexible in operation. Such systems are suitable for surveillance and ecological study as they produce no noise and don't disturb the aquatic animals nearby.

Bio-mimetic AUVs are incapable of carrying heavy payloads and achieving high speed. AUVs used for these applications generally use multiple propellers or thrusters for propulsion

along with rudders and fins for directional control. AUVs presented in Shome and Das [4], Ferguson [12], Jun et al. [31], Hiller et al. [32], Hyakudome [33], Alam et al. [44], Isa and Rizal A. [79], STARFISH Hong et al. [34], Maya National Institute Of Oceanography(NIO) [68] and AQUA EXPLORER 1000 Kato et al. [24] use wings and rudder along with propeller for motion. AUVs presented in He et al. [38], Li et al. [41] and Yue et al. [39] use servo controlled water jet propellers whereas AUVs in Ma et al. [40], Fittery et al. [37] and Wan et al. [42] use servo controlled hydraulic pump for propulsion. Bluefin21 AUV General Dynamics Mission Systems [6] uses a gimbaled, ducted thruster. AUV can follow complex trajectories with fixed thrusters using different control algorithms. Typhoon AUV Allotta et al. [80], SPARUS II AUV Font et al. [81], Girona 500 AUV Wirth et al. [45], P-SURO AUV Li et al. [43], Hovering AUV General Dynamics Mission Systems [82] and AUV presented in Hung and Na [46] are some examples of such AUVs with fixed thrusters. Kinematics and dynamics relations of different AUVs are discussed in the next section.

2.4 Kinematics and Dynamics

Kinematic model of a robot is the mathematical correlation between the inertial, non-inertial frame and links of a robot which defines the position, velocity and acceleration of different parts of the robot with respect to some frame of reference. Dynamic model correlates forces and moments with the position and velocity of the robot. A rigid body AUV is considered as a single link manipulator and its kinematic model correlates the body-fixed frame and the earth-fixed frame as shown in (Fig. 2.3). The Body-fixed frame is attached to the geometrical center of the vehicle with axes in the directions of surge, sway and heave respectively. Earth-fixed or inertial (X, Y, Z) frame coincides with the North-East-Down directions and fixed to a point on the water surface.

As presented in table 2.1 coordinates along X, Y, Z axis (x, y, z) and rotational angle about these axis (ϕ, θ, ψ) constitute the position and orientation vectors of AUV Center of Gravity (C.G) in the inertial frame presented as $\eta = [\eta_1^T, \eta_2^T]^T$; where $\eta_1 = [x, y, z]^T$, $\eta_2 = [\phi, \theta, \psi]^T$. Linear and angular velocity of the AUV C.G in the body fixed frame is denoted as $\nu = [\nu_1^T, \nu_2^T]^T$; where $\nu_1 = [u, v, w]^T$ and $\nu_2 = [p, q, r]^T$.

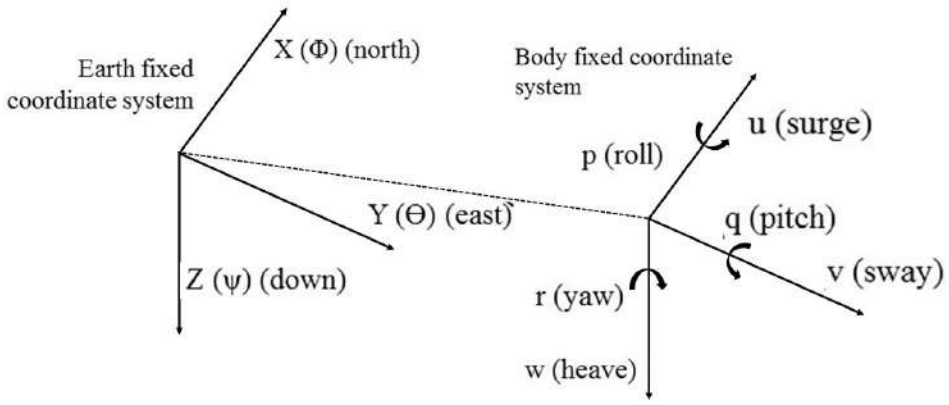

Figure 2.3: Definition of reference frame and relative motion

Table 2.1: Standard SNAME (1950) notations for Marine vessels

DOF	Motion Descriptions	Positions and Orientations	Linear and Angular Velocities
1	Motions in the X- direction(surge)	x	u
2	Motions in the Y- direction(sway)	y	v
3	Motions in the Z- direction(heave)	z	w
4	Rotations about the X-axis(roll)	ϕ	p
5	Rotations about the Y-axis(pitch)	θ	q
6	Rotations about the Z-axis(yaw)	ψ	r

Parameters in both the frames can be correlated using Euler transformation presented as:

$$\dot{\eta} = J(\eta_2)\nu \tag{2.1}$$

where $J(\eta_2)$ is the Jacobian matrix. Detailed derivation of the kinematic and dynamic model is presented in Fossen [83, 84], Antonelli [85].

Accurate dynamic model is essential for an AUV for its control and navigation. Fossen and Fjellstad [86] have presented non-linear modeling of a 6 degree of freedom marine vehicles which can be extended for a rigid body AUV. The interaction between the motion of an AUV and different related forces and torques can be expressed as:

$$M\dot{v} + C(v)v + D(v)v + g(\eta) = \tau \tag{2.2}$$

where $M = M_{RB} + M_A$; M_{RB} and M_A are the constant inertia and added mass matrix of the AUV respectively, $C(\nu) = C_{RB}(\nu) + C_A(\nu)$; $C_{RB}(\nu)$ and $C_A(\nu)$ are the Coriolis and Centripetal matrix

of the rigid body, and the added mass respectively, $D(\nu)$ is the Damping matrix containing drag and lift terms, $g(\eta)$ is the vector of restoring forces and moments which includes gravitational and buoyancy forces, and τ is the vector of body-fixed forces from the actuators. Hydrodynamic added mass can be interpreted as virtual mass added to a system because when the body accelerates or decelerates it must move some volume of the surrounding fluid as it moves through it. Added mass matrix M_A depends on the shape of the AUV. M_A is positive and symmetrical for submersed bodies.

Different modern tools such as CAD modeling and CFD analysis techniques can be used to find close estimates of these above-mentioned parameters. Different system identification techniques have to be employed to accurately measure these system parameters by comparing the simulated results with the experiments. Weiss and Noel [87] presented a method to develop the dynamic model for underwater vehicles in real-time by system identification, which can be used for position and velocity estimation. This method uses Recursive Least Squares estimator to minimize the square of the error between the modeled and measured response to find-out the unknown parameters. Yue et al. [39] presented a dynamic model for the spherical robot 'SUR-II' along with parameter estimation to determine the hydrodynamic added mass matrix to damping matrix. Here CFD analysis using ANSYS FLUENT^{TM} is used for parameter estimation. Shome and Das [4], Hyakudome [33], Isa and Rizal A. [79], Allotta et al. [80], Shen et al. [88], Hosseini et al. [89], Chin et al. [90], Ngatini et al. [91], Wang et al. [92], Sarhadi et al. [93], Liu et al. [94], Bae et al. [95] presented kinematic and dynamic model of the AUVs similar to the model discussed above. Silva and Sousa [96] discussed different dynamic models for simulation and control of underwater vehicles. A simplified approach towards the solution of a dynamic model is discussed.

Drag and lift forces are exerted on the AUV due to skin friction between the AUV structure and surrounding fluid. AUV body structure affect these forces. Drag and lift coefficients can be experimentally determined with full scale or scaled models Mahfouz et al. [97], Julca Avila et al. [98]. Though these experiments can produce accurate properties but are often expensive with complex setup and measurement sensors requirements. Computational approach with CFD software packages such as Autodesk CFD Cely et al. [99], ANSYS FLUENT^{TM} He et al. [38],

Yue et al. [39], Ma et al. [40], Alam et al. [44], Star-CCM Chin et al. [100], ANSYS CFX^{TM} Yang et al. [101] and FSI solver Luo et al. [102] have been successfully used to estimate and study different hydrodynamic properties with good accuracy. Yang et al. [101] and Cely et al. [99] have verified the estimated system parameters from computational approach with full scale and scaled model experiments respectively. The k-ε turbulent model in ANSYS FLUENT^{TM} is popularly used to estimate drag and lift coefficient in hydrodynamic simulations with good accuracy by Yue et al. [39], He et al. [38], Mansoorzadeh and Javanmard [103], and Menter et al. [104].

During the underwater motion AUV has to displace surrounding water from its path by imparting kinetic energy, which has to be supplied by the actuators. To consider this effect equivalent mass is added to the system which is called added or virtual mass. For a submersed body, added-mass is constant and depends on the geometry of the system. The added-mass coefficients have been determined with WAMIT Chin et al. [100], Yang et al. [101], Eng et al. [105], ANSYS AQUA^{TM} Chen and Yan [106], ANSYS CFX^{TM} Moelyadi and Riswandi [107]. Strip theory has also been used to determine the added mass coefficients numerically Severholt [108]. In this method the system is considered to be a slender body having length considerably longer than the width and depth. The body is divided into thin sections, for which the 2D added mass coefficients are estimated and the 3D added mass coefficients are calculated by integrating the 2D coefficients over the length Lewis [109]. Dong from Lawrence Livermore National Laboratory (LLNL) Dong [110] and Newman in his book Marine Hydrodynamics Newman [111] have presented empirical relations of 2D and 3D added mass coefficients derived from experimental data for submerged body of different shapes. Other parameters such as inertia, position of center of buoyancy (C.B) and center of gravity (C.G) can be determined by developing a detailed CAD model of the system using software package such as SOLIDWORKS^{TM}. MATLAB^{TM} is a useful software package for simulating the developed kinematic Liu et al. [94] and dynamic models for understanding the behavior of the system. MATLAB^{TM} can also be used for desired trajectory generation, optimization Bae et al. [95].

For various practical applications such as retrieval of objects and repair work etc., underwater manipulators are essential. Work-class ROVs with remotely operated underwater manipu-

lators are being used for underwater intervention and manipulation works. These systems are very expensive because of the requirement of skilled operators, high-bandwidth communication link and they have to be deployed form the ships with sophisticated control stations. Apart from these, operator fatigue is also a major issue. Cheaper autonomous intervention systems can effectively replace these expensive manipulator systems. Such Intervention AUVs (I-AUVs) can be easily deployed from less sophisticated surface vehicles and require less human intervention. 'ODIN' Choi et al. [112] and 'OTTER' Wang et al. [113] are some of the first AUVs to be equipped with simple 1-DOF robotic arm. Lane et al. [114] presented the 'AMADEUS' project for cooperative manipulation using a 7-DOF electro-mechanical arm with-in a water tank. "UNION" project Rigaud et al. [115] demonstrated a coupled AUV-manipulator system with a AUV VORTEX and a 7-DOF robotic arm. ALIVE I-AUV described in Evans et al. [116] is one of the early projects to use autonomous manipulator system in the field. The I-AUV was aimed for docking to sub-sea structure autonomously, using sonar, vision sensors and manipulators. Kadiyam et al. [117] is a comparative study on fixed and vectored thruster configuration for I-AUV applications.

Dynamic modeling of AUVs with manipulator becomes more complex when the hydrodynamic effect of the manipulator on the AUV motion is considered. Following are some study on dynamic model of AUVs coupled with manipulators and other external accessories. Wang et al. [118] presented a lightweight multi-link manipulator structure for minimizing the dynamic coupling between the manipulator and the AUV. Wilson et al. [119] presented a dynamic model for AUV coupled with a two-link manipulator with its control design and numerical simulation. Zhao et al. [61] discussed the mathematical models of individual flipper joints of the turtle-like robot and coupling of the joints for oscillatory cooperative movement for swimming. Shibata et al. [120] presented a joint mechanism which is a combination of flexible and rigid parts and can be deformed by a prismatic actuator driven by hydraulic pressure for underwater manipulation. Santhakumar and Kim [121] discussed detailed modeling and simulation of dynamic coupling in an AUV and its manipulator system. Jie and Wang [122] presented an underwater robot with two hanging torpedoes and developed a dynamic model for the robot considering the forces exerted by the torpedoes on the robot. Generally underwater robots rely on tethered com-

munication. The cable affects the dynamics of these vehicles. Schjolberg and Egeland [123] presented dynamic model of a robotic system connected to the ship by a cable.

A flexible AUV such as a robotic fish or snake has a body consisting of multiple links. In case of such AUVs, kinematic and dynamic modeling becomes more complex. The dynamic model of such robots correlates different forces along with the forces generated because of the link movements and the motion of the AUV. Some studies with Mathematical modeling of such multi-link flexible AUVs are presented here. Yang et al. [47] presented dynamic model for a 3 joint 4 link robotic fish. Ashar et al. [55] used different link movement patterns for different motion of the fish robot. Kinematic relations have been developed for these movement patterns, which are further used in the control system. Vo et al. [56], Choi et al. [124] and Yu et al. [59] developed kinematic and dynamic models of their flexible robot for control and navigation. AUVs have to use different control systems and path planning algorithms for navigation in the highly dynamic underwater environment which are discussed in the following section.

2.5 Planning and Control

After the development of an accurate dynamic model, one needs to develop a control system for the AUV to work properly. Control system regulates the actuator output to obtain required velocity and position. AUV controller has three major operations: planning, control and error diagnostic. Depending on the mission objective and environmental constrains, path-plan is developed. Control enables the AUV to follow this path and replanning is done if some constrain is violated. The highly non-linear behavior of AUV, dynamic underwater environment forces and uncertainties in system parameters are some major challenges faced during the design of a control system for an AUV. Multi-link flexible body AUVs and additional manipulators add more complexity to the problem. AUVs to operate in these highly dynamic environment, controller gains have to be tuned during AUV motion. Thus adaptive or self-tunning controllers are highly desirable. But still classic control technique such as PID is commonly used in AUVs because of its ease of implementation. Schjolberg and Egeland [123] adopted a classical PID control strategy for control of the underwater robot and presented stability analysis of the system by Lyapunov theory. A simple PID controller was used by Jung et al. [60] to control the

motion of a slide-slipping fish robot on a flow aided path. Fittery et al. [37] used a simple PD controller with an on-board gyro sensor for estimation of heading angle of the micro-pumps of an egg-shaped AUV. Isa and Rizal A. [79] developed an open loop controller for a propeller-driven underwater glider. Shome and Das [4] implemented a PID controller for 'AUV-150'. Wilson et al. [119] presented a PID controller having a linearised feedback. Schillai et al. [125] used a depth PID control along with sonar to evaluate the terrain collision risk associated with AUVs used in photographic surveys of sea-floor.

Apart from simple controllers, researchers have developed some advanced control strategies such as non-linear control, adaptive control, sliding mode control and neural network control to address complex dynamic control problem associated with AUVs. Some of these control methods adapted for AUVs are discussed by Parhi and Kundu [126] and Yuh [127]. Hyaku-dome [33] used a linear quadratic optimum controller with integral action. Sarhadi et al. [93] proposed an adaptive PID control with anti-windup compensator for an AUV. Such adaptive control strategies are better equipped to handle variable system parameters. Xiang et al. [128] developed a control strategy to move an AUV along a horizontal path in both fully-actuated and under-actuated configurations. A non-linear controller was used for an under-actuated AUV which was later adopted for the fully-actuated system.

Fuzzy controllers based on fuzzy logic are most popular control techniques. Fuzzy logic is a mathematical system which considers analog inputs in form of logical variable which can take continuous values between 0 to 1. This method reduces mathematical complexity. Kato et al. [24] developed a PID and a fuzzy controller for maintaining the altitude of a cable tracking AUV and also discussed the cable tracking experiment with sensors, sonar and PID control. Hung and Na [46] used a Hybrid fuzzy PID controller where the incremental fuzzy logic controller is used in place of the proportional term with integral and derivative terms intact. Yu et al. [59] used two-stage control law for posture control of the robotic fish. First one is the fast position approach, which is a modified proportional control for the fish to swim faster towards the target and the second one is the accurate posture adjusting using a time-varying feedback stabilization control for position and directional accuracy. Here fuzzy logic and behavior based control were used for coordination of multiple fish robots. Vo et al. [56] developed the dynamic model of

a fish robot based on Lagrange method. The Sliding Mode Controller (SMC) and the Fuzzy Sliding Mode Controller (FSMC) were proposed to achieve the straight and turning motion of the fish robot. Feasibility and the quality of the controllers were verified using numerical simulations. Li et al. [41] used Fuzzy Sliding Mode Controller for a spherical AUV to control the direction of the water-jet thruster for navigation. Yu et al. [129] proposed a non-linear single input fuzzy controller coupled with a 3D guidance law for path following problem of an under-actuated AUV. Londhe and Patre [130] designed an adaptive fuzzy sliding mode control for trajectory tracking AUV considering the system non-linearity. Yan et al. [131] discussed an adaptive integral sliding mode control for under-actuated AUVs with unknown dynamics. A dual closed-loop integral sliding mode control design is used with outer loop for velocity estimation and inner loop for actual control input to actuators for trajectory tracking. Khodayari and Balochian [132] presented a self adapting fuzzy PID controller based on the non-linear model of the AUV and the stability of the controller is presented with different simulations.

Neural network controllers have gained popularity and seen a large scale adoption in recent years because of exponential advancements in computer infrastructure. Artificial neural networks are computing systems inspired by biological neural network with machine learning algorithms for data processing. Li and Lee [133] designed a neural network adaptive controller for an AUV. Here neural network was used to approximate unknown dynamics in the pitch motion. Wang et al. [92] proposed a neural network PID controller for an amphibious spherical robot. The stability of the controller was analysed according to the Lyapunov method. Shojaei [134] studied a 3D target tracking control for an under-actuated AUV with multilayer neural network.

As discussed above, the control strategies in general are developed with a objective to make the AUV follow a predefined path or target taking care of the unknown dynamics, system non-linearity and unknown disturbances. Shen et al. [88] presented non-linear model predictive control for trajectory tracking AUV. Here six DOF AUV model was presented in three coupled subsystems and distributed model predictive control was implemented. Santhakumar and Asokan [51] presented a nonlinear back-stepping controller to overcome modeling errors. Xia et al. [135] presented a line-of-sight (LOS) based adaptive trajectory tracking controller for an

under-actuated AUV with consideration of system non-linearity, uncertain ocean currents and input saturation etc. Here kinematic and dynamic models of AUV are developed with ocean currents and extended disturbance observers (EDO) are utilized to estimate the ocean currents. Chowdhury et al. [136] presented a behaviour-based control to achieve local goals while tracking a desired path. Lamraoui and Qidan [137] presented a active disturbance rejection control strategy for a path following AUV in presence of fast-varying disturbance by waves and ocean currents. Here the generalized extended state observer (GESO) and Harmonic ESO (HESO) is used for disturbance estimation. Rout and Subudhi [138] presented a model predictive controller for an under-actuated system. Sarkar et al. [139] has developed energy efficient trajectory tracking Controller for underwater navigation. Yan et al. [140] presented a coordination control for multiple AUVs for trajectory following problem. In this work a leader AUV with accurate sensors lead the fleet of multiple AUVs. Kimura et al. [21] presented control strategy for SOTAB-I (SOTAB; Spilled Oil Tracking Autonomous Buoy) Allibert et al. [141] presented a vision-based non-linear control technique for pipeline following. Apart from following a path or target, control strategies can be developed to control depth, increase energy efficiency, achieve bio-mimetic propulsion, autonomous docking etc. Hong et al. [34] presented a depth controller design for a positively buoyant torpedo-shaped AUV named as 'STARFISH'. Here, the effect of buoyancy on both pitch and heave dynamics of an AUV was studied and a controller scheme was proposed that specifically compensates for the positive buoyancy. A cascaded dual loop design with inner sliding mode control and outer proportional control with feed-forward loop was used for depth or altitude control for the terrain following AUV for collision avoidance. Yang et al. [47] described a control method according to propulsion algorithm for improving energy efficiency and obstacle avoidance of the fish robot "Ichthus". Mahapatra et al. [142] presented a non-linear path following control algorithm for diving motion in vertical plane. Zhao et al. [61] presented a central pattern generator (CPG) based control model for propulsion of a turtle-like robot. The controller generates oscillatory movement of the four mechanical flippers which results in different swimming gaits. Liu et al. [143] presented a convolutional neural network control for detection and pose estimation for docking. Kundu and Parhi [144] presented frog leaping algorithm for 6DOF motion controller for with obstacle avoidance. Kadiyam et al.

[145] showed an actuator fault-tolerant back-stepping control for under actuation case. Bak et al. [146] presented hovering control with PID based control design with decomposition and compensation method.

2.6 Navigation and Localization

AUVs navigate underwater autonomously based on predefined strategy. Localization is a vital component in navigation which helps an AUV to follow the predefined path precisely and reach the final destination. Non-availability of Global Positioning System (GPS) and high-frequency radio signals in the underwater environment makes localization and navigation very challenging for AUVs. Maintaining accuracy in AUV's position for a long mission is a difficult task. Accuracy in position deteriorates over time because of variations in AUV motion and absence of an external reference. Therefore, over time different innovative methods have been developed to tackle these problems using a combination of numerical technique and real-time sensor data. As discussed by Stutters et al. [147] AUV navigation can be broadly classified as:

- *Inertial navigation*: Inertial navigation uses different sensor data to estimate vehicle′s relative velocity and position. Acceleration, rotational speed and magnetic field intensity data are obtained from accelerometer, gyroscope and magnetometer sensors respectively. These three sensors are part of the Inertial Measurement Unit (IMU). Other sensor data such as relative velocity from Doppler velocity log (DVL) sonar, positioning data from GPS, depth data from pressure sensor etc. are used to minimize the error in estimated position.
- *Acoustic navigation*: Acoustic navigation uses multiple acoustic transponders to estimate AUV's position using time of flight concept.
- *Geophysical navigation*: Geophysical navigation uses unique features in the surrounding as reference to estimate AUV′s position and navigate. Different sensors capable of detecting and identifying these features are used.

AUVs are equipped with different sensors which can provide real-time quantitative data of the surrounding. All these sensor data have to be processed together using some techniques to

obtain an optimal estimate of the vehicle position. Some of those techniques are Kalman Filters (KFs), Particle Filters (PFs), and Simultaneous localization and mapping (SLAM). From these techniques, KFs and PFs are numerical techniques for sensor fusion. These numerical methods are prone to drift over time. In SLAM method localization is achieved by identifying areas of the environment, the robot has already passed through. Stutters et al. [147] and Paull et al. [148] discussed different navigation and localization methods in detail.

2.6.1 Inertial navigation systems

INS calculates relative position and orientation of a dynamic system relative to a known starting point, orientation, and velocity using the data from motion sensors (accelerometers), and rotation sensors (gyroscopes). INS is a compact, inexpensive and self-contained system which does not require external references. Therefore It can be used for inexpensive small AUVs. However, INS can accumulate error over time because the estimated relative velocity and position are the result of mathematical integration of the accelerometer and gyroscopic sensor data. Errors in the measurement of the sensor data and errors introduced in integration lead to a significant drift in the estimated position and velocity. Therefore, the estimated position from INS needs to be compared with the data from other systems such as depth sensor, compass, DVL sonar, acoustic Doppler current profiler (ADCP) Sonar for short missions and from GPS on long missions. Depth sensor, compass, GPS costs between 100-1000 USD where as DVL and ADCP Sonar cost 20k-200k USD. A low cost INS set-up uses GPS, but the AUV has to resurface in interval. When operating in greater depth resurfacing is not an option AUV has to relay on INS with DVL or ADCP Sonar.

P-SURO AUV Li et al. [43] used an INS system along with depth sensor, sonar and vision system with Kalman filter for navigation. Thompson et al. [16] used Kearfott inertial navigation system (INS) with Doppler velocity log, a Paroscientific pressure sensor, and an ultrashort baseline (USBL) and acoustic modem for communications in their mapping AUV. Shome and Das [4] used EKF with INS and DVL for navigation of ‘AUV-150’. Ashar et al. [55] used an INS using a 10-DOF IMU for a fish robot. Tal et al. [149] proposed a navigation system for small AUV using INS and DVL fusion with partial DVL measurement.

2.6.2 State estimator

As discussed above Kalman Filters (KFs), Particle Filters (PFs), and Simultaneous localization and mapping (SLAM) are some of the popular state estimators used for AUV localization with available sensor data. KFs and PFs commonly used with INS and acoustic navigation where as SLAM with geophysical navigation. Kalman Filter (KF) is used to derive the best estimate of position from different sensors used. The KF estimates the state of a system from multiple uncertain observations using a predict update cycle. A physical model describing AUV motion can be highly non-linear where the KF fails. In such non-linear model case, an Extended Kalman Filter (EKF) can be used. EKF uses a first-order Taylor series to approximate the non-linear processes. Xiaoping Yun et al. [150] developed an INS navigation system for small AUV using low-cost IMU and GPS unit. An Asynchronous Kalman Filter is used to improve position estimation. Allotta et al. [151], Choi et al. [152] Used EKF for AUV localization. Font et al. [81] developed a navigation system with two parallel EKF, one using the positioning system GPS and other Ultra Short Base Line (USBL) acoustic modem. Panish and Taylor [7] presented the development of a high accuracy INS for AUVs developed by Bluefin Robotics using different sophisticated laser and fibre optic gyros with sonar. Mu et al. [153] proposed a modified algorithm combining least square method with EKF. This proposed LS-EKF is compared with EKF and observed to reduce localization errors. Ngatini et al. [91] presented position estimation of AUV based on the dynamic model using the Ensemble Kalman Filter (EnKF) and the Fuzzy Kalman Filter (FKF) and shown that EnKF is better in estimating the trajectory of dynamic equation of AUV motion. Choi and Lee [57] proposed an effective movement for the navigation of the fish-like robot using the heuristic method. Kinsey et al. [154] presented a system to estimate position and velocity of an ROV for the navigation using non-linear dynamic model. Here EKF and non-linear observer (NLO) methods were used for position estimation, and it is observed that NLO performed better than KF. Shao et al. [155] used a adaptive EKF for AUV navigation. Allotta et al. [80, 156] used Unscented Kalman Filter (UKF) for AUV navigation and presented a comparative study with EKF approach. Jung et al. [60] presented a navigation strategy for an AUV in a flowing medium. A biomimetic robot moving in uniform flow using a side-slipping maneuver was used to showcase the stability of the proposed strategy.

Accurate dynamic model of AUVs are essential for navigation, but error in parameter estimation and some unknown parameters introduce error in navigation. Shariati et al. [157] proposed a method to estimate the non-linear dynamic model of the AUV using PF combined with EKF. Simulated results by the estimated model is compared with the experimental results to validate the model.

Navigation algorithms can also be target-specific such as tracking oil spill, gas leakage or underwater communication cables etc. In these cases different visual and chemical makeup sensors data are incorporated in the navigation algorithm to track these specific targets. Kimura et al. [21] described the guidance control simulation for designing the underwater robot SOTAB, that tracks oil-spill autonomously and gathers oceanographic data. Numerical simulation was adopted to estimate the maneuverability of this robot. To compute the hydrodynamic derivatives of the robot, USAF DATCOM Method and CFD were used. Modalavalasa et al. [158] proposed target tracking by EKF using bearing and elevation measurements. Kato et al. [24] presented an autonomous underwater robot "AQUA EXPLORER 1000" (AE1000) used for inspection of underwater telecommunication cables. AEl000 can find and track buried underwater cables with a cable tracking sensor, and the underwater footage of the sea-floor is saved on a built-in Video Cassette Recorder (VCR).

Among the three navigation systems INS is suitable for low-cost small-scale AUVs for short missions and long missions with GPS where resurfacing is allowed. Acoustic navigation is costlier with better accuracy. This need transponders to be fitted to support surface vehicles, GPS buoys or to be placed on seabed. Which are time consuming process and before starting each operation the transponders has to be referred globally. These limitations can be eliminated by using acoustic modems. Acoustic modems are suitable for cooperative navigation. When existing information of the environment is available such as repetitive routine operations geophysical navigation can be utilized with low cost optical sensors or high precision costlier sonar sensors and different SLAM techniques.

2.7 Summary of Literature Review

A critical review on underwater vehicles has been carried out considering the past literature. In the literature review, a detailed study of UUVs with applications and different research aspects such as structural design and analysis, propulsion, dynamics, control, navigation, localization, and path planning are discussed. Most of the underwater systems available are bulky and expensive. These systems require specialized equipment to deploy, have high maintenance and operation cost and cannot be operated in narrow terrains such as rivers, frozen ice-covered lakes. An affordable compact underwater robotic system will be a very useful tool for small-scale marine industries, entertainment industries, individuals, and environmental groups etc. Neutral buoyancy, lightweight, modular design, intuitive control, and easy deployment are some of the key requirements for a compact UUV. A closed-frame structure will be better with low drag resistance and will help avoid river weeds and other debris in lakes and rivers. Most underwater submersible vehicles have cylindrical structures because of less drag, less stress concentration, and the ability to withstand more pressure. However, a hull with circular cross-sections will have more buoyancy than an elliptical one with the same length and similar diameter and major axis as it will displace more water. The weight must be increased to make it neutrally buoyant in a fixed buoyant system. Moreover, most internal components are rectangular in shape, so the unused portions in a cylindrical structure will lead to high weight and buoyancy. Thus different shapes can be explored further for compact UUVs.

The use of non-traditional materials and manufacturing techniques can drastically reduce the cost and manufacturing complexity. Most of the underwater systems are developed with metal structures. Complex hydrofoil structures are difficult to manufacture and costly with traditional materials and techniques. Composite materials can be used in such cases for ease of manufacturing, high strength and other properties comparable and sometimes better than traditional materials. Kang et al. [65] presented an underwater glider made of carbon fiber composite with similar strength but 40% less weight compared to high tensile aluminum. Here stress and buckling analysis is used to show that the glider can withstand the underwater pressure at 200m depth with 1.8 factor of safety. Glass fiber composites are used in marine structures and flexible pressure vessel due to its properties such as corrosion resistance and high resilience. Glass fiber

composite has not been used for UUVs. But use of this material will reduce manufacturing cost, vehicle weight and improve strength. AUVs nowadays are adapting modular design in the body structure [4, 6, 68]. The whole AUV is a combination of different modules such as propulsion, sensor modules which can be easily and quickly replaced in case of a failure as well as can be interchanged with different modules according to the mission requirements. Such modular design are highly versatile and incur less maintenance cost. During motion, AUV experiences drag and lift forces because of the friction between the body and surrounding water, which affect the dynamics of AUV. Body structure greatly affects these forces. Fluid-structure interaction study of the AUV with the surrounding water is essential to predict the drag and lift. Minimizing these forces using different numerical and optimization technique, increases the efficiency of the AUVs.

Stability, performance, and structural analysis using numerical or experimental techniques can help develop a robust underwater robotic system. A popular Computational Fluid Dynamics (CFD) software ANSYS FLUENT^{TM} is being used for the hydrodynamic study of the AUVs. Such performance study can help in selection of actuators to be used depending on the system applications. AUVs experience hydrostatic pressure due to water head and hydrodynamic pressure due to their movement. AUV body can deform or get damaged due to excess pressure, which increases with depth. Researchers are using 'Finite Element Method'(FEM) for stress and buckling analysis of the hull structure which helps in selection of proper material, thickness of the wall as well as set the operational depth limit of the AUVs. ANSYS^{TM} static structural module coupled with Fluent can be used for such analysis.

AUVs depend on its propulsion system to travel in the underwater environment. Bio-mimetic AUVs mimic propulsion technique as well as body structure of aquatic animals. These AUVs travel in water using undulatory propulsion. In this technique pressure difference is created in water by moving some part of their body in a wave-like pattern. Bio-mimetic AUVs are incapable of carrying heavy payloads and achieving high speed. AUVs used for these applications generally use multiple propellers or thrusters for propulsion along with rudders and fins for directional control.

Underwater systems can be used as ROVs or AUVs depending on requirements. For the

UUVs to be used as an AUV required basic sensors, controller and robust control algorithms are essential. Accurate kinematic and dynamic model of the system are useful for development of the AUV. Study of Kinematic and dynamic model of different AUVs will help in developing accurate models for the AUV and also in system parameter estimation. To understand the interaction of environmental forces acting on the system experimentation with full scale or scaled models can be performed. Though these experiments can produce accurate properties but are often expensive with complex setup and measurement sensors requirements. Computational approach with CFD software packages such as Autodesk CFD, ANSYS FLUENT^{TM}, STAR CCM^{TM}, ANSYS CFX^{TM} has been successfully used to estimate different hydrodynamic properties with good accuracy.

During the underwater motion AUV has to displace surrounding water from its path by imparting kinetic energy, which has to be supplied by the actuators. To consider this effect equivalent mass is added to the system which is called added or virtual mass. For a submersed body, added-mass is constant and depends on the geometry of the system. Strip theory has also been used to determine the added mass coefficients numerically Severholt [108]. In this method the system is considered as a slender body having length considerably longer than the width and depth. The body is divided into thin sections, for which the 2D added mass coefficients are estimated and the 3D added mass coefficients are calculated by integrating the 2D coefficients over the length Lewis [109]. Dong from Lawrence Livermore National Laboratory (LLNL) Dong [110] and Newman in his book Marine Hydrodynamics Newman [111] have presented empirical relations of 2D and 3D added mass coefficients derived from experimental data for submerged body of different shapes. In most of the AUVs the added mass has been neglected but by considering the effect, accuracy of the model can be improved significantly. Other parameters such as inertia, position of center of buoyancy (C.B) and center of gravity (C.G) can be determined by developing a detailed CAD model of the system using software package such as SOLIDWORKS^{TM}. MATLAB^{TM} is an useful software package for simulating the developed kinematic [94] and dynamic models for understanding the behavior of the system. MATLAB^{TM} can also be used for desired trajectory generation, optimization [95].

Localization is a vital component in navigation which helps an AUV to follow the pre-

defined path precisely and reach the final destination. Non-availability of Global Positioning System (GPS) and high-frequency radio signals in the underwater environment makes localization and navigation very challenging for AUVs. Maintaining accuracy in AUV's position for a long mission is a difficult task. Accuracy in position deteriorates over time because of variations in AUV motion and absence of an external reference. As discussed by Stutters et al. [147] from different techniques, INS is best economical localization solution for a small scale AUV. INS calculates relative position and orientation of a dynamic system relative to a known starting point, orientation, and velocity using the data from accelerometers, and gyroscopes by integration. Errors in the measurement of the sensor data and errors introduced in integration lead to a significant drift in the estimated position and velocity. Therefore, the estimated position from INS needs to be compared with the data from other sensors using state estimators such as Kalman Filter (KF). KF is used to derive the best estimate of position from different sensors used. A physical model describing AUV motion is highly non-linear where the KF fails. In such non-linear model case, an Extended Kalman Filter (EKF) can be used. For a small low-cost AUV, INS with mems IMU, depth and GPS sensor with EKF can be used for localization.

After the development of an accurate dynamic model, one needs to develop a control system for the AUV to work properly. Control system regulates the actuator output to obtain required velocity and position. AUV controller has three major operations: planning, control, and error diagnostic. Depending on the mission objective and environmental constrains, path-plan is developed. Control enables the AUV to follow this path and re-planning is done if some constrain is violated. The highly non-linear behavior of AUV, dynamic underwater environment forces and uncertainties in system parameters are some major challenges faced during the design of a control system for an AUV. AUVs to operate in these highly dynamic environments, controller gains must be tuned during AUV motion. For unstructured underwater environment adaptive or self-tuning controllers are highly desirable. In uncertain environments soft computing techniques such as Fuzzy logic and Neural networks are popular tools to control the system. Thus adaptive Fuzzy-PID, Neuro-Fuzzy controllers can be developed for AUV navigation. Classical controllers such as PID is also popular because of its ease of implementation. From a detailed

literature review it is observed that most of the underwater vehicles use some form of the PID controller for autonomous trajectory tracking. Hence PID controller is used as the fundamental controller in the present work.

Fuzzy controllers based on fuzzy logic are most popular control techniques. Fuzzy logic is a mathematical system which considers analog inputs in form of logical variable which can take continuous values between 0 to 1. This method reduces mathematical complexity. PID parameters are difficult to tune for complex coupled non-linear AUV model. Using fuzzy rules these parameters can be adjusted to address the system modeling uncertainties making the controller adaptive.

Neural network controllers have gained popularity and seen a large-scale adoption in recent years because of exponential advancements in computer infrastructure. Artificial neural networks are computing systems inspired by biological neural network with machine learning algorithms for data processing. A Neuro-Fuzzy controller can be used to develop an accurate dynamic model of the system considering the environmental forces and will help adapt to different environments on the go.

Chapter 3

DESIGN AND DEVELOPMENT OF THE AUV

3.1 Introduction

Compact affordable underwater robotic systems can be a very useful tool in the hands of individuals and small-scale marine industries. As discussed in the previous chapter neutral buoyancy, modular design, use of composite materials are some of the key elements in development of an affordable compact underwater system. Numerical validation of the designed structure for performance, dynamic stability and structural rigidity is essential for developing a reliable device. Software and hardware architecture along with presence of required sensors are essential towards ease of operation of the device. This chapter presents the design and development of an affordable, compact underwater robot, which is organized into the following sections. In the section 3.2, system requirements and their design solutions are discussed. Design analysis involving stability, stress and hydrodynamic analysis are also mentioned here. Manufacturing of the robot structure is presented in section 3.3. Section 3.4, discusses the field test result of the developed robot. The summary of the work is discussed in section 3.5.

3.2 Mechanical Design

The objective of this chapter is to develop a compact, affordable underwater robot to be used in static and dynamic underwater environments. The robot should be easy to transport and deploy without requiring any specialized equipment. It should be able to operate up to a depth of 100 meters. Non-traditional materials and manufacturing techniques can be employed

to minimize the cost, improve product life and efficiency. A fixed buoyancy system can be developed instead of a variable buoyancy to reduce the cost. The robot should be neutral buoyant for better battery life. The vehicle will be used for exploration and monitoring purposes, so it should be equipped with the required sensors. The design of the UUV is discussed in the following sub-section.

3.2.1 UUV structure

Design requirements of the UUV to fulfill the objectives mentioned above are summarized in the following sub-section.

Design requirements

The basic challenge is to come up with a compact yet functional design while maintaining the overall cost low. Also, it should address the practical problems faced while developing a reliable underwater robot.

- The total weight of the UUV must be less than 15 kg for ease of transportation, which is also the safe load carrying capacity for an individual.
- The maximum length must be less than 1 m for better maneuverability and ease of transportation.
- The interior volume of the UUV should be watertight and should be more than 6000 cubic centimeters (cc) to accommodate internal components but not more than 9000 cc to avoid excess buoyancy.
- Modular structure for ease of accessibility, manufacturing, and assembly.
- UUV must be neutrally buoyant for better efficiency.
- Should able to travel at 1.5 - 2 m/s, ideal velocity for the survey.
- Should have a closed frame structure to avoid external interference such as river-weeds.

UUV will use fixed position, bi-directional thrusters instead of fins and rudders to avoid manufacturing complexity and keep the cost low. An underwater robot requires a minimum of three

thrusters for its motion in 3D space. One of the thrusters will be used for vertical motion and the other two for motion in horizontal direction. The UUV will be neutrally buoyant; thus, only one thruster can be used for vertical motion. As buoyancy and gravitational forces cancel each other out, there will be no unbalancing forces in the vertical direction. The use of a fixed buoyancy system instead of a variable one reduces the cost. The UUV Centre of Gravity (C.G.) must coincide vertically with the Centre of Buoyancy (C.B.) to avoid pitch and roll. The C.G of the structure must be close to the central truster to avoid tilt during vertical motion.

Component Selection

Thrusters are the most important component which will be selected after design analysis. For design purposes, thrusters are assumed to be 500 grams and with dimensions of 10 cm diameter and 15 cm length. UUVs can have onboard power, or power can be transmitted using a separate power cable along with the communication cable. For a small compact ROV low-cost rechargeable onboard battery is the best option to avoid complexities in transportation and deployment. The compact size of the ROV restricts the use of power sources such as solar and fuel cells etc. Two batteries will be used, one as primary and the other as a backup power source. Commercially available 5000 mAh three-cell lithium polymer batteries are used as this is readily available and economical. These batteries will supply 12 volt D.C. power which is ideal for most of the thrusters. Apart from thrusters and batteries, a few other essential components were selected for the operation of the UUV, such as Raspberry Pi computer, Pixhawk controller, sensor housing containing temperature and pressure sensor, camera, and power distribution module. The UUV can be used as ROV with assisted operation modes such as depth hold and stability mode with the mentioned components. The UUV can be used for some AUV applications such as trajectory tracking, obstacle avoidance, with some additional sensors. But for full autonomy in dynamic environments, control modules need to be upgraded.

Hull geometry

The design of the UUV is carried out using the CAD modeling software SOLIDWORKS^{TM}. Initially, the weight and dimensions of the internal components are recorded as given in Table

3.1. Equivalent CAD models of these components are developed as shown in Fig. 3.2. During the design of the hull, keeping the vertical thruster at the center, other components are to be arranged around it to maintain the C.G. of the UUV close to C.G. of the thruster (Fig. 3.2). Using MATLAB Optimization Toolbox^{TM} a multi-objective linear search optimization was carried out with the objective function to minimize the combined C.G (Center of Gravity) position from the geometric center. Using MATLAB Optimization Toolbox^{TM} a multi-objective linear search optimization was carried out with the objective function to minimize the combined C.G position from the geometric center. The upper and lower bounds are selected to avoid overlap of the objects. Optimal x-coordinate of the components' C.G. are presented in the Table. 3.1 and arrangement is shown in the Fig. 3.2. In this optimal configuration, C.G. is at 0.84 mm from the center of the central thruster.

Table 3.1: Internal components present in the UUV

Component Name	Weight (in kg)	Dimensions (in m)
Thruster	0.50	ϕ0.100 x 0.150
Battery	0.38	0.145 x 0.050 x 0.026
Camera module	0.20	0.070 x 0.060 x 0.080
Sensor Housing	0.10	0.060 x 0.050 x 0.050
Raspberry Pi	0.16	0.120 x 0.060 x 0.050
Pixhawk	0.15	0.080 x 0.050 x 0.050
Power distribution board	0.13	0.120 x 0.080 x 0.050
Communication Module	0.10	0.080 x 0.050 x 0.050

Table 3.2: Optimized component position

Component name	Optimized position (in m)
Side Thruster	-0.12
Battery	0.12
Camera module	0.21
Sensor Housing	-0.28
Raspberry Pi	0.20
Pixhawk	-0.11
Power distribution board	0.11
Communication Module	-0.23

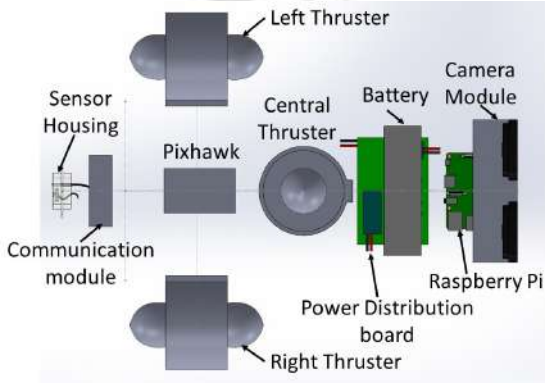

Figure 3.2: Arrangement of internal components

After fixing the position of the internal components, a side section of the encloser is developed (Fig. 3.3), considering the dimensions of the internal components. The front section of the structure is made of two flat surfaces with an inclination of 60° to vertical. Flat transparent

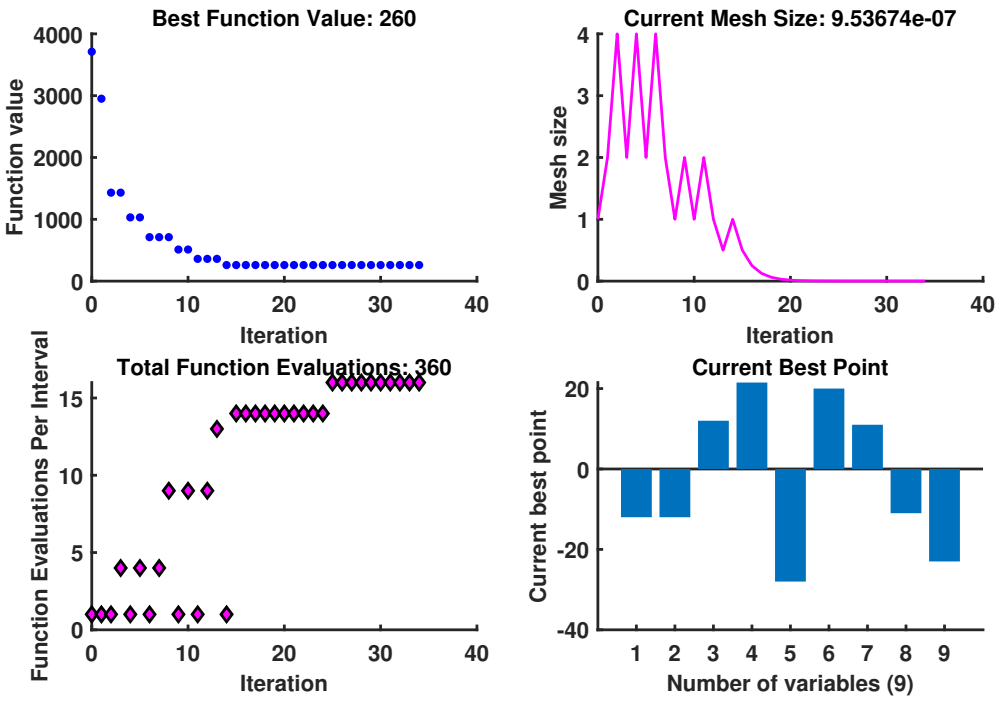

Figure 3.1: Component position optimization

plates can be used on these flat surfaces to give a good field of view for the cameras to be placed inside. The use of flat transparent panels instead of a hemispherical structure reduces cost and manufacturing complexity. A parametric fluid flow study of the 2D section is conducted with ANSYS FLUENT^{TM} and optimization tool (Fig. 3.4) to find the optimal shape of the cross-section having minimum drag coefficient. Simulation setup is presented in the Fig. 3.3. Here the flow field is developed by subtracting UUV shape from the rectangular domain. The inlet wall was selected with velocity inlet, outlet wall with pressure outlet and other walls with symmetry boundary condition. Inlet velocity was defined as 4 m/s with 603916 Pa gauge pressure. The parameters h_1 and h_3 (Fig. 3.3) are varied in each step to find the optimal shape with least drag coefficient. The optimal shape is found with h_1 and h_3 values as 70 mm and 56 mm respectively with drag coefficient 1.14.

Most underwater submersible vehicles have cylindrical structures because of less drag, less stress concentration, and the ability to withstand more pressure. However, a hull with circular cross-sections will have more buoyancy than an elliptical one with the same length and similar diameter and major axis as it will displace more water. The weight has to be increased to make it neutrally buoyant in a fixed buoyant system. Moreover, most internal components are

rectangular in shape, so the unused portions in a cylindrical structure will lead to high weight and buoyancy. Therefore slightly elliptical cross-section according to the internal component dimensions is selected (Fig. 3.5). A closed frame structure with the selected cross and optimal side sections (Fig. 3.6) is developed, enclosing the internal components. Fig. 3.6 shows the placement of internal components inside the closed frame structure. The C.G. of the system is maintained to be close to the center point of the central thruster. A closed frame structure will help reduce the drag and avoid external interference such as river weeds.

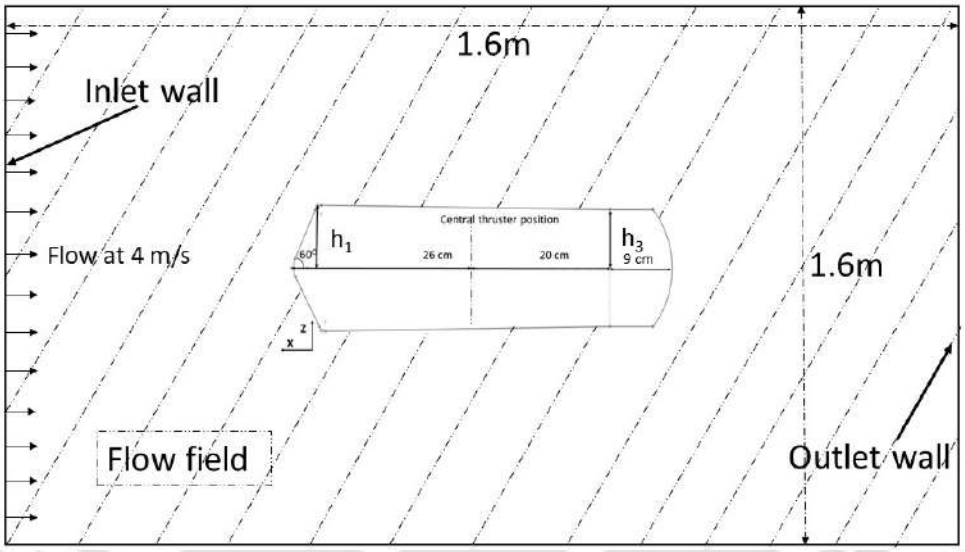

Figure 3.3: Side section view of the structure

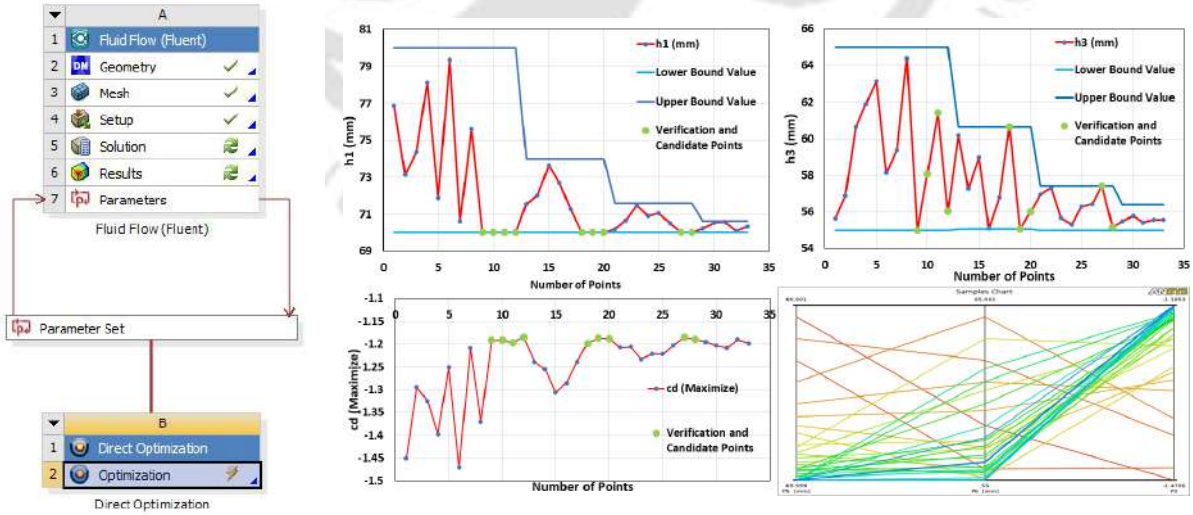

Figure 3.4: ANSYS^{TM} Parameter optimization

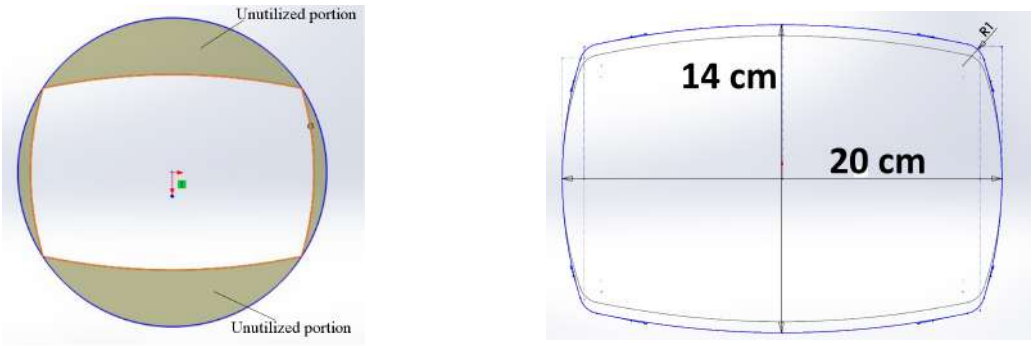

Figure 3.5: Cross-section of the UUV

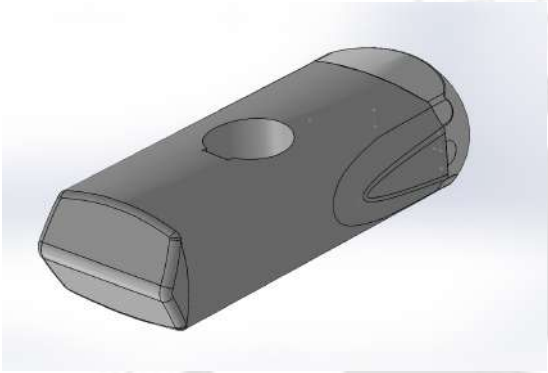

Figure 3.6: UUV hull structure

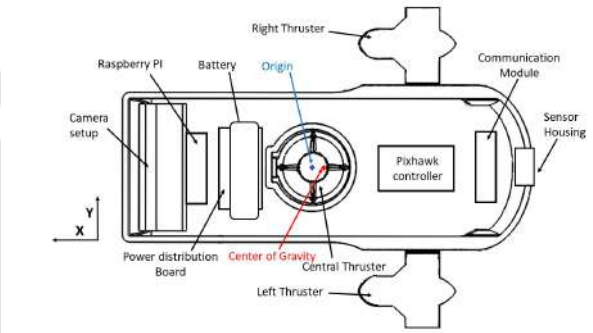

Figure 3.7: Section view of structure showing arrangement of internal components

3.2.2 Design Analysis

The UUV structure is designed in SOLIDWORKS^{TM}, keeping in mind the static stability, neutral buoyancy, accessibility of internal components, ease of manufacturing, space requirement, and size of internal components. The UUV will work in the complex underwater environment; thus, static and dynamic stability, hydrodynamic characteristics, and structural rigidity must be analyzed before manufacturing. ANSYS^{TM} is a Finite Element Method (FEM), and ANSYS FLUENT^{TM} is a Finite Volume Method (FVM) based design and simulation software. For hydrodynamic and structural analysis, ANSYS FLUENT^{TM} and ANSYS^{TM} static structural modules have been used, respectively.

Material

The objective here is to develop a neutrally buoyant underwater structure. Thus, the structure should be lightweight yet strong to withstand underwater pressure. Fiber Reinforced Plastic (FRP) has a higher strength-to-weight ratio than traditional materials like aluminum. Glass fiber

composite is a popular choice for marine applications because of its good corrosion resistance property. FRP also has high-stress resistance capability. Moreover, traditional materials like aluminum and steel require highly complex and costly manufacturing processes. Thus the use of FRP will reduce the manufacturing cost to a great extent. FRP is a combination of a matrix medium and fibers to reinforce them. For glass FRP, sheets woven from fibers made of glass strands are used. The fiber orientation in the matrix gives directional properties to the FRP. To have uniform properties, one randomly oriented glass fiber, and two woven glass fiber mats, each of 3 mm thickness, will be used alternatively. The cured FRP sheet with this arrangement has 12 mm thickness. Here macro-mechanical GFRP properties obtained by testing of the cured sheet (Sangu [159]) are considered for simulation, which are given in the Table 3.3. In case of macro-mechanical property, equivalent properties of all layers together are considered for analysis instead of modeling each layer.

Table 3.3: Glass FRP properties

Density	2100 kg/m^3
Shear modulus	10 GPa
Poisson's Ratio	0.28
Young's modulus	26.9 GPa
Ultimate Tensile strength	278 MPa

3.2.3 CFD Analysis

3D unsteady simulations have been carried out using FVM solver ANSYS FLUENT^{TM}. This numerical analysis simulates fluid flow around a structure to find the drag and lift forces acting on the structure due to skin friction. Here flow of water past the submersed UUV structure is studied.

Modeling

CFD analysis of a complex 3D model is time-consuming and requires high computational power. Therefore to get effective results in less time, the UUV model has to be simplified. In the hydrodynamic analysis, only the fluid-structure interaction at the outer solid and fluid interface is studied. So, the internal details of the UUV are irrelevant. Therefore a simplified single

solid model is developed by filling the internal hollow spaces. The new modified model (Fig.) is imported to ANSYS Workbench^{TM} from SOLIDWORKS^{TM}. After generating the model, a cylindrical encloser is developed surrounding the UUV structure, which is the fluid volume. The solid interface is considered to be rigid and static. The UUV volume is subtracted from the cylindrical volume to remain with the final flow field, as shown in Fig. 3.9.

Meshing

The hydrodynamic analysis is mostly affected by the mesh quality. Grids with high refinement yield good results but increase computational time. Therefore grid size has to be selected, making a balance between the computational time and result quality. Thus a grid independent test is conducted to select meshing with minimum elements without having much deviation in the results. For one of such tests number of elements are varied from 10,25,953 to 158,84,806 as shown in Table. 3.4 (Fig. 3.8) and fine mesh with 14,54,076 tetrahedral elements with 268731 nodes is selected for simulation. Fig. 3.9 highlights the dense mesh at the solid-fluid interface with inflation layer to capture the field of interest.

Table 3.4: Drag Coefficient (C_d) variation with number of Mesh element

Mesh element no.	Drag Coefficient (C_d)
1025953	0.2640
1183601	0.2691
1262075	0.2383
1380693	0.2649
1454076	0.2655
1584806	0.2670

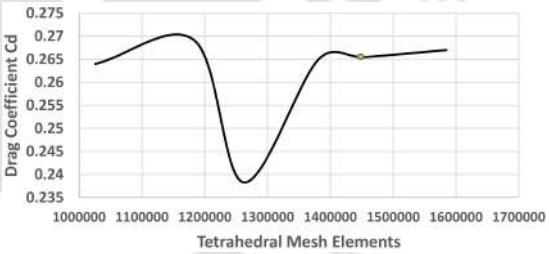

Figure 3.8: Grid independent test

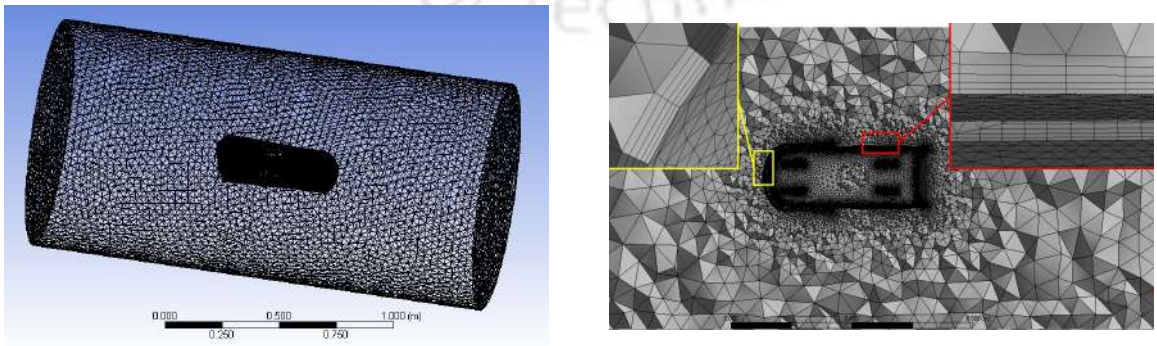

Figure 3.9: Meshed flow field

Simulation setup and boundary conditions

After the meshing, the domain is imported into the Fluent Solver. The flow around the UUV is turbulent in nature. It is evident from the Reynolds number ($R = uL/\nu$) calculation. Reynolds number is found to be more than $5x10^5$ with kinematic viscosity(ν) of water at 20^0C as $10^{-6}m^2/s$, characteristic length(L) as 0.56 m, and flow velocity(u) varying from 1 to 4 m/s. Hence, the standard k-ε turbulent model (He et al. [38], Yue et al. [39], Mitra et al. [71], Mansoorzadeh and Javanmard [103], Menter et al. [104]) is used to carry out the simulation. Near solid fluid interface, standard wall function is used with $y^+ \approx 50$. First layer thickness of Boundary layer grid (y) is calculated (Sharma and Sharma [160]) to be 3.1×10^{-4}m. In simulation setup the encloser boundary is selected with symmetry type, the inflow face is selected with velocity inlet and outflow face with pressure outlet type. The gauge pressure is selected as the total pressure at a water depth. Fig. 3.10 shows detailed boundary conditions.

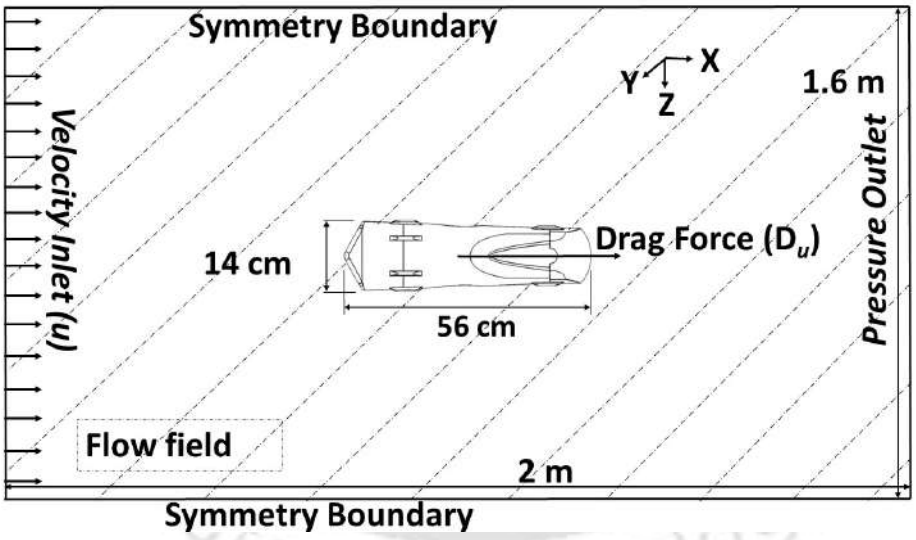

Figure 3.10: Boundary conditions and computational domain

Simulation is carried out at 50 m and 100 m depth with 2 m/s flow velocity and drag coefficient obtained as 0.260 and 0.263 respectively. There is a very small increase in the drag coefficient over depth. Furthermore, the robot will be mostly used in freshwater bodies such as lakes, rivers and dams. Thus for practical purpose the flow simulations are carried out at 50 m depth. The simulations are carried out with the water flowing past the static UUV at different velocities, which is equivalent to the UUV moving in static water. The objective of the simulations is to obtain the drag and lift forces developed on the UUV structure because of the flow

at different velocities. The solution is initialized with an inlet velocity and pressure at 50 m water depth. Here the velocity mentioned is the horizontal planar velocity along the length of the UUV. The velocity and pressure contour of a simulation carried out with 4 m/s inlet velocity and 50 m water depth is shown in Fig. 3.11 and Fig. 3.12.

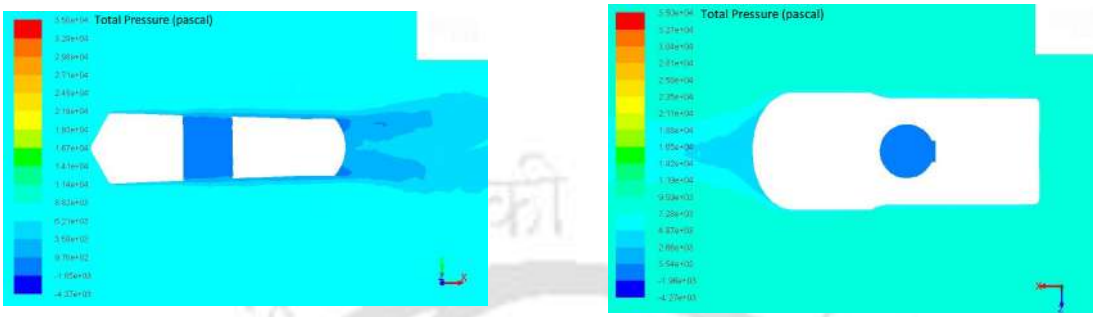

Figure 3.11: Pressure contour at 50 m water depth with 4 m/s inlet velocity

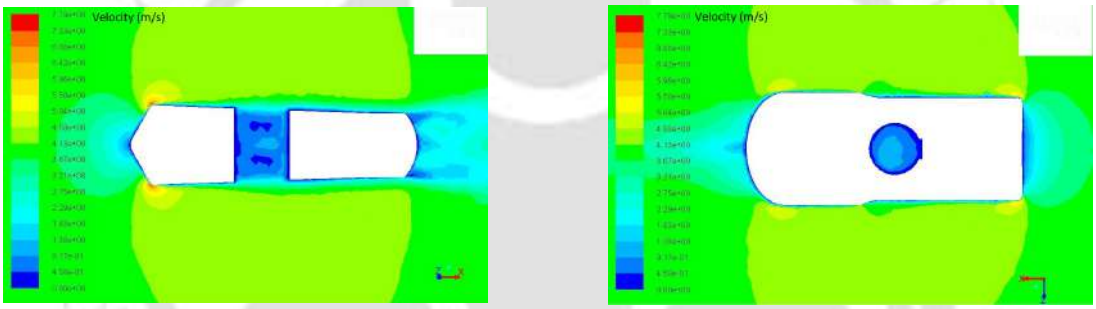

Figure 3.12: Velocity contour at 50 m water depth with 4 m/s inlet velocity

Required Thrust

Above mentioned simulations are carried out at different inlet velocities along the horizontal axis, i.e., along the length of the UUV, starting from 1 m/s to 4m/s in 0.5 m/s steps. Each simulation provided average drag and lift forces. Because of the symmetrical structure, the lift force is negligible and thus is neglected for this analysis. The average drag force obtained for different inlet velocities are mentioned in the Table 3.5.

Table 3.5: Drag at different flow velocity

Flow velocity (m/s)	Avg. Drag (N)
1.0	4.115
1.5	9.003
2.0	15.352
2.5	24.352
3.0	40.058
3.5	56.847
4.0	83.355

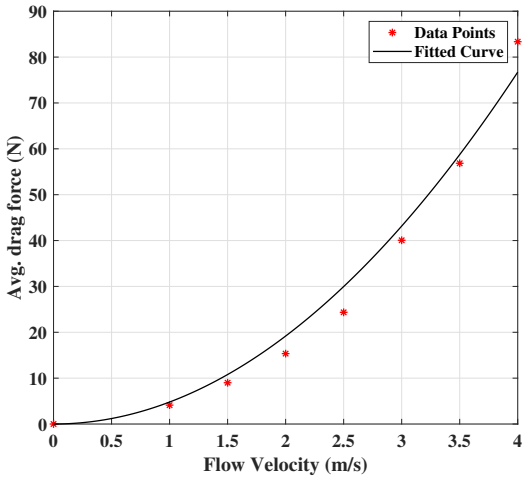

Figure 3.13: Drag vs Velocity

To determine an empirical relation between the drag force and the flow velocity, a quadratic curve (Fig. 3.13) is fitted using MATLAB^{TM} and the data in the Table 3.5.

From Fig. 3.13 the relationship between the drag and the velocity is found to be

$$D = 4.795u^2 + 1.16 \times 10^{-19}u \tag{3.1}$$

Here 'u' is the flow velocity in the horizontal plane, and 'D' Drag force developed.

The UUV has a symmetrical structure about the middle horizontal plain; therefore the lift force is negligible. The drag force is acting on the UUV structure because of the friction between the UUV and the fluid medium. The force generated by the two thrusters placed on the side of the UUV has to balance the drag force as well as supply the required thrust for the UUV to move. Using the empirical relation, for the UUV to move at a speed of 2 m/s in static water, the thrusters have to exert 19.18 N of force. The UUV to move at 2 m/s against a flow of 1.5 m/s, where the relative velocity is 3.5 m/s the thrusters have to exert 58.7 N of force. These forces will be the sum of the output of two thrusters; thus, an individual thruster should be able to exert a force of 10 N to 29.4 N for the above scenario. Thus for the UUV to be able to travel at 3.5 m/s in static water or 2 m/s upstream in a flow of 1.5 m/s, a thruster capable of exerting 30 N of force should be selected for the use.

Propulsion Systems

Three fixed position bi-directional thrusters are to be used for the propulsion of the UUV. One central thruster for vertical motion and two side thruster for planar motion in a horizontal plane. From the above analysis, thruster should be able to exert around 30 N of force. As per the requirements, commercially available T200 thrusters ([161] Fig. 3.14) from BlueRobotics are selected to be used. These thrusters can exert up to 34.8 N of force when running at 12 V and up to 50 N of force when running at 16 V. Specification of the thrusters are presented in the Table 3.6. Moreover, these thrusters are designed for marine robotics applications. Thus it can be used in various underwater environments such as oceans, lakes, and rivers. The T200 is made of high-strength, UV-resistant polycarbonate injection molded plastic. The core of the motor is sealed and protected with an epoxy coating, and it uses high-performance plastic bearings instead of steel bearings that rust in saltwater. It has an integrated ESC (Electronic Speed Controller) exposed to water, so the heating of ESC will not be an issue.

Table 3.6: Specification of the thruster BlueRobotics [161]

Max Thrust Forward @12V	34.8 N
Max Thrust Forward @16V	49.9 N
Max Thrust Reverse @12V	29.43 N
Max Thrust Reverse @16V	40.02 N
Min Thrust	0.1 N
Operating Voltage	6-20 volts
Max Power	180 Watts @12V
Weight in Air	422 g
Weight in Water	210 g

Figure 3.14: T200 thruster BlueRobotics [161]

3.2.4 Structural Analysis

Submersed UUV experiences stress because of the hydrostatic load due to the water column and hydrodynamic load because of its movement in underwater. If the UUV structure is not capable of withstanding these loads, then the structure will fail. Thus stress analysis is essential to ensure the structural rigidity of the UUV. The UUV is intended to be used for the underwater survey in the lakes, rivers, and oceans up to a depth of 50 to 100 m. Thus the UUV structure should maintain its structural rigidity at 100 m depth. As mentioned in the previous section, the wall thickness of the structure is 12mm.

Total pressure acting on the UUV is obtained from the flow simulations mentioned above by substituting the gauss pressure as the hydrostatic pressure at different depths varying from 50 m to 100 m and inlet velocity as 4 m/s. The pressure profile from the simulation is exported to the ANSYS^{TM} static structural module. FRP is selected as the UUV body material, and the simulation is carried out to obtain the maximum von Mises stress which is presented in the Table. 3.7. Maximum von Mises stress at 100 m depth is found to be 151.35 MPa, which gives a factor of safety of 1.84 compared to the 278 MPa limiting stress of the material. Thus theoretically, the UUV can maintain its structural rigidity at the maximum depth of 100 m though in rivers average depth is around 50 m. The simulation output, i.e., von Mises stress at 100 m, is presented in the Fig. 3.15. The deformation shown in the Table. 3.7 is the maximum localized elastic deformation. The used glass fiber composite material is linear elastic in nature. Thus localized deformation can be present under loading conditions, but as the von Mises stress developed is well below the ultimate stress, failure will not happen. Maximum deformation at 100 m depth of water is found to be 1.32 mm, which is observed in the middle part. This deformation is the flexing of the body sell which will come back to its original shape after the load is removed.

There will be a transparent acrylic flat plate rigidly fixed to the front face of the UUV. The plate will be subjected to hydrostatic pressure due to water depth and hydrodynamic pressure due to UUV motion from the outside and one atmospheric pressure from inside. Static structural analysis has been carried out to understand the structural rigidity of the plate. Total pressure from the flow simulation at 100 m depth at 4m/s flow is subjected to the outer face, one atmospheric pressure to the inner face, and the side faced are fixed for the simulation. The maximum stress developed is 29 MPa 2.6 times less than the limiting stress (75 MPa) of the acrylic. Thus, the transparent panel won't fail at 100 m depth. It may be noted that the UUV structure is divided into three parts. Stress analysis has been carried out for these parts separately. The Joint holes are fixed and 1081325 Pa pressure is applied on the outer faces. Also, similar analysis has been carried out considering the assembled structure (Fig.3.21). As shown in the Figs. 3.18,3.19,3.20 maximum von-Mises stress developed for the sections at 100 m depth is below 151 MPa, which is 1.8 times less than the ultimate stress of the material. Thus the UUV

structure will be able to withstand the water pressure at 100 m depth.

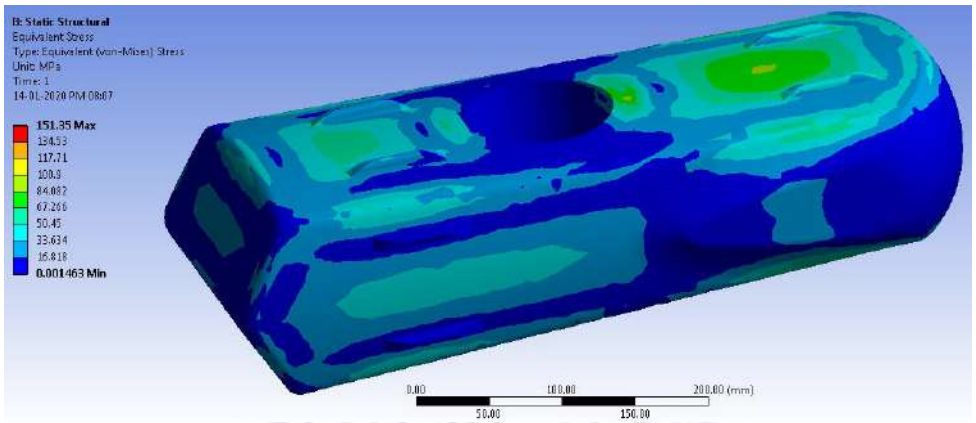

Figure 3.15: von Mises stress at 100 m depth

Table 3.7: Estimated stress and deformation at different depth

Depth (m)	Max Deformation (mm)	Eq von Mises stress (MPa)	FoS
50	0.72	82.60	3.36
60	0.84	96.35	2.88
70	0.96	110.10	2.52
80	1.08	123.85	2.24
90	1.20	137.60	2.02
100	1.32	151.35	1.84

Table 3.8: Maximum total pressure on the transparent panel

Depth (m)	Total Pressure (MPa)
50	0.612
100	1.116

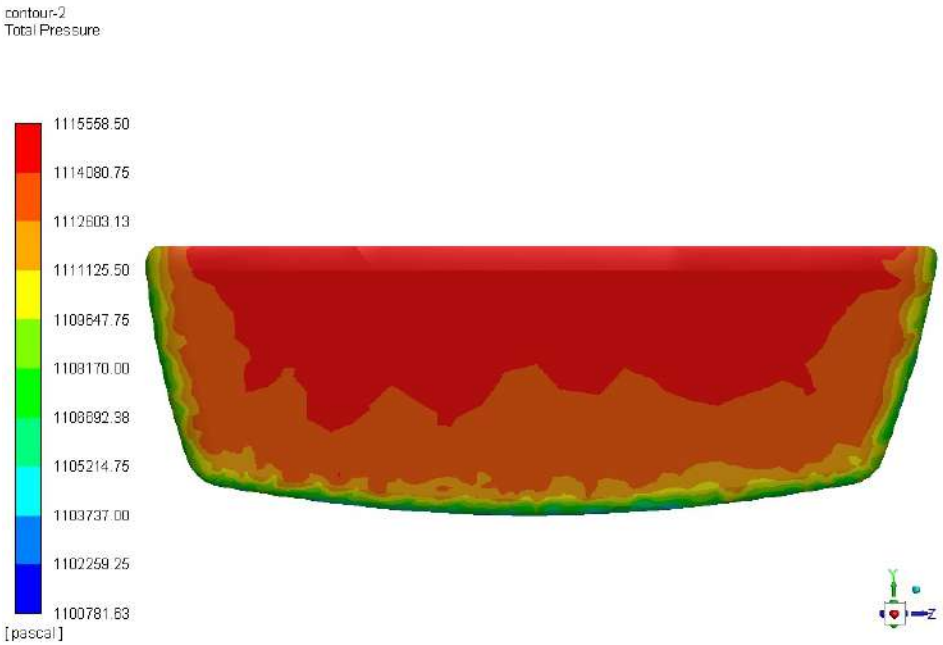

Figure 3.16: Total pressure at 100 m depth

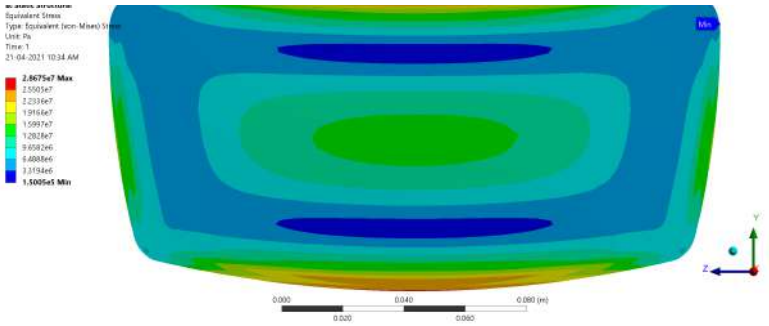

Figure 3.17: von Mises stress at 100 m depth

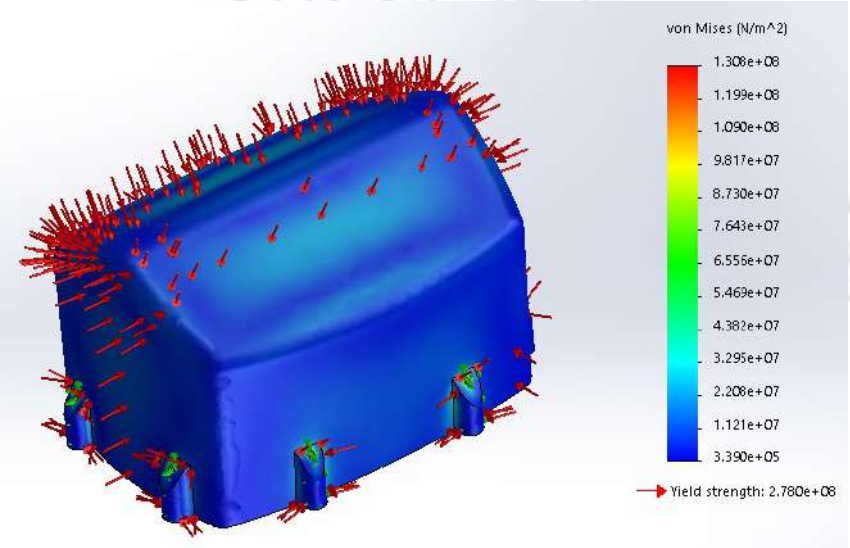

Figure 3.18: von Mises stress at 100 m depth of the front part

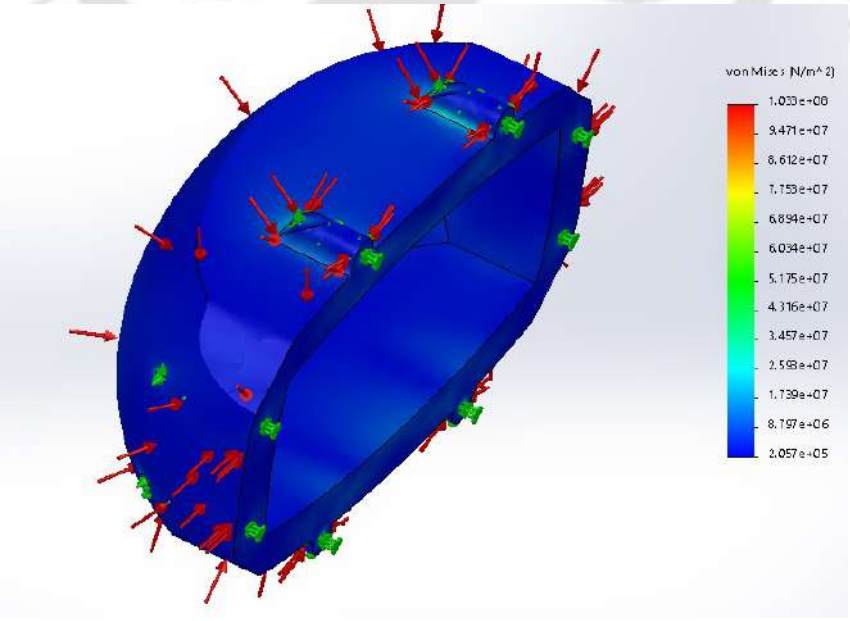

Figure 3.19: von Mises stress at 100 m depth of the end part

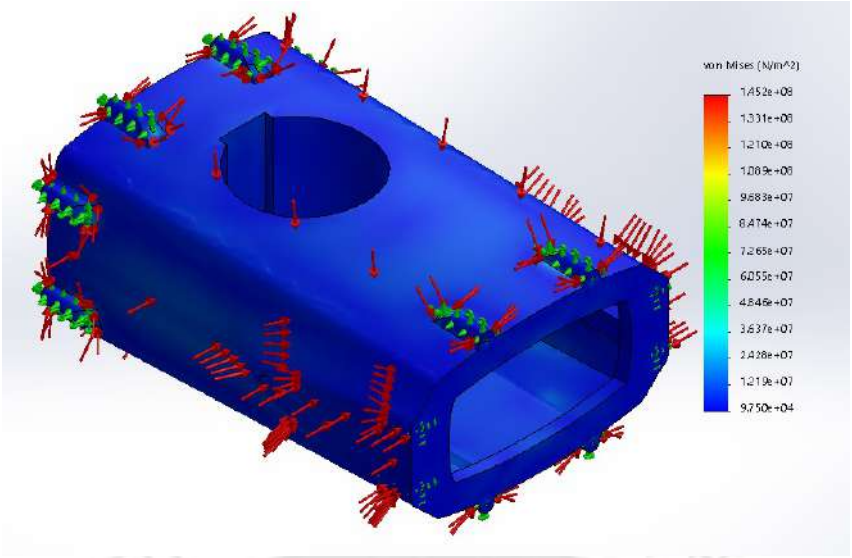

Figure 3.20: von Mises stress at 100 m depth of the middle part

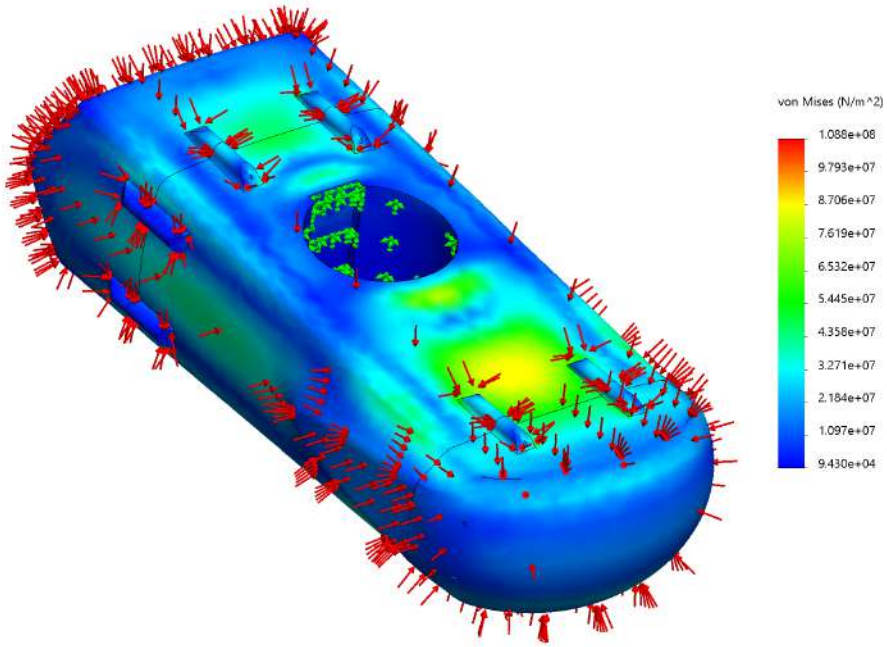

Figure 3.21: von Mises stress at 100 m depth of the assembled body

3.2.5 Final Design

A water displacement model (Fig. 3.22) of the UUV is developed to determine the buoyancy characteristics. The C.B., i.e., the C.G. of the water displacement model, is obtained from this. This water model is developed by creating an all solid model identical to the designed UUV and selecting the material as water. C.B. is found to be at (-1.67, 0, 0) cm from the origin along the

X, Y, Z axis. The center of the central hole in the middle plain is considered as the origin. The weight of this model gives the buoyant force, which was found to be 12.1 kg. For the UUV to be neutrally buoyant, the buoyant force and the weight should be equal. Therefore four balancing blocks are added inside the UUV to balance the buoyant force and help maintain the C.G. of the UUV to lie on the vertical line passing through the C.B.

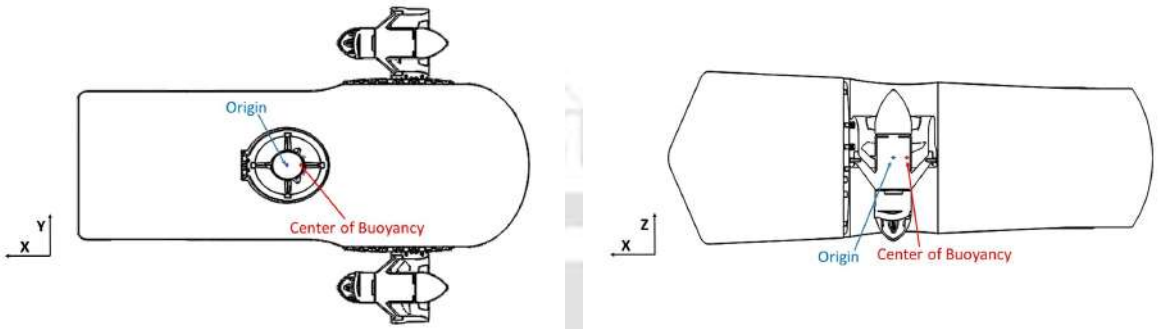

Figure 3.22: section view of water model

The hull is divided into three parts, as shown in the Fig. 3.23, keeping in mind the ease of accessibility of internal components and ease of manufacturing and assembly. The front section houses the camera module and front balancing block. The mid-section houses the battery, thrusters, power distribution board, and raspberry pi. The central thruster is to be placed in the pass-through hole in this section. The sensor housing and communication module are to be placed in the tail section. Each section is to be assembled with screw joints with silicon rubber gaskets in between to form a watertight joint. The gaskets rest on the protruding surface from the midsection on both sides, and front and tail sections will be fitted onto it. The UUV body surrounds the gasket from three sides, and the other side is exposed to the surrounding. When screwed under pressure, it will create a watertight joint. This Modular structure provides accessibility of internal components for easy repair, up-gradations, and modification. Modular structure will be versatile for various mission objectives as modules or sections with different sensor sets can be interchanged for different missions. For example, the UUV can be used for autonomous operations by interchanging the tail section, which will have a different communication module and antenna instead of a tether connection and a control module as per requirement.

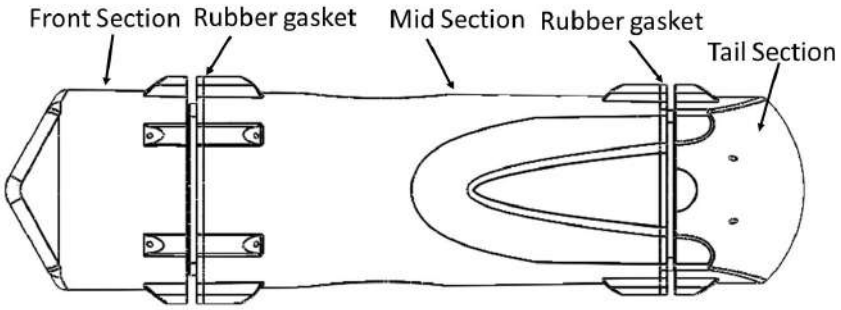

Figure 3.23: Three-part modular structure

As mentioned above the UUV is 55 cm long and 43 cm wide. A detailed CAD model is presented in the Fig. 3.24. The main objective was to develop a compact underwater system for shallow water application with an affordable price tag. The use of composite material reduces the cost involved in manufacturing and leads to a lighter body. A structure with an elliptical cross-section is designed, instead of a conventional cylindrical body, to reduce the buoyancy. The design kept in the view for space for the internal components and maintained C.G. close to the central thruster position. Dimensions of the cross-section were decided based on the dimensions of the central thruster, battery, and camera setup and further optimized for the minimum drag coefficient. The flat front surfaces are kept at an angle to avoid using a transparent hemispherical structure and reduce the cost. Slanting the surfaces from front to bottom will help in reducing drag. Thus, the resultant shape is the result of a design process with a major focus on cost reduction and manufacturing simplicity. The stability study of the proposed design is presented in the following section.

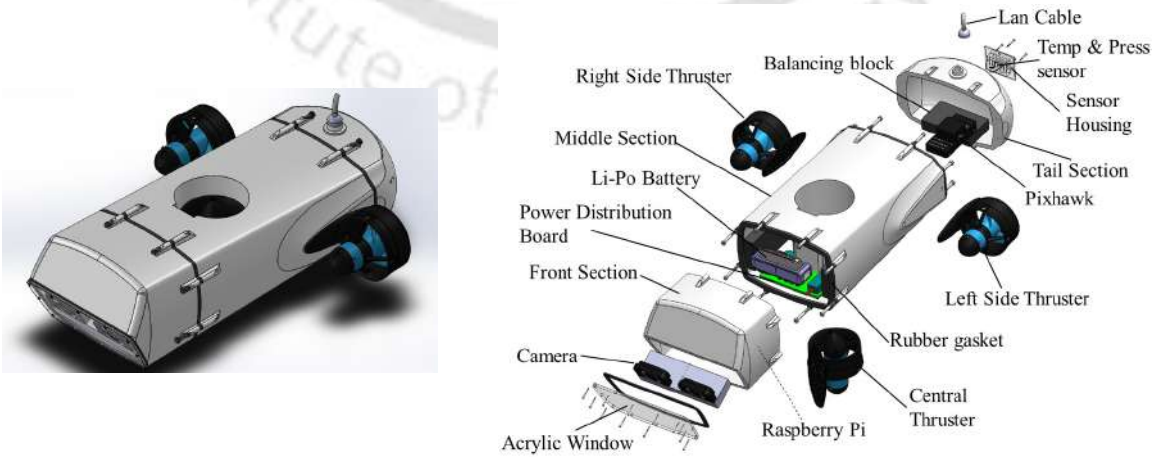

Figure 3.24: Detailed UUV CAD model

3.2.6 Stability Analysis

From the CAD model, it is observed that the UUV displaces 12.1 kg of water. The C.B. is found to be at (-1.67, 0, 0) cm from the origin along the X, Y, Z axis. Four cast-iron balancing blocks are added to the model to balance the buoyant force and keep the C.G. in the same vertical line as the C.B. to avoid any unbalancing torque. After adjusting the balancing block dimensions and positions, the C.G. of the whole model is at (-1.67, 0, -0.97) cm from the origin along the X, Y, Z axis, as shown in Fig. 3.7. A comparison of the position of the C.G. and the C.B. along with the origin is shown in the Fig. 3.25. As the C.G. and C.B. are aligned along the same vertical line, there is no unbalancing torque. During the submerged condition, the weight and the buoyant force cancel each other, so no unbalance force in the vertical direction. The position of C.G. 0.97 cm below the C.B. provides better roll-over stability. The origin of the ROV coincides with the central thruster. Therefore the vertical thrust will act at the origin, which is 1.67 cm away from the C.G. Thus, low vertical speed will have a low pitch, and high vertical speed will have high pitch motion, as shown in the Fig. 3.26. For general use with low vertical speed the pitch motion is negligible. If required with high speed, this pitch motion can help better maneuverability and the ability to have a more complex motion with only three thrusters. This is to be noted that this pitch motion is the consequence of the distance between the C.G. of the UUV and central thruster and cannot be actively controlled.

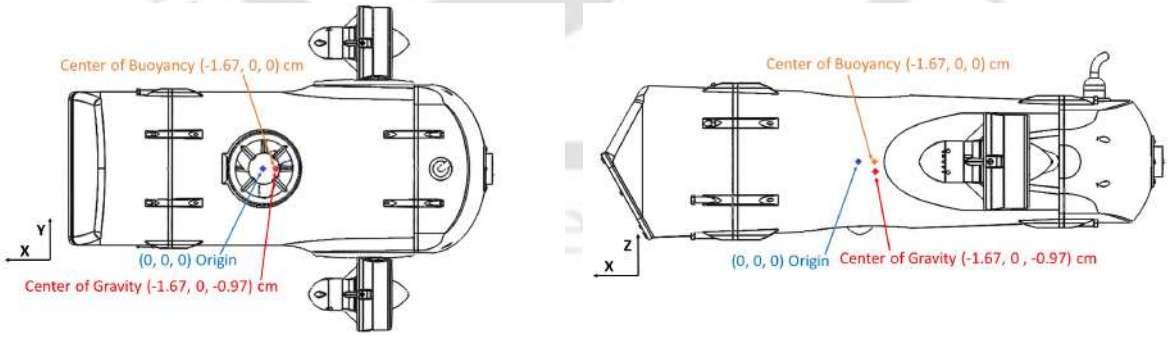

Figure 3.25: Origin, C.G. and Centre of buoyancy position

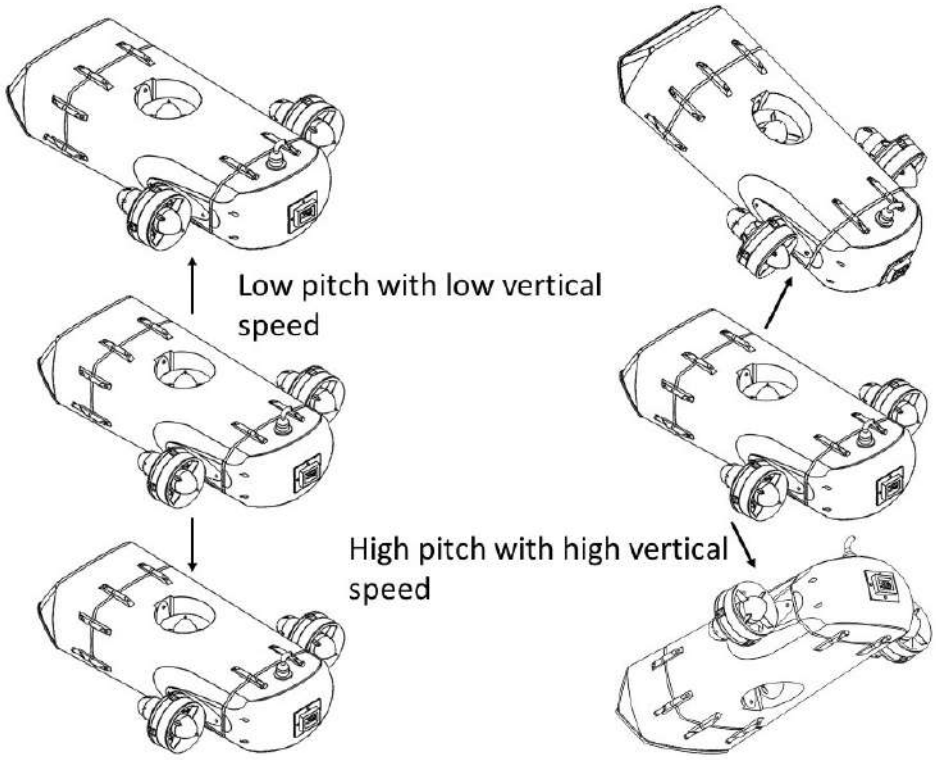

Figure 3.26: Pitch motion

3.3 UUV Development

After the design analysis, the UUV is manufactured. GFRP is used for the UUV structure to reduce the cost and complexity of manufacturing associated with traditional materials. The UUV body is manufactured in parts using the hand molding technique with simple tools.

3.3.1 UUV body manufacturing

Manufacturing of the UUV started with the development of a real-size thermocol replica of the CAD model. For this purpose, a hot wire cutting setup is developed as shown in Fig. 3.27. The templates from the cad model are pasted on the thermocol blocks, and using the hot wire cutting setup and using sandpaper, required shapes are obtained. As the UUV is developed in parts, the thermocol models are also produced in parts. For ease of manufacturing, the mid-section is further divided into two parts. These thermocol models are reinforced with glue and cotton clothes. The detailed manufacturing process is presented in the flow diagram (Fig. 3.28).

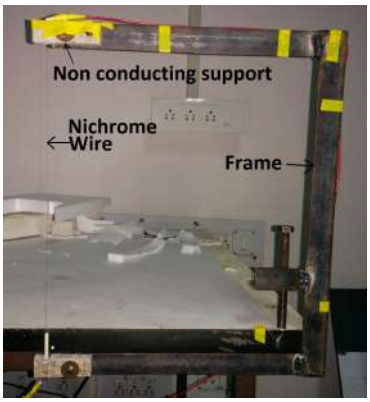

Figure 3.27: Hot wire cutting setup

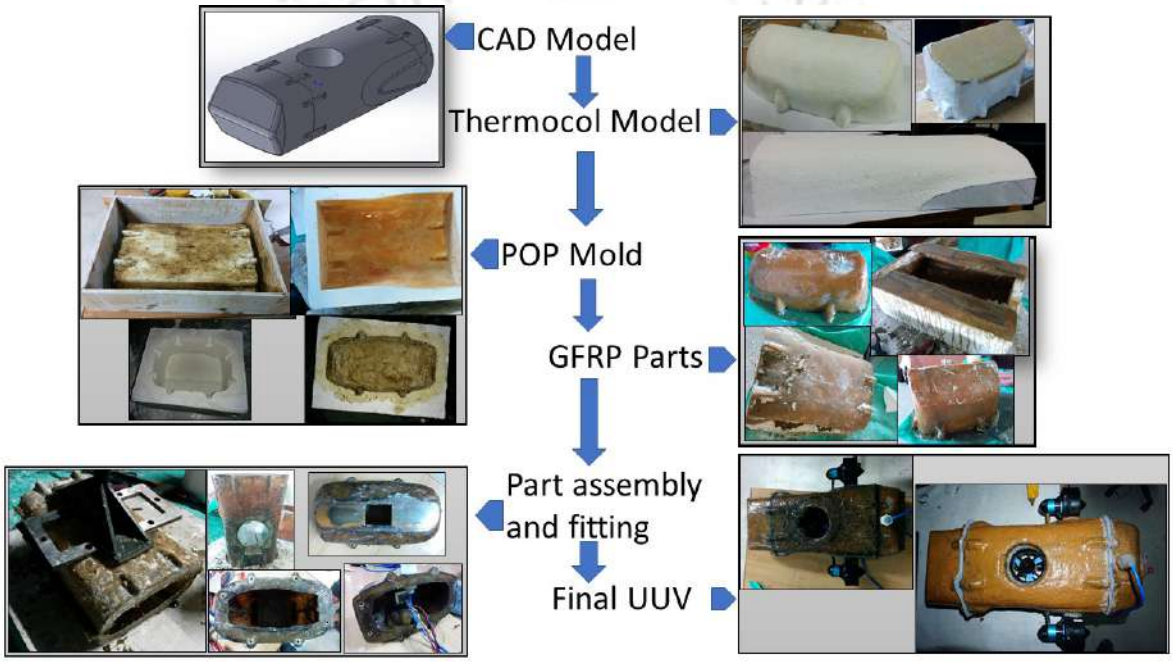

Figure 3.28: Flow diagram of UUV manufacturing process

Using the thermocol models and wooden boxes, Plaster Of Paris (POP) molds have been prepared for each part. POP molds are left to dry for 24 hours. After the molds are ready, one layer of grease and two layers of gel-coat are applied to the molds. A layer of gel-coat on top of glass fiber and matrix would give the structure its water-resistant properties. Then for each part, two layers of random and one layer of 90^0 woven glass fiber sheets along with the matrix are applied. Matrix is a chemical solution of three chemicals epoxy-based vinyl ester resin, cobalt naphthenate as the initiator, methyl ethyl ketone peroxide as curing agent, mixed with 100:1:5 ratio by volume, respectively. After curing, the matrix solution becomes hard plastic, and the glass fiber enforces to give it strength. Then the parts are allowed to dry for 24 hours.

After the parts are dried and ready, the parts are removed from the molds. Then two parts of the mid-section are joined. Then the three distinct sections are ready for further assembly.

3.3.2 Assembly

The three sections are to be joined with screw joints. First, the surfaces to be joined are leveled. Holes are drilled by aligning the parts for the passage of the screw. Nuts with washers are embedded in the body itself to create better joint pressure and a watertight joint. Silicon rubber gaskets are made for the joints. Then the thrusters are mounted on the midsection. Two side thrusters are mounted on the planes on the side of the body. For the central thruster, a pass-through cylindrical hole was created. After mounting the thrusters, passages for the cables are appropriately sealed. During manufacturing in the locations for holes and passages, cut-outs were made in the fiber layers. Later drilling was done for cleaner passage without damaging the fiber layers. To further strengthen the cut-outs, fiber layers are added to the edge of the holes. On the front section, a transparent acrylic sheet is mounted in front of the camera mount.

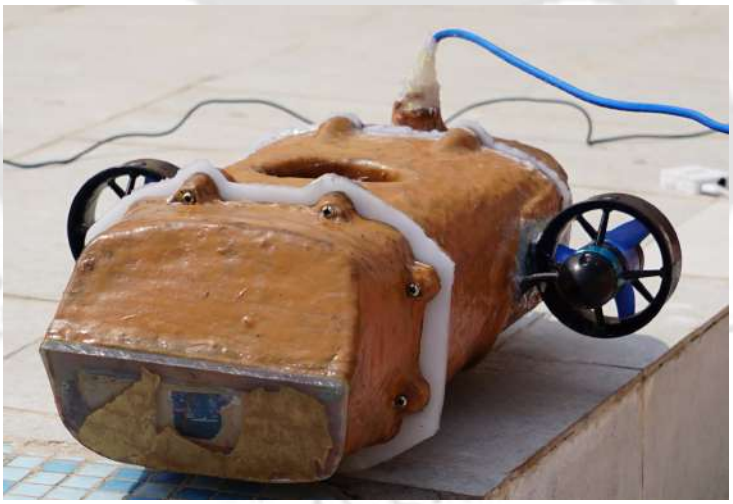

Figure 3.29: Assembled UUV

3.3.3 Sensor integration

For UUVs, sensors are essential as they will be used for exploration and survey to collect underwater footage and scientific information such as temperature, pressure, etc. Initially, only temperature, pressure sensor, and camera setup (Fig. 3.31) are used. Pressure data can be used to

estimate the depth of the UUV from the water surface. The pressure sensor used has a resolution of 0.2 mbar or a depth resolution of 2mm and can work up to a depth of 300 m underwater. The temperature sensor used has an accuracy of $\pm 0.1^0$C and can work up to a depth of 975 m. These sensors had to be exposed to the external water and also connected to the internal components. A sensor housing is developed using thick acrylic sheets, silicone gel, and marine epoxy have been used to make it watertight. The sensor housing is mounted to the tail section. The camera setup is placed in the front section behind the transparent acrylic window.

Figure 3.30: Sensor housing

Figure 3.31: Camera

3.3.4 Control and communication system

The UUV must be in constant communication with the remote station when operated as ROV to be controlled by an operator. The communication channel helps to transmit the live underwater footage, sensor data, and control signals. Inside the UUV, a single-board computer Raspberry Pi is used to manage all the electronics components. Raspberry Pi is connected to a computer in the control station by LAN cable after going through a network booster. Open-Source companion computer platform in the raspberry-pi helps collect the sensor data and live underwater footage, transmit to the computer at the other end, and interpret and communicate the received control signal to the Pixhawk controller for thruster operation. Pixhawk controller, connected to the raspberry pi, is the brain of the UUV and controls the robot motion. Pixhawk has an open-source software “Ardusub,” which is capable of ROV and AUV operations such as manual, stability and depth hold control, obstacle avoidance by sonar, and trajectory tracking with an acoustic positioning system. The thrusters and sensors are connected to the Pixhawk. In the case of ROV, Pixhawk controls the thrusters as per the signal received from the operator. Whereas, in the case of AUV, the Pixhawk controls the thrusters depending on the control

algorithms and sensor input. Single board Raspberry Pi computer and Pixhawk controller is capable of handling ROV and basic AUV operations such as predefined trajectory tracking but will fall short for full autonomy in the dynamic environment. A more capable system, such as "Nvidia Jetson nano," flow, and other sensor upgradations will be essential for full autonomy. The computer in the control station uses an open-source software called "Q Ground Control." The software displays the sensor data, live footage and also interprets and maps the keypress in the controller to predefined signals and transmit to the Raspberry Pi.

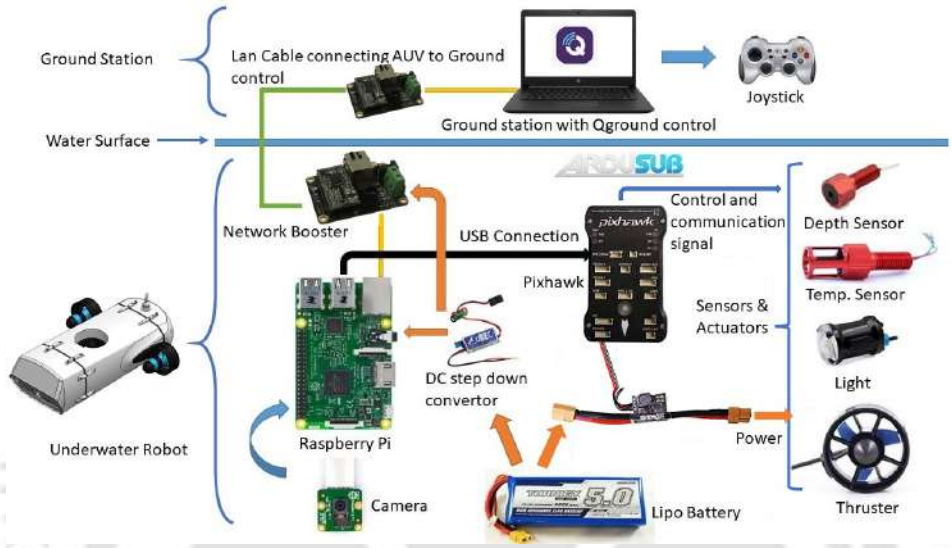

Figure 3.32: Internal connection layout

3.3.5 Power distribution

Two 5500 mAh lithium polymer(Li-Po) battery batteries are used as the power source for the UUV. A power distribution board (Fig. 3.33) has been developed to manage connections from the battery to the electronic components. To avoid the inconvenience of disassembly and assembly of the UUV for recharging of the batteries, a three-way switch and a charging connection are placed in the sensor housing (Fig. 3.30), which facilitates external balanced charging of the Li-Po batteries. The charging port is embedded in the sensor housing and sealed. The switch helps select the connection of the battery to the charging port, power distribution board, or no connection. The power distribution board passes power to the thrusters and light. The raspberry pi works on 5 Volts; thus a dc-dc step-down buck converter is used to convert the 12 volts from the battery to 5 Volts. The power consumptions of different electronic components

are presented in the Table. 3.9.

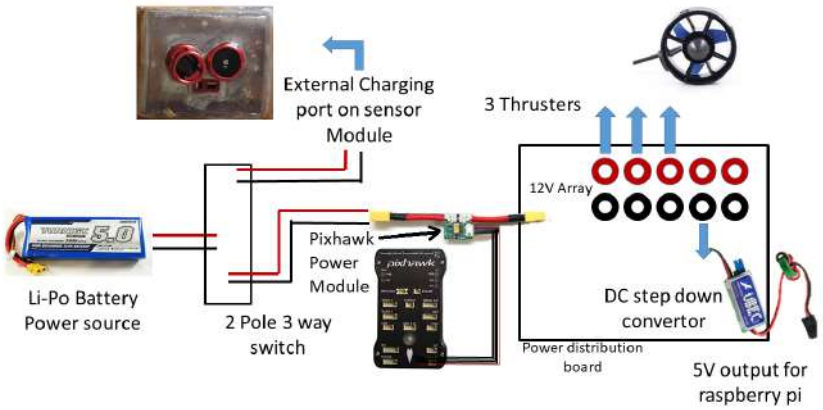

Figure 3.33: Power distribution setup

Table 3.9: Power rating of electronic components

Component	Max Power	Average power
Raspberry Pi	12.5 Watts	8 Watts
Pixhawk	2.5 Watts	2 Watts
Communication module	3 Watts	2 Watts
Side thruster	180 Watts	100 Watts
Central thruster	180 Watts	50 Watts

From the Table. 3.9 average power consumption of the UUV is around 262 Watts. With two 5500 mAh batteries, the UUV can operate from 30 minutes to 1 hour, depending on use. The UUV is assembled with all the mechanical and electronic components. Cost analysis of the UUV is discussed in the following section.

3.3.6 Cost analysis

The objective is to develop an affordable, compact underwater robot, which can be helpful for educational institutes, small-scale industries, environmentalists, marine biologists, etc. Table. 3.10 presents the development cost associated with the UUV with the cost of different components. Thrusters are one of the significant costs associated with the compact UUV; thus, a minimum number of thrusters are used. The use of open-source software, non-traditional material, and manufacturing techniques help maintain a low cost of the UUV. This is a prototype, and the cost can be further reduced. 1500 USD, which is just above 1 lakh INR, is an affordable price range for an underwater robot. The cost of the system can be further reduced with

mass manufacturing. “BlueROV2” from BlueRobotics is a popular high-performance compact ROV with a starting price of around 3000 USD. It has two thrusters for vertical motion and four thrusters for horizontal movement, thus having superior motion control. BlueROV2 is rated for 100 m depth and has an open frame structure. This ROV is suitable for variable payload sensor integration and expansion, depending on the application. Though BlueROV2 is a high-performance system with the price on the higher side. “GLADIUS MINI” is one of the affordable ROV systems costing around 1200 USD. But with logistics and customs, it will be an expensive option. This is a compact close-frame system rated for 100 m depth. But the system is just to be used for video footage collection not suitable for scientific research as custom payload and expansion capability is not there. Hopefully, the developed UUV with an affordable price tag and further sensor integration capability and modular structure for easy repair and mission versatility may attract small-scale industries, researchers, and communities to use it for various applications and their benefit.

Table 3.10: Component price

Component	Price (USD)	Price (INR)
Thrusters	670	50,250
UUV Body	180	13,500
Rapberry Pi	56	4,200
Pixhawk	42	3,150
Camera	56	4,200
Temperature sensor	85	6,375
Pressure sensor	104	7,800
Cable	200	15,000
Miscellaneous	57	4,275
Total	1500	1,12,500

3.3.7 Motion mechanism

The UUV has three fixed position bidirectional thrusters for motion. Among these three thrusters, two are placed in the side for horizontal motion and one in the middle for vertical motion. The central thruster is not exactly placed at the C.G. of the UUV and has an offset of 1.67 cm (Fig. 3.25). Thus, a pitch motion can be developed using a single vertical thruster with a high thrust, as shown in Fig. 3.26. The absence of thrusters for lateral movement makes the system under-actuated and four degrees of freedom system considering the pitch motion. As the

thrusters are fixed with the UUV body, the robot is a single rigid link manipulator. All motion directions are presented in the Fig. 3.34, 3.35. Using the three thrusters, the UUV can travel in the 3d underwater space with ease. The UUV can rotate about a point using side thrusters in opposite directions thus, has a very low turning radius which is helpful in narrow terrains. The UUV can also be used in curved paths with a large turning radius using side thrusters in the same direction with varying thrusts.

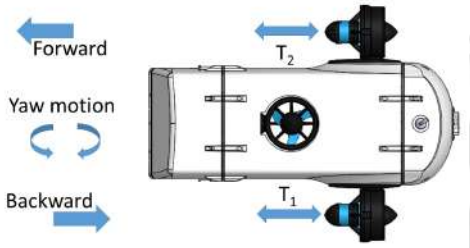

Figure 3.34: Motion in the horizontal plane

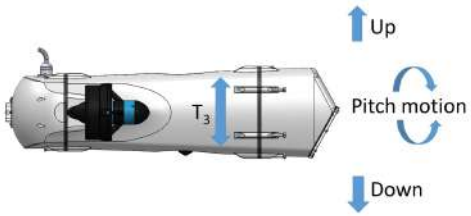

Figure 3.35: Motion in the vertical plane

3.4 Testing

After manufacturing the UUV structure and assembly of the desired components, a few tests have been carried out to ensure the working of the UUV.

3.4.1 Water leakage and Neutral buoyancy test

The structure needs to be watertight to avoid any water leakage. Special care has been taken to ensure no water leakage. During manufacturing, all the ports have been adequately sealed. In the joints, soft silicon rubber with vacuum grease and high joint pressure has been used. Each part has been checked for no water leakage. After assembly, the model has been placed inside a water drum for 24 hours to ensure watertight joints.

The structure floats when the model is deployed in water without the balancing blocks (Fig. 3.36). Then the required weight is found out and added in the form of cast iron balancing blocks surrounding the C.G. in predefined positions until the UUV is fully submersed (Fig. 3.37). The balancing blocks are a combination of multiple units of the same cross-section. Thus, these blocks can be removed during future component up-gradations as per requirement.

Few of these units can be removed, maintaining the C.G. to make the UUV positively buoyant as overall weight will decrease. Positively buoyant structure will come back to the surface in case of power failure thus making recovery easy. The UUV was coming back to a few cms below the water surface when the thrusters are turned off. The network cable used is not a neutrally buoyant cable causing this effect. Later the cable is upgraded to a neutral buoyant one making the whole system neutrally buoyant. Details of the balancing blocks are presented in table 3.11. After adding the balancing blocks, the net weight of the UUV is found to be 13.6 kg, 1.5 kg more than the designed model. But the weight of the balancing block had to decrease as the model weight is more than the design weight, and some internal components such as wires are not considered during design.

Table 3.11: Balancing blocks

Object	Designed		Final	
	Weight (kg)	Dimensions (cm × cm × cm)	Weight (kg)	Dimensions (cm × cm × cm)
Front Balancing block	1.123	13 × 6 × 2	0.950	11 × 6 × 2
Tail Balancing block	0.864	10 × 6 × 2	0.600	7 × 6 × 2
Middle Balancing block	2.246	26 × 6 × 2	2.246	26 × 6 × 2

Figure 3.36: Floating UUV

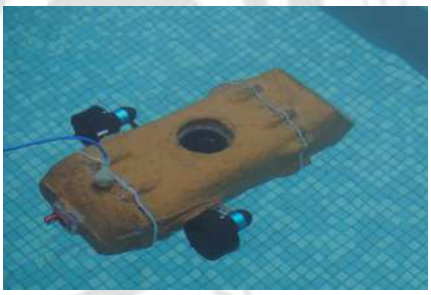

Figure 3.37: Fully submersed UUV

3.4.2 Field test

An initial field test is conducted in the swimming pool. The "Q Ground Control" software is used for live temperature, pressure data, and video footage monitoring, as shown in the Fig. 3.38, which is the screen shot of the topside computer running Q Ground Control. The Q Ground Control software has recording option to record the live footage transmitted from the camera inside the UUV. The hand controller is connected to the laptop, and using the controller, UUV can travel forward, backward and make the left and right turn. The UUV travel

speed could also be changed using the controller. Figure. 3.39 presents the UUV moving in the underwater space. The footage is recorded by a separate underwater camera placed inside the swimming pool.

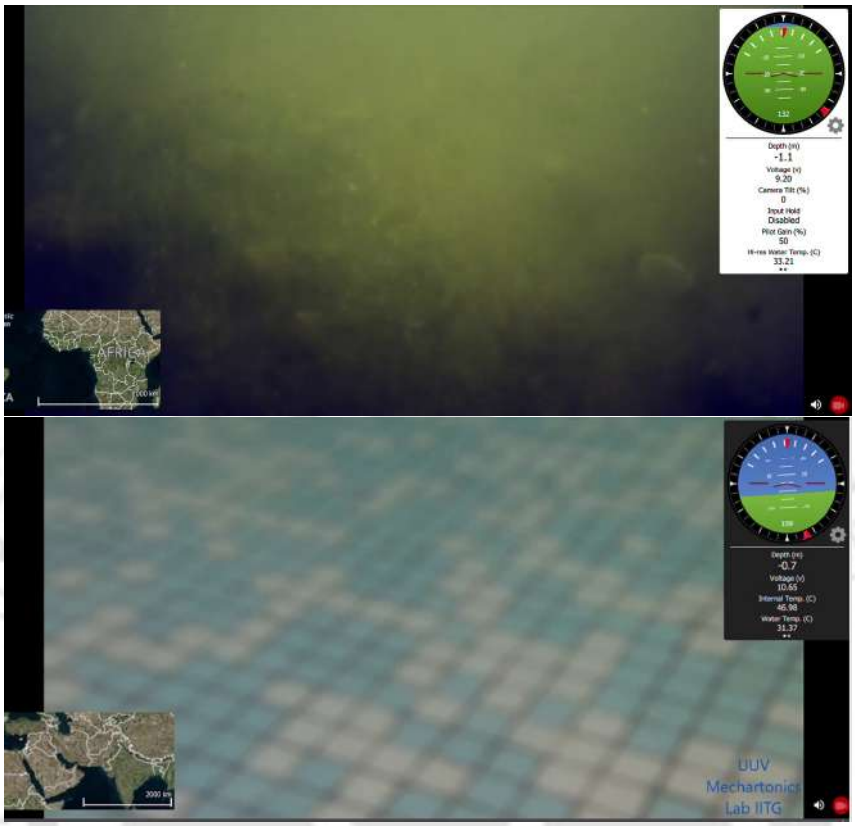

Figure 3.38: Live video and sensor data on ground station

Figure 3.39: UUV moving in the underwater environment

After multiple successful runs in the swimming pool, the UUV is ready for the field test in rivers and lakes. To verify the robustness of the UUV, multiple runs are carried out in lakes and rivers without any failure (shown in Fig. 3.40, 3.41). The Pixhawk in the UUV obtains the velocity data from the integrated IMU, and depth sensor data, using extended Kalman filter (EKF). 3D velocity magnitude vs. time of test runs in lake and river are presented in the Fig. 3.42 and 3.43, respectively. During the river test, the flow speed of the water is registered to be 2.6 m/s, and the UUV is able to move upstream against the flow (Fig. 3.41). Still, it is challenging to maintain the motion direction with manual operation. The depth achieved during this test is 5m. It is difficult to control the UUV motion direction in the river during rainy seasons with a flow speed more than 2 m/s. Control algorithms and flow sensors need to be used for proper control. UUV can be operated easily in manual mode during other seasons when flow speed is around 1 m/s at maximum. The velocity data shows that the UUV can achieve around 4 m/s in still water. Velocity magnitude is less in the flowing river as the UUV has to move against the flow. Figure. 3.44 presents the depth of the UUV during operation in depth hold mode. Here the UUV maintains a depth of 1.1 m and comes back to the preset depth after disturbance from an external force. Figure. 3.45 presents voltage drop with time during a field test in a lake. Here the battery voltage drops from 11.6 V to 10.8 V, which is 80% to around 20% capacity of

a single battery during 30 min run. During testing, the UUV operates approximately 45 mins with a single battery; thus, the system with two 5500 mAh Li-Po batteries can work for around 90 mins. The system is also deployed in a river dam (Fig. 3.46) and the depth achieved during this test is around 18m (Fig. 3.47). A temperature profile study was carried out during this test to find the temperature variation with water depth (Fig. 3.48).

Figure 3.40: Field test in a lake

Figure 3.41: Field test in a river

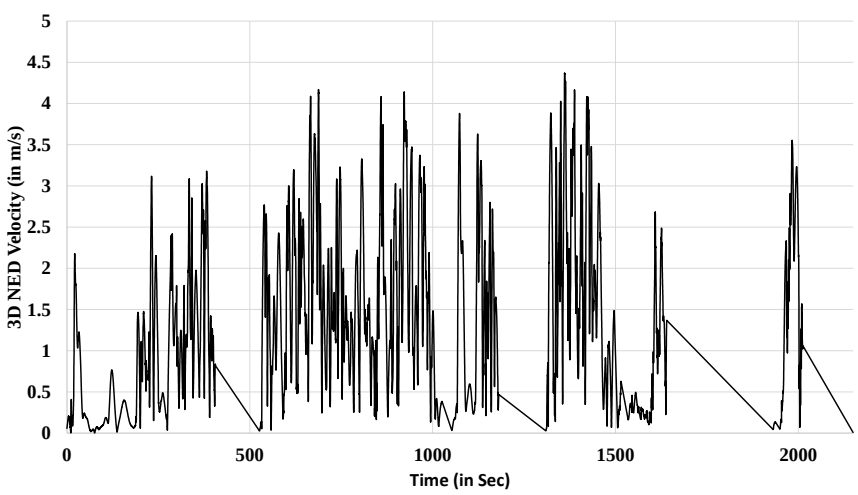

Figure 3.42: 3D velocity with time from lake test

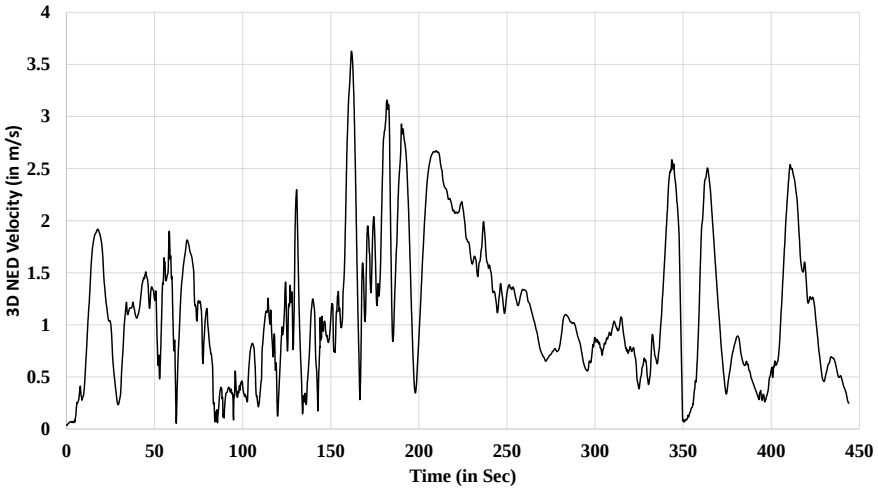

Figure 3.43: 3D velocity with time from river test

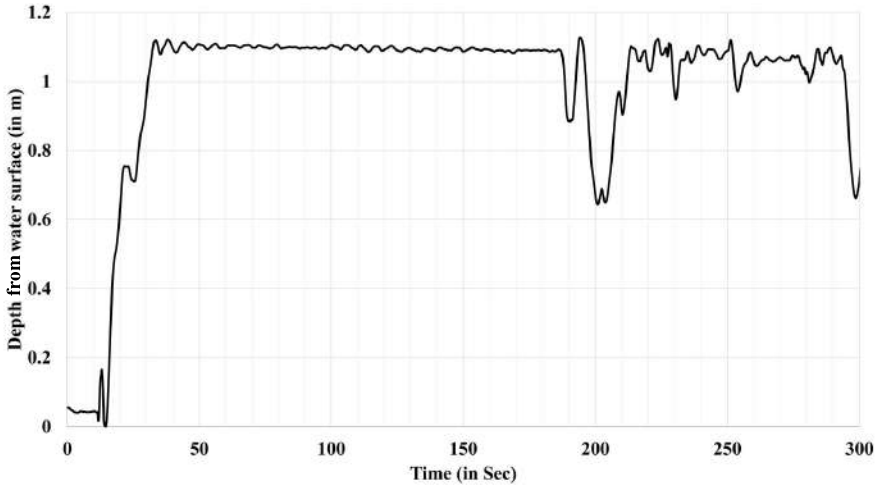

Figure 3.44: Depth in depth hold mode

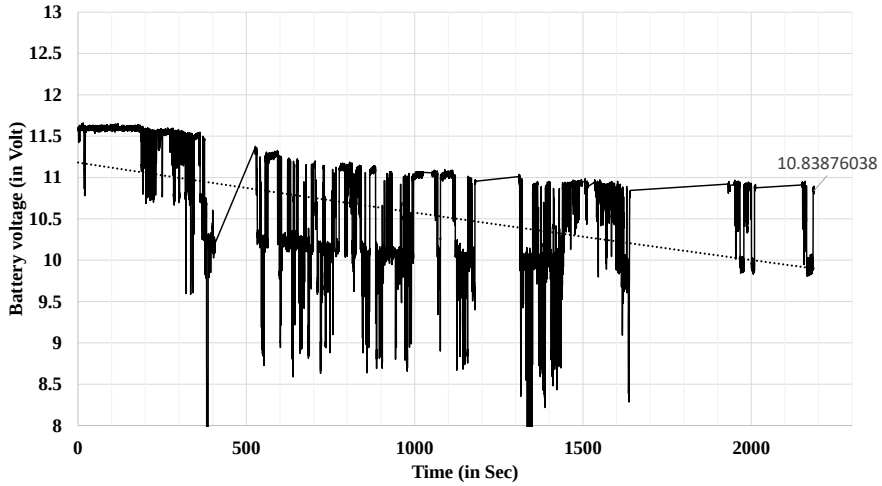

Figure 3.45: Battery voltage drop with time

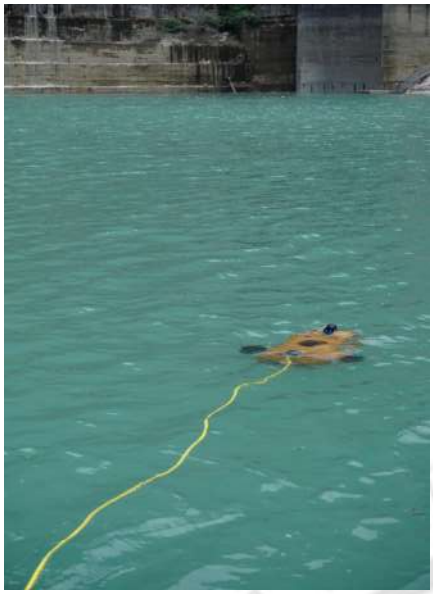

Figure 3.46: Field test in a dam

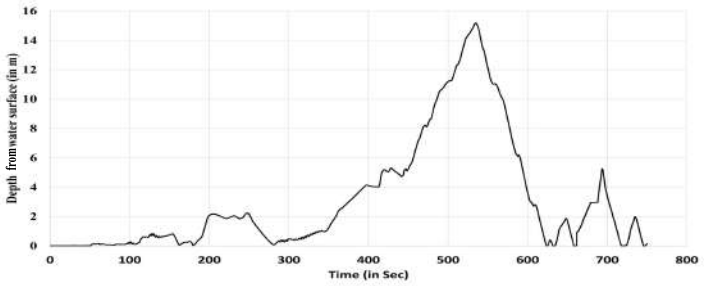

Figure 3.47: Depth with time

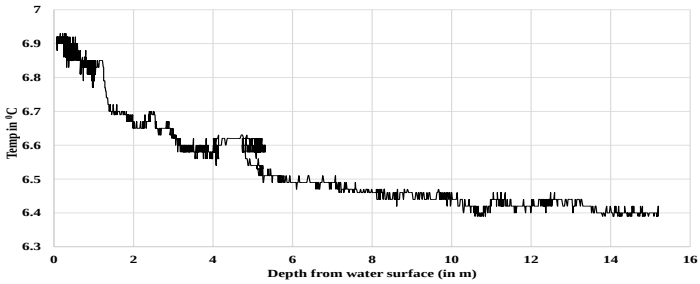

Figure 3.48: Temperature variation with depth

3.5 Summary

The design and development of an affordable, compact underwater robotic system is presented in this chapter. First different system requirements are identified based on the final application of the UUV. Different internal components are selected and their optimal position is determined with a linear optimization search for clash-free placement maintaining over all C.G close to the central thruster. A optimal side section is developed with parametric fluid flow study with ANSYS FLUENT^{TM}. Then using CAD modeling software SOLIDWORKS^{TM} a compact, closed frame, neutrally buoyant and three-part modular structure has been developed. The UUV design is numerically analyzed for performance and structural rigidity. First, the hydrodynamic study is carried out using the CFD software ANSYS FLUENT^{TM} to find out the drag experienced by the UUV during its motion. According to the simulation results, the thrusters are selected for the vehicle to achieve 2 m/s speed. The FEM analysis carried out to find the stress developed at different water depths showed that the UUV structure could withstand underwater pressure up to 100 m depth with factor of safety 1.84. Stability analysis has been carried out to ensure roll-over stability. After validating the UUV design, the structure was manufactured in parts using GFRP. GFRP gave the UUV its strength and corrosive resis-

tant properties with lightweight and reduced the manufacturing cost. Three parts of the structure are manufactured, fitted with different components, and assembled together to make the UUV. The UUV houses rechargeable Li-Po batteries as the power source, pressure and temperature sensors, camera setup for live underwater footage, raspberry pi and pixhawk for control, three thrusters for propulsion, balancing blocks for neutral buoyancy, and other electronic and mechanical components. The UUV has been tested for water leakage, neutral buoyancy and static stability. Successful testing of the UUV in the swimming pool, lake and the river demonstrated that the UUV could be used for live monitoring and exploration. The UUV could be controlled from the ground using a laptop and controller where the laptop displaying the live sensor data and underwater footage is connected to the UUV using a LAN cable. Such an affordable compact UUV can be a useful tool for small-scale industries, environmentalists, and researchers in their exploration, monitoring, and study of underwater environments, small and big. The UUV is successfully used as a ROV, but to be used as an AUV, robust control algorithms need to be incorporated in the pixhawk controller. For this purpose a detailed mathematical model of the system is required, which is presented in the next chapter.

Chapter 4

DYNAMIC ANALYSIS OF THE AUV

4.1 Introduction

AUVs work autonomously using on-board sensors for understanding the surroundings, propulsion system for navigation and an on-board computer for decision making. For navigation and motion control of the AUV in an unknown dynamic environment, accurate kinematics and dynamics model is essential. System properties need to be evaluated for developing the mathematical model. These properties can be experimentally determined with full scale or scaled models. Though these experiments can produce accurate properties but are often expensive with complex setup and sensor requirements. Computational approach with CFD software packages such as ANSYS FLUENT^{TM} have been successfully used to estimate different hydrodynamic properties with good accuracy. Strip theory has been used to determine the added mass coefficients numerically. Other parameters such as inertia, C.B and C.G can be determined by developing a detailed CAD model of the system. MATLAB^{TM} is used for simulating the developed kinematics and dynamics model for understanding the behavior of the system. This chapter presents mathematical modeling of the developed compact AUV, including the system parameter estimation in five sections. Following the introductory section is the section 4.2 which, presents the developed AUV and detailed mathematical model of the system. Section 4.3, discusses the system parameter estimation using CAD modeling and CFD analysis. Developed simulation platform, experimental result and its comparison with the developed model is presented in section 4.4. Summary of the chapter is presented in section 4.5.

4.2 AUV and System Model

A compact affordable underwater robot is developed as presented in the previous chapter. For the system to be used as an AUV a robust controller has be developed and an accurate mathematical model of the system is essential for the controller. Detailed mathematical modelling of the system is discussed in this section.

4.2.1 Kinematics

Kinematics of a system interprets its motion in the global frame. The AUV has a rigid structure and fixed actuators. AUV kinematic model expresses its velocity measured in the body-fixed frame relative to the the earth-fixed frame. The Body-fixed frame (B-frame) or the local frame is the coordinate system with origin at the AUV geometrical center with axes along the surge, sway and heave direction respectively. Earth-fixed(N-frame) or global (X, Y, Z) frame with the axes along North-East-Down directions and origin fixed at the water surface.

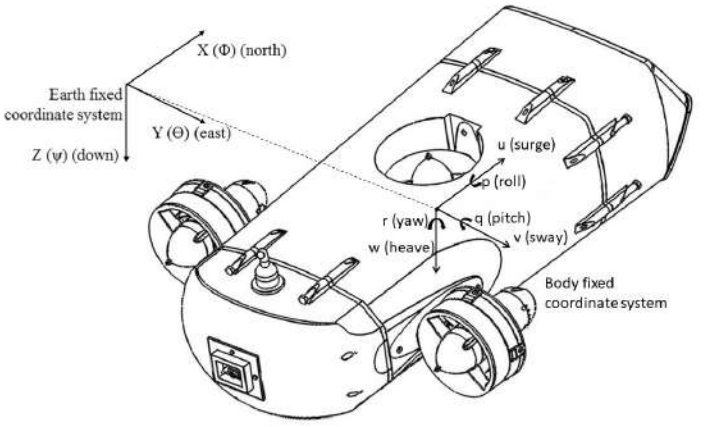

Figure 4.1: AUV reference frames

As presented in the Table 4.1 position along north, east and down direction x, y, z and rotational angle about these axis ϕ, θ, ψ constitute the position and orientation vectors of the AUV in global perspective and noted as $\eta = [\eta_1^T, \eta_2^T]^T$; where $\eta_1 = [x, y, z]^T$, $\eta_2 = [\phi, \theta, \psi]^T$. Linear and angular velocity of the AUV is expressed in the body fixed frame $\{b\}$ or the local frame as the sensors for measurement of these parameters are mounted in the AUV. These parameters are notated as $\nu = [\nu_1^T, \nu_2^T]^T$; where $\nu_1 = [u, v, w]^T$ and $\nu_2 = [p, q, r]^T$.

Table 4.1: Standard notations for AUV state vector

DOF	Motion Descriptions	Positions and Orientations	Linear and Angular Velocities
1	Motions in the X- direction(surge)	x	u
2	Motions in the Y- direction(sway)	y	v
3	Motions in the Z- direction(heave)	z	w
4	Rotations about the X-axis(roll)	ϕ	p
5	Rotations about the Y-axis(pitch)	θ	q
6	Rotations about the Z-axis(yaw)	ψ	r

Motion parameters in global and local frames are correlated using Euler transformation presented as (Fossen [84]):

$$\dot{\eta} = J\nu = \begin{bmatrix} J_1(\eta_2) & 0 \\ 0 & J_2(\eta_2) \end{bmatrix} \nu \tag{4.1}$$

where

$$J_1(\eta_2) = \begin{bmatrix} c(\psi)c(\theta) & -s(\psi)c(\phi)+c(\psi)s(\theta)s(\phi) & s(\psi)s(\phi)+c(\psi)c(\phi)s(\theta) \\ s(\psi)c(\theta) & c(\psi)c(\phi)+s(\phi)s(\theta)s(\psi) & -c(\psi)s(\phi)+s(\theta)s(\psi)c(\theta) \\ -s(\theta) & c(\theta)s(\phi) & c(\theta)c(\phi) \end{bmatrix} \tag{4.2}$$

$$J_2(\eta_2) = \begin{bmatrix} 1 & s(\phi)t(\theta) & c(\phi)t(\theta) \\ 0 & c(\phi) & -s(\phi) \\ 0 & s(\phi)/c(\theta) & c(\phi)/c(\theta) \end{bmatrix} \tag{4.3}$$

where $s(\phi) = sin(\phi)$, $c(\phi) = cos(\phi)$ and $t(\phi) = tan(\phi)$.

Here for $\theta = \pm\frac{\pi}{2}$ the $tan(\theta)$ is infinite and the $J_2(\eta_2)$ is undefined. This creates a singularity for the kinematic equation. For the AUV the C.B lies above the C.G and both are vertically aligned thus a restoring torque is acting during roll and pitch motion. Therefore the pitch angle θ is not going to be $\pm\frac{\pi}{2}$ and singularity is avoided. Most of the time the global motion parameters are know and local parameters can be obtained using the inverse kinematic relations given below.

$$\nu = J^{-1}\dot{\eta} \tag{4.4}$$

4.2.2 Dynamics

Dynamic model of a system interprets how different forces acting on the system such as actuation, inertia, and environmental forces affect the system motion. Thus an accurate dynamic model can estimate the required actuation force for desired AUV motion and is essential for autonomous control and navigation. The AUV motion in 6 degrees of freedom and different forces and torques acting on the system can be correlated and expressed in the body-fixed frame as given by the following equation (Fossen [84], Fossen and Fjellstad [86]):

$$M\dot{v} + C(v)v + D(v)v + g(\eta) = \tau \tag{4.5}$$

Here $M = M_{RB} + M_A$ in which, M_{RB} is the inertia matrix and M_A is the added mass matrix of the AUV, $C(\nu) = C_{RB}(\nu) + C_A(\nu)$ in which $C_{RB}(\nu)$ and $C_A(\nu)$ are the rigid body and added mass coriolis and centripetal matrix respectively, $D(\nu)$ is the hydrodynamic damping matrix which includes drag and lift terms, $g(\eta)$ is the vector containing the restoring forces such as buoyancy and gravity, and τ is the vector of containing forces and moments exerted by the actuators.

The equation of motion can also be written in the global or NED frame as given below.

$$M^\star(\eta)\ddot{\eta} + C^\star(v,\eta)\dot{\eta} + D^\star(v,\eta)\dot{\eta} + g^\star(\eta) = \tau^\star \tag{4.6}$$

where,

$$\begin{aligned} \dot{\eta} &= J(\eta)v \iff v = J^{-1}(\eta)\dot{\eta} \\ \ddot{\eta} &= J(\eta)\dot{v} + \dot{J}(\eta)v \iff \dot{v} = J^{-1}(\eta)[\ddot{\eta} - \dot{J}(\eta)J^{-1}(\eta)\dot{\eta}] \end{aligned} \tag{4.7}$$

$$\begin{aligned} M^\star(\eta) &= J^{-T}(\eta)MJ^{-1}(\eta) \\ C^\star(v,\eta) &= J^{-T}(\eta)[C(v) - MJ^{-1}(\eta)\dot{J}(\eta)]J^{-1}(\eta) \\ D^\star(v,\eta) &= J^{-T}(\eta)D(v)J^{-1}(\eta) \\ g^\star(\eta) &= J^{-T}(\eta)g(\eta) \\ \tau^\star &= J^{-T}(\eta) \end{aligned} \tag{4.8}$$

Inertia matrix

M_{RB} is the inertia matrix of the rigid AUV structure (Fossen [84]).

$$M_{RB} = \begin{bmatrix} mI_{3x3} & -mS(r_g) \\ mS(r_g) & I_b \end{bmatrix}$$
$$= \begin{bmatrix} m & 0 & 0 & 0 & mz_g & -my_g \\ 0 & m & 0 & -mz_g & 0 & mx_g \\ 0 & 0 & m & my_g & -mx_g & 0 \\ 0 & -mz_g & my_g & Ix & -I_{xy} & -I_{xz} \\ mz_g & 0 & -mx_g & -I_{yx} & Iy & -I_{yz} \\ -my_g & mx_g & 0 & -I_{zx} & -I_{zy} & Iz \end{bmatrix} \tag{4.9}$$

Here m is the mass of the AUV, I_b is the inertia tensor of the system expressed in local-frame, $r_g = [x_g, y_g, z_g]^T$ is the C.G of the robot measured from the origin in the local-frame and $S(a)$ is the skew symmetric matrix of vector a. These parameters are constant for the AUV and depend on the mass distribution.

A submersed body while accelerating or decelerating have to push the surrounding fluid in-order to move as a result transfer kinetic energy to otherwise stationary fluid. To consider this effect virtual mass is added to the system which is refereed as hydrodynamic added mass. M_A is the added mass inertia matrix which is expressed as follows (Fossen [84]).

$$M_A = -\begin{bmatrix} X_{\dot{u}} & X_{\dot{v}} & X_{\dot{w}} & X_{\dot{p}} & X_{\dot{q}} & X_{\dot{r}} \\ Y_{\dot{u}} & Y_{\dot{v}} & Y_{\dot{w}} & Y_{\dot{p}} & Y_{\dot{q}} & Y_{\dot{r}} \\ Z_{\dot{u}} & Z_{\dot{v}} & Z_{\dot{w}} & Z_{\dot{p}} & Z_{\dot{q}} & Z_{\dot{r}} \\ K_{\dot{u}} & K_{\dot{v}} & K_{\dot{w}} & K_{\dot{p}} & K_{\dot{q}} & K_{\dot{r}} \\ M_{\dot{u}} & M_{\dot{v}} & M_{\dot{w}} & M_{\dot{p}} & M_{\dot{q}} & M_{\dot{r}} \\ N_{\dot{u}} & N_{\dot{v}} & N_{\dot{w}} & N_{\dot{p}} & N_{\dot{q}} & N_{\dot{r}} \end{bmatrix} = \begin{bmatrix} m_{11} & m_{12} & m_{13} & m_{14} & m_{15} & m_{16} \\ m_{21} & m_{22} & m_{23} & m_{24} & m_{25} & m_{26} \\ m_{31} & m_{32} & m_{33} & m_{34} & m_{35} & m_{36} \\ m_{41} & m_{42} & m_{43} & m_{44} & m_{45} & m_{46} \\ m_{51} & m_{52} & m_{53} & m_{54} & m_{55} & m_{56} \\ m_{61} & m_{62} & m_{63} & m_{64} & m_{65} & m_{66} \end{bmatrix} \tag{4.10}$$

Here $m_{11} = -X_{\dot{u}}$, is the added mass force in the X-direction due to motion along the surge direction and $m_{66} = -N_{\dot{r}}$, is added moment of inertia due to rotation about yaw. For a submersed

body beyond a depth of 20 meters moving at low speed added mass coefficients are not function of the wave excitation frequencies and are positive constants. The coefficients only depend on the geometry of the submersed body. Added mass matrix is symmetrical, thus 21 unknown parameters has to be determined. This number will decrease with the presence of plane of symmetry in the structure. The AUV is symmetrical about the xy and xz plains. Following Lewis [109] for slender body added mass matrix is given as follows.

$$\begin{bmatrix} m_{11} & 0 & 0 & 0 & 0 & 0 \\ 0 & m_{22} & 0 & m_{24} & 0 & m_{26} \\ 0 & 0 & m_{33} & 0 & m_{35} & 0 \\ 0 & m_{42} & 0 & m_{44} & 0 & m_{46} \\ 0 & 0 & m_{53} & 0 & m_{55} & 0 \\ 0 & m_{62} & 0 & m_{64} & 0 & m_{66} \end{bmatrix} \tag{4.11}$$

Coriolis and centripetal matrix

$C_{RB}(\nu)$ is the coriolis and centripetal matrix of the rigid AUV structure (Fossen [84]).

$$C_{RB}(\nu) = \begin{bmatrix} 0_{3x3} & -mS(r_g) \\ mS(r_g) & I_b \end{bmatrix}$$

$$= \begin{bmatrix} 0 & 0 & 0 \\ 0 & 0 & 0 \\ 0 & 0 & 0 \\ -m(y_g q + z_g r) & m(y_g p + w) & m(z_g p - v) \\ m(x_g q - w) & -m(z_g r + x_g p) & m(z_g q + u) \\ m(x_g r + v) & m(y_g r - u) & -m(x_g p + y_g q) \end{bmatrix} \begin{bmatrix} m(y_g q + z_g r) & -m(x_g q - w) & -m(x_g r + v) \\ -m(y_g p + w) & m(z_g r + x_g p) & -m(y_g r - u) \\ -m(z_g p - v) & -m(z_g q + u) & m(x_g p + y_g q) \\ 0 & -I_{yz} q - I_{xz} p + I_z r & I_{yz} r + I_{xy} p - I_y q \\ I_{yz} q + I_{xz} p - I_z r & 0 & -I_{xz} r - I_{xy} p + I_x p \\ -I_{yz} r - I_{xy} p + I_y q & I_{xz} r + I_{xy} q - I_x p & 0 \end{bmatrix} \tag{4.12}$$

$C_A(\nu)$ is the coriolis and centripetal matrix due to the added mass effect (Fossen [84]).

$$C_A = \begin{bmatrix} 0 & 0 & 0 & 0 & -c_3 & c_2 \\ 0 & 0 & 0 & c_3 & 0 & -c_1 \\ 0 & 0 & 0 & -c_2 & c_1 & 0 \\ 0 & -c_3 & c_2 & 0 & -d_3 & d_2 \\ c_3 & 0 & -c_1 & d_3 & 0 & -d_1 \\ -c_2 & c_1 & 0 & -d_2 & d_1 & 0 \end{bmatrix} \tag{4.13}$$

Here

$$c_1 = X_{\dot{u}}u + X_{\dot{v}}v + X_{\dot{w}}w + X_{\dot{p}}p + X_{\dot{q}}q + X_{\dot{r}}r$$

$$c_2 = Y_{\dot{u}}u + Y_{\dot{v}}v + Y_{\dot{w}}w + Y_{\dot{p}}p + Y_{\dot{q}}q + Y_{\dot{r}}r$$

$$c_3 = Z_{\dot{u}}u + Z_{\dot{v}}v + Z_{\dot{w}}w + Z_{\dot{p}}p + Z_{\dot{q}}q + Z_{\dot{r}}r$$

$$d_1 = K_{\dot{u}}u + K_{\dot{v}}v + K_{\dot{w}}w + K_{\dot{p}}p + K_{\dot{q}}q + K_{\dot{r}}r$$

$$d_2 = M_{\dot{u}}u + M_{\dot{v}}v + M_{\dot{w}}w + M_{\dot{p}}p + M_{\dot{q}}q + M_{\dot{r}}r$$

$$d_3 = N_{\dot{u}}u + N_{\dot{v}}v + N_{\dot{w}}w + N_{\dot{p}}p + N_{\dot{q}}q + N_{\dot{r}}r$$

And $X_{\dot{u}}$, $Y_{\dot{v}}$ .... are added mass coefficients.

Hydrodynamic damping matrix

$D(\nu)$ is the Damping matrix. For AUVs damping effect is due to the drag and lift forces exerted on the system by the surrounding fluid due to skin friction.

$D(\nu) = D_l(\nu) + D_n(\nu)$, where $D_l(\nu)$ is the linear damping and $D_n(\nu)$ is the non-linear damping matrix. As the linear and non-linear damping cannot be effectively separated these parameters will be estimated together. Due to existing symmetry in the AUV structure the non-diagonal terms will be neglected.

$$D_l(\nu) = -\begin{bmatrix} X_u & 0 & 0 & 0 & 0 & 0 \\ 0 & Y_v & 0 & 0 & 0 & 0 \\ 0 & 0 & Z_w & 0 & 0 & 0 \\ 0 & 0 & 0 & K_p & 0 & 0 \\ 0 & 0 & 0 & 0 & M_q & 0 \\ 0 & 0 & 0 & 0 & 0 & N_r \end{bmatrix} \tag{4.14}$$

The axial quadratic drag:

$$X = -\left(\frac{1}{2}\rho C_d A_f\right)u|u| = X_{u|u|}u|u| \tag{4.15}$$

Where $X_{u|u|} = \frac{\partial X}{\partial(u|u|)} = -\frac{1}{2}\rho C_d A_f$, ρ is the density of the surrounding fluid, C_d is the coefficient of drag, A_f is the reference area.

Quadratic damping matrix:

$$D_n(\nu) = -\begin{bmatrix} X_{u|u|}|u| & 0 & 0 & 0 & 0 & 0 \\ 0 & Y_{v|v|}|v| & 0 & 0 & 0 & 0 \\ 0 & 0 & Z_{w|w|}|w| & 0 & 0 & 0 \\ 0 & 0 & 0 & K_{p|p|}|p| & 0 & 0 \\ 0 & 0 & 0 & 0 & M_{q|q|}|q| & 0 \\ 0 & 0 & 0 & 0 & 0 & N_{r|r|}|r| \end{bmatrix} \tag{4.16}$$

Gravitational and buoyancy matrix

$g(\eta)$ is the vector of forces and moments due to gravitational and buoyancy effects.

$$g(\eta) = \begin{bmatrix} f_b + f_g \\ r_b \times f_b + r_g \times f_g \end{bmatrix} \tag{4.17}$$

Where $f_g = R^{BN^{-1}}[0,0,W]^T$ with $W = mg$ is the gravitational force vector in N-frame

and $f_b = R^{BN^{-1}}[0,0,-B]^T$ with $B = \rho g \nabla$ is the buoyancy force vector in N-frame

where g is the acceleration due to gravity 9.81 m / s^2 , ρ is the fluid density, ∇ is the displaced fluid volume, $r_b = [x_b, y_b, z_b]^T$ is the position of C.B in the B-frame $r_g = [x_g, y_g, z_g]^T$ is the position of C.G in the B-frame

$$g(\eta) = \begin{bmatrix} (W-B)sin(\theta) \\ -(W-B)cos(\theta)sin(\phi) \\ -(W-B)cos(\theta)cos(\phi) \\ -(y_gW - y_bB)cos(\theta)cos(\phi) + (z_gW - z_bB)cos(\theta)sin(\phi) \\ (z_gW - z_bB)sin(\theta) + (x_gW - x_bB)cos(\theta)cos(\phi) \\ -(x_gW - x_bB)cos(\theta)sin(\phi) - (y_gW - y_bB)sin(\theta) \end{bmatrix} \tag{4.18}$$

Actuator force and torque matrix

τ is the vector containing force and torque acting on the AUV by the actuators.

$$\tau = LU \tag{4.19}$$

where L matrix represent the thruster position and orientation.

$$L = \begin{bmatrix} 1 & 0 & 0 & 0 & 0 & -l_1 \\ 1 & 0 & 0 & 0 & 0 & l_2 \\ 0 & 0 & 1 & 0 & l_5 & 0 \end{bmatrix}^T \tag{4.20}$$

and U is the vector presenting the trust output from the individual thrusters.

$$U = [T_1, T_2, T_3]^T \tag{4.21}$$

The AUV has three thrusters for propulsion. The central thruster is used for heave motion, whereas the other two thrusters are used for surge motion. T_1 and T_2 are the thrust output of the two side thrusters as indicated in the Fig. 4.2 and T_3 is the thrust output of the heave thruster. Fig. 4.3 presents the thruster positions from the origin of the body-frame. Matrix L contains the distance of the actuators from the origin in local frame as shown in Fig. 4.3. Here $l_1 = l_2 = 16.3$ cm and $l_5 = 0.09$ cm.

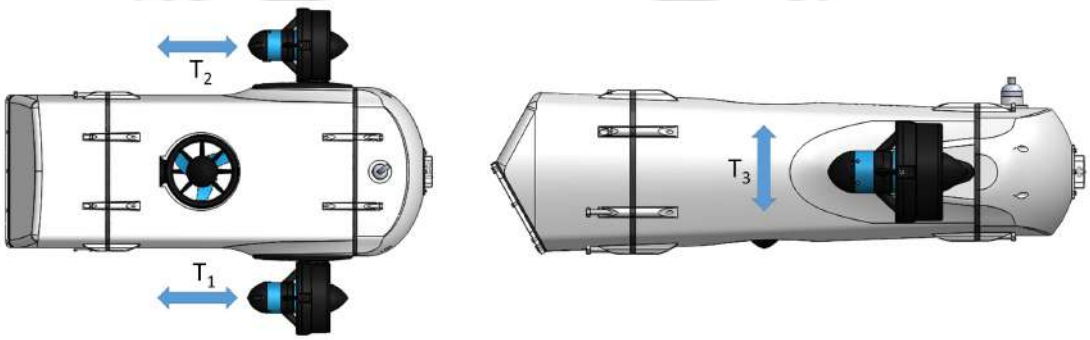

(a) Side thruster (b) Central thruster

Figure 4.2: Thrust output T_1, T_2 and T_3

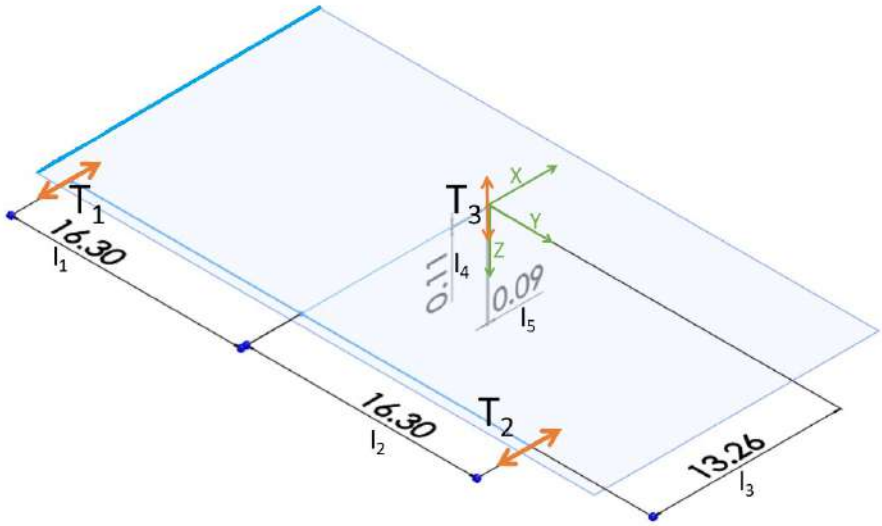

Figure 4.3: Thruster position

A detailed 6 DOF dynamic model for the AUV is presented. The model is further simplified with the following assumptions with justifications.

- The AUV operates at low speed (maximum 2 m/s).
- Because of the low operating speed and symmetrical structure of the AUV the lift forces are negligible.
- The C.G lies 0.97 cm vertically below the C.B thus, a restoring torque is present which prevents any significant roll or pitch motion. Single thruster is present around the C.G for vertical motion. Therefore roll and pitch motions are neglected.
- The AUV is neutrally buoyant, thus the buoyancy force and weight of the system cancel each other.
- For the submersed body beyond a depth of 20m, moving at low speed will have no wave interaction.
- The surge and heave motions are independent.

With these assumptions, pitch and roll motions are neglected and surge, heave, and yaw motions are considered. Therefore the 6 DOF AUV model can be simplified to a 3 DOF model, considering sway, pitch and roll to be zero state vectors. Because of the decoupling of the DOF, the hydrodynamic damping matrix is diagonal. The system is neutrally buoyant thus the gravi-

tational and buoyancy force cancel each other out and the restoring force matrix vanishes. The 3 DOF mathematical model is summarised as follows:

Position and orientation in Global-frame: $\eta = [x, y, z, \psi]^T$

Linear and angular velocity in Body-frame: $\nu = [u, v, w, r]^T$

The kinematic correlation is presented as:

$$\dot{x} = ucos(\psi) - vsin(\psi); \;\; \dot{y} = usin(\psi) + vcos(\psi); \;\; \dot{z} = w; \;\; \dot{\psi} = r \tag{4.22}$$

and the dynamic correlation in body-frame as:

$$M\dot{\nu} + C(\nu)\nu + D_l(\nu)\nu + D_n(\nu)\nu = \tau \tag{4.23}$$

$$\begin{bmatrix} m - X_{\dot{u}} & 0 & 0 & -my_g \\ 0 & m - Y_{\dot{v}} & 0 & mx_g - Y_{\dot{r}} \\ 0 & 0 & m - Z_{\dot{w}} & 0 \\ -my_g & mx_g - Y_{\dot{r}} & 0 & I_z - N_{\dot{r}} \end{bmatrix} \begin{Bmatrix} \dot{u} \\ \dot{v} \\ \dot{w} \\ \dot{r} \end{Bmatrix} + \left\{ \begin{bmatrix} 0 & 0 & 0 & -m(x_g r + v) + Y_{\dot{v}} v + Y_{\dot{r}} r \\ 0 & 0 & 0 & -m(y_g r - u) - X_{\dot{u}} u \\ 0 & 0 & 0 & 0 \\ m(x_g r + v) - Y_{\dot{v}} v - Y_{\dot{r}} r & m(y_g r - u) + X_{\dot{u}} u & 0 & 0 \end{bmatrix} + \right.$$
$$\left. \begin{bmatrix} X_u & 0 & 0 & 0 \\ 0 & Y_v & 0 & 0 \\ 0 & 0 & Z_w & 0 \\ 0 & 0 & 0 & N_r \end{bmatrix} + \begin{bmatrix} X_{u|u|}|u| & 0 & 0 & 0 \\ 0 & Y_{v|v|}|v| & 0 & 0 \\ 0 & 0 & Z_{w|w|}|w| & 0 \\ 0 & 0 & 0 & N_{r|r|}|r| \end{bmatrix} \right\} \cdot \begin{Bmatrix} u \\ v \\ w \\ r \end{Bmatrix} = \begin{bmatrix} T_1 + T_2 \\ 0 \\ T_3 \\ -l_1 T_1 + l_2 T_2 \end{bmatrix} \tag{4.24}$$

The 3 DOF coupled non-linear equation presented here considers different forces acting on the system and their correlation with the AUV motion. The model can be used to estimate the actuation force required for desired AUV motion. The equation will be complete by substituting the system parameters introduced. These parameters are measured and estimated in the following section.

4.3 System Parameter Estimation

System parameters defined in the previous section have to be determined to complete the dynamic model. The mass, buoyancy, inertia, position of C.G and C.B are determined using a detailed CAD model and physical measurements. CFD software package ANSYS FLUENT^{TM} is used for hydrodynamic damping parameter estimation, where as the added mass coefficients

are estimated using numerical technique.

4.3.1 Inertia and Buoyancy

Individual components used in the system are designed in the SOLIDWORKS^{TM} software using the weight and dimension measurements of the components. Components are assembled and a detailed CAD model (Fig. 4.4) is developed. Inertia and position of C.G are determined from this CAD model and verified by physical measurements. To estimate the buoyancy parameter, a solid replica of the AUV is developed by filling the internal hollow spaces. Water is selected as material for this structure. Weight of this water model is the buoyancy and its C.G is the C.B. The estimated system parameters are mentioned in the Table. 4.2.

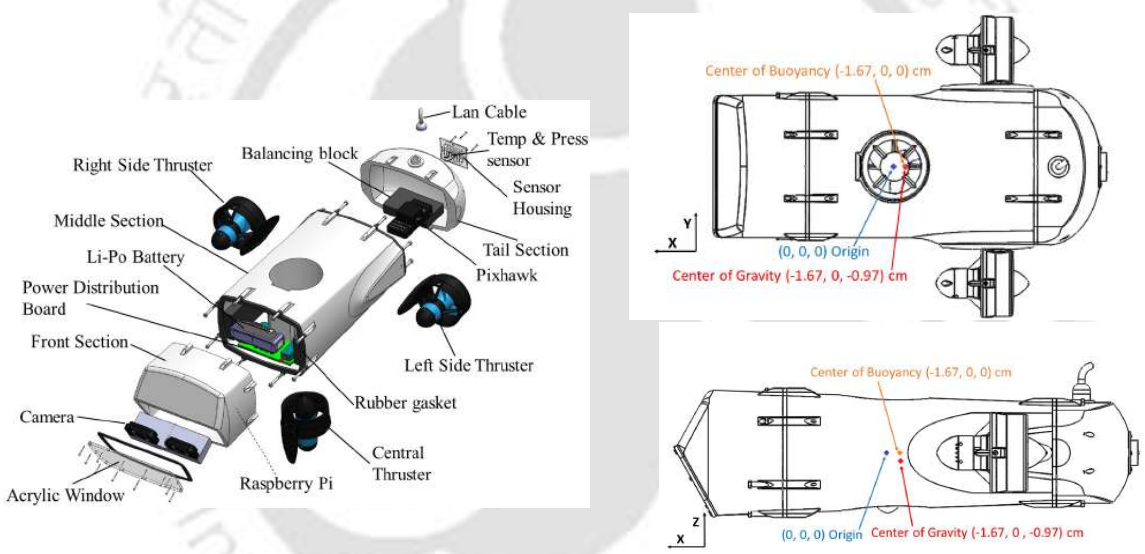

Figure 4.4: Detailed CAD model of the AUV

Table 4.2: Estimated system parameters from CAD model.

Parameter	Value
m	14.700 kg
W	144.060 N
B	144.060 N
I_{xx}	0.110 kg.m^2
I_{yy}	0.290 kg.m^2
I_{zz}	0.360 kg.m^2
l_1	0.163 m

Parameter	Value
x_g	-0.0167 m
y_g	0 m
z_g	-0.0097 m
x_b	-0.0167 m
y_b	0 m
z_b	0 m
l_5	0.0009 m

4.3.2 Added Mass Estimation

The AUV has to impart kinetic energy to accelerate the surrounding fluid from its path in order to move as AUV and fluid cannot occupy the same space at the same time. This effect is considered by adding virtual mass to the system and the virtual mass is called "added-mass". Here the slender body theory is used to estimate the added mass of the robot. The system is considered to be a slender body having length considerably longer than the width and depth. The body is divided into thin sections (Fig. 4.5) for which the 2D added mass coefficients are estimated from the literature (Fig. 4.5). Following the formulations from the handbook: Principles of Naval Architecture Vol III., (1989) Soc. Naval Arch. and Marine Engineers (Lewis [109]), the 3D added mass coefficients are estimated by integrating the 2D coefficients over the length as presented in the eq. 4.25. 2D and 3D coefficients are mentioned as a_{ij} and m_{ij} respectively for added mass effect in i-direction due to motion in j-direction. The solid AUV CAD model is sliced into multiple sections, 10 mm apart in the middle portion and 5 mm apart in the front and back. The cross-sections are approximate rectangles and ellipses. Empirical formulas for 2D added mass coefficients for appropriate cross-sections from the literature Dong [110], Newman [111] are used for calculations as shown in Fig. 4.7. With the measured dimensions of the individual cross-sections from the CAD model, 2D added mass coefficients are calculated and integrated over the length to find out the 3D coefficients. For longitudinal added mass coefficient, a parallelepiped formula Dong [110] is used as shown in the Fig. 4.8 as the AUV is have approximately rectangular cross-sections for most of its length. The parallelepiped selected is just enclosing the AUV as shown in the Fig. 4.8. Table. 4.3 presents the calculated 3D added-mass.

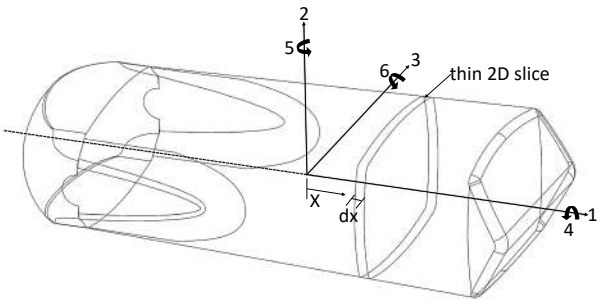

Figure 4.5: 3D slender body

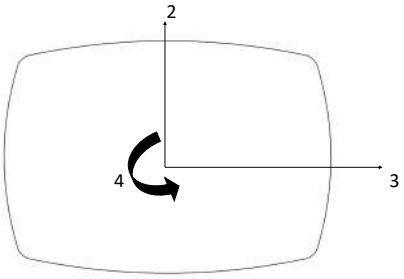

Figure 4.6: 2D cross section of the slender body

$$m_{22} = \int_L a_{22}dx;\ \ m_{33} = \int_L a_{33}dx;\ \ m_{44} = \int_L a_{44}dx;$$
$$m_{55} = \int_L x^2 a_{33}dx;\ \ m_{66} = \int_L x^2 a_{22}dx;\ \ m_{26} = \int_L x\, a_{22}dx; \tag{4.25}$$

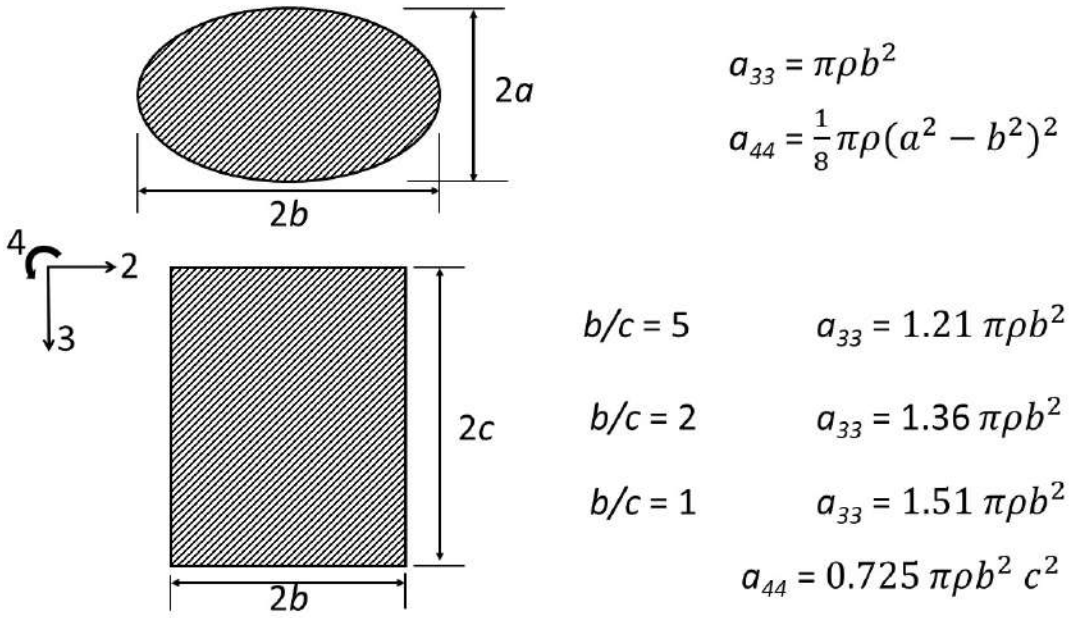

Figure 4.7: 2D added mass coefficient for different geometry (Dong [110], Newman [111])

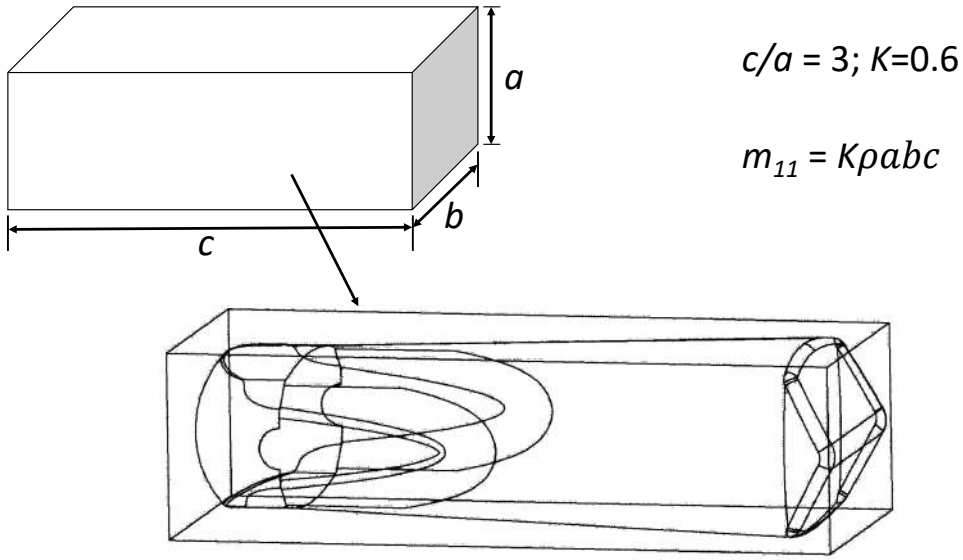

Figure 4.8: 3D added mass coefficient

Table 4.3: 3D added mass

	Added mass (in kg)
m_{11}	11.8000
m_{22}	11.9400
m_{33}	23.8050
m_{44}	0.6900
m_{55}	0.0007
m_{66}	0.0004
m_{26}	0.0575

4.3.3 Hydrodynamic Damping

Hydrodynamic damping parameters are obtained by estimating the drag forces experienced by the AUV because of the skin friction between the AUV structure and the surrounding fluid. CFD solver ANSYS FLUENT^{TM} is used for the purpose and the simulation setup and solution is discussed in this section.

Computational Domain

Multiple simulations have been carried out for motion along surge, sway, heave, and yaw directions. Furthermore varying flow velocities have been considered for simulation along each direction. A simplified AUV model is imported into ANSYS^{TM} design module. Computational domain has been developed by creating an enclosure surrounding the AUV model. Size of the domain is kept at least thrice the size of the model to avoid interference from the domain boundary. Then the AUV structure is subtracted from the domain using the boolean operation and only the flow field remained. Depending on the flow direction, faces of the domain are marked as inlet and outlet planes. The domain for the yaw simulation consist of two sections, outer rectangular section and inner cylindrical section. The two sections are separated by a sliding interface as shown in Fig. 4.12. Figure. 4.9, 4.10, 4.11, and 4.12 show the simulation setup and flow vector for simulations along different flow directions.

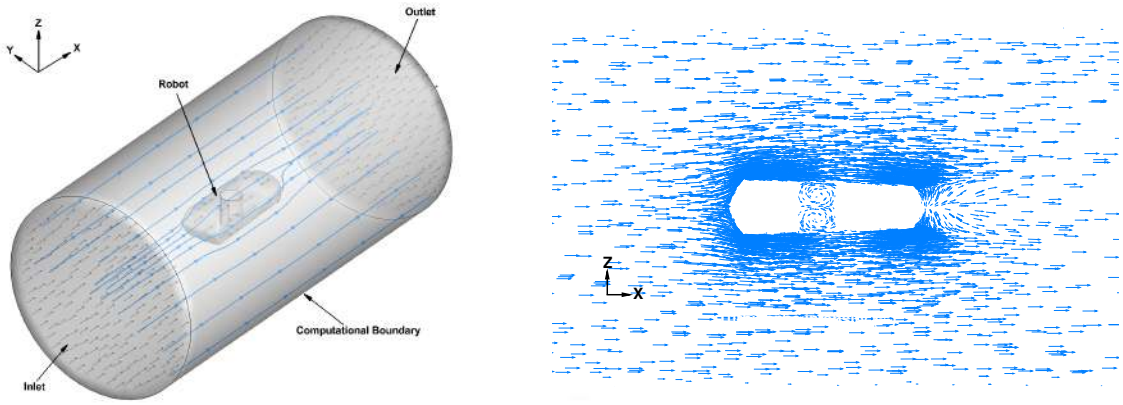

(a) (b)

Figure 4.9: (a)Simulation setup (b)Flow vector for simulation for surge motion

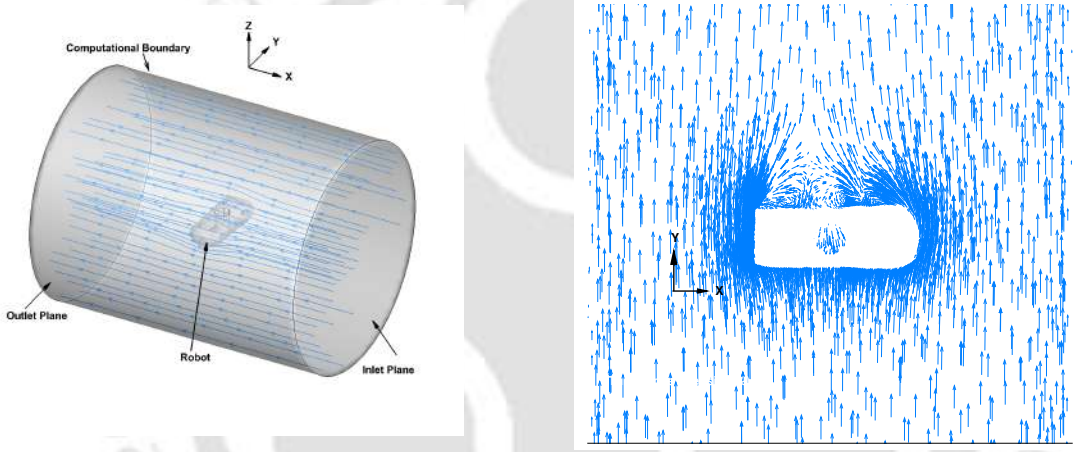

(a) (b)

Figure 4.10: (a)Simulation setup (b)Flow vector for simulation for sway motion

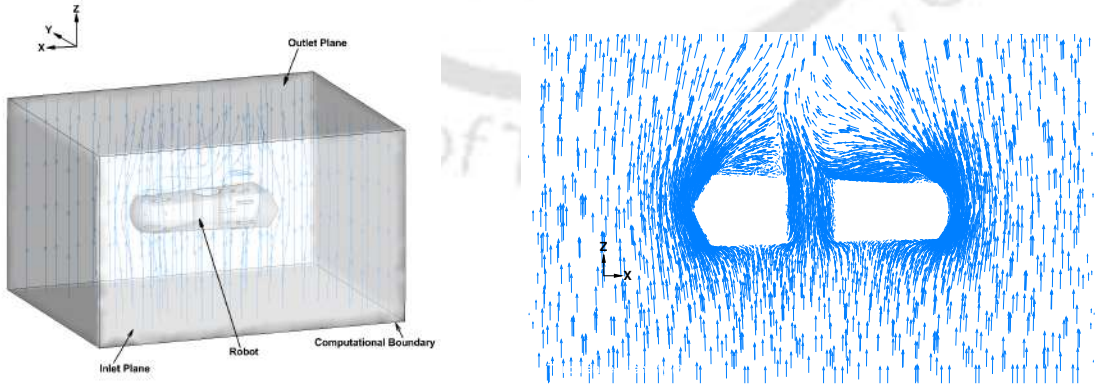

(a) (b)

Figure 4.11: (a)Simulation setup (b)Flow vector for simulation for heave motion

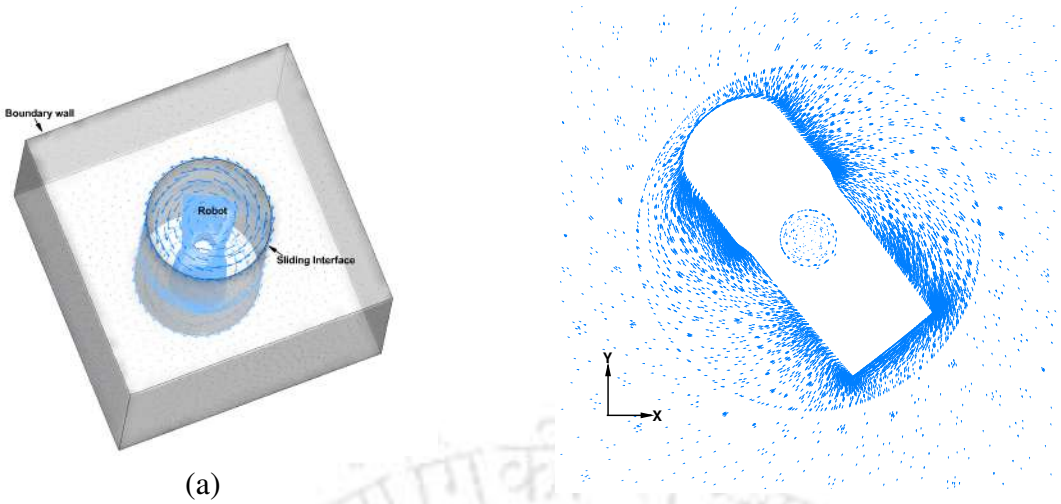

(a) (b)

Figure 4.12: (a)Simulation setup (b)Flow vector for simulation for yaw motion

Simulation Setup

The 3D computational domain is discretized with ANSYS FLUENT^{TM} meshing with unstructured tetrahedral grids (Fig. 4.14). Edge and body sizing operation is used to create a dense mess around the AUV wall boundary for better accuracy. In FEM or FVM, large number of elements give good results as it can capture the physics better. But more elements increase computational complexity and takes more time and resources. Thus a grid independent test is conducted to select meshing with minimum elements without having much deviation in the results. For one of such tests number of elements are varied from 10,25,953 to 158,84,806 as shown in Table. 4.4 (Fig. 4.13) and fine mesh with 14,54,076 tetrahedral elements with 268731 nodes is selected for simulation.

After meshing boundary conditions are applied to the computational domain. Multiple simulations are carried out with inlet flow velocity varying from 1 to 4 m/s, 0.25 to 1.5 m/s and 0.5 to 2 m/s for flow along surge, sway, and heave direction, respectively. Depending on the flow configuration uniform velocity is prescribed at the inlet plane where as pressure outlet boundary condition is prescribed at the outlet plane. These simulations are conducted with gauge pressure 603916 Pa, which is absolute pressure at 50 m water depth. For the yaw simulation the AUV body wall is given no-slip boundary condition and considered as moving wall with rotational-speed varying from 20 to 50 rpm. Side walls are given symmetry boundary condition.

The flow around the AUV structure is turbulent in nature. k-ε turbulent model is used to estimate drag and lift coefficient in the hydrodynamic simulations (Yue Yue et al. [39], He et al. [38], Mansoorzadeh and Javanmard [103], and Menter et al. [104]). Near solid fluid interface, standard wall function is used with $y^+ \approx 50$. For the transient simulations time-step size used is 0.001 second with minimum number of time step is considered to be 20,000. But in several simulations dynamic steady state is achieved well before that.

Table 4.4: Drag Coefficient (C_d) variation with number of Mesh element

Mesh element no.	Drag Coefficient (C_d)
1025953	0.2640
1183601	0.2691
1262075	0.2383
1380693	0.2649
1454076	0.2655
1584806	0.2670

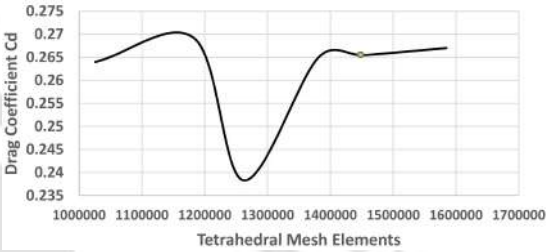

Figure 4.13: Grid independent test

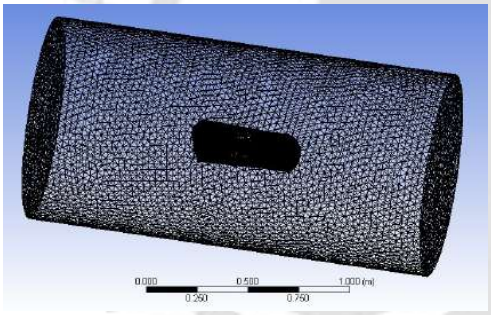

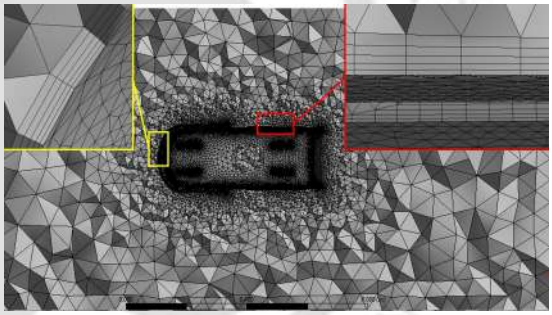

Figure 4.14: Meshed flow field

Simulation Result

Multiple simulations are carried out with varying inlet velocity conditions for different flow directions. Simulations are carried out till dynamic steady state is reached for the drag coefficient. For each simulation along surge, sway and heave the time average drag coefficient is obtained. Negligible lift coefficients are obtained due to the symmetrical structure of the AUV and thus neglected. Using the drag coefficient values the drag forces are estimated using the following expression

$$D_u = \frac{1}{2}\rho C_d A_f u^2 \tag{4.26}$$

where D_u is the drag force experienced due to motion in surge direction, ρ is the density of the surrounding fluid, C_d is the coefficient of drag and A_f is the projected area in Y-Z plane. The projected area is determined to be 0.029239 m^2 from the CAD model. Figure 4.15 shows the turbulence intensity, velocity, and pressure contour from the simulation carried at 2.5 m/s inlet velocity along X-axis. From the velocity contour plot the maximum velocity is observed at the top and bottom edge of the nose where as the least velocity is observed at the stagnation point and the wake region. In the wake region low pressure and high turbulence intensity is observed. The C_d value reached dynamic steady state around 6 seconds and the time average value of 0.267 is considered for further calculations.

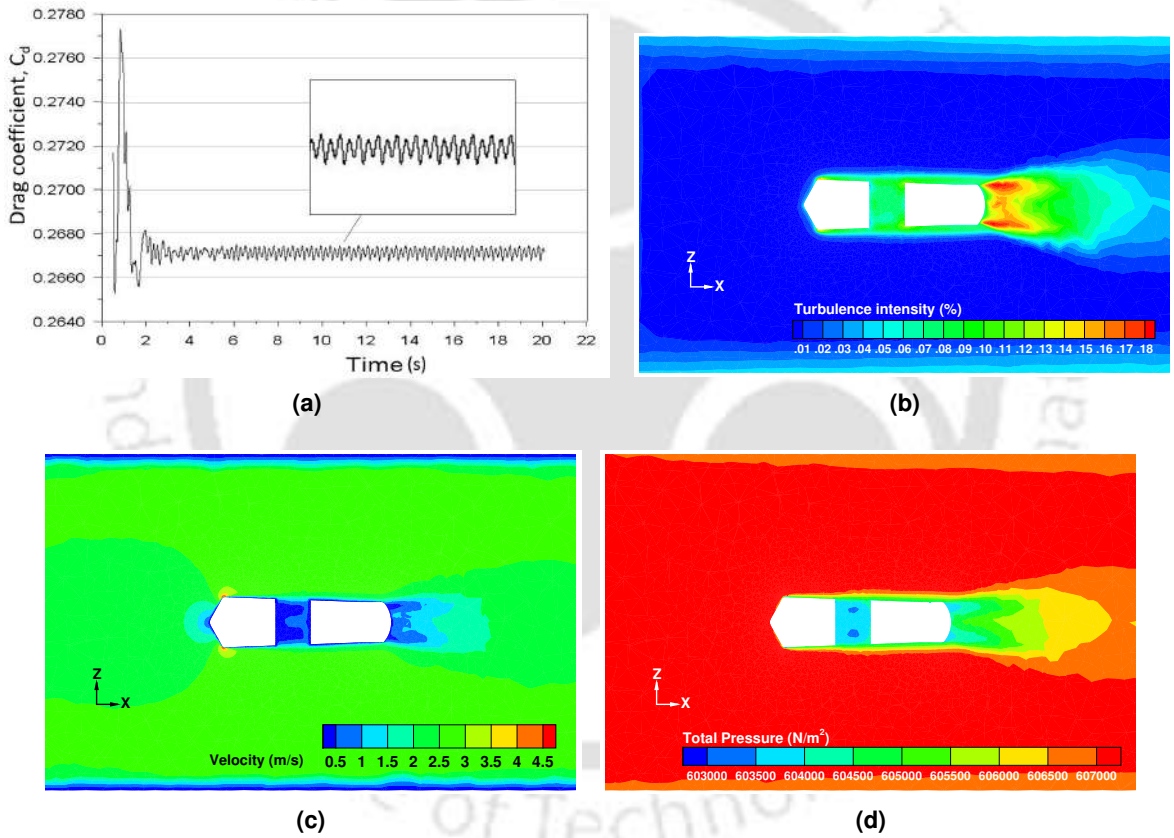

Figure 4.15: (a)Variation of drag coefficient with time (b)Turbulence intensity (%) contour (c)Velocity magnitude (m/s) contour (d)Total pressure (m/s^2) contour for 2.5 m/s flow in the X-direction

Drag coefficient and Drag force obtained for various flow velocities are presented in the Table. 4.5. An quadratic curve (Fig. 4.16) is fitted using MATLAB^{TM} with the results obtained from simulation and the developed relationship between the drag force experienced and the flow velocity is presented as:

$$D_u = 4.795u^2 + 1.16 \times 10^{-19}u \tag{4.27}$$

Here 'D_u' is the drag force experienced and 'u' is the velocity along the X-axis. Here 1.16×10^{-19} is the linear damping and 4.795 is the quadratic damping parameter.

Table 4.5: Variation of drag coefficient and average drag force with flow velocity along X-direction

Flow velocity (m/s)	Drag coefficient C_d	Avg. drag force (N)
1.0	0.282	4.115
1.5	0.274	9.003
2.0	0.263	15.352
2.5	0.267	24.352
3.0	0.305	40.058
3.5	0.318	56.847
4.0	0.357	83.355

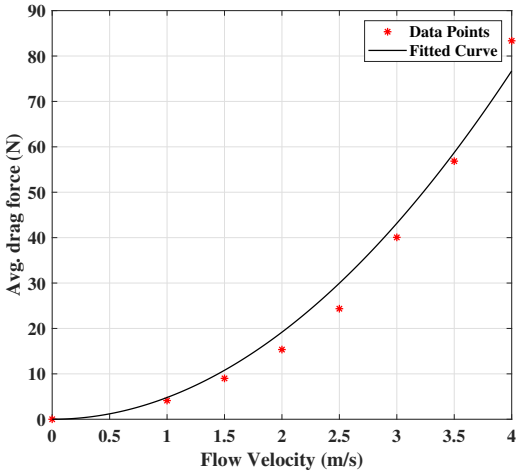

Figure 4.16: Avg. drag vs flow velocity in X-axis

Similar simulation with flow along Y-axis and Z-axis are carried out to estimate the rest hydrodynamic damping parameters. Figure 4.17 shows the turbulence intensity, velocity, and pressure contour from the simulation carried at 1.5 m/s inlet velocity along Y-axis. The C_d value reached dynamic steady state around 3 seconds and the time average value of 1.0351 is considered.

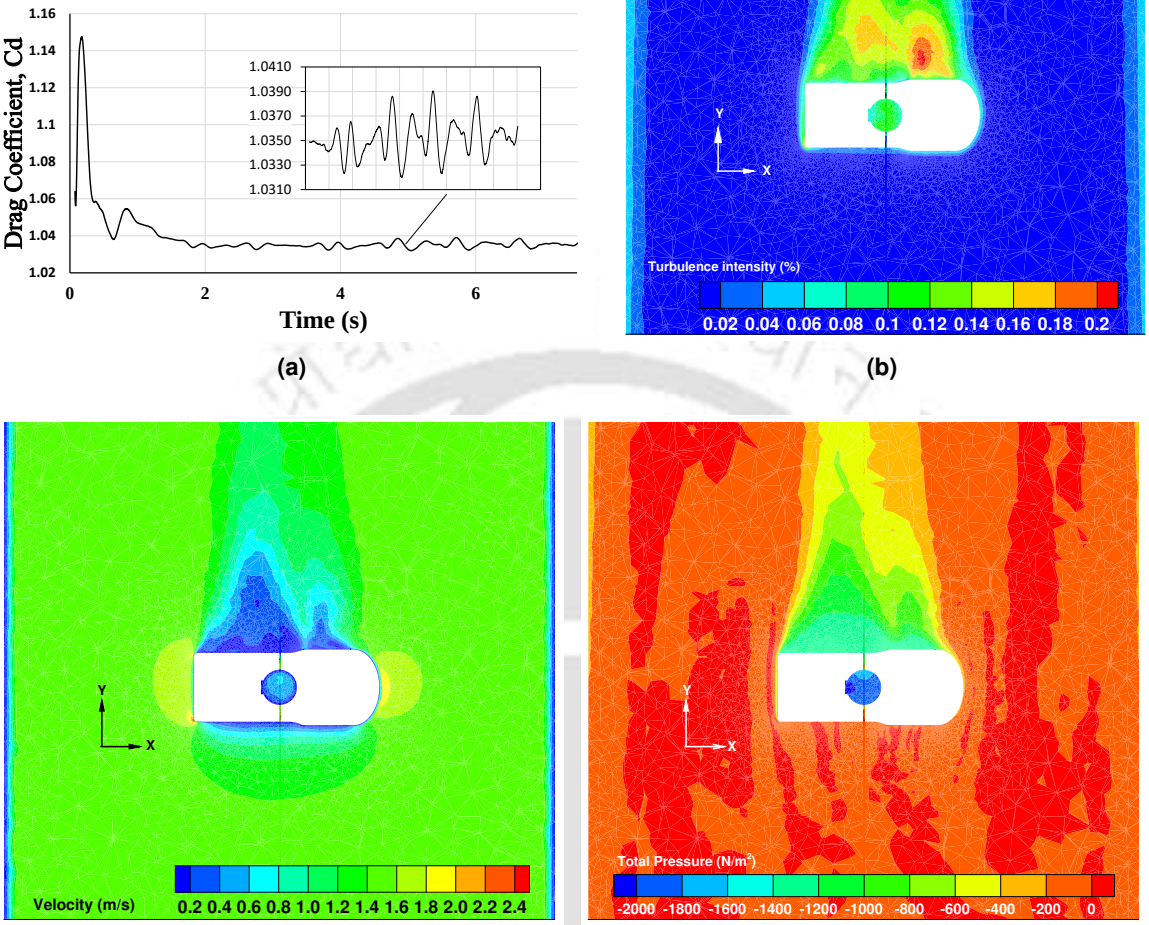

Figure 4.17: (a)Variation of drag coefficient with time (b)Turbulence intensity (%) contour (c)Velocity magnitude (m/s) contour (d)Total pressure (m/s^2) contour for 1.5 m/s flow in the Y direction

Table 4.6: Variation of drag coefficient and average drag force with flow velocity along Y-direction

Flow velocity (m/s)	Drag coefficient C_d	Avg. drag force (N)
0.25	1.38	2.33
0.50	1.22	8.26
0.75	1.13	17.27
1.00	1.09	29.52
1.25	1.06	44.76
1.50	1.03	63.07

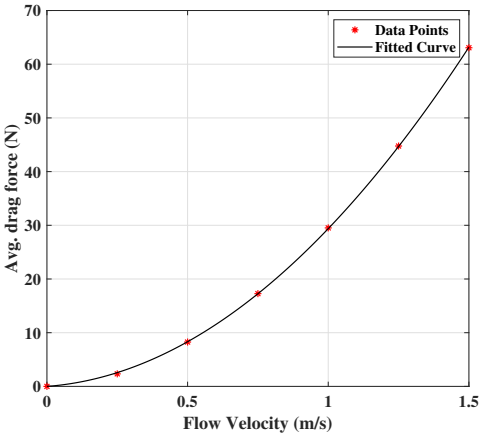

Figure 4.18: Avg. drag vs flow velocity in Y-axis

Drag coefficient and drag force obtained for various flow velocities are presented in the Table 4.6. An quadratic curve (Fig. 4.18) is fitted using MATLAB^{TM} with the results obtained from simulation and the developed relationship between the drag force and the flow velocity is presented as follows:

$$D_v = 25.48v^2 + 3.902v \tag{4.28}$$

Here 'D_v' is the drag force experienced and 'v' is the velocity along the Y-axis.

Figure 4.19 shows the turbulence intensity, velocity, and pressure contour from the simulation carried at 1.25 m/s inlet velocity along Z-axis. From Fig. 4.19 it is observed that high turbulence intensity and low pressure zone are developed on the top side of the AUV.

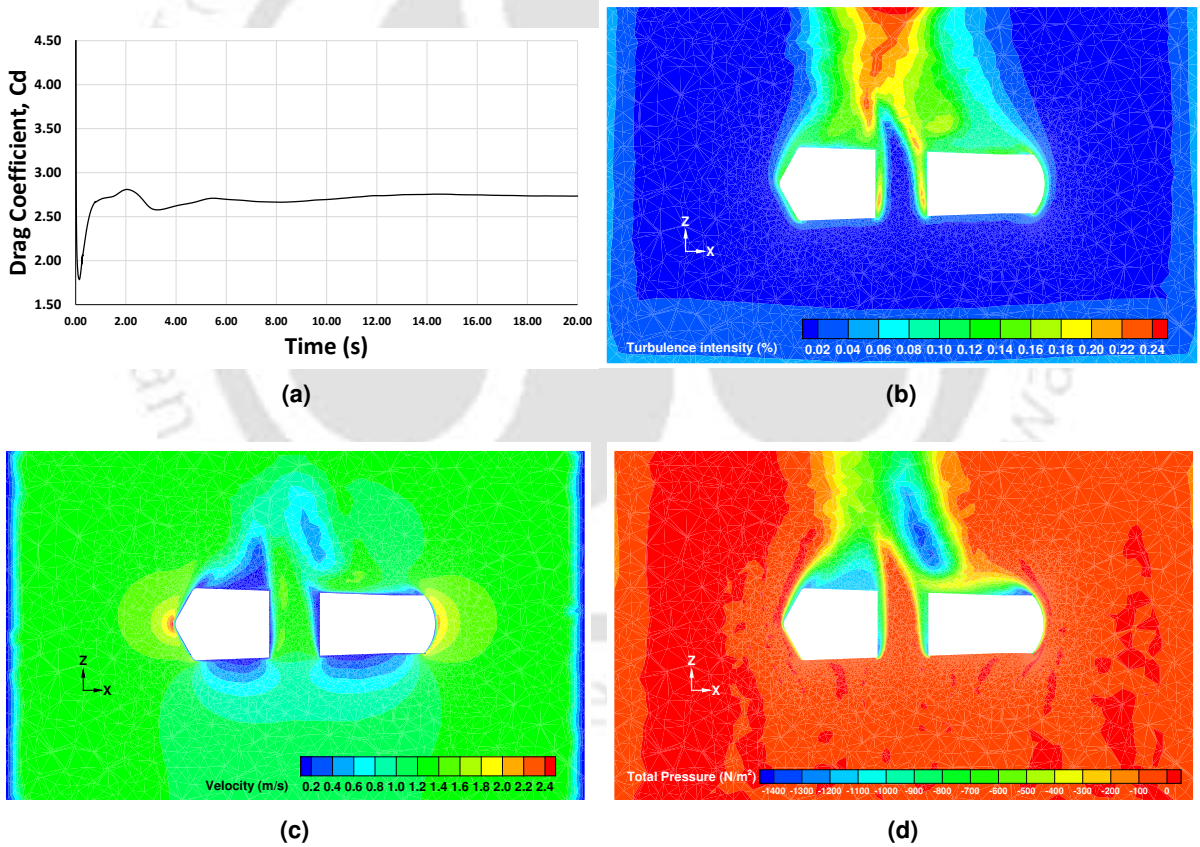

Figure 4.19: (a)Variation of drag coefficient with time (b)Turbulence intensity (%) contour (c)Velocity magnitude (m/s) contour (d)Total pressure (m/s^2) contour for 1.25 m/s flow in the Z direction

After quadratic curve fitting of the simulated results the relationship between the drag and

the flow velocity is presented as:

$$D_w = 125.5w^2 + 6.574w \tag{4.29}$$

Here 'D_w' is the drag force experienced and 'w' is the velocity along the Z-axis.

Table 4.7: Variation of drag coefficient and average drag force with flow velocity along Z direction

Flow velocity (m/s)	Drag coefficient C_d	Avg. drag force (N)
0.50	2.72	34.14
0.75	2.73	77.09
1.00	2.61	131.03
1.25	2.58	202.22
1.50	2.59	292.33
1.75	2.60	400.51
2.00	2.55	512.67

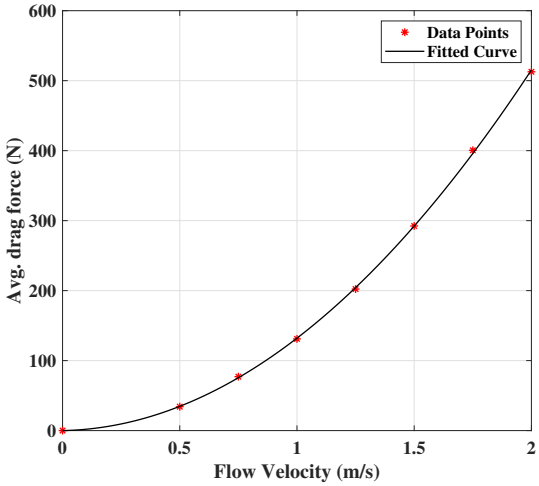

Figure 4.20: Avg. drag vs flow velocity in Z-axis

Moment coefficients obtained in the yaw simulations are used to estimate the torque using the following expression.

$$M_z = \frac{1}{2}\rho C_m A_c L_c (Rr)^2 \tag{4.30}$$

where M_z is the drag torque experienced due to angular motion about the heave direction, ρ is the density of the surrounding fluid, C_m is the moment coefficient, L_c is the characteristic length, $R = L_c/2$, r is the angular velocity, and A_c is the projected area in X-Y plain. The projected area is determined to be 0.1005 m^2 from the CAD model. Figure 4.21 presents the turbulence intensity, velocity, and pressure contour from the simulation carried at 40 rpm rotational velocity about Z-axis in accordance with the physics of the problem.

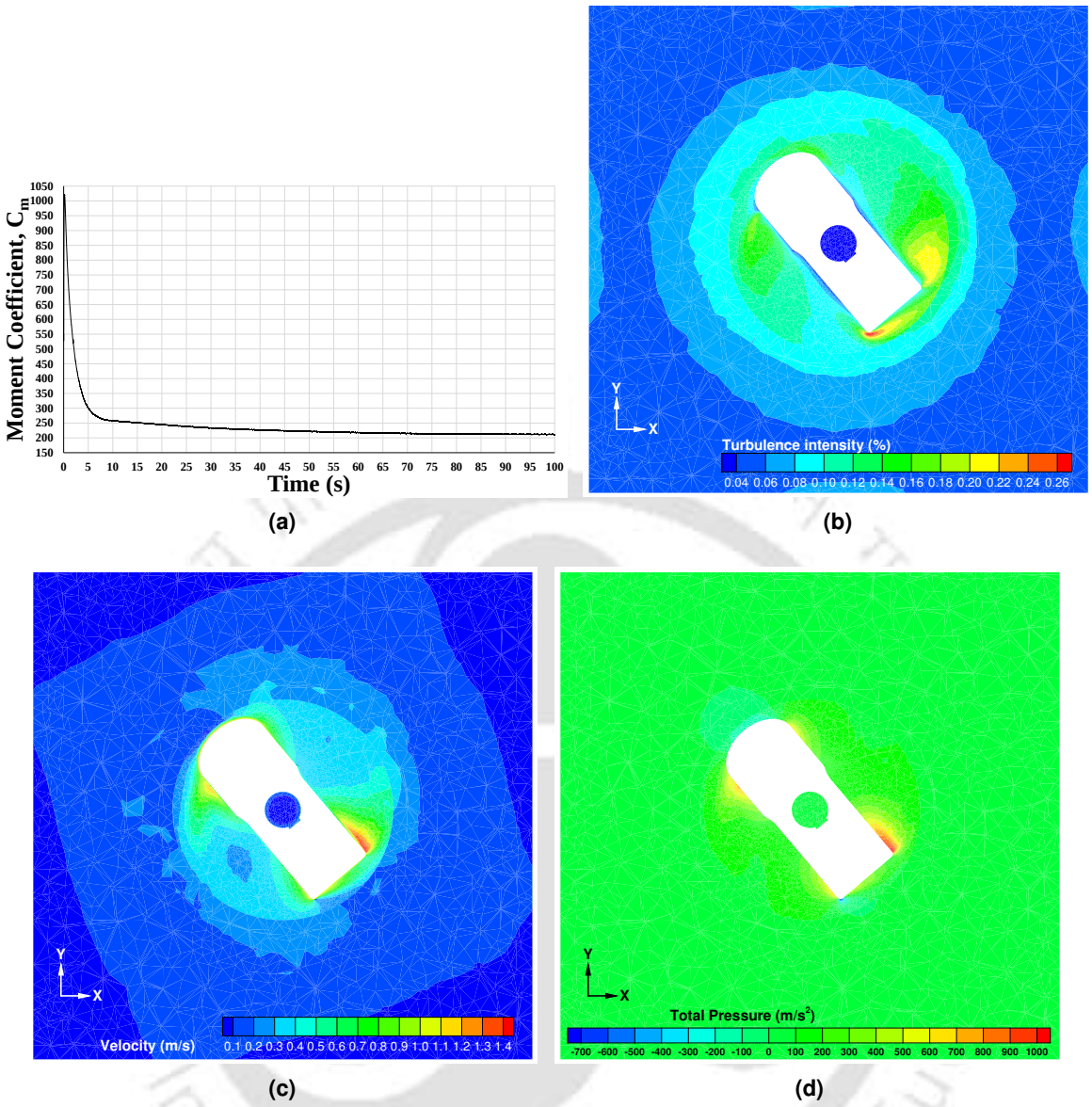

Figure 4.21: (a)Variation of moment coefficient with time (b)Turbulence intensity contour (c)Velocity contour (d)Total pressure contour for 40 rpm angular velocity about Z-direction

Moment coefficient and average torque obtained form simulations are presented in the Table. 4.8. An quadratic curve (Fig. 4.22) is fitted using MATLAB^{TM}. The relationship between the torque and the angular velocity is presented as:

$$M_w = \begin{cases} 2.414r^2 - 11.53r + 14.37 & ; \ r \geq 2 \\ 0 & ; \ r < 2 \end{cases} \tag{4.31}$$

Here 'M_w' is the torque experienced and 'r' is the angular velocity about the Z-axis. Here 1.16×10^{-19} is the linear damping and 4.795 is the quadratic damping parameter.

Table 4.8: Variation of torque with angular velocity about Z direction

Angular Velocity (rad/s)	Moment Coefficient C_m	Avg. torque (Nm)
2.09	62.6	0.60
3.14	117.0	.54
4.19	202.0	7.79
5.23	337.0	20.30

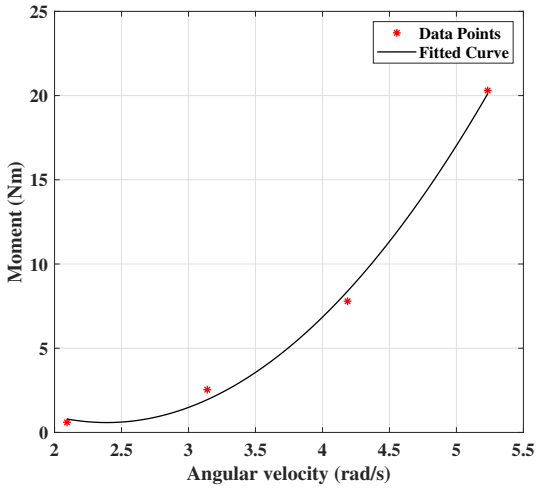

Figure 4.22: Avg. torque with angular velocity (rad/s)

From the above equations the linear and quadratic damping terms are obtained which are presented in the Table. 4.9.

Table 4.9: Estimated hydrodynamic damping parameters

Direction	Linear Damping	Quadratic Damping
Surge	0	4.79
Sway	3.90	25.48
Heave	6.57	125.50
Yaw	-11.53	2.41

4.3.4 Thruster Input

The correlation between the input Pulse Width Modulation (PWM) signal and the corresponding thrust output of the thrusters used, need to be developed to complete the AUV model. Then the input parameters can be selected depending on the thrust requirement by the AUV. Experimental data of the thrust output and the corresponding control signal input is available from the thruster manufacturer BlueRobotics [161]. The plot of the input PWM signal and the thrust output is presented in the Fig. 4.23. PWM signal varies from 1500 to 1900 for forward thrust and 1100 to 1500 for backward thrust.

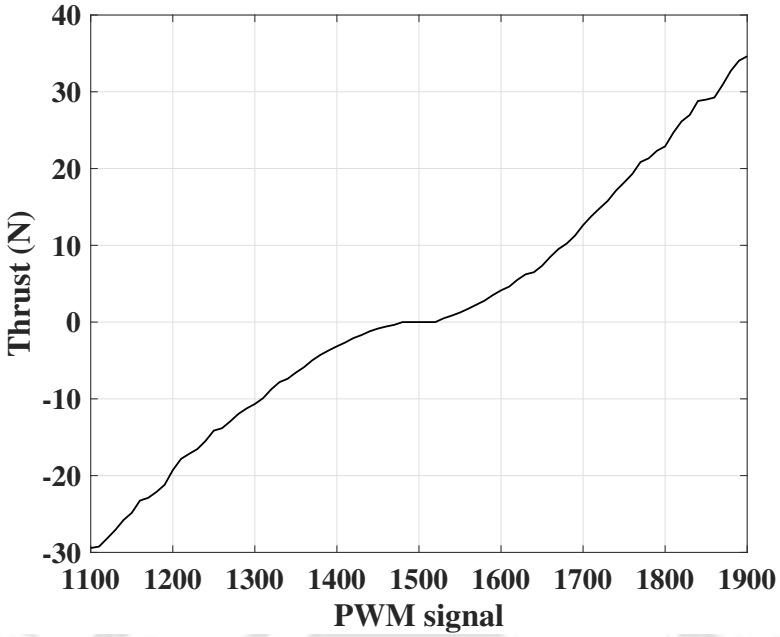

Figure 4.23: Thrust vs Input signal (BlueRobotics T200BlueRobotics [161])

With these data-set two cubic curves are fitted for forward and backward thrust as shown in Fig. 4.24. The correlation between the thrust output and the PWM signal is obtained as:

$$T_B = -2.015^{-7}P^3 + 0.00067P^2 - 0.638P + 128.8 \tag{4.32}$$

$$T_F = -3.955^{-7}P^3 + 0.00213P^2 - 3.724P + 2119 \tag{4.33}$$

where, T_B is the Backward Thrust, T_F is the Forward Thrust and P is the PWM signal. These expressions can be used to find out the thrust developed for corresponding PWM signal.

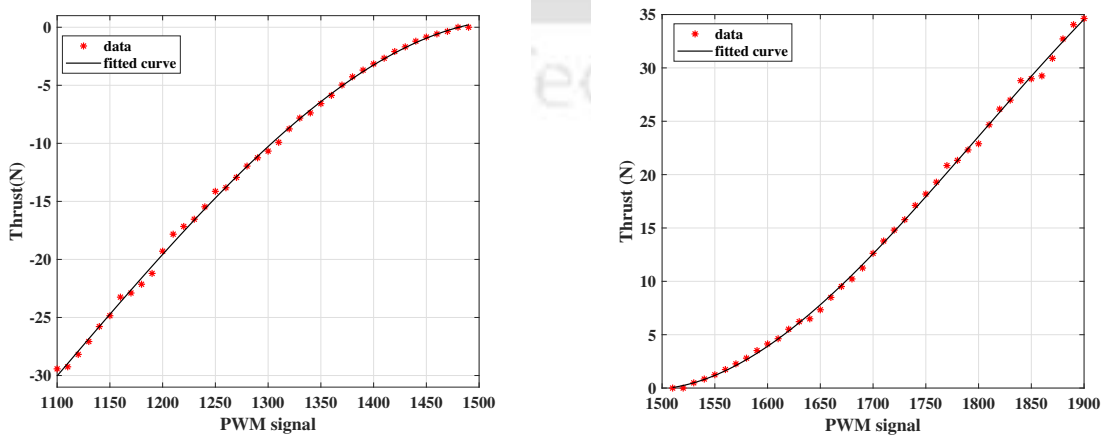

(a) Backward (b) Forward

Figure 4.24: Variation of PWM signal with thrust in (a) backward and (b) forward direction

When used with the controller, the PWM signal corresponding to the required thrust will be communicated to the actuators. For this purpose the following expressions can be used to estimate the control signal for corresponding thrust.

$$P = 0.01098T_B^3 + 0.6703T_B^2 + 22.78T_B + 1472 \tag{4.34}$$

$$P = 0.008409T_F^3 - 0.5479T_F^2 + 19.88T_F + 1524 \tag{4.35}$$

These correlations are developed by cubic curve fitting as shown in Fig. 4.25.

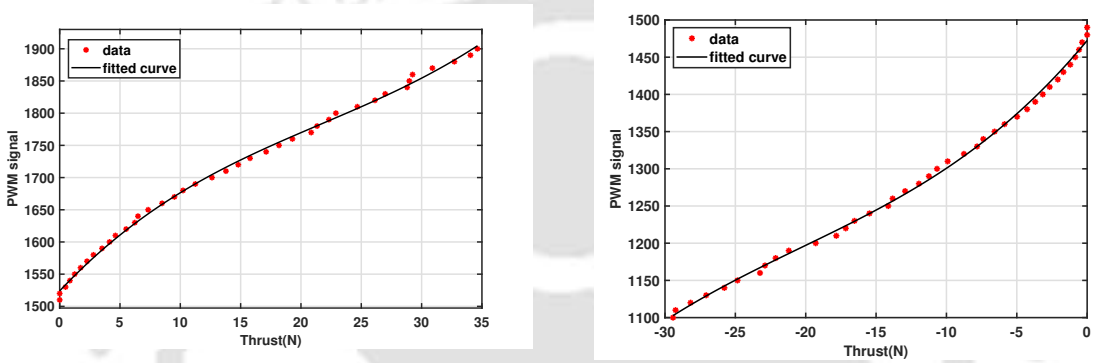

(a) Backward (b) Forward

Figure 4.25: Variation of thrust with PWM signal in (a) backward and (b) forward direction

4.4 Simulation and Field Test

Detailed mathematical model with system parameter estimation is presented in the previous section. Using this developed model, a simulation platform is created in the MATLAB^{TM} Simulink^{TM} environment. Multiple simulations has been carried out to verify the basic behaviour of AUV motion. Further more the field test results are compared with the simulated results with same input conditions to validate the developed model and results are presented in this section.

4.4.1 Simulink Model

A MATLAB^{TM} Simulink^{TM} model (Fig. 4.26) is created using the developed AUV model. The SIMULINK^{TM} model estimates the AUV position depending on the PWM signal input

to the thrusters. Using the developed empirical relations in the previous section, thrust of the individual actuators are calculated. The palnt model is simulated with equal control signals to the side thrusters generating a linear motion of the AUV as shown in Fig. 4.27(a). Figure 4.27(b) presents a simulated scenario of the AUV along a curved path generated with unequal control signal to the side thrusters.

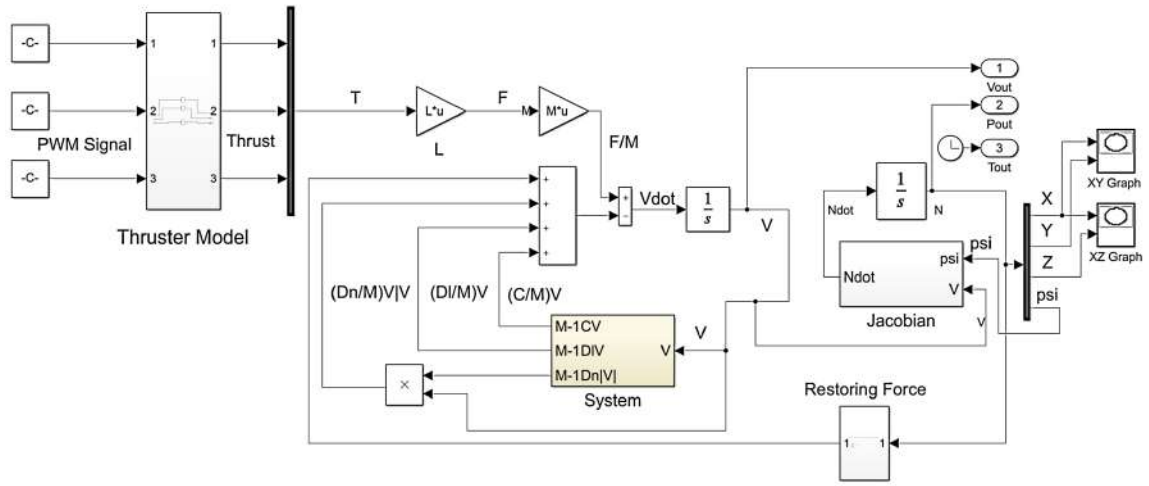

Figure 4.26: Robot plant model

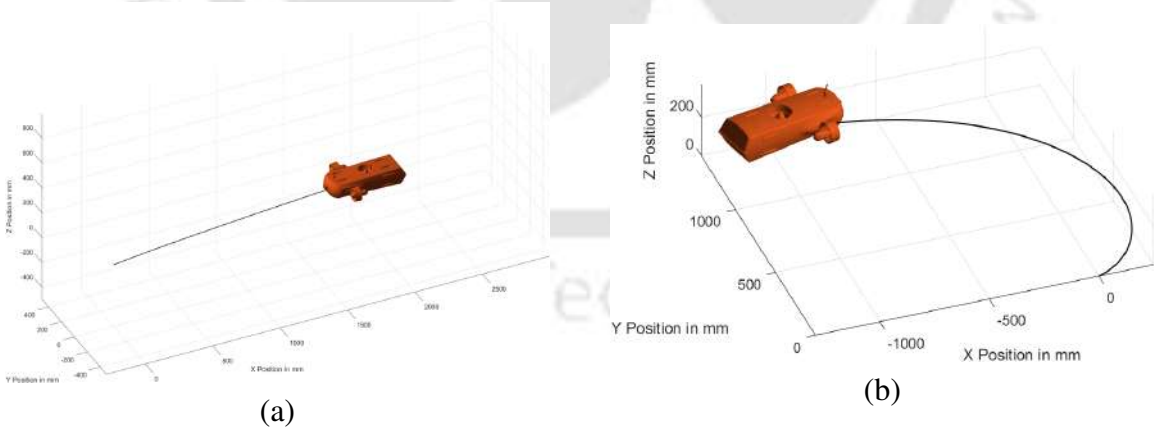

(a) (b)

Figure 4.27: Simulation of plant model for (a)linear trajectory (b)curved trajectory

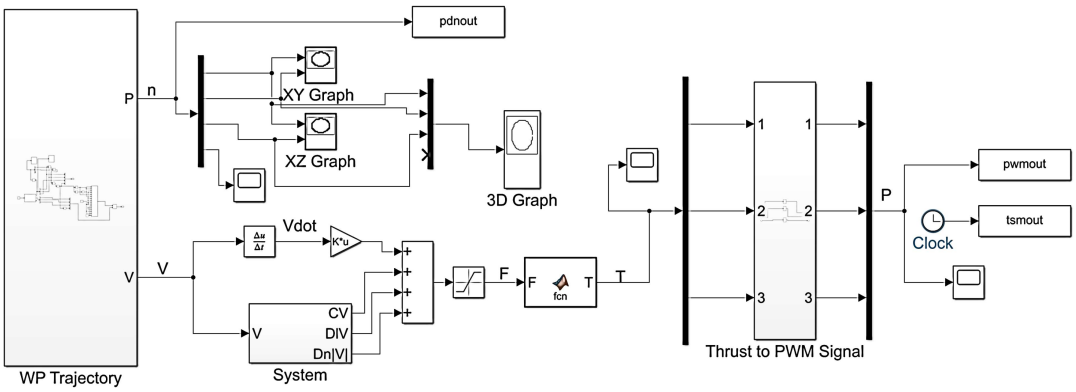

Figure 4.28: Open-loop controller

For AUV applications, the system model is used to estimate the control signal inputs for the actuators for the desired motion of the AUV. First, in path-planning the desired path of the AUVs or trajectories are developed in terms of position, velocity and accelerations in the global frame. Then the position, velocity and acceleration are converted to the body frame using the inverse kinematic model. Further the body-frame motion parameters are used to estimate the actuation force and thus the input PWM signals using the dynamic model. In open loop controllers, the required actuator input signal for desired motion output are estimated, without any feedback. Such an open loop controller is developed in MATLAB^{TM} Simulink^{TM} (Fig. 4.28). This controller uses a way-point trajectory generated with B-spline method. The controller is simulated with way-points (0 0 0), (0 1 1), (1 1 1.5), (1 0 2), (2 0 1.5),and (2 1 1) presented in Fig. 4.28 and the estimated control signal is presented in Fig. 4.30.

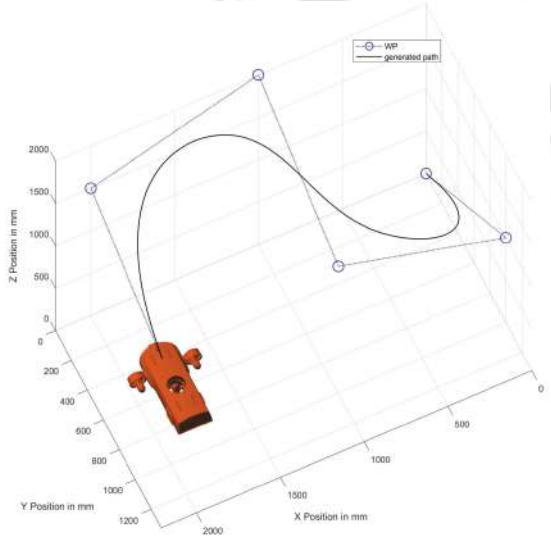

Figure 4.29: Simulation of open-loop controller

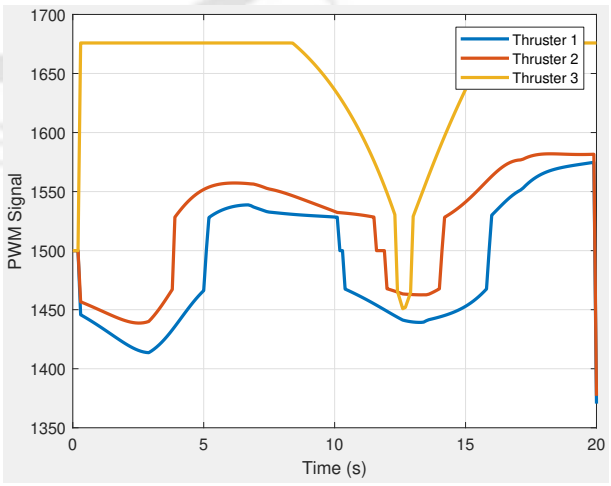

Figure 4.30: Estimated PWM signal

4.4.2 Field Test

The Underwater robot is deployed successfully in different water bodies. For validating the dynamic model of the system the PWM signal inputs to the thrusters and the depth sensor readings are recorded during a field run of the robot in a lake (Fig. 4.31). The developed MATLAB^{TM} model is simulated with the recorded PWM signals. The depth output of the simulation is compared with the actual depth sensor reading for the field operations presented in the Fig. 4.33. The depth data is selected for comparison as the AUV has a depth sensor with a resolution of 2 mm which can measure upto 300 m depth. From the Fig. 4.33 it is observed that the overall trend of the predicted heave motion by the model matches the actual heave motion from the field run. But there exist 4.5% and 13.63% percent error in estimation of maximum depth the AUV travelled during the heave motion. Similarly recorded PWM signals from another field run in a river dam (fig. 4.32) is simulated in MATLAB^{TM} with the developed model and the comparison of the model prediction with recorded depth data is presented in the fig. 4.34. Here the AUV model successfully predicted the overall trend of the actual heave motion but there exist 0.1% error in prediction of maximum depth achieved. It may be noted that the consideration of added-mass improved the over all prediction. The errors present may be due to unknown environmental forces and conditions which are difficult to model. Thus a robust feedback controller development is essential, which can compensate for the errors and accurate desired motion can be achieved.

Figure 4.31: Field test in a lake

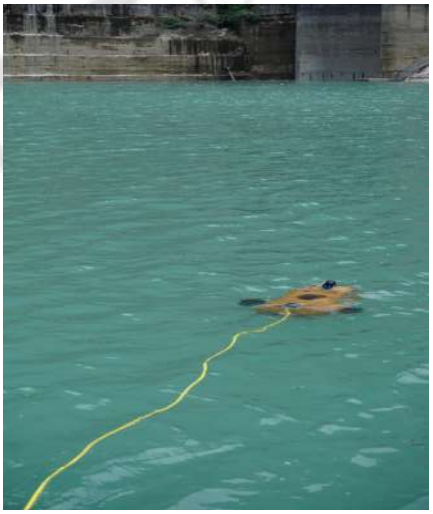

Figure 4.32: Field test in a dam

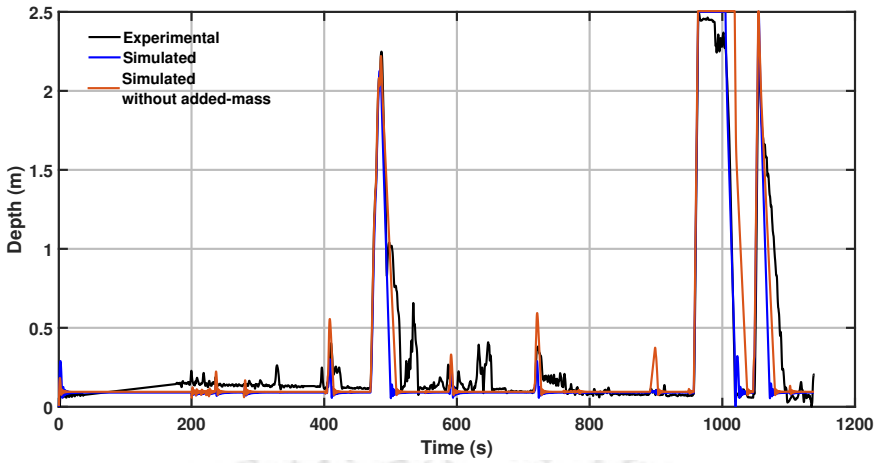

Figure 4.33: Variation of depth during field test in lake vs simulated output

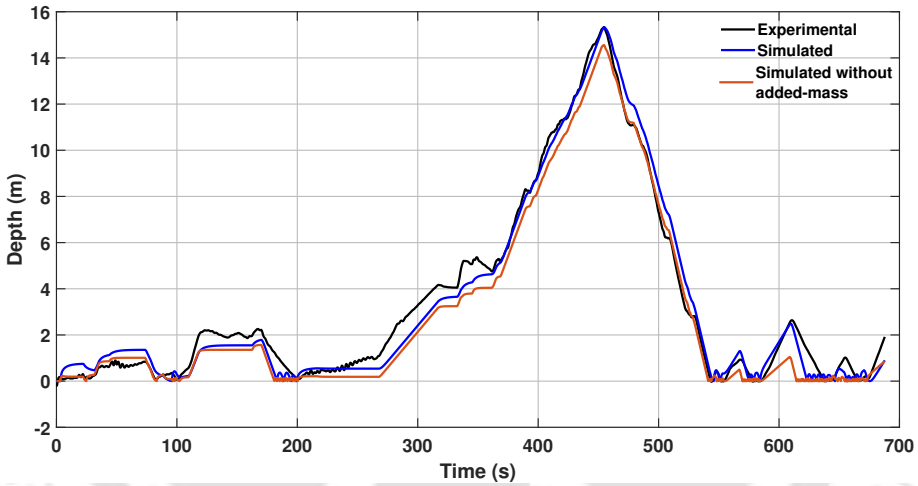

Figure 4.34: Variation of depth during field test in dam vs simulated output

4.5 Summary

Detailed mathematical modeling of the developed AUV is presented in this Chapter. Inertia, C.G and C.B are estimated with a detailed CAD model developed with the software "SOLIDWORKS". To determine hydrodynamic damping parameters, multiple CFD analysis has been carried out with ANSYS FLUENT^{TM} package. Motion along surge, sway, heave, and yaw are simulated to find drag forces acting at different velocities. With estimated forces at different velocities, relationships are established to find out drag forces at different motion conditions. Added mass coefficients are determined numerically using the slender body theory. From the experimental data of the actuators empirical relations have been established between control

signal and thrust output. MATLAB^{TM} Simulink^{TM} model is developed to simulate different AUV motion conditions. Inverse kinematic model is developed to estimate the control signal for the AUV to follow a way-point trajectory developed with B-spline method. Control signal recorded from the field tests are simulated to validate the developed dynamic model with reasonable accuracy. Though the model is able to predict the overall trend of the motion but there exist 4.5% error in prediction of maximum traveled depth during heave motion. For another such comparison with experimental data of the upgraded model with neutral buoyant cable, the error is 0.1%. The developed mathematical model of the system is further used in development of closed loop control system for autonomous operation, which is discussed in the next chapter.

Chapter 5

NAVIGATION, PLANNING AND CONTROL OF THE AUV

5.1 Introduction

An AUV to work autonomously should be able to reach a static or dynamic target or follow a predefined path. To achieve this autonomy a guidance system works closely with the system controller. Guidance system generates next desired position of the AUV depending on the predefined target and the control system helps the AUV achieve that target location by adjusting the propeller output. Guidance system uses way-point navigation with Line-Of-Sight(LOS) technique. Localization is another vital component in navigation, as the system needs to aware of its location in-order to reach a target. Among different navigation systems, Inertial Navigation System (INS) is suitable for small-scale AUVs for short missions and long missions with GPS where resurfacing is allowed. In this chapter, following the introductory section, section 5.2 presents a 3D guidance system for the AUV using LOS technique. Section 5.3 discusses the development of PD and PID based closed-loop control systems. An INS system for localization is presented in the section 5.4. Summary of the chapter is presented in section 5.5.

5.2 3D Guidance system

LOS is a most widely used guidance system for its simplicity and ease of implementation. LOS technique uses a very simple strategy illustrated in Fig. 5.1 that is to constrain the AUV motion close to the LOS vector between the start point and target. The desired orientation angle is calculated by finding the line between the current position and the desired position using the

following equation.

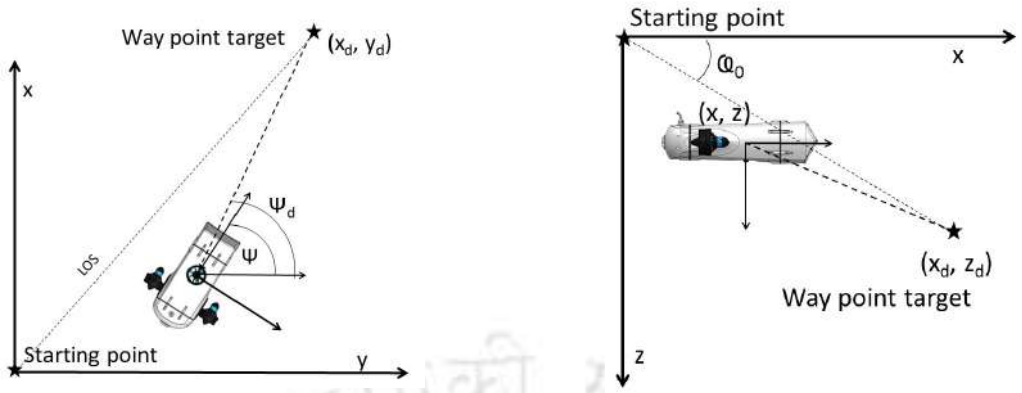

Figure 5.1: LOS Guidance system

$$\Psi_{desired} = \tan^{-1}\left(\frac{y_k - y(t)}{x_k - x(t)}\right) \tag{5.1}$$

Where (x_k, y_k); k = 1, 2 . . . N are the x y coordinates of the N waypoints, and $(x(t), y(t))$ are the x y coordinates of the AUV position at time t.

Heave motion is independent of surge and sway motion but to follow the LOS vector closely the desired Z directional depth should be proportional to the current horizontal height between the AUV and the target. To obtain this desired depth first the angle between the line from start point (x,y,z) to target (x_p, y_p, z_p) and the horizontal plane is calculated using the following equation.

$$\varphi_0 = \tan^{-1}\frac{z_p - z}{\sqrt{(x_p - x)^2 + (y_p - y)^2}} \tag{5.2}$$

For the AUV to keep moving towards the target, along this angle, the desired depth can be calculated from the following equation.

$$z_d(t) = z_p - \tan\varphi_0 \times \sqrt{(x_p - x(t))^2 + (y_p - y(t))^2} \tag{5.3}$$

With desired positions and tracking errors from the guidance system the control system have to control the thruster forces to closely follow the path. Once the AUV is with in certain acceptable radius of the waypoint it is considered that the target is reached and next waypoint is selected. The radius of acceptance (r_a) is generally selected twice the size of the AUV at maximum and

depends on the application. The radius of acceptance is tracked using the equation given below.

$$r(t)^2 = [x_p - x(t)]^2 + [x_p - x(t)]^2 + [x_p - x(t)]^2 \leq r_a^2 \tag{5.4}$$

5.3 Closed-loop Control

The AUV has to follow a predefined path and its motion underwater is controlled with the thrust generated by the actuators. Thus a control system is required to estimate appropriate input signals to the thrusters to produce the required thrust. The required thrusts are estimated using feedback from the position sensors or dynamic model of the system. A closed-loop controller will help AUV follow the desired path.

5.3.1 PD Controller

Development of a simple open-loop control system based on the dynamic model of the AUV is presented in detail in the previous chapter. The AUV is a 4 DOF coupled non-linear system. In this chapter a partitioning control law is used and the controller is divided into a model-based portion and a servo portion. System parameters ($M_{RB}, C_{RB}, D_l and D_n$) comes in the model-based portion and the servo portion is independent.

As stated in the previous chapter the open-loop equation of the model can be expressed as follows:

$$M_{RB}\ddot{X} + C_{RB}\dot{X} + D_l\dot{X} + D_n\dot{X} = f \tag{5.5}$$

The controller for this system is decomposed into two parts. Model-based portion utilizes $M_{RB}, C_{RB}, D_l and D_n$. The model-based portion is reduced to unit mass system and the control gains in the servo portion are tuned for unit mass.

The model-based portion is of the form

$$f = \alpha f' + \beta \tag{5.6}$$

For the system to appear as unit mass α and β are selected as:

$$\alpha = M_{RB}, \beta = C_{RB}\dot{X} + D_l\dot{X} + D_n\dot{X} \tag{5.7}$$

Substituting in Eq. 5.6, system equation for unit mass system becomes

$$\ddot{X} = f' \tag{5.8}$$

If the trajectory is given by a function of time, $X_d(t)$, which is double differentiable can provide desired position and velocity. The positional error between desired and final position can be defined as $e = X_d - X$. Designed control law to compute f' is given as follows:

$$f' = \ddot{X}_d + K_d\dot{e} + K_p e \tag{5.9}$$

Where K_d and K_p are the derivative and proportional control gains, respectively. Combining this control law with Eq. 5.8 on may get the following equations.

$$\ddot{X} = \ddot{X}_d + K_d\dot{e} + K_p e \tag{5.10}$$

$$\ddot{e} + \ddot{X}_d + K_d\dot{e} + K_p e = 0 \tag{5.11}$$

In this method control gain tuning is simple and independent of the system parameters and the critical damping condition is given by:

$$K_d = 2\sqrt{K_p} \tag{5.12}$$

The designed control law is implemented with the AUV system using MATLAB^{TM} Simulink^{TM} software shown in Fig. 5.2.

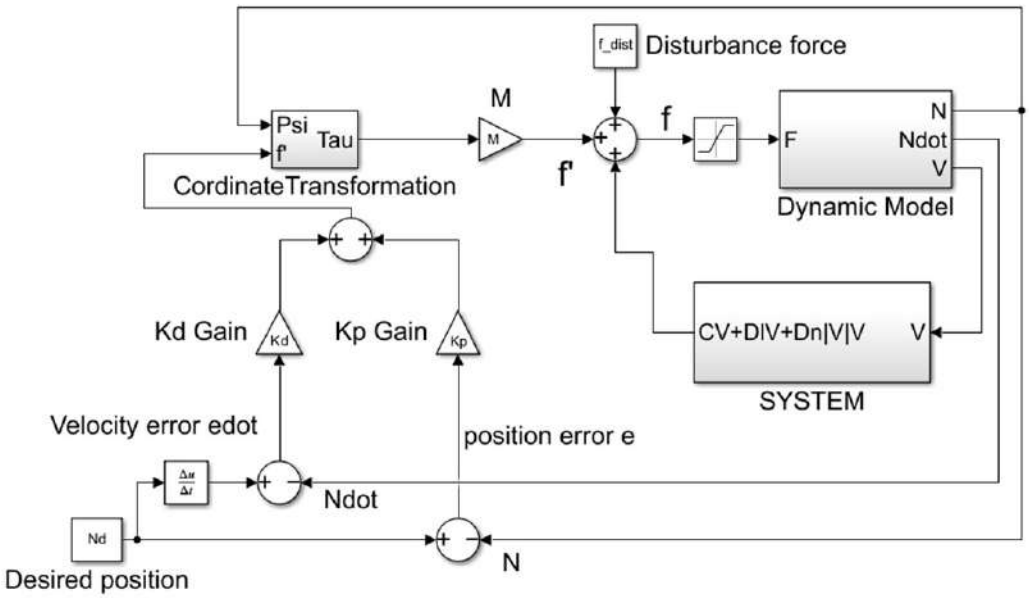

Figure 5.2: PD controller

After developing the control system and the guidance system in MATLAB^{TM} Simulink^{TM} the gain parameters are tuned to receive quick and stable output. Tuned gain parameters are presented in the Table 5.1. Model is simulated with target position at (10, 7, 6) m along the x, y , z directions in global frame with origin at the starting point of the AUV. Force limiter is used to limit the thrust input not to go beyond the maximum possible thrust output. As each thruster can produce maximum of 34 N of force a saturation block is used to maintain the upper limit of the force out from the controller. Simulated result of the virtual model reaching the target position is presented in the Fig. 5.3 and the tracking error is shown in Fig. 5.4. Figure 5.5 represents the 3D position tracking of the robot. It can be observed from the Fig. 5.4 that Y degree of freedom has a constant steady state error of 20 cm. Error is due to the absence of active thrust in sway-direction. A PID controller can help element this constant steady state error which is presented in the next section.

Table 5.1: Controller gain parameters

positions	k_p	velocities	k_v
x	0078.70	u	17.69
y	0000.71	v	01.68
z	0232.97	w	30.53
ψ	2162.00	r	92.99

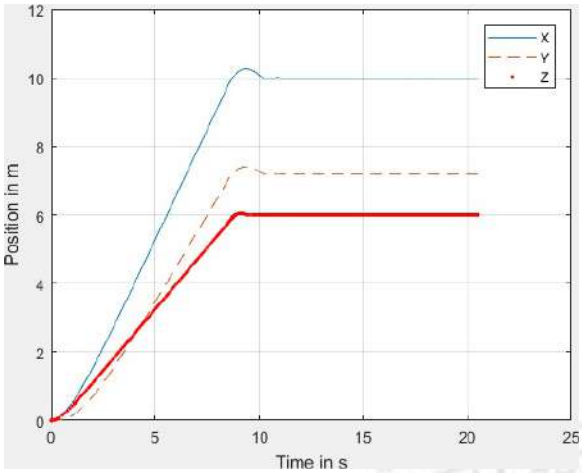

Figure 5.3: Position with time

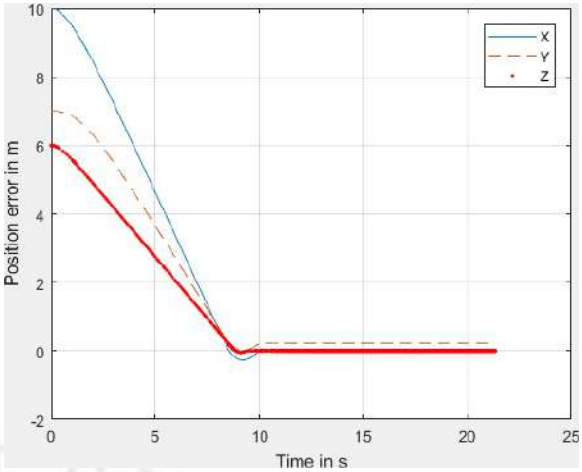

Figure 5.4: Tracking error with time

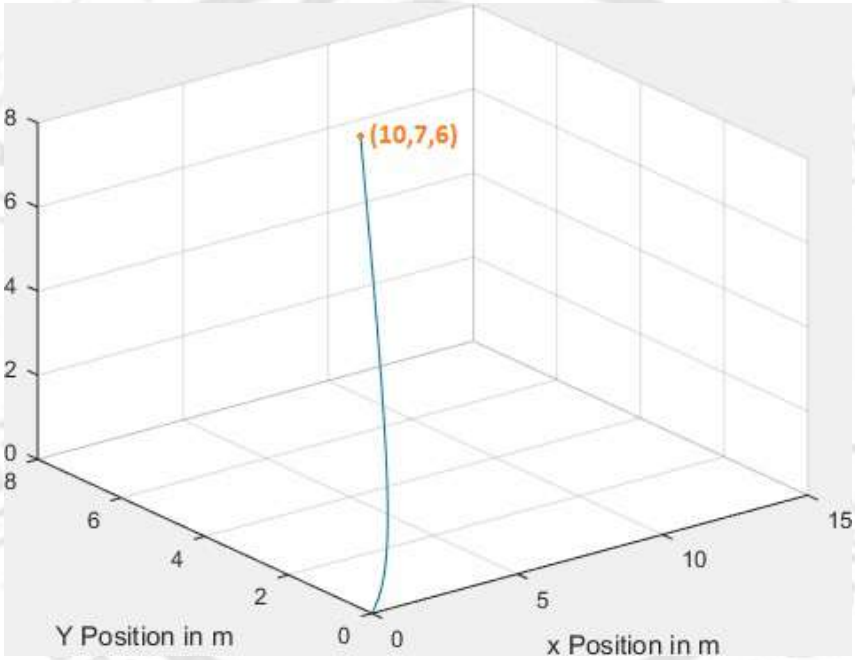

Figure 5.5: 3D position tracking

5.3.2 PID Control

For the PID controller the integral term is introduced in the the control law as follows. The same partitioning control law is used and the controller is divided into a model-based portion and a servo portion. System parameters ($M_{RB}, C_{RB}, D_l and D_n$) comes in the model-based portion and the servo portion is independent.

Designed control law to compute f' :

$$f' = \ddot{X}_d + K_d\dot{e} + K_p e + k_i \int e dt \tag{5.13}$$

Combining this control law with the eq. 5.8,

$$\ddot{X} = \ddot{X}_d + K_d\dot{e} + K_p e + k_i \int e dt \tag{5.14}$$

$$\ddot{e} + K_d\dot{e} + K_p e + k_i \int e dt = 0 \tag{5.15}$$

In presence of a constant steady-state error, the modified control law for this unit mass system can be presented as follows.

$$\ddot{e} + K_d\dot{e} + K_p e + k_i \int e dt = f_{dist} \tag{5.16}$$

Here f_{dist} is the disturbance.

Simulink Model

The designed control law is implemented with the AUV system using MATLAB^{TM} Simulink^{TM} software shown in Fig 5.7. Desired positions and velocities from the guidance system are the input to the controller. Depending on the input the controller estimates the thrust of the propellers and run the thrusters. The feedback loop which incorporates a localization system, feeds the live position and orientation data. Controller over time tries to minimize the error. In this simulation reverse plant model is used to estimate the position instead of a localization system. Saturation block is used to restrict the thrust output to go beyond the maximum possible value. Each thruster can produce maximum of 34 N force when operating at 12V. For the AUV to maintain its path close to the LOS vector Eqn. 5.3 is used to calculate the desired $Z_d(t)$ in each iteration.

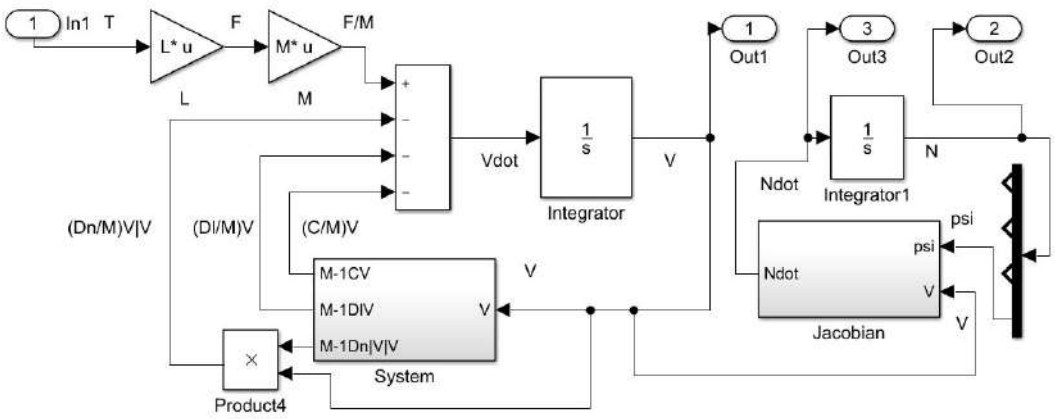

Figure 5.6: PLANT MODEL

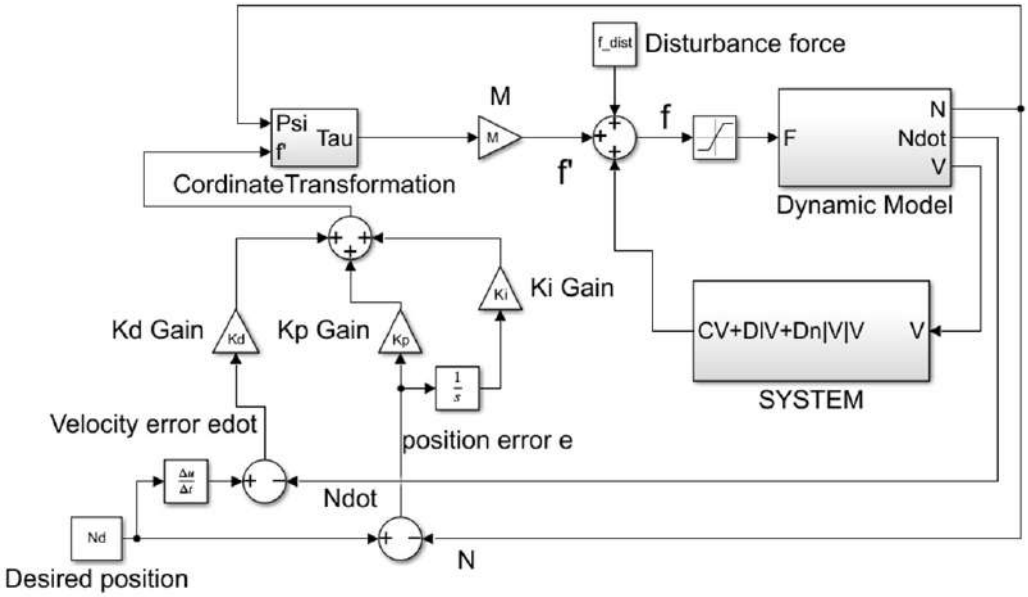

Figure 5.7: SIMULINK model of PID controller

Simulation Result

Control gain tuning is independent of the system parameters as control partitioning technique is used. To tune the control gains, initially the system equation is reduced to be linear by considering non-linear term coefficients to be zero. Then the K_p value is calculated from the critically damped condition of the linear system considering the damping ratio to be 0.5. Staring with this K_p value the final value is selected by trail and error method till quick stable response without much oscillation and overshoot is achieved. Then differential gain K_d selection started

from critical damping condition and adjusted with trail and error. In presence of steady state error small Ki value is introduced. The tuned gains are presented in Table. 5.2 After tuning the

Table 5.2: Controller gain parameters

position	k_p	k_i	velocity	k_v
x	78.70	0	u	17.69
y	0.71	-2.1	v	1.68
z	232.97	0	w	30.53
ψ	2162.00	0	r	92.99

gain values the SIMULINK model is used for simulation with target 3D point as (10,7,6) m. Figure 5.8 presents the position tracking with time and the Fig. 5.9 presents the error tracking with time. Comparing error tracking of the PID controller shown in Fig. 5.9 with PD controller shown in Fig. 5.4 shows the PID controller greatly reduces the steady-state error, generated because of cross-coupling and external disturbances. Maximum steady-state error is presented in the Table. 5.3.

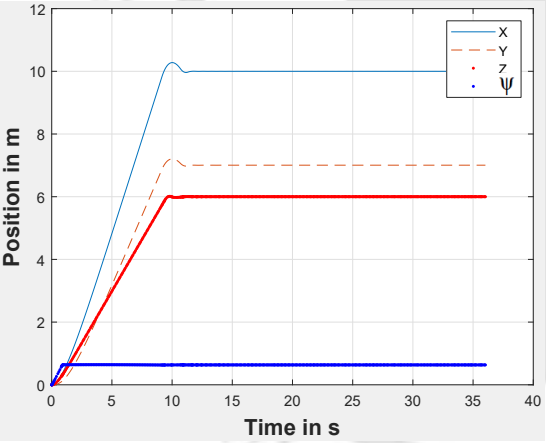

Figure 5.8: PID POSITION TRACKING

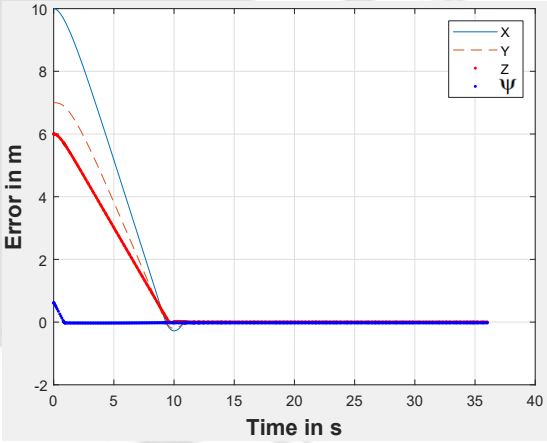

Figure 5.9: PID Error Tracking

Table 5.3: Steady-state error

Direction	Steady-state error
x	4.1 x 10^{-5} m
y	0.0050 m
z	0.0002 m
ψ	0.0226 rad

2D Multi Way-point Trajectory

AUV to work autonomously need to follow a predefined path. The path is generated by connecting multiple way-points with straight lines. LOS strategy is used to closely follow the LOS vector connecting the way-points. From the target way-point and current position desired yaw angle and Z-position is calculated using formulas mentioned in the section(). Radius of acceptance is considered to be 20 c.m and once the position is within this radius the next way-point is selected as the target position. Simulation for a zig-zag multi way-point path is carried out and the position and error tracking results are presented in Fig. 5.10 and Fig. 5.11, respectively. Way-points are (0,0) (3,4) (6,1) (8,4). In the PID controller control gains are not universal, thus for a different path the controller has to be tuned separately. The tuned control gains for this 2D path is presented in the Table. 5.4. Desired position input and the controller output along x-axis and y-axis are presented in Fig. 5.12 and Fig. 5.13 respectively. It may be noted that the next target position is selected when the current position enters inside the acceptance radius of the desired value.

Table 5.4: Controller gain parameters

position	k_p	k_i	velocity	k_v
x	17.00	0	u	17.69
y	0.71	-0.1	v	01.68
z	232.97	0	w	30.53
ψ	2162.00	0	r	92.99

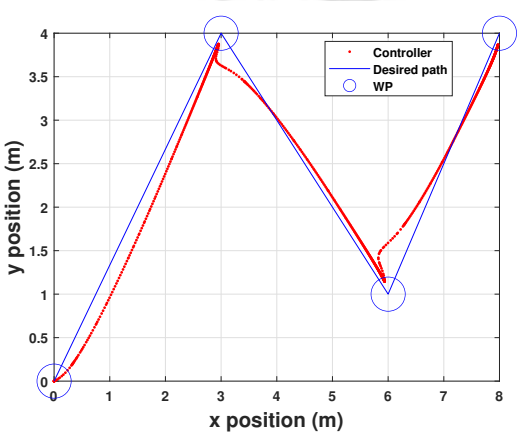

Figure 5.10: Position with time

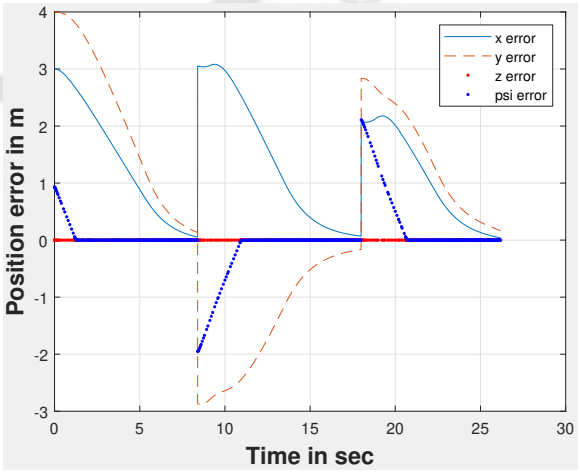

Figure 5.11: Position error with time

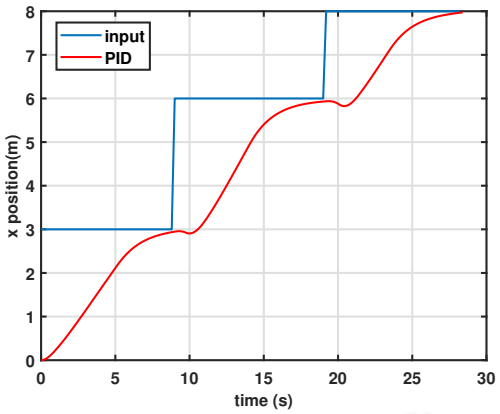

Figure 5.12: X position with time

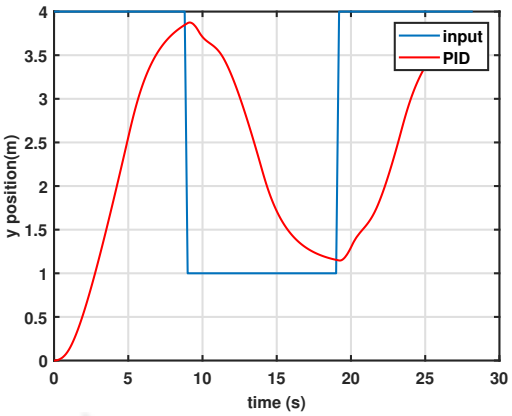

Figure 5.13: Y position error with time

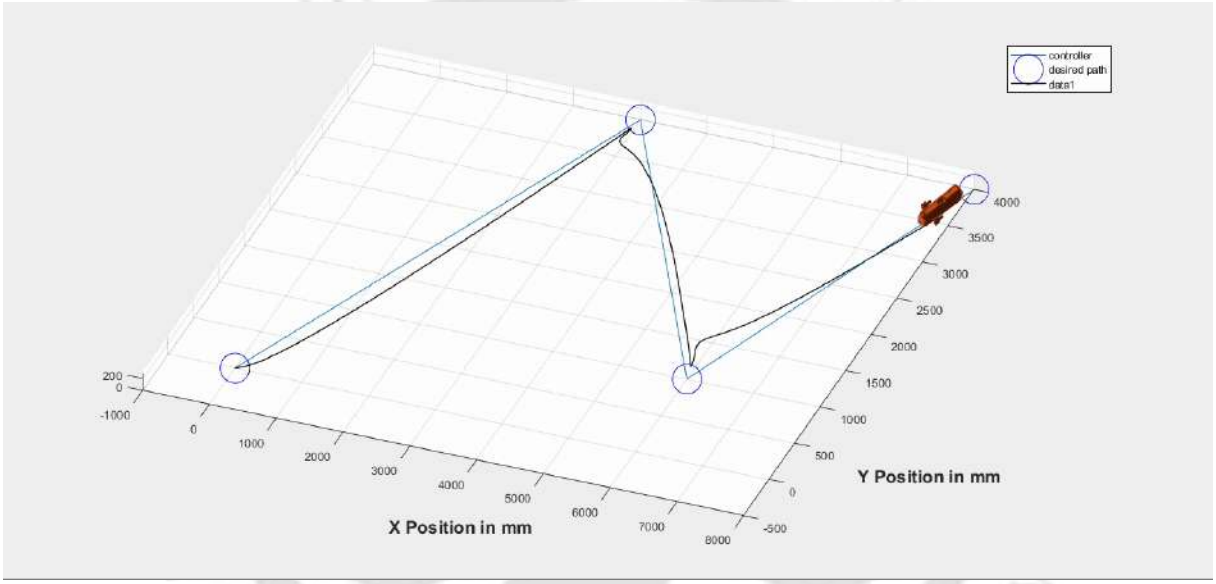

Figure 5.14: SIMULINK WAY-POINT TRACKING SIMULATION

3D Multi Way-point Trajectory

Simulation for a curved multi way-point path is carried out. Way-points are 10 equidistant points in x and z axes from 0 to 6 and 0 to 3, respectively and y-coordinates are in form of a sine function of x-coordinates. The tuned control gains for this 3D path is presented in the Table. 5.5. The position tracking result is presented in Fig. 5.15. The error tracking is presented in Fig. 5.16. Desired position input and the controller output along x-axis, y-axis and z-axis are presented in Fig. 5.17,5.18 and 5.19, respectively. The plots shows the PID controller achieves the desired position without overshooting or oscillations. When the position of the robot is within the acceptance radius of the waypoint the next target waypoint is selected and controller

gradually minimises the errors and achieve the target position.

Table 5.5: Controller gain parameters

position	k_p	k_i	velocity	k_v
x	12.00	0	u	17.69
y	0.71	-0.1	v	1.68
z	20.00	0	w	30.53
ψ	200.00	0	r	92.99

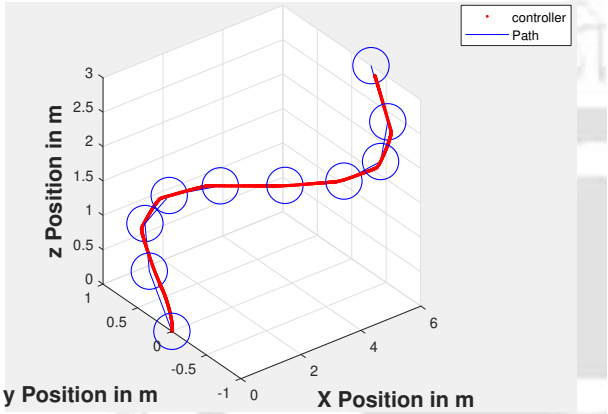

Figure 5.15: Position with time

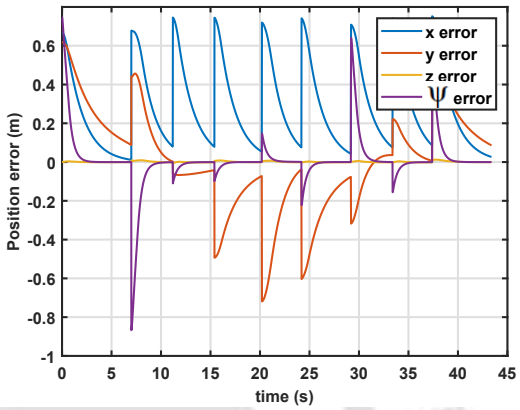

Figure 5.16: Position error with time

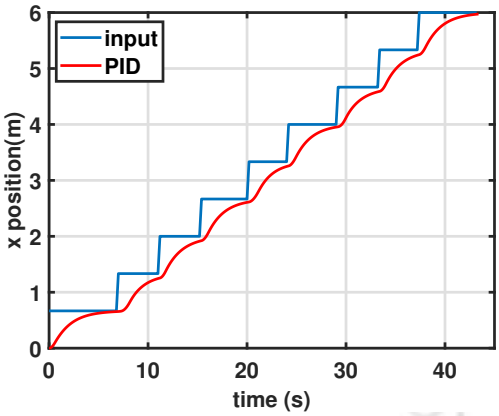

Figure 5.17: X position with time

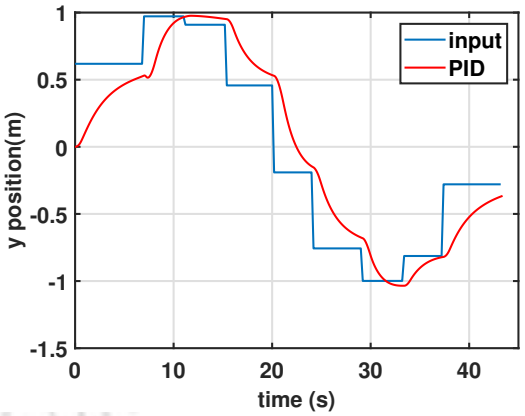

Figure 5.18: Y position with time

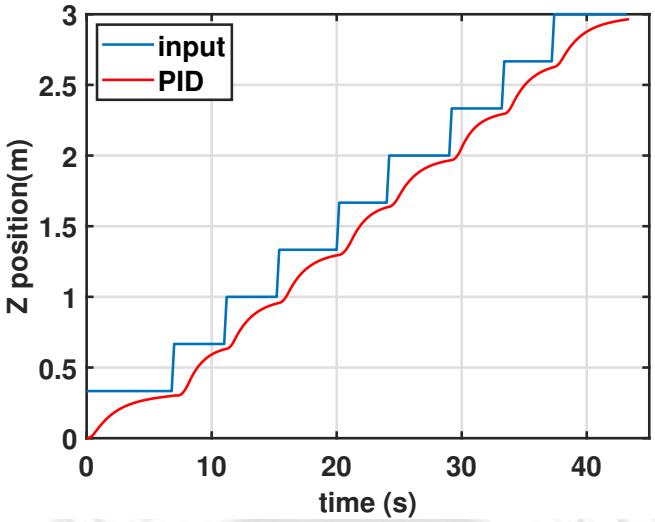

Figure 5.19: Z position with time

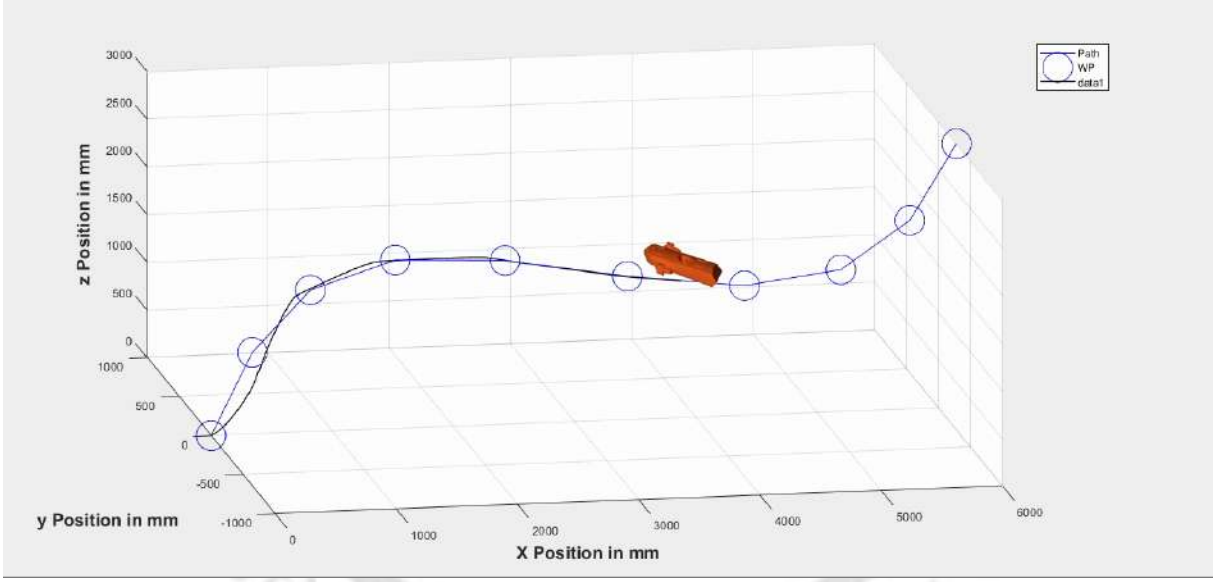

Figure 5.20: 3D WAY-POINT TRACKING SIMULATION

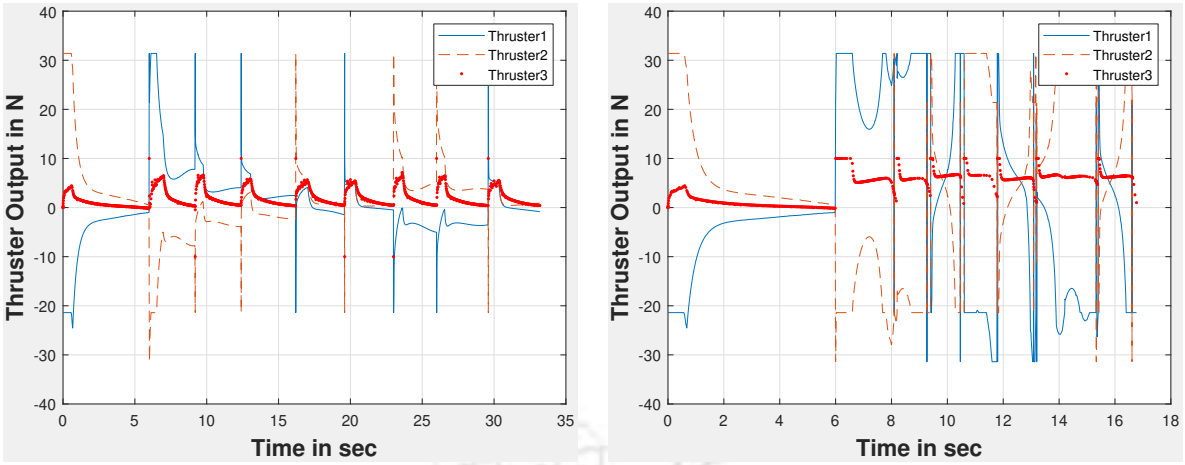

Figure 5.21: Thrust output from controller for (a) zero velocity (b) continuous velocity at way-point

As shown in Fig. 5.21 (a) the controller slows down and the thrust output drops to zero but by implementing a constant velocity at the way points as shown in the Fig. 5.21 (b) the thrust output is maintained at a constant level at the waypoints without slowing down and the path can be achieved quicker.

5.4 Inertial Navigation System

INS calculates relative position and orientation of a dynamic system relative to a known starting point, orientation, and velocity using the data from motion sensors (accelerometers), and rotation sensors (gyroscopes). INS is a compact, inexpensive and self-contained system which does not require external references. Therefore, it can be used for inexpensive small AUVs. However, INS can accumulate error over time because the estimated relative velocity and position are the result of mathematical integration of the accelerometer and gyroscopic sensor data. Errors in the measurement of the sensor data and errors introduced in integration lead to a significant drift in the estimated position and velocity. Therefore, the estimated position from INS needs to be compared with the data from other sensors using a techniques like Kalman Filter to produce accurate state. These state estimation techniques are discussed further in the following section.

5.4.1 State estimator

AUVs are equipped with different sensors which can provide real-time quantitative data of the surrounding. All these sensor data have to be processed together using some techniques to obtain an optimal estimate of the vehicle position which are called state estimators. Some of these techniques are Kalman Filters (KFs), Particle Filters (PFs), and Simultaneous localization and mapping (SLAM). From these techniques, KFs and PFs are numerical techniques for sensor fusion.

Kalman Filter (KF) is used to derive the best estimate of position from different sensors used. The KF estimates the state of a system from multiple uncertain observations using a predict update cycle. A physical model describing AUV motion can be highly non-linear where the KF fails. In such a non-linear model case, an Extended Kalman Filter (EKF) can be used. EKF uses a first-order Taylor series to approximate the nonlinear processes to linear system. This method will fail for systems with high non-linearity. Unscented Kalman Filter (UKF) uses the true nonlinear models and approximates a Gaussian distribution of the state random variable by selecting suitable sigma points with known mean $\bar{x}$ and covariance P_x. Non-linear function is calculated for each points. The statistics of the transformed points are calculated to form an estimate of the non-linearly transformed mean and covariance.

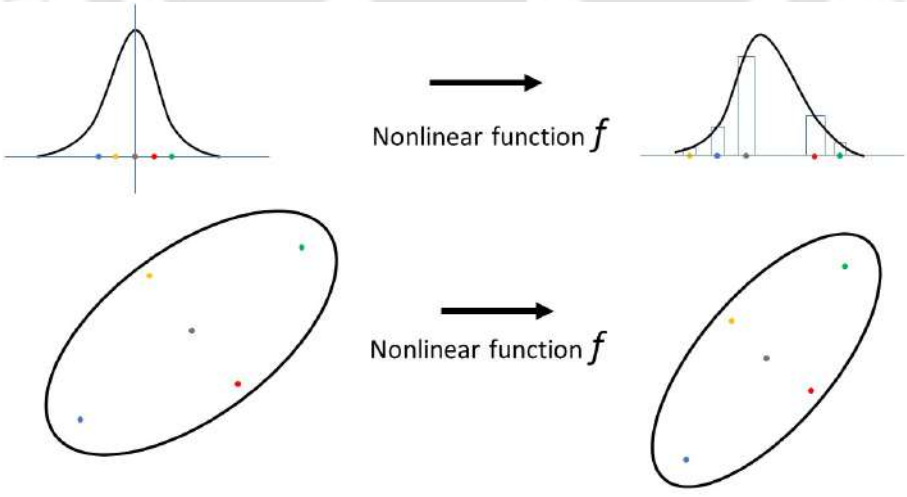

Figure 5.22: UKF Sigma point

The AUV state equation for non-linear system and sensor measurements can be expressed

as follows.:

$$x_k = f(x_{k-1}) + w_{k-1} \tag{5.17}$$

$$y_k = H(x_k) + v_k \tag{5.18}$$

where x_k, x_{k-1} are AUV state vectors at time k, $k-1$, respectively; $f(x_{k-1})$ non-linear state transition function; w_{k-1} is system noise; y_k sensor measurement vector; $H(x_k)$ is non-linear observation matrix; v_k is the measurement noise. The system noise and measurement noise with covariance matrix Q_k, R_k are assumed to be Gaussian white noise.

$$\begin{aligned} Cov[w_k, w_j] = E[w_k, w_j^T] = Q_k \delta_{kj}, E[w_k] = 0 \\ Cov[v_k, v_j] = E[v_k, v_j^T] = R_k \delta_{kj}, E[v_k] = 0 \\ Cov[w_k, v_j] = E[w_k v_j^T] = 0 \end{aligned} \tag{5.19}$$

The UKF algorithm can be presented in following steps:

Step 1: Initialize the state parameter and corresponding covariance.

$$\hat{x_0} = E(x_0) \tag{5.20}$$

$$P_0 = E[x_0 - \hat{x_0}][x_0 - \hat{x_0}]^T = E(x_0) \tag{5.21}$$

where x_0, $\hat{x_0}$ denote the initial and mean state information, P_0 initial covariance matrix.

Step 2: Update parameters

The sigma points and weights are calculated as follows:

$$x_k = \{\hat{x_k}, \hat{x_k} + [\sqrt{(n+|\lambda)P_{x,k}}]_i, \hat{x_k} - [\sqrt{(n+|\lambda)P_{x,k}}]_i\}, (i = 1, 2, ..., n) \tag{5.22}$$

$$W_i^{(m)} = W_i^{(c)} = \begin{cases} \lambda/(n+\lambda), i = 0 \\ 1/[2(n+\lambda)], i = 1, ..., 2n \end{cases} \tag{5.23}$$

where $W_i^{(m)}$ $W_i^{(c)}$ denote the weighted values of the mean and covariance, respectively; $x\,N(x, Px)$, x, P_x denote the mean and covariance of coordinates, respectively; λ is the proportional param-

eter; and $x_{i,k}$ is the weighted point that approximates the random variable distribution. One may calculate the prediction sigma points, the state value, and the covariance matrix as follows.

$$x_{i,k}^{-} = q[x_{i,k}](i = 1, ..., 2n) \tag{5.24}$$

$$\hat{x}_k^{-} = \sum_{i=0}^{2n} W_i^{(m)} x_{i,k}^{-} \tag{5.25}$$

$$P_{x,k}^{-} = \sum_{i=0}^{2n} W_i^{(c)} [x_{i,k}^{-} - \hat{x}_k^{-}][x_{i,k}^{-} - \hat{x}_k^{-}]^T + Q_k \tag{5.26}$$

where Q_k denotes the state noise covariance matrix.

Step 3: prediction value of measurement.

$$\hat{z}_k^{-} = \sum_{i=0}^{2n} W_i^{(m)} H[x_{i,k}^{-}] \tag{5.27}$$

Step 4: variance and covariance matrix.

$$P_{z,k} = \sum_{i=0}^{2n} W_i^{(c)} H[x_{i,k}^{-} - \hat{z}_k^{-}] H[x_{i,k}^{-} - \hat{z}_k^{-}]^T + R_k \tag{5.28}$$

$$P_{xz,k} = \sum_{i=0}^{2n} W_i^{(c)} x_{i,k}^{-} - \hat{x}_k^{-} H[x_{i,k}^{-} - \hat{z}_k^{-}]^T \tag{5.29}$$

where R_k is the measurement noise covariance matrix

Step 5: calculate the Kalman gain.

$$K_k = P_{xz,k} P_{z,k}^{-1} \tag{5.30}$$

Step 6: Update the state vector and the covariance matrix.

$$\hat{x}_k = \hat{x}_k^{-} + K_k[\hat{z}k - \hat{z}_k^{-}] \tag{5.31}$$

$$P_x = P_{x,k}^{-} - K_k P_{z,k} K_k^T \tag{5.32}$$

Matrix operation makes the process comparatively easier and as the non-linear function is calculated at sigma points the Jacobian is not required.

5.4.2 Sensor fusion for localization

AUV localization is essential for underwater navigation. Here INS is used for this purpose. INS will fuse the IMU, GPS, depth sensor and dynamic model output to estimate the state of the AUV. For development of INS and simulation work mathematical models of the above mentioned sensors are developed. As discussed in the previous section the measurement noise are assumed to be Gaussian white noise. Thus the sensor models are developed by adding white noise to the corresponding output from the dynamic model. Sensor properties and models are presented below.

IMU

Inertial Measurement Unit (IMU) houses accelerometer, gyroscope and magnetometer sensors and the acceleration, rotational speed and magnetic field intensity data are obtained from them respectively. IMU acceleration measurements are integrated twice and gyro outputs are integrated once to obtain positions and orientations. But with error bias, magnetic interference and error with integration the position results drift with time. INS calculates relative position and orientation of a dynamic system relative to a known starting point, orientation, and velocity using the data from motion sensors (accelerometers), and rotation sensors (gyroscopes) as shown in the Fig. 5.23. A IMU model is developed as shown in the Fig. 5.24.

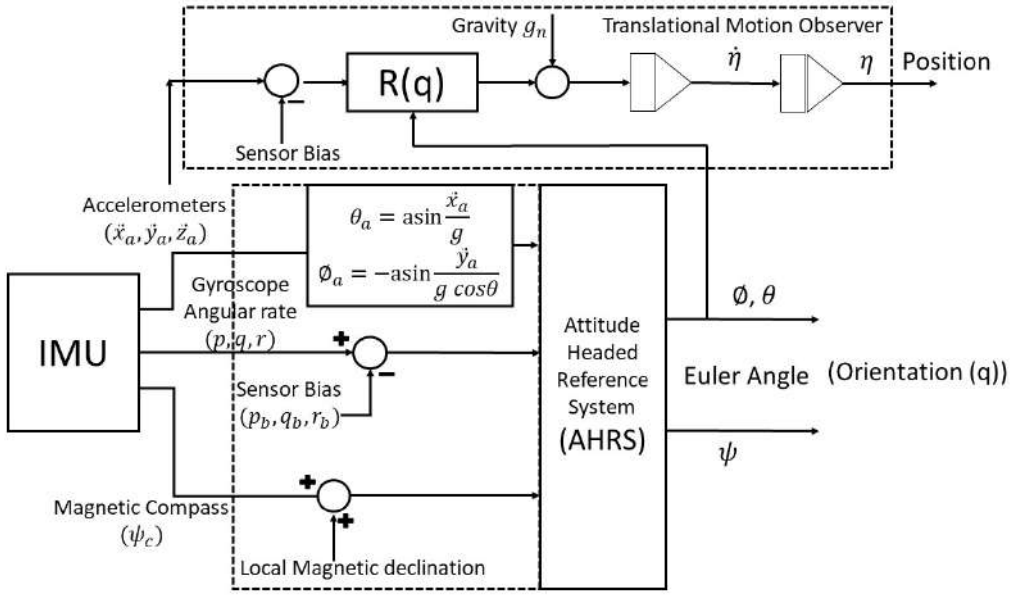

Figure 5.23: IMU observer structure

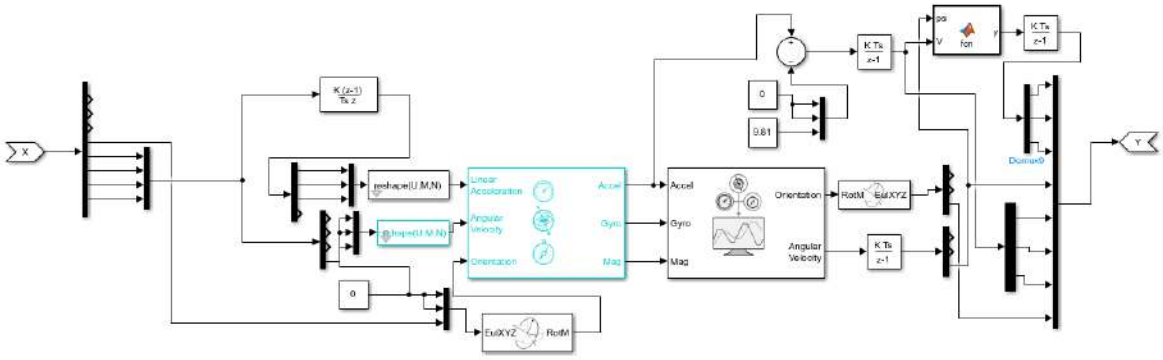

Figure 5.24: Dveloped IMU sensor model

Here LSM303D MEMS Ultra-compact high-performance eCompass module with 3D accelerometer and 3D magnetometer is used and the sensor properties are presented in the table below.

Table 5.6: IMU Sensor Properties

IMU	
Communication:	I2C: 100 kHz SPI: 400 kHz
Accelerometer	
measurement range: sensitivity: noise density:	$\pm$2 g,..., $\pm$16 g 0.244 mg/LSB for Linear acceleration FS = $\pm$8 g 150 ug/$\sqrt{Hz}$
Magnetometer	
measurement range: sensitivity: noise density:	$\pm$2 gauss,..., $\pm$12 gauss 0.320 mgauss/LSB for Magnetic FS = $\pm$8 gauss 5 mgauss/RMS
Gyro	
measurement range: sensitivity: noise density:	$\pm$245 dps,..., $\pm$2000 dps 17.5 mdps/digit 0.011 dps/$\sqrt{Hz}$

GPS

Global Positioning System (GPS) signal only works to few cm depth from water surface. GPS and high frequency radio signals in the underwater environment makes localization and navigation very challenging for AUVs. But GPS can be used to obtain the initial condition data as well as can be used for eliminating the bias build by surfacing the AUV intermittently. Here NEO-7 GNSS module is used for GPS. GPS sensor properties are presented in the table below.

Table 5.7: GPS Sensor Properties

GPS	
Horizontal position accuracy: Frequency of signal: Max navigation update rate: Velocity accuracy: Heading accuracy	Autonomous 2.5 m 0.25 Hz, ..., 10 MHz 10 Hz 0.1 m/s 0.5 degrees
Operational limits:	
Dynamics: Altitude: Velocity:	4 g 50,000 m 500 m/s

Depth Sensor

The pressure sensor used has a resolution of 0.2 mbar or a depth resolution of 2mm and can work upto a depth of 300m underwater and communicates over I2C.

Sensor Fusion

Considering the sensor noise the sensor models are developed by adding these noise to the corresponding output from the dynamic model. Fig. 5.25,5.26,5.27 and 5.28 present the position and orientation output from different measurement sources.

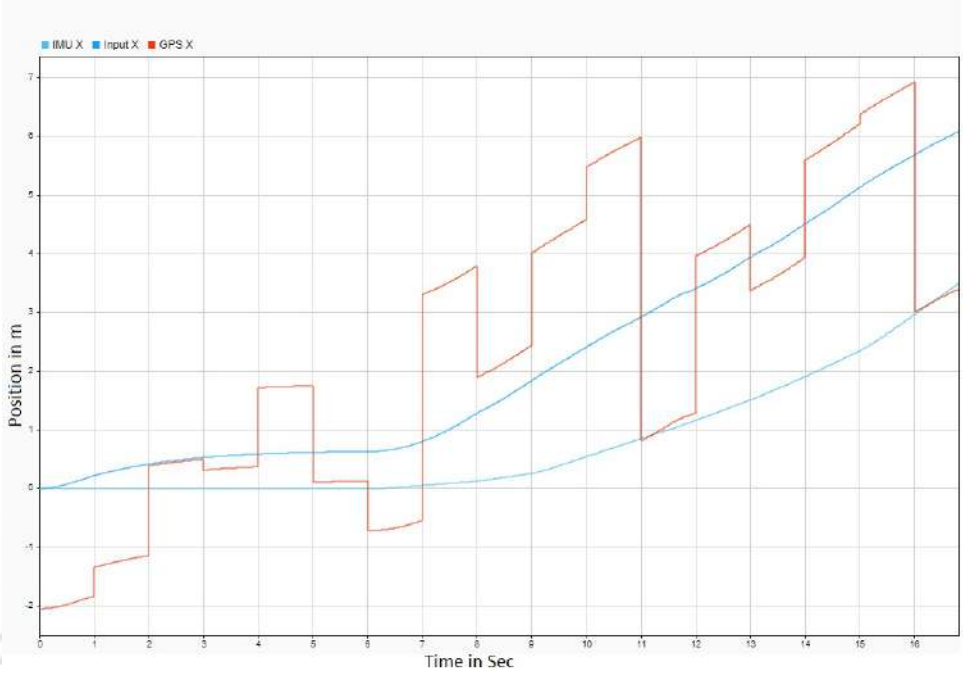

Figure 5.25: Position in X axis

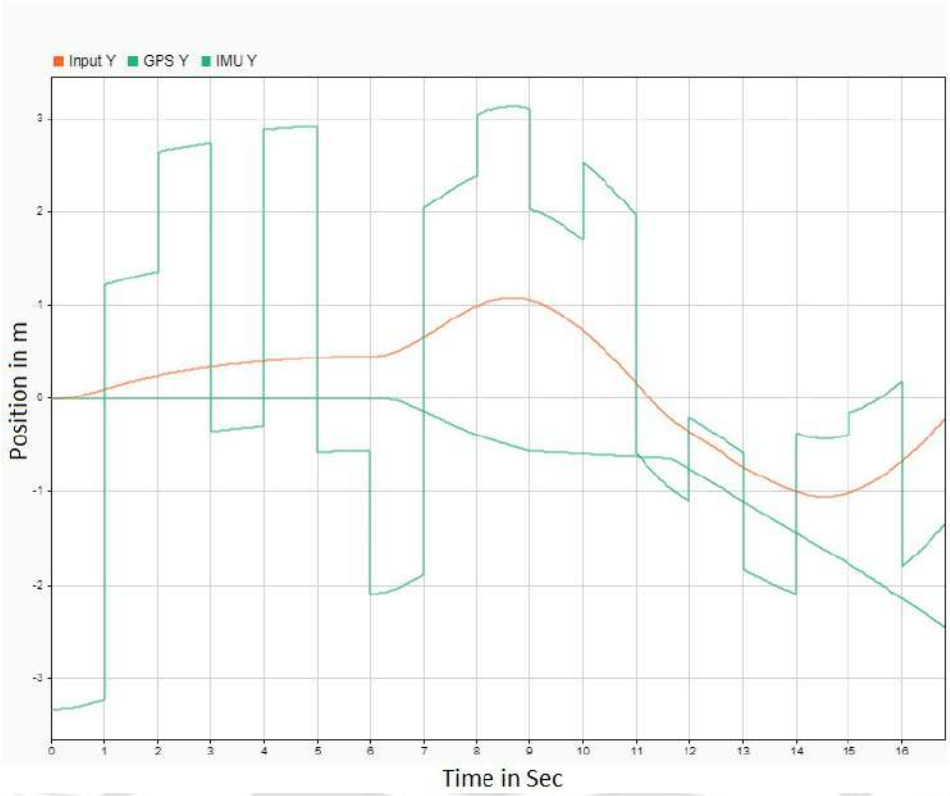

Figure 5.26: Position in Y axis

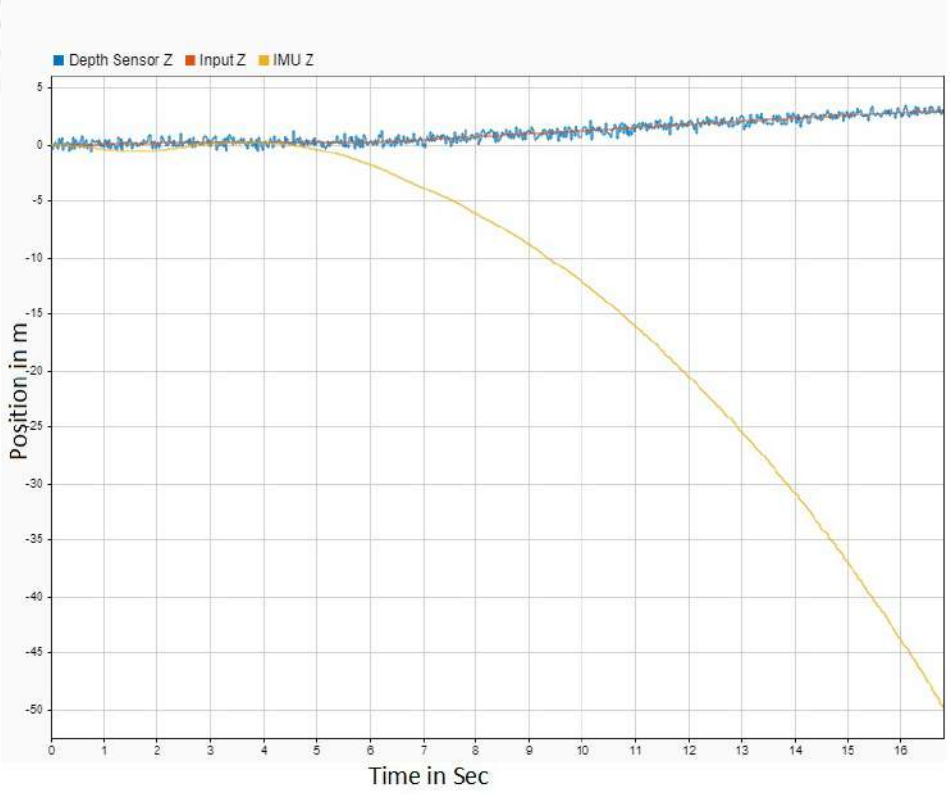

Figure 5.27: Position in Z axis

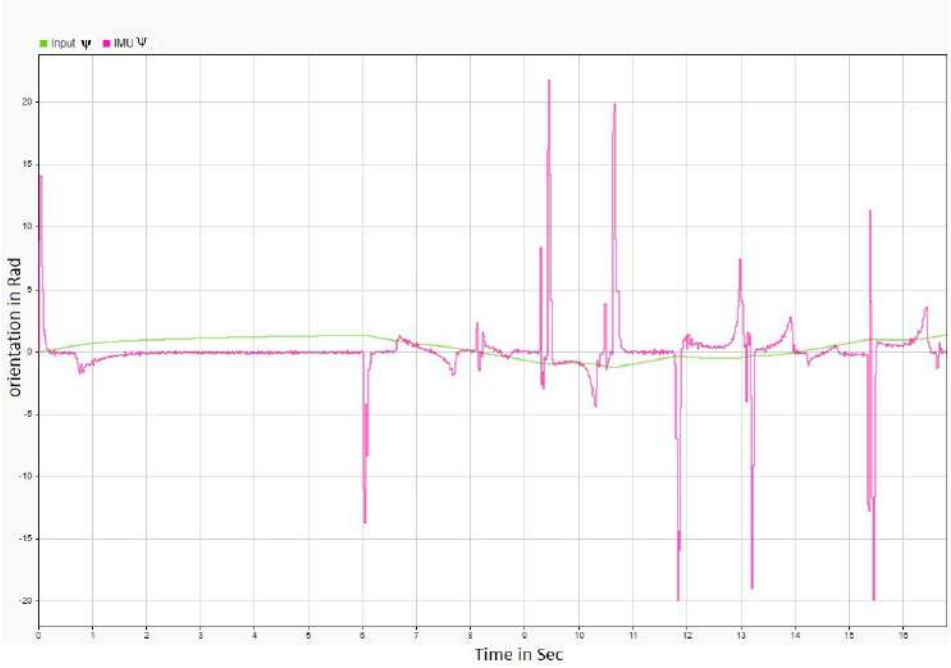

Figure 5.28: Orientation about Z axis

The INS is developed in the MATLAB^{TM} Simulink^{TM} software as shown in Fig. 5.29. The AUV model is presented in the "stateTransitionFcn" and three measurements are considered from IMU, GPS, and depth sensor. Covariance matrices are defined according to the measurement noise and sensor resolution. Fig. 5.30 shows the model depth output and UKF depth estimate. The UKF estimate is close to the depth sensor data rather than the IMU data. The IMU depth estimates deviates from the true value due to accumulation of error (Fig. 5.27). UKF estimate is close to the confident sensor data.

AUV model:

$$\begin{aligned} \dot{\eta} &= J(\eta)v \\ M\dot{v} + C(v)v + D(v)v &= \tau \end{aligned} \tag{5.33}$$

Sate-space model:

$$\begin{aligned} \dot{x} &= Ax + Bu \\ x &= [\eta^T v^T]^T, u = \tau \\ A &= \begin{bmatrix} 0 & J(\eta) \\ 0 & -M^{-1}(C+D) \end{bmatrix}, B = \begin{bmatrix} o \\ M^{-1} \end{bmatrix} \end{aligned} \tag{5.34}$$

System state vector is defined as follows.

$x = [\eta^T v^T]^T = [x, y, z, \psi, u, v, w, r]^T$

Sensor measurement vector is defined as:

$$y_k = [\eta_x^{IMU}, \eta_y^{IMU}, \eta_z^{IMU}, \eta_\psi^{IMU}, \nu_u^{IMU}, \nu_v^{IMU}, \nu_w^{IMU}, \nu_r^{IMU}, \eta_x^{GPS}, \eta_y^{GPS}, \eta_z^{depth}]_k^T$$

System state evolution and sensor measurement equation are expressed as:

$$\begin{aligned} x_k &= f(x_{k-1}) + w_{k-1} \\ [\eta]_k &= [\eta]_{k-1} + \Delta T[B] + w_{k-1} \end{aligned} \tag{5.35}$$

$[B]$ contains system parameters, $[\Delta T]$ discrete sample time .

$$y_k = H(x_k) + v_k \tag{5.36}$$

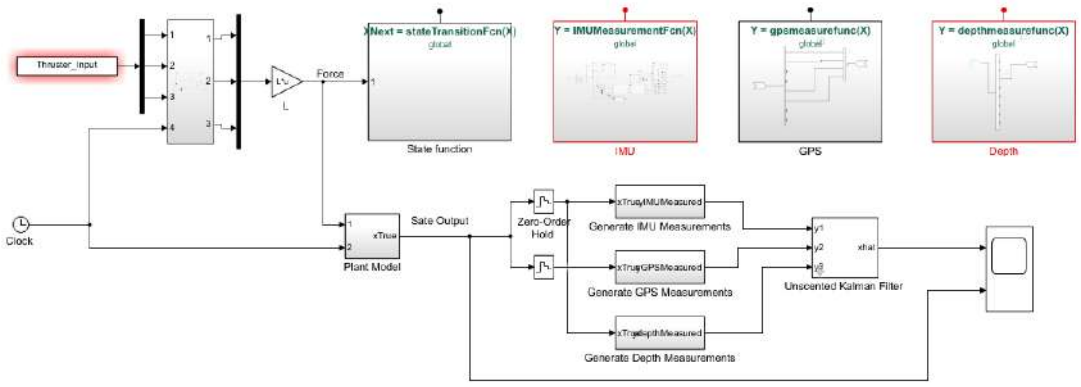

Figure 5.29: Localization system

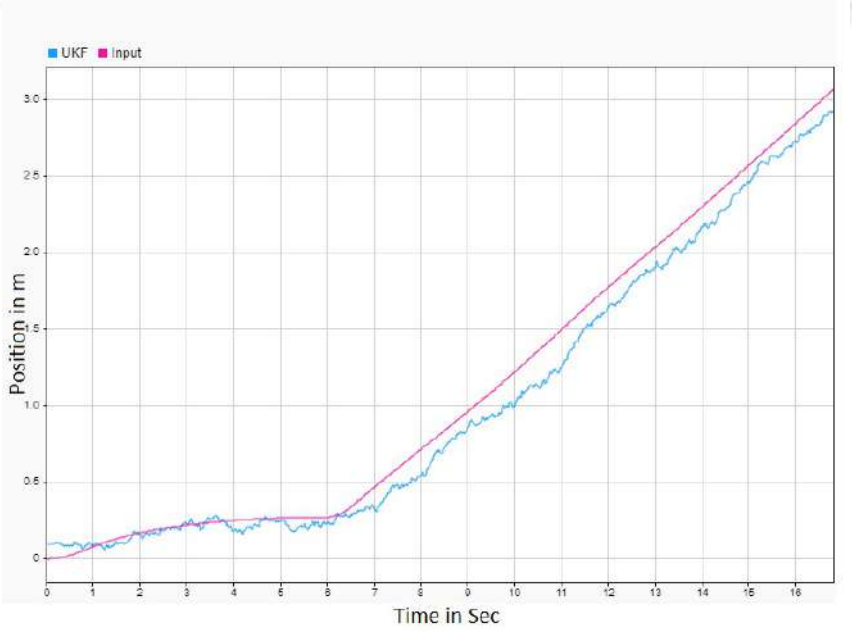

Figure 5.30: UKF vs model depth output

5.5 Summary

Guidance and close-loop control system developed for the AUV is presented in this chapter. Guidance system generates desired trajectory for way-point navigation using LOS strategy. Here the AUV will closely follow the line of sight vector between the target way-point and starting position. The next way-point will be selected once the AUV is within the acceptance radius of the way-point. A control system has to work closely with the navigation system to enable the AUV to reach a target position. Here initially a PD controller is developed, but the existing steady state error due to under-actuation leads to development of a PID close-loop control strategy. The controller is developed using MATLAB^{TM} Simulink^{TM} and simulated with different target points. The PID control gains are tuned heuristically to reach the target point without much oscillation and overshoot. A path with multiple way-points is also simulated. PID controller is also compared with PD controller to show that the steady state error found in case of the PD controller for the under-actuated system is minimized by the PID controller. The AUV uses Inertial navigation for localization. IMU, GPS and depth sensor outputs along with the output of system dynamic model are fused together using the state estimator UKF to estimate the AUV position and orientation. UKF is best suited for this coupled non-linear system. For the simulation GPS and depth sensor models are developed considering the system model output and sensor bias. The position estimate is used in the feedback loop of the control system to maintain the path of the AUV close to the desired path. As shown in this chapter the PID controller has to be tuned for different paths and the controller gains are not universal. Thus a adaptive controller is highly desirable and practical. Development of an robust adaptive controller is presented in the next chapter.

Chapter 6

ADAPTIVE CONTROL OF THE AUV

6.1 Introduction

Dynamic model based PID controller developed in the previous chapter is able to follow different trajectories, but the controller gains have to be tuned for each trajectories. Thus use of an adaptive controller is highly practical for an AUV working in dynamic underwater conditions. In uncertain environments soft computing techniques such as Fuzzy logic and Neural networks are popular tools to control the system. Fuzzy controller based on fuzzy logic is one of the most popular adaptive control technique. Fuzzy logic is a mathematical system which considers analog inputs in form of logical variable which can take continuous values between 0 to 1. PID parameters are difficult to tune for complex coupled non-linear AUV model. Using fuzzy rules these parameters can be adjusted to address the environmental disturbance making the controller adaptive. Neural network controllers have gained popularity and seen a large-scale adoption in recent years because of exponential advancements in computer infrastructure. Artificial neural networks are computing systems inspired by biological neural network with machine learning algorithms for data processing. A Neuro-Fuzzy system can be used to develop an accurate black box model of the system considering the environmental forces which will help to adapt to different environments. In this chapter, following the introductory section, section 6.2 presents a self adaptive Fuzzy-PID controller and a comparison study with the developed PID controller. Development of the Neuro-Fuzzy controller is discussed in the section 6.3. The summary of the chapter is presented in section 6.4.

6.2 Self adaptive Fuzzy-PID controller

As the PID controller has to be tuned for individual path, little deviation from the path due to dynamic environmental disturbance will cause the PID controller to fail. In such scenario use of Fuzzy controller to adapt to variation of the path brings robustness to the controller. A PID controller with some allowed variations in the control gains can be formulated as follows.

$$\begin{aligned} u(t) &= (K_p(t)e(t)) + \int_0^t (K_i(\tau)e(\tau))d(\tau) + \frac{d}{dt}(K_d(t)e(t)) \\ &= [k_p^0 + \Delta k_p(t)]e(t) + \int_0^t [k_i^0 + \Delta k_i(\tau)]e(\tau)d(\tau) + \frac{d}{dt}([k_d^0 + \Delta k_d(t)]e(t)) \end{aligned} \tag{6.1}$$

where, $K_p(t) = k_p^0 + \Delta k_p(t)$; $K_i(t) = k_i^0 + \Delta k_i(t)$; $K_d(t) = k_d^0 + \Delta k_d(t)$ are the control gains with some allowable variation.

k_p^0, k_i^0, k_d^0 are the PID controller gains similar to that presented in the previous chapter. These parameters are time independent.

$\Delta k_p(t), \Delta k_i(t), \Delta k_d(t)$ are time variant and adapted during simulation. These parameters can be obtained from the fuzzy controller. Using these parameters the control law can be presented as follows.

$$u(t) = u(t)^0 + \Delta u(t) \tag{6.2}$$

where,

$$\begin{aligned} u(t)^0 &= [k_p^0 e(t)] + \int_0^t [k_i^0 e(\tau)]d(\tau) + k_d^0 \frac{de(t)}{dt} \\ \Delta u(t) &= [\Delta k_p(t)e(t)] + \int_0^t [\Delta k_i(\tau)e(\tau)]d(\tau) + \frac{d}{dt}[\Delta k_d(t)e(t)] \end{aligned} \tag{6.3}$$

Here a Fuzzy Logic Controller (FLC) is proposed for generating $\Delta k_p(t)$, $\Delta k_i(t)$, $\Delta k_d(t)$. The FLC uses the fuzzy linguistic variables NL, NM, NS, ZR, PS, PM, PL which represent Negative Large, Negative Medium, Negative Small, Zero, Positive Small, Positive Medium, and Positive Large, respectively. The FLC has two inputs. One is the system error ($e(t)$) and the other one is error rate ($\dot{e}(t)$). To produce the three signals, the FLC needs three outputs. Consequently, the FLC has two inputs and three outputs that are shown in Fig. 6.1.

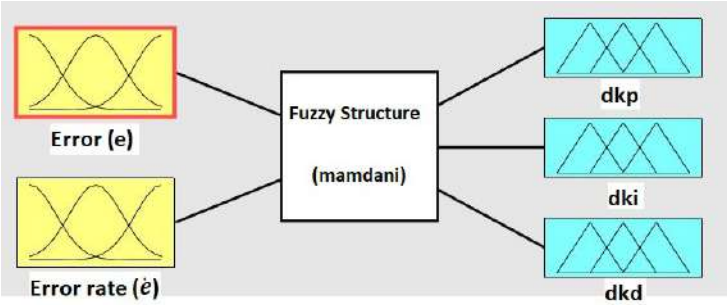

Figure 6.1: Fuzzy logic controller

When the error is large, k_p should be large to have fast response. A smaller value of k_d prevents instantaneous value of error rate to be very large. In order to avoid the overshoot due to a larger system response, the integral action should be limited, thus k_i value should be very small. When the error is medium, in order to ensure fast system response and have small overshoot, k_p should be reduced, while larger k_d increases the impact of system response, k_i should be in medium range. When error is small, to ensure that the system has the ideal steady state performance, k_p should be large and k_i should be small. Considering these facts fuzzy rules for k_p, k_d and k_i are designed which are presented in the Tables. 6.1, 6.2 and 6.3.

Table 6.1: FLC rules for $\Delta k_p(t)$

$\dot{e}$ \ e	NL	NM	NS	Z	PS	PM	PL
NL	PL	PL	PM	PM	PS	PS	Z
NM	PL	PL	PM	PM	PS	Z	Z
NS	PM	PM	PM	PS	Z	NS	NM
Z	PM	PS	PS	Z	NS	NM	NM
PS	PS	PS	Z	NS	NS	NM	NM
PM	Z	Z	NS	NM	NM	NM	NL
PL	Z	NS	NS	NM	NM	NL	NL

The membership functions for the inputs and the outputs are trimf and gbellmf, respectively. Here gbellmf and trimf represent generalized bell curve membership function and triangular curve member function respectively in fuzzy logic as shown in the Fig. 6.2. FLC input and output range of the membership functions and the parameter values are presented in the Table. 6.4.

Table 6.2: FLC rules for $\Delta k_i(t)$

$\dot{e}$ \ e	NL	NM	NS	Z	PS	PM
NL	NL	NL	NL	NM	NM	Z
NM	NL	NL	NM	NM	NS	Z
NS	NM	NM	NS	NS	Z	PS
Z	NM	NS	NS	Z	PS	PS
PS	NS	NS	Z	PS	PS	PM
PM	Z	Z	PS	PM	PM	PL
PL	Z	Z	PS	PM	PB	PB

Table 6.3: FLC rules for $\Delta k_d(t)$

$\dot{e}$ \ e	NL	NM	NS	Z	PS	PM
NL	PS	PS	Z	Z	Z	PL
NM	NS	NS	NS	NS	Z	NS
NS	NL	NL	NM	NS	Z	PS
Z	Z	Z	Z	Z	Z	Z
PS	NL	NM	NS	NS	Z	PS
PM	NM	NS	NS	NS	Z	PS
PL	PS	Z	Z	Z	Z	PL

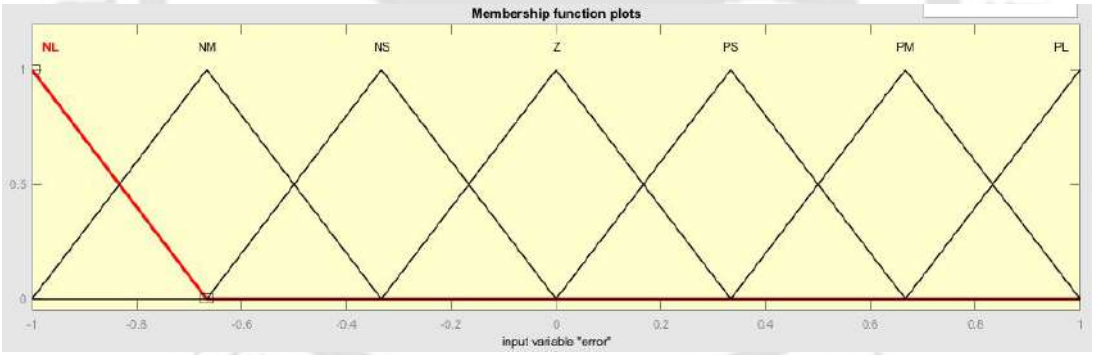

(a)

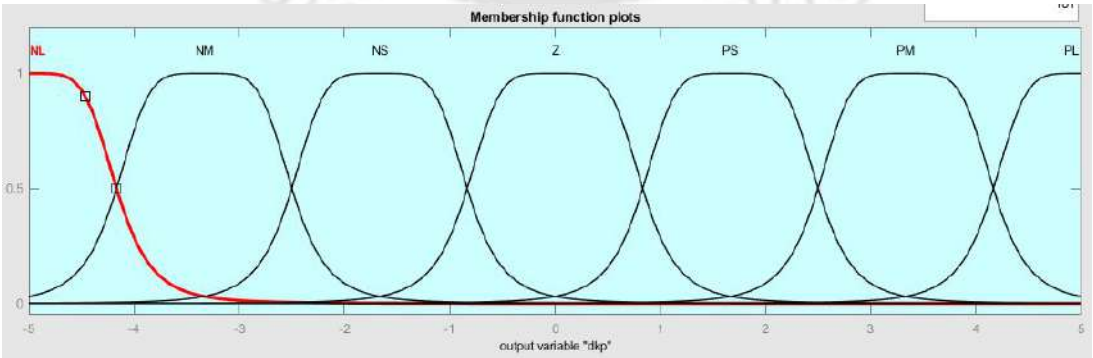

(b)

Figure 6.2: Fuzzy Logic Membership Functions (a) trimf and (b) gbellmf

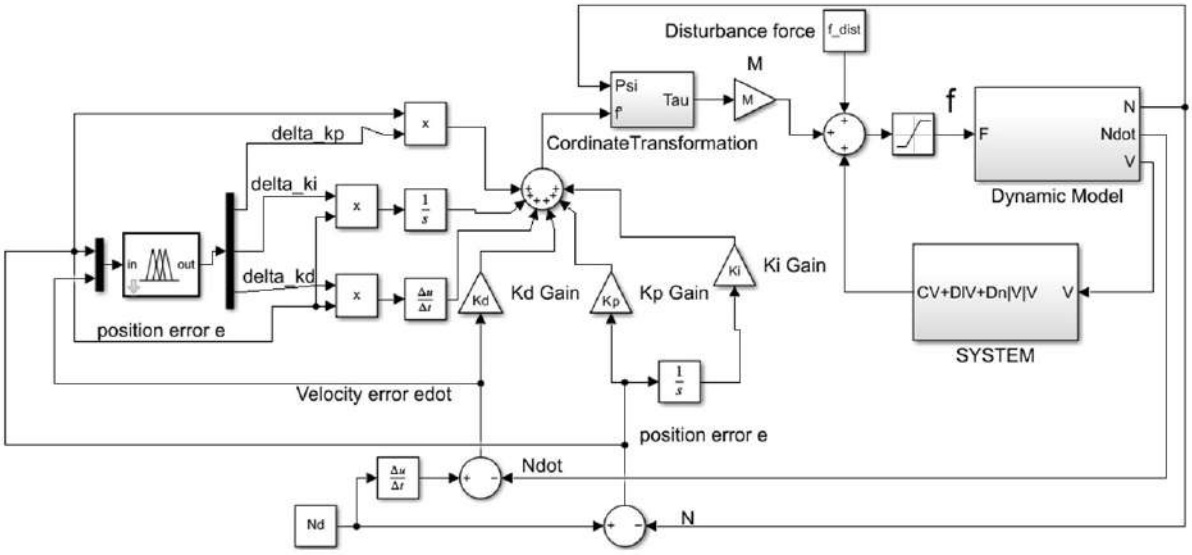

Figure 6.3: Fuzzy-PID controller

Table 6.4: FLC input output parameter range

	$\dot{e}$	e	$\Delta k_p(t)$	$\Delta k_i(t)$	$\Delta k_d(t)$	k_p^0	k_i^0	k_d^0
X	[-1 1]	[-0.5 0.5]	[-5 5]	-	[-9 9]	10	-	17.7
Y	[-0.7 0.7]	[-1 1]	[-0.3 0.3]	[-0.06 0.06]	[-1.5 1.5]	0.7074	-0.1	1.68
Z	[-0.2 0.2]	[-0.4 0.4]	[-9 9]	-	[-15 15]	18	-	30.527
ψ	[-4 4]	[-1300 1300]	[-100 100]	-	[-50 50]	200	-	90

Simulation Result

Developed self adaptive Fuzzy-PID controller is simulated in MATLAB^{TM} Simulink^{TM} for multi waypoint trajectory. Controller was able to flow the 3D trajectory successfully. For comparison and validation of the Fuzzy-PID controller the same multi Way-point path is simulated with PID and Fuzzy-PID controller changing the control gains. Control gain parameters used on this simulation for both the controllers are presented in the Table. 6.5. As the the control gains are not the tuned parameters the PID controller failed to follow the path (shown in Fig. 6.4), where as the adaptive Fuzzy-PID controller was able to follow the trajectory (shown in Fig. 6.5). The error tracking results of the Fuzzy-PID controller is presented in the Fig. 6.6. The desired position input and the controller output along X-axis, Y-axis and Z-axis are presented in

the Fig. 6.7,6.8 and 6.9, respectively. This may be noted that the results shows the Fuzzy-PID controller can adjust the controller gains and adapt to dynamic environmental conditions.

Table 6.5: Controller gain parameters considered for simulation

position	k_p	k_i	velocity	k_v
x	10	0	u	17.69
y	0.71	-2	v	1.68
z	18	0	w	30.53
ψ	160	0	r	50

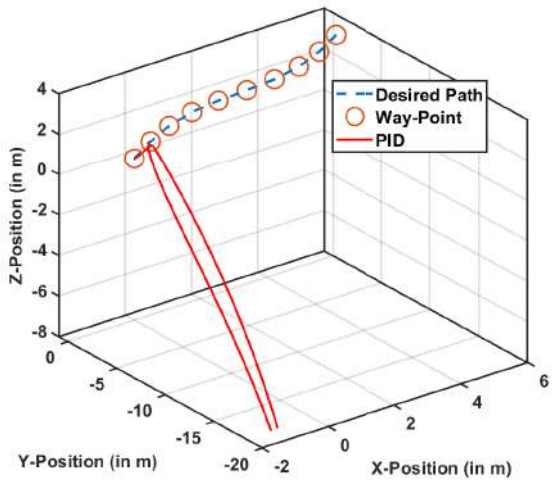

Figure 6.4: Position Tracking PID controller

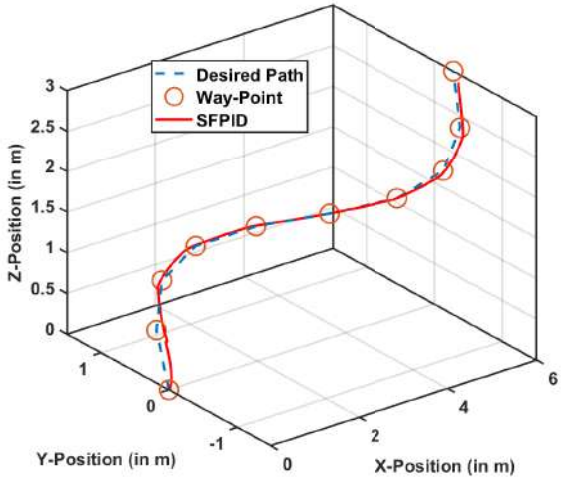

Figure 6.5: Position Tracking Fuzzy-PID controller

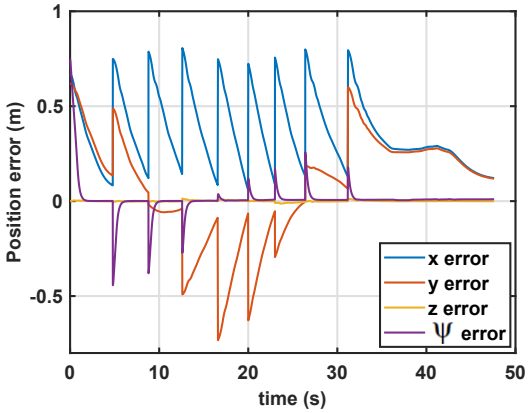

Figure 6.6: Error tracking Fuzzy-PID controller

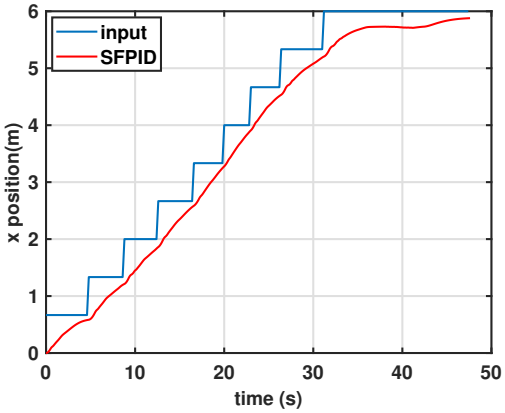

Figure 6.7: X position with time

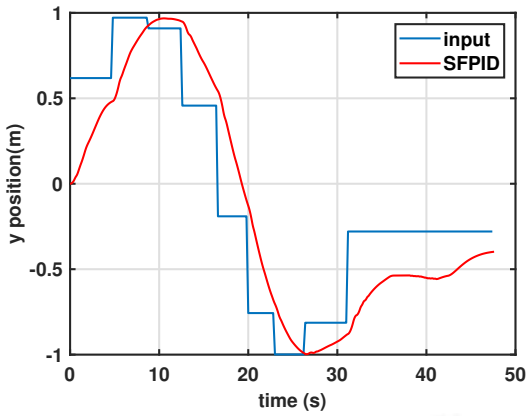

Figure 6.8: Y position with time

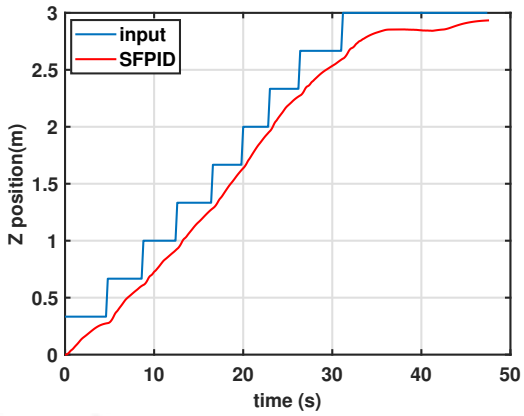

Figure 6.9: Z position with time

To further showcase the robustness of the controller, simulation is carried out with a different waypoint trajectory without tuning the controller for the path. Position tracking of the PID and SFPID controller is presented in the Fig. 6.10. It may be noted that the SFPID was able to adapt to the scenario and achieve the targeted waypoints but the PID controller was failed to achieve the waypoints and deviated from the path thus the SFPID controller performance is far superior than that of the PID controller as it can adapt deviations in the path. The same effect can be observed in the error tracking as shown in Fig. 6.11 where the error increases before decreasing and takes longer time by PID than the SFPID. Position tracking along x and y axis as shown in Fig. 6.12 and 6.13, respectively for the PID and SFPID controller shows the same effect.

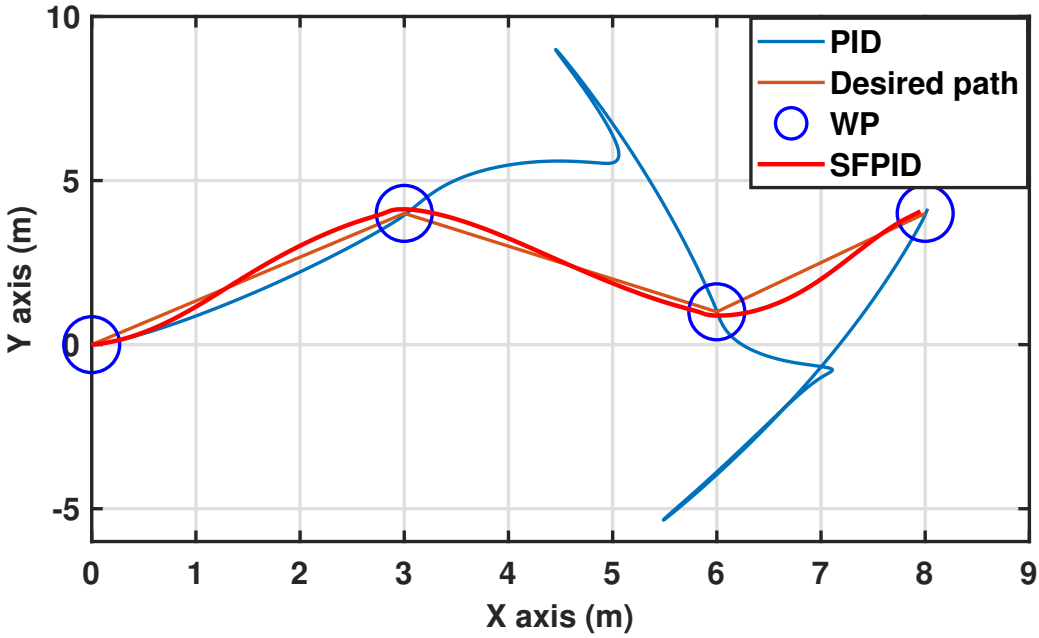

Figure 6.10: Position tracking with time for PID and SFPID controller

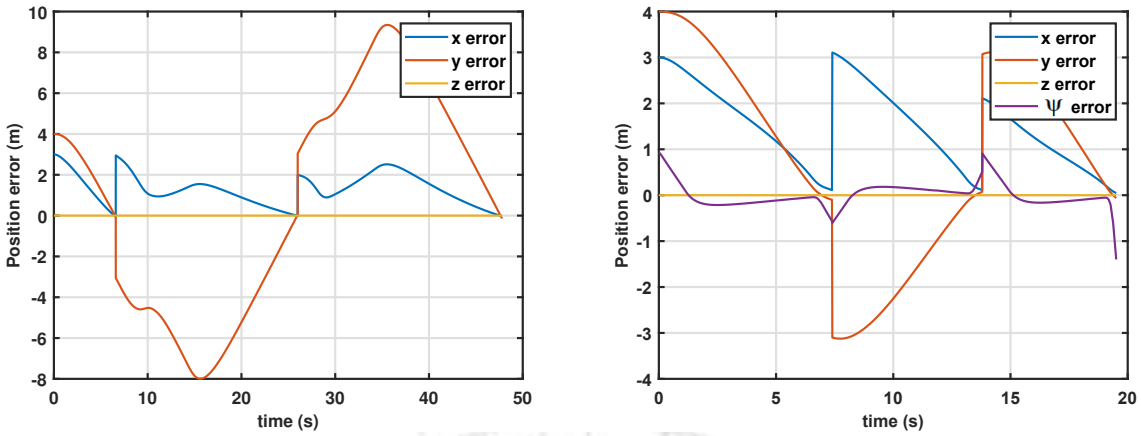

(a) (b)

Figure 6.11: Error tracking (a) PID (b) SFPID

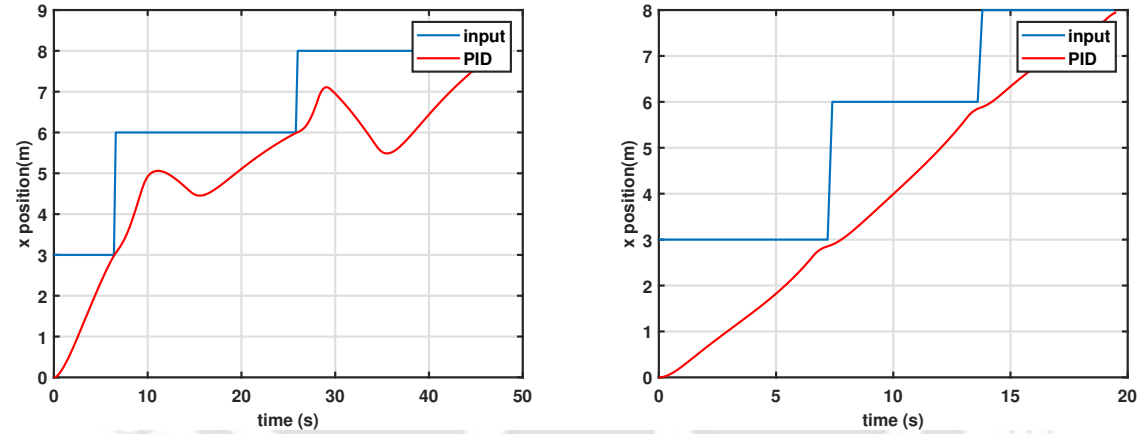

(a) (b)

Figure 6.12: X position with time (a) PID (b) SFPID

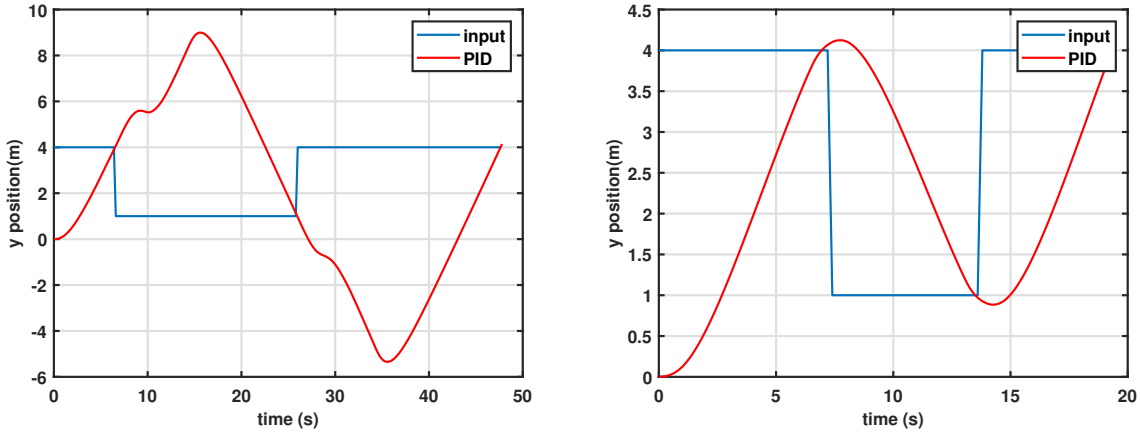

(a) (b)

Figure 6.13: Y position with time with (a) PID (b) SFPID

Under External disturbance

To study the controller performance under external disturbance force such as river and ocean currents simulation is carried out with considering sinusoidal disturbance forces (Bak et al. [146]) as follows:

$$f_{dist} = [3sin(t), 2sin(t), cos(t), 0]^T \tag{6.4}$$

Position plot (Fig. 6.14) of the SFPID controller under external disturbance shows the controller is able to achieve all the targeted waypoints successfully but not always along the least distance path due to presence of external force. Tuned PID controller under same conditions failed(Fig. 6.15) to achieve last two way points and deviated from the path under external disturbance.

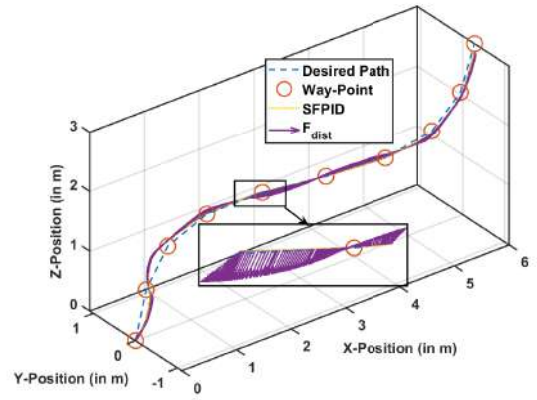

Figure 6.14: Position tracking with external disturbance of SFPID

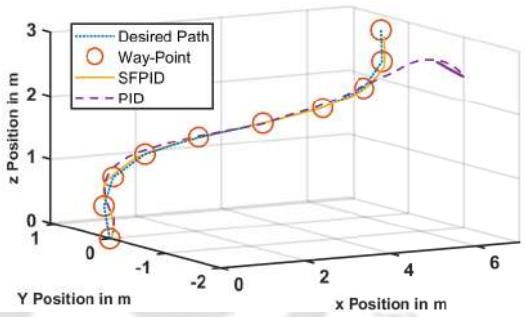

Figure 6.15: Position tracking with external disturbance of PID vs SFPID

6.3 Adaptive Neuro-Fuzzy Controller

Fuzzy-PID controller will help adapt to different trajectories without specifically tuning the controller for that path. Dynamic unknown environmental forces still may deviate the AUV from its trajectory. To consider the unknown system parameters in the controller design, a Neuro-Fuzzy controller is developed with accurate dynamic model of the system considering the environmental forces and will help adapt to different environments. Adaptive Neuro-Fuzzy Inference Systems (ANFIS) of MATLAB^{TM} is used for development of the NN model of the

system. Control system of the AUV is presented in the Fig. 6.17. The desired state from the motion planning and the actual state is compared and error is feed into the controller. Controller output are the forces which are supplied to the thrusters for AUV motion. These forces are also used by the dynamic model of the system to estimate the state of the AUV. This estimate along with measurement from the IMU, GPS and depth sensors are fused to provide an accurate AUV position using UKF. The dynamic model used here is not that accurate as some assumptions are considered during derivation of the coupled non-linear system model. Using the ANFIS module of MATLAB^{TM} a system correlation can be developed between the thrust input and the experimental AUV position from the INS. This system model will be accurate and will have environmental effect which are otherwise difficult to model. This process is presented in the Fig. 6.16(a). This experiment will be an initial process to develop the system model for a particular environment. Fig. 6.16(b) represent the controller during operation of the AUV. Error between the Fuzzy-PID controller output and the ANFIS model will be used to update the model thus the controller will adapt to the unknown variable environmental effects.

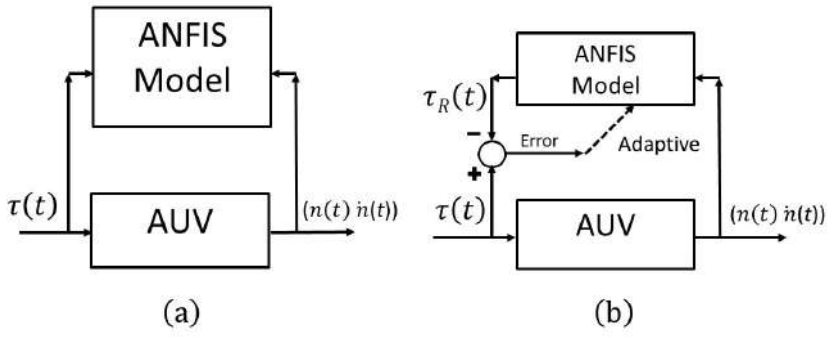

Figure 6.16: Neuro-Fuzzy Control

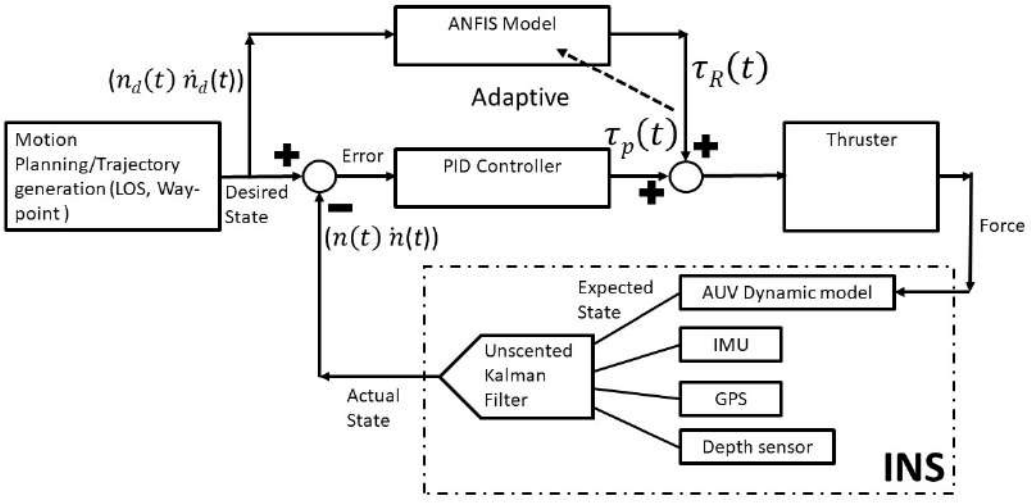

Figure 6.17: AUV Control system

Neural Network Model

During the field test in the river dam the control input signal to the thrusters, accelerometer, gyroscope, and depth sensor data are recorded. Controller signal and sensor data are produced at a different rate. First, the data are converted to time series data and synchronized. Two independent NN models are fitted for horizontal and vertical motion, respectively each with ten hidden layers and two output layers (Fig. 6.18). The NN model is trained with the experimental data using the Levenberg-Marquard algorithm using the MATLAB^{TM} Deep Learning Toolbox^{TM}. The horizontal and vertical motion model is fitted with 0.85 and 0.83 regression value(Fig. 6.19, 6.20), respectively. For both the models the correlation is established between the position and velocity as input and thrust produced as output.

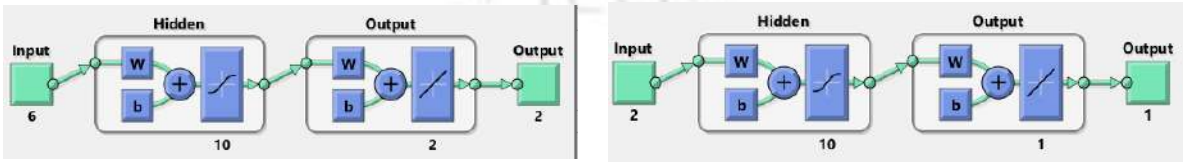

(a) (b)

Figure 6.18: Neural Network model of (a) horizontal motion and (b) vertical motion

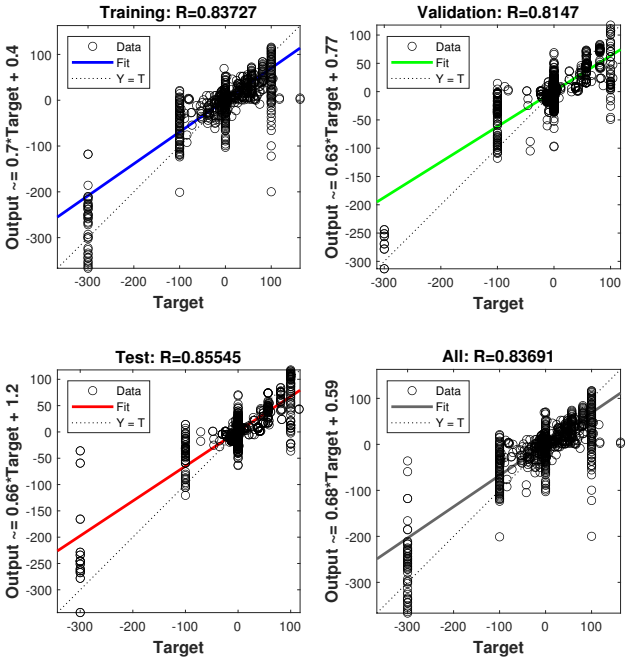

Figure 6.19: Regression of fitted NN horizontal motion model

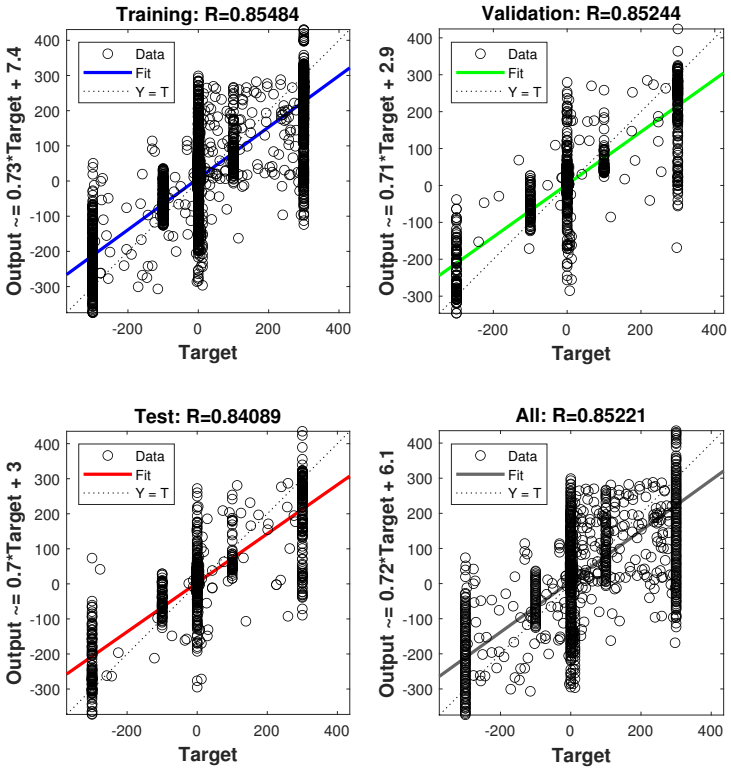

Figure 6.20: Regression of fitted NN vertical motion model

Simulation

The developed NN models is used in parallel with the developed PID controller to improve the controller performance to address the unknown system behavior. The Nuero-Fuzzy PID controller is developed in MATLAB^{TM} Simulink^{TM} (Fig. 6.21). Successful simulations show good controller performance. NFPID is able to handle trajectories without specifically tuning the gains for the path (Fig. 6.22) like the SFPID controller. During a field run the NN model can be updated for the current environment and can provide good performance in dynamic environment. Comparison of the error tracking as shown in the Fig. 6.11; position tracking along x, y, and z axis (Fig. 6.12, 6.13) for the NFPID and SFPID controller show slightly better performance of the NFPID controller but both the controller are able to follow the trajectories. SFPID controller takes 10 second longer to complete the trajectory but struggles with the last way-point. Controllers relays on the PID controller gains. The controllers will be able to handle deviations from the path due to environmental disturbances but for a drastically different path the PID controller gains have to be tuned.

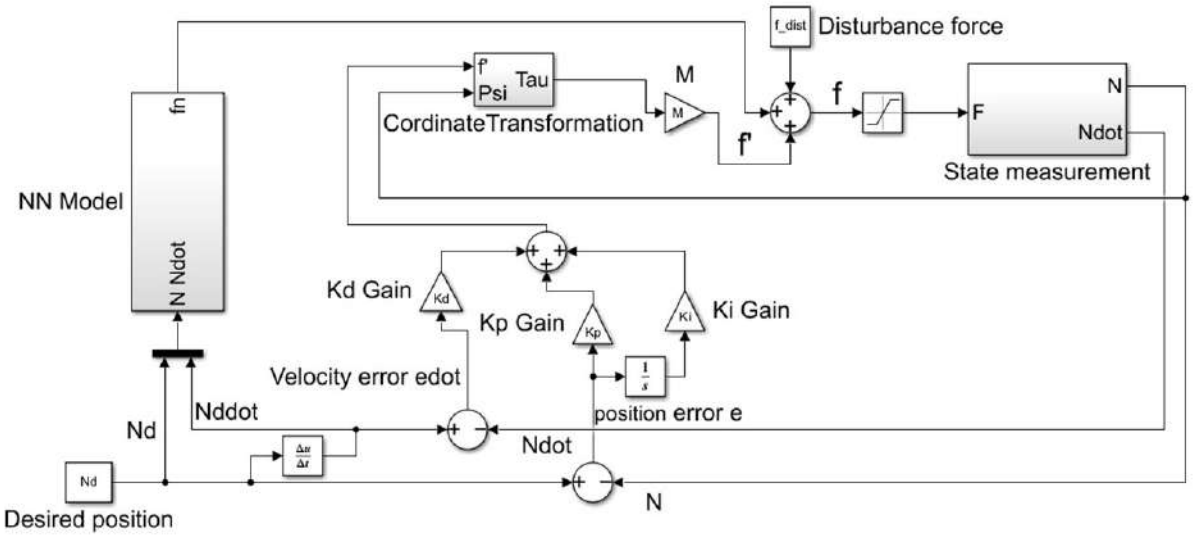

Figure 6.21: Neuro-Fuzzy Controller

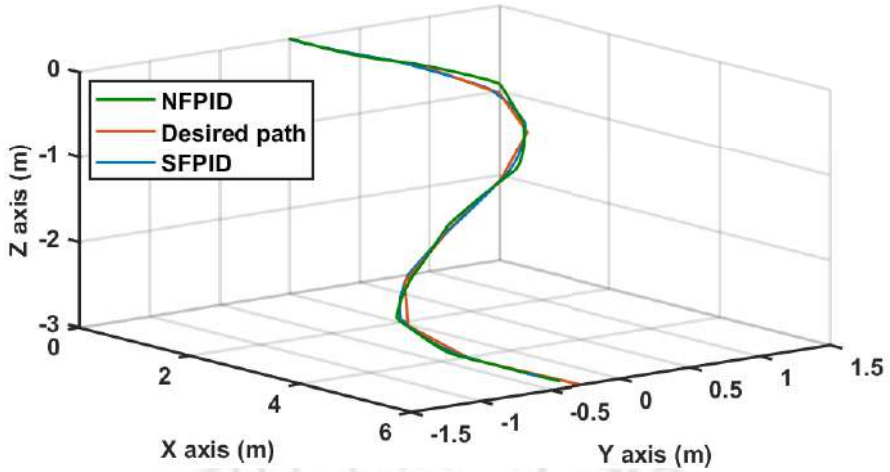

Figure 6.22: Position tracking with time

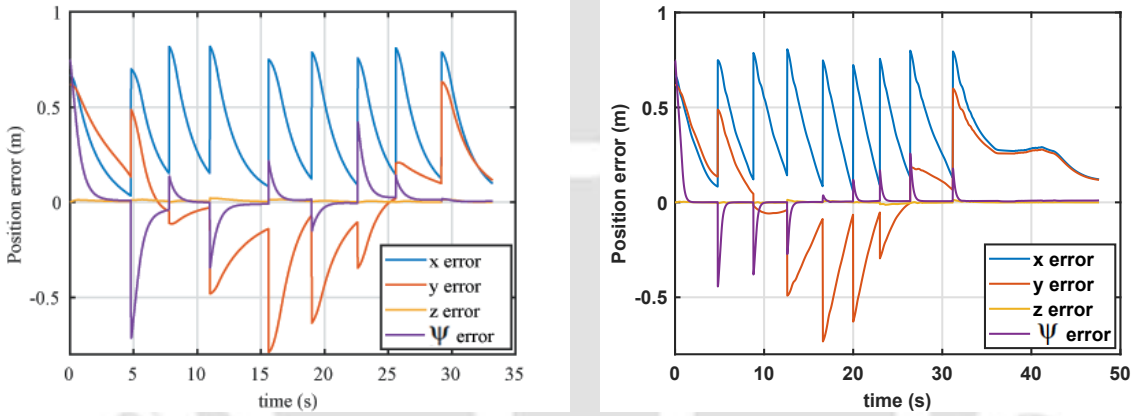

Figure 6.23: Error tracking (a) NFPID (b) SFPID

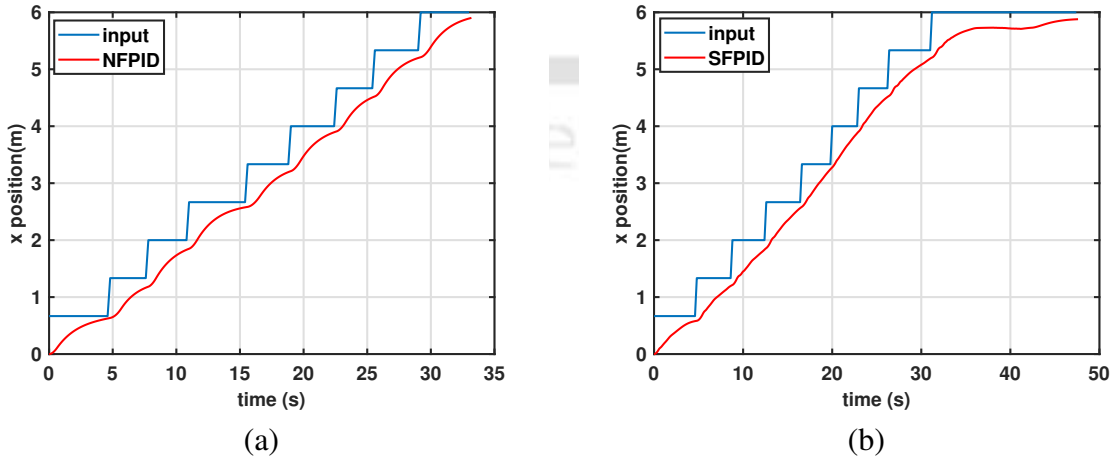

Figure 6.24: X position with time (a) NFPID (b) SFPID

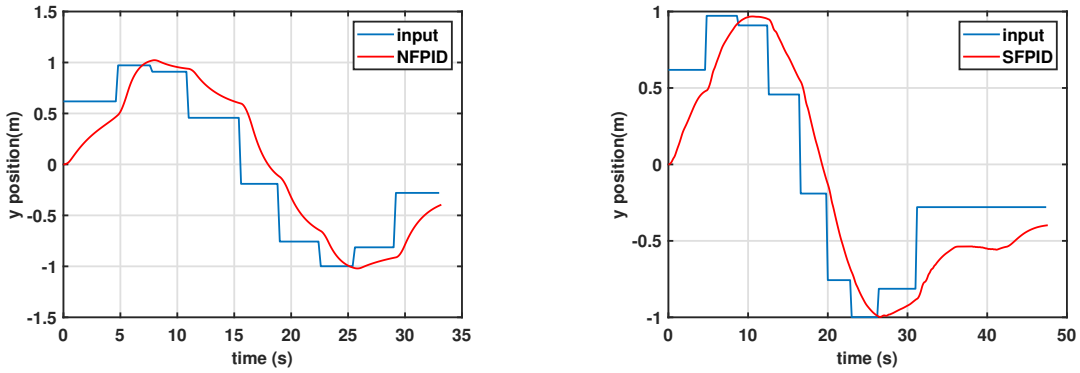

(a) (b)

Figure 6.25: Y position with time(a) NFPID (b) SFPID

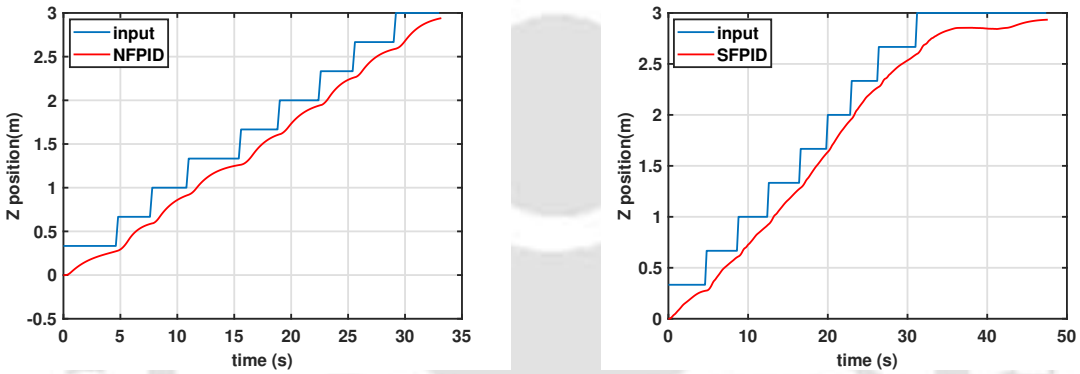

(a) (b)

Figure 6.26: Z position with time (a) NFPID (b) SFPID

External disturbance

To study the controller performance under external disturbance force such as river and ocean currents simulation is carried out with considering sinusoidal disturbance forces (Bak et al. [146]) as follows:

$$f_{dist} = [3sin(t), 2sin(t), cos(t), 0]^T \tag{6.5}$$

Position plot (Fig. 6.14) of the NFPID controller under external disturbance shows the controller is able to achieve all the targeted waypoints successfully but not always along the least distance path due to presence of external force.

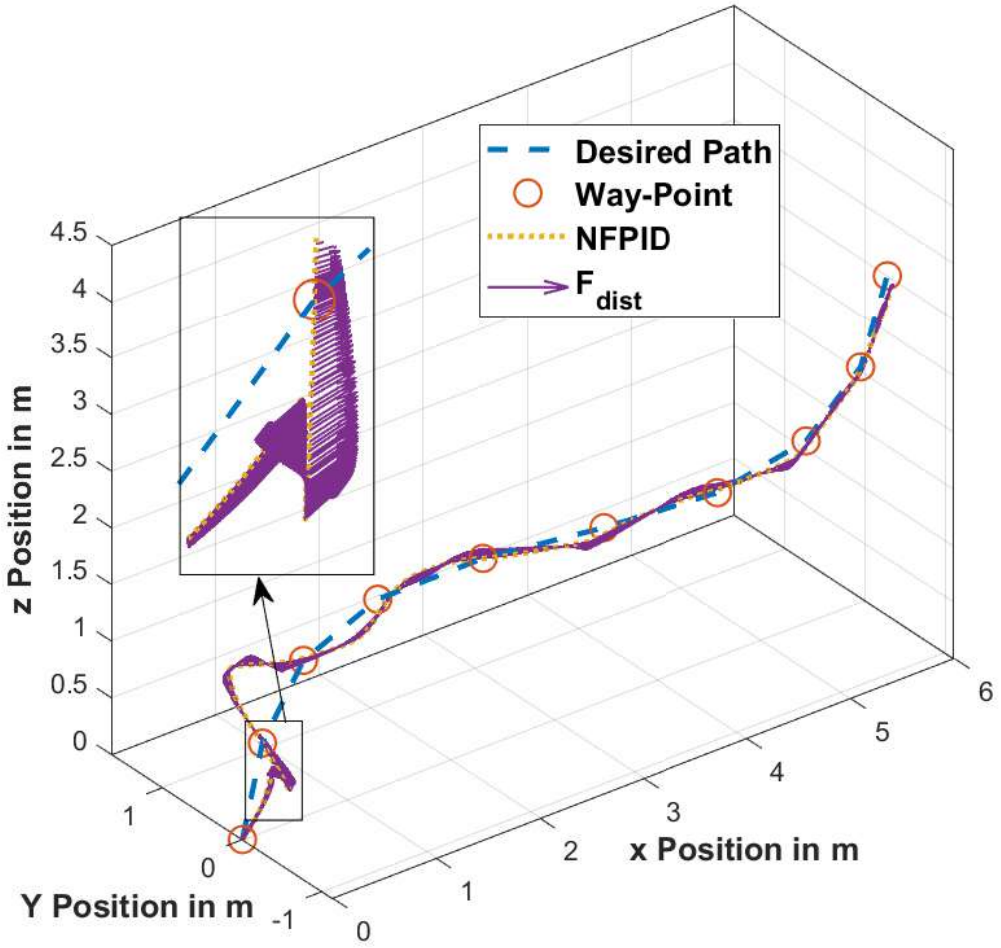

Figure 6.27: Position tracking with external disturbance of NFPID

Comparative simulation study is carried out under higher magnitude external disturbance force as follow.

$$f_{dist} = [5sin(t), 4sin(t), 3cos(t), 0]^T \tag{6.6}$$

SPID controller under same conditions failed(Fig. 6.15) to achieve the way points and deviated from the path under external disturbance. While the NFPID controller is able to achieve the way-points but is not able to move along the shortest path due to presence of high external disturbance.

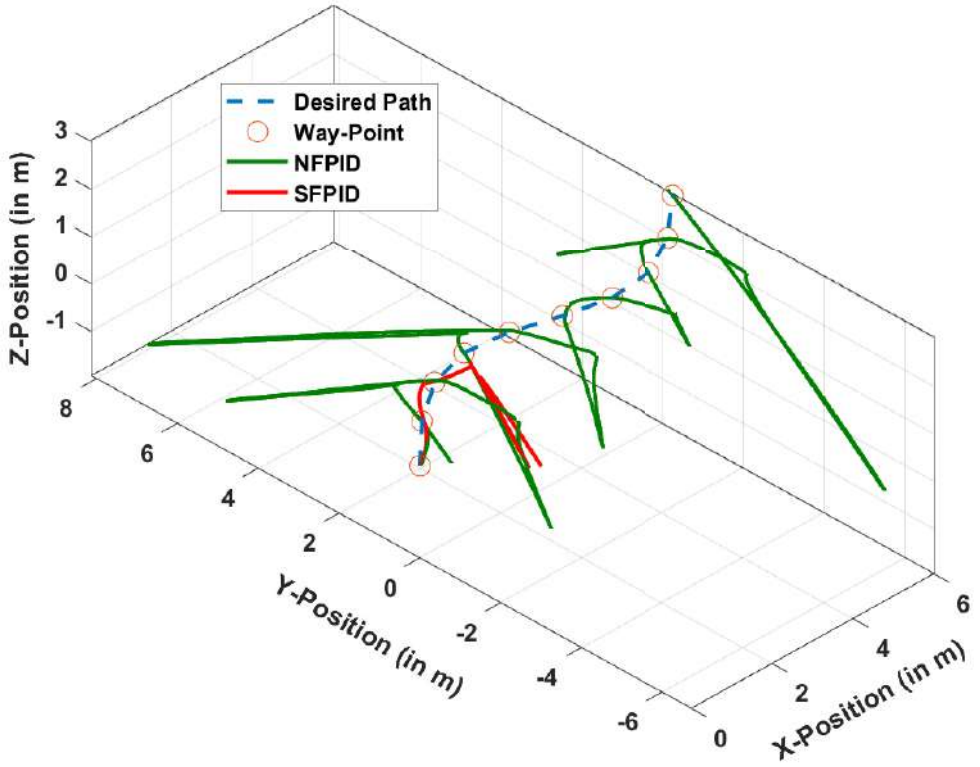

Figure 6.28: Position tracking with external disturbance of NFPID

6.4 Summary

In this chapter a self adaptive Fuzzy-PID controller is developed using fuzzy logic system to estimate the variations in the PID controller gains. Successful simulations with MATLAB^{TM} Simulink^{TM} model show case the controller can adapt to different trajectories. Comparative study of the Fuzzy-PID and PID controller is also presented to show the advantage of the adaptive controller. Simulation with external disturbance is also presented to show the robustness of the controllers. Adaptive network-based fuzzy inference system (ANFIS) is used to develop Neural Network (NN) model of the AUV with the field test data. The performance of the developed NN model is verified with another set of experimental data. This NN system is used in parallel with the PID system to address unknown system parameters and handle dynamic environmental forces. The developed controller is successfully simulated to show case its robustness and excellent dynamic stability.

Chapter 7

CONCLUSION AND FUTURE WORK

7.1 Introduction

In this chapter, the conclusions related to the design, development of an UUV and control system developed for AUV operation is presented. A compact UUV is designed and developed keeping in mind the identified requirements. A detailed mathematical model of the system is developed with system parameter identification and validated with experimental results. Both simple and adaptive controllers are developed for autonomous operation and simulations are carried out to showcase its stability. The general and specific conclusions are given in the next sections. The scope of future work is also highlighted in this chapter.

7.2 General Conclusion

In this work, a compact UUV is designed and developed. First the design requirements are identified for a compact underwater robot. Different essential internal components are selected and equivalent CAD models are developed. As a single thruster is used for vertical motion, the C.G. of the UUV must be close to the C.G. of the central thruster. To achieve this objective, linear search optimization is carried out using the MATLAB^{TM} Optimization Toolbox^{TM} to find the optimal position of the components along the X-axis. After fixing the position of the internal components, a side section of the encloser is developed, considering the dimensions of the internal components. A parametric fluid flow study of the 2D section is conducted with ANSYS FLUENT and optimization tool to find the optimal shape of the cross-section having

minimum drag coefficient. Slightly elliptical cross-section is selected to have less buoyancy. A closed frame structure with the selected cross section and the optimal side sections is developed with 3D modeling software SOLIDWORKS^{TM}. The hydrodynamic study is carried out using the CFD software ANSYS FLUENT^{TM} to find out the drag experienced by the UUV during its motion. According to the simulation results, the thrusters are selected for UUV to achieve 2 m/s speed. The FEM analysis is carried out to find the stress developed at different water depths showed that the UUV structure could withstand underwater pressure up to 100m depth with 1.84 factor of safety. After validating the UUV design, the structure was manufactured using glass fiber composite. The UUV is installed with required controllers (Pixhawk and Raspberry pi) and sensors (temperature, pressure) for both ROV and AUV operations. System is successfully operated in a lake, a pool, a river, and a dam. Field test of the UUV shows operational details of the UUV.

After development of the UUV next objective was to develop a robust controller. To achieve this goal, first the kinematic and dynamic model for the existing underwater robot is developed in 6 DOF. To simplify the complex dynamic model some assumptions were made. According to the assumptions the dynamic model has been converted to 4 DOF model neglecting the pitch and roll motion. Inertia and buoyancy parameters are estimated using detailed CAD model and physical measurements. Added mass matrix is calculated using slender body theory. Hydrodynamic parameters are estimated with CFD analysis for surge, sway, heave,and yaw motion. An empirical correlation between the input signal and thrust output is developed with the experimental data. MATLAB^{TM} Simulink^{TM} model and simulation platform is developed with the UUV model. Developed SIMULINK model is verified with open loop simulations for linear and curved path. Comparison of experimental field data and the system model output shows matching trend in prediction of heave motion.

A 3D guidance system is developed using waypoint technique and LOS strategy. The guidance system has to work with controller for the AUV to maneuver and follow the defined path. Inertial navigation system is developed to be used in the feedback loop of the controller to estimate accurate state of the AUV. INS used UKF to predict the AUV state, taking input from dynamic model, depth sensor, GPS, IMU measurements. Using the developed dynamic model

a closed-loop PID controller is developed using partitioning law for this non-linear coupled system. Controller gain parameters are selected to achieve a quick and stable response. The controller is simulated for specified target location as well as multi way-point 2D and 3D trajectory and results are discussed.

A self adaptive fuzzy PID controller is developed using the developed PID controller and Fuzzy logic and simulated with MATLAB^{TM} Simulink^{TM}. A comparative study between the PID and Fuzzy-PID controller is carried out show-casing that the Fuzzy-PID controller can adapt to deviation introduced in the tuned parameters, where as the PID controller failed to do so. Thus, the SFPID controller can adapt to deviations in the trajectory due to environmental disturbances. Independent Neural-Network models are developed for heave and planner motion with experimental data collected during field trials. The developed Neural network models predict the robot motion with minimal error. Neural network model is used in parallel with the PID system for adapting to various environmental conditions and unknown model behaviour. Simulation with external disturbance is also presented to show the robustness of the controllers. The NFPID controller is able to handle higher disturbance than the SFPID controller

7.3 Specific Conclusion

In this section specific conclusions related to design and development of a compact UUV have been presented.

7.3.1 Design and development of the UUV

- Linear search optimization is carried out to find the optimal position of the components maintaining the overall C.G close to the C.G of the central thruster. With the components at the optimal positions the C.G is found to be at 0.84 mm from the center.

- A parametric fluid flow study of the 2D section is conducted with ANSYS FLUENT^{TM} and optimization tool to find the optimal shape of the cross-section having minimum drag coefficient. The optimal shape is found with h_1 and h_3 parameter values as 70 mm and 56 mm respectively.

- CFD analysis has been carried out with the designed model to find out drag force at different flow speeds. Empirical correlation has been developed between the flow speed and drag force and actuator capable of producing 30 N of thrust is selected to achieve 2 m/s speed.

- Finite element stress analysis has been carried out with ANSYS^{TM} static structural module to show the designed model can withstand water pressure at 100 m depth with 1.84 factor of safety.

- The C.B is found to be 9.7 mm above the C.G along the same vertical line making the system stable from rollover. C.G is 1.67 cm away from the center along the vertical direction creating a possibility of pitch motion with high vertical thrust.

- A compact underwater robot is developed with following specifications:
  - length 55 cm, Width 43 cm, height 15 cm and weight 14.7kg.
  - It has a neutral buoyant, three-part modular structure.
  - Two 90 $^{\circ}$ woven and one random glass fiber layers are used for manufacturing.
  - System is designed for speed of 2m/s and a depth up to 100m.
  - Temperature sensor with a accuracy of $\pm$ 0.10C, a Depth sensor with a resolution of 2mm, and low light camera is used.

- During the river trial at Brahmaputra river, the UUV was able to move upstream against a flow of 2.6 m/s. Depth achieved during this trail is 5 m and speed as indicated by the Pixhawk controller is around 2.5 m/s.

- UUV is also deployed in a river dam upto a depth of 20 m.

- During a 30 min test run UUV battery voltage dropped from 11.6 V to 10.8 V, which is 80% to around 20%. Thus with a single 5500 mAh Li-Po battery the system can run around 45 mins.

7.3.2 Kinematic and dynamic modeling of the UUV

- A 6 DOF kinematic and dynamic model of the AUV is developed considering different forces acting on the system and simplified to a 4 DOF model with appropriate assumptions.
- Inertia and buoyancy parameter are estimated using Detail CAD model and physical measurements.
- Hydrodynamic parameter estimation is carried out with multiple CFD simulations along surge, sway, heave, and yaw motion. Linear and Quadratic damping parameters along surge, sway, heave, and yaw direction are (1.16×10^{-19}, 4.795), (3.902, 25.48), (6.574, 125.5), and (-11.53, 2.414), respectively.
- Experimental motion data from the lake run and mathematical model output with experimental data input shows a matching trend with 4.5% and 13.63% error in prediction of depth.
- Experimental motion data from the river dam run with upgraded neutral buoyant cable and mathematical model output with experimental data input shows a matching trend with 0.1% error in prediction of depth.
- Consideration of added mass effect improves the overall motion prediction of the mathematical model close to the experimental results.

7.3.3 Planning, localization, and control of the UUV

In this section specific conclusions related to planning, localization, and control of the UUV is highlighted.

- 3D guidance system is developed for way-point trajectory with LOS strategy. Here the the system try to follow the line of sight vector between the start point and the target. The acceptance radius is considered to be 0.2 m.

- Simulation of the developed PD controller with the target point at (10,7,6) shows a steady state error of 20 cm along Y axis. The error exist due to under-actuation in the system.
- Simulation of the developed PID controller with the target point at (10,7,6) shows a steady state error of 5 mm along Y axis.
- PID controller is successfully simulated for a 2D way-point path with way-points at (0,0) (3,4) (6,1) (8,4). The tuned proportional, integral, and derivative controller gains parameters along x, y, z and ψ are (17,0,17.7), (0.71,-0.1,1.68), (232.97,0,30.5), and (2162,0,92.99), respectively.
- PID controller is successfully simulated for a 3D way-point path with way-points are 10 equidistant points in x and z axes from 0 to 6 and 0 to 3 respectively and y-coordinates are in form of a sine function of x-coordinates. The tuned proportional integral and derivative controller gain parameters along x, y, z and ψ are (12,0,17.7), (0.71,-0.1,1.68), (20,0,30.5), and (200,0,92.99), respectively.
- Constant velocity criteria introduced at the way points reduced time taken to complete the path by 50%.
- UKF is used to predict AUV state taking input from dynamic model, depth sensor, GPS, IMU measurement. Sensor models developed introducing noise to the dynamic model output for simulation.
- UKF output show case estimated state close to confident sensor data.

7.3.4 Adaptive controller design for the UUV

Specific conclusions related to adaptive controller design is presented in this section.

- Fuzzy-PID controller is developed by introducing fuzzy system to adjust the PID controller gains.
- Comparison study of the PID and Fuzzy-PID system shows the adaptive nature of the controller. Where the PID controller is unable to complete more than 2 way-points and

deviate from the path the Fuzzy-PID system is able to complete the trajectory successfully.

- The controller is successfully simulation for different trajectories without tuning showcasing the robustness of the controller and comparison with PID controller shows better performance of the SFPID controller.
- The SFPID controller is able to handle external sinusoidal disturbance of the magnitude 3 N and The PID controller failed to achieve the waypoint under the disturbance.
- Neural network model for AUV heave motion is fitted with experimental data with regression value 0.83.
- A separate Neural network model for AUV horizontal motion is trained with experimental data with regression value 0.85.
- The NN models are used in parallel with the PID controller to develop the neuro-fuzzy controller and successfully simulated for way-point trajectory. The comparison between the SFPID and the NFPID shows slightly better performance by the NFPID as the SFPID takes 10 seconds longer to complete the trajectory and struggles with the last way-point.
- The NFPID controller is able to handle external sinusoidal disturbance of the magnitude 5 N and The SPID controller failed to achieve the waypoint under the disturbance.

7.4 Scope of Future Work

In the preset work a compact low-cost AUV has been developed with a robust trajectory tracking controller for autonomous operation. There are many scope to extend the present work in order to enhance the AUV autonomy and operational efficiency.

- The UUV structure can be further optimized with more complex hydrofoil shape and the structure can be developed with a composite 3D printer.
- Presently the AUV is a fixed buoyancy system and option of a variable buoyancy ballast system can be explored in the future.

- Addition of other sensors such as dissolved oxygen, turbidity, sonar etc. can be explored to expand the vehicle capability.
- In this work fixed way-point navigation has been used. Development of a navigation system for dynamic target tracking will add dynamic object following capability.
- Improvement of localization using stereo vision sensors can be explored for low-cost localization solutions.
- Development of low-cost acoustic localization system can be explored for localization.
- In this work the developed controllers are simulated, these will be further implement in the AUVs and real-world performance will be studied.
- Development of control system for obstacle avoidance with vision and sonar sensors will be helpful in an unknown dynamic environment for collision avoidance.
- Manipulator can be added to the system for Intervention AUV operation.

References

[1] Remotely Operated Vehicle Committee of the Marine Technology Society. Rovs - a brief history. www.rov.org/history/. Online; accessed 5-March-2020.

[2] H.R. Widditsch. SPURV-The First Decade. Technical report, Applied Physics Laboratory, University of Washington, Oct 1973.

[3] Kongsberg Maritime. Remus 6000. https://geo-matching.com/auvs-autonomous-underwater-vehicles/remus-6000. Online; accessed 5-March-2020.

[4] S. N. Shome and S. K. Das. Development of modular shallow water AUV : issues & trial results . *Journal of The Institution of Engineers (India): Series C*, 93:217–228, Aug 2012.

[5] AUVAC. Autonomous undersea vehicle application center. http://auvac.org/. Online; accessed 5-March-2020.

[6] General Dynamics Mission Systems. Bluefin-21. http://gdmissionsystems.com/bluefinrobotics/vehicles-batteries-and-services/bluefin-21, . Online; accessed 5-March-2020.

[7] Robert Panish and Mikell Taylor. Achieving high navigation accuracy using inertial navigation systems in autonomous underwater vehicles. In *Proceedings of the OCEANS IEEE International Conference, Spain*, pages 1–7. Jun 2011.

[8] B. Allotta, R. Costanzi, A. Ridolfi, O. Salvetti, M. Reggiannini, M. Kruusmaa, T. Salumae, D M Lane, G. Frost, N. Tsiogkas, M. Cocco, L. Gualdesi, G. Lacava, D. Roig, H T Gundogdu, M I C Dede, S. Baines, S. Tusa, P. Latti, and D. Scaradozzi. The ARROWS Project: robotic technologies for underwater archaeology. *IOP Conference Series: Materials Science and Engineering*, 364(1): 012088, Jun 2018.

[9] Enrico Simetti and Giuseppe Casalino. Manipulation and Transportation With Cooperative Underwater Vehicle Manipulator Systems. *IEEE Journal of Oceanic Engineering*, 42(4):782–799, Oct 2017.

[10] Mario Prats, David Ribas, Narcís Palomeras, Juan Carlos García, Volker Nannen, Stephan Wirth, José Javier Fernández, Joan P. Beltrán, Ricard Campos, Pere Ridao, Pedro J Sanz, Gabriel Oliver, Marc Carreras, Nuno Gracias, Raúl Marín, and Alberto Ortiz. Reconfigurable AUV for intervention missions: a case study on underwater object recovery. *Intelligent Service Robotics*, 5(1): 19–31, Jan 2012.

[11] Pedro J Sanz, Pere Ridao, Gabriel Oliver, Giuseppe Casalino, Carlos Insaurralde, Carlos Silvestre, Claudio Melchiorri, and Alessio Turetta. TRIDENT: Recent Improvements about Autonomous Underwater Intervention Missions. In *IFAC Proceedings Volumes*, volume 45, pages 355–360, 2012.

[12] J. Ferguson. Under-ice seabed mapping with AUVs. In *Proceedings of the OCEANS'09 IEEE International Conference, Bremen: Balancing Technology with Future Needs*, pages 1–6. May 2009.

[13] Chris Kaminski, Tristan Crees, James Ferguson, Alexander Forrest, Jeff Williams, David Hopkin, and Garry Heard. 12 days under ice - An historic AUV deployment in the Canadian High Arctic. In *Proceedings of the IEEE/OES International Conference on Autonomous Underwater Vehicles*, 2010.

[14] Kangsoo Kim, Tamaki Ura, Kenji Nagahashi, Takayuki Asanuma, Takatoshi Matsuzawa, Kenji Nakane, Tadamasa Obata, Hisashi Koyama, Yuuji Ooyabu, and Ryuichi Nagata. Towards AUV-based iceberg profiling and gouging survey in arctic sea: The first Japanese under-ice AUV deployment in Okhotsk Sea. In *Proceedings of the IEEE International Symposium on Underwater Technology (UT)*, 2013.

[15] Colin Morice, Sandor Veres, and Stephen McPhail. Terrain referencing for autonomous navigation of underwater vehicles. In *Proceedings of the 2009 OCEANS International Conference, Europe*, pages 1–7. May 2009.

[16] D. Thompson, D. Caress, C. Paull, D. Clague, H. Thomas, and D. Conlin. MBARI mapping

AUV operations: In the Gulf of California. In *Proceedings of the OCEANS IEEE International Conference*, pages 1–5. Oct 2012.

[17] E. Desa, R. Madhan, P. Maurya, G. Navelkar, A. Mascarenhas, S. Prabhudesai, S. Afzulpurkar, and S. Bandodkar. The small maya auv - initial field results. *International Ocean Systems*, 11(1): 6–9, 2007.

[18] Robert K. Katzschmann, Joseph DelPreto, Robert MacCurdy, and Daniela Rus. Exploration of underwater life with an acoustically controlled soft robotic fish. *Science Robotics*, 3(16):eaar3449, Mar 2018.

[19] A U V Tri-ton. Detailed 3D Seafloor Imaging of Kagoshima Bay by. In *Proceedings of the IEEE International Conference on Underwater Technology (UT)*, pages 1–6. Feb 2013.

[20] A. Alvarez, A. Caffaz, A. Caiti, G. Casalino, E. Clerici, F. Giorgi, L. Gualdesi, A. Turetta, and R. Viviani. FOLAGA: A VERY LOW COST AUTONOMOUS UNDERWATER VEHICLE FOR COASTAL OCEANOGRAPHY. In *IFAC Proceedings of the 16th Triennial World Congress*, volume 38, pages 31–36, Prague, Czech Republic, 2005.

[21] R Kimura, M Choyekh, N Kato, H Senga, H Suzuki, M Ukita, and K Kamezuka. Guidance and Control of an Autonomous Underwater robot for Tracking and Monitoring Spilled Plumes of Oil and Gas from Seabed. In *Proceedings of the Twenty-third International Offshore and Polar Engineering (ISOPE) Conference*, volume 9, pages 366–371, 2013.

[22] Giacomo Marani, Song K Choi, and Junku Yuh. Underwater autonomous manipulation for intervention missions AUVs. *Ocean Engineering*, 36(1):15–23, Jan 2009.

[23] Marco Jacobi. Autonomous inspection of underwater structures. *Robotics and Autonomous Systems*, 67:80–86, May 2015.

[24] Naomi Kato, Y. Ito, J. Kojima, S. Takagi, K. Asakawa, and Y. Shirasaki. Control performance of autonomous underwater vehicle "AQUA EXPLORER 1000" for inspection of underwater cables. In *Proceedings of the OCEANS International Conference*, volume 1, pages I/135–I/140, aqua1000, 1994. IEEE.

[25] Kawasaki Subsea (UK) Limited. Kawasaki auv, Feb 2019. Accessed: 2019-03-05.

[26] H. Nakajoh, T. Miyazaki, T. Sawa, F. Sugimoto, and T. Murashima. Development of 7000m work class ROV "KAIKO Mk-IV". In *Proceedings of the OCEANS IEEE International Conference, Monterey*, pages 1–6. Sep 2016.

[27] J. Padial, S. Dektor, and S. M. Rock. Correlation of imaging sonar acoustic shadows and bathymetry for ROV terrain-relative localization. In *Proceedings of the OCEANS IEEE International Conference, TAIPEI*, pages 1–10. Apr 2014.

[28] Kim R Reisenbichler, Mark R Chaffey, Francois Cazenave, Robert S Mcewen, Richard G Henthorn, E Robert, and Bruce H Robison. Automating MBARI ' s midwater time-series video surveys : the transition from ROV to AUV. In *Proceedings of the OCEANS MTS IEEE International Conference, Monterey*, pages 1–9. Sep 2016.

[29] Stein M Nornes, Martin Ludvigsen, and Asgeir J. Sorensen. Automatic relative motion control and photogrammetry mapping on steep underwater walls using ROV. In *Proceedings of the OCEANS MTS IEEE International Conference, Monterey*, pages 1–6. Sep 2016.

[30] Avilash Sahoo, Santosha K. Dwivedy, and P.S. Robi. Advancements in the field of autonomous underwater vehicle. *Ocean Engineering*, 181:145–160, Jun 2019.

[31] Bong Huan Jun, Jin Yeong Park, Fill Youb Lee, Pan Mook Lee, Chong Moo Lee, Kihun Kim, Young Kon Lim, and Jun Ho Oh. Development of the AUV 'ISiMI' and a free running test in an Ocean Engineering Basin. *Ocean Engineering*, 36(1):2–14, 2009.

[32] Thomas Hiller, Arnar Steingrimsson, and Robert Melvin. Expanding the small AUV mission envelope; longer, deeper & more accurate. In *Proceedings of the IEEE OES International Conference on Autonomous Underwater Vehicles (AUV)*, 2012.

[33] Tadahiro Hyakudome. Design of autonomous underwater vehicle. *International Journal of Advanced Robotic Systems*, 8(1):131–139, 2011.

[34] E. Y. Hong, H. G. Soon, and M. Chitre. Depth control of an autonomous underwater vehicle, STARFISH. In *Proceedings of the OCEANS'10 IEEE International Conference, SYDNEY*, pages 1–6. May 2010.

[35] Marc Carreras, Juan David Hernandez, Eduard Vidal, Narcis Palomeras, David Ribas, and Pere Ridao. Sparus II AUV—A Hovering Vehicle for Seabed Inspection. *IEEE Journal of Oceanic Engineering*, 43(2):344–355, Apr 2018.

[36] Benedetto Allotta, Steven Baines, Fabio Bartolini, Fabio Bellavia, Carlo Colombo, Roberto Conti, Riccardo Costanzi, Can Dede, Marco Fanfani, Jonathan Gelli, Hilal Tolasa Gundogdu, Niccolo Monni, Davide Moroni, Marco Natalini, Maria Antonietta Pascali, Fabio Pazzaglia, Luca Pugi, Alessandro Ridolfi, Marco Reggiannini, Daniel Roig, Ovidio Salvetti, and Enis I. Tekdemir. Design of a modular Autonomous Underwater Vehicle for archaeological investigations. In *OCEANS 2015 - Genova*, pages 1–5. May 2015.

[37] A. Fittery, A. Mazumdar, M. Lozano, and H. H. Asada. Omni-Egg: A smooth, spheroidal, appendage free underwater robot capable of 5 DOF motions. *Proceedings of the OCEANS MTS IEEE International Conference on Harnessing the Power of the Ocean*, 2012.

[38] Yanlin He, Liwei Shi, Shuxiang Guo, Ping Guo, and Rui Xiao. Numerical simulation and hydrodynamic analysis of an amphibious spherical robot. In *Proceedings of the IEEE International Conference on Mechatronics and Automation (ICMA)*, pages 848–853, 2015.

[39] Chunfeng Yue, Shuxiang Guo, and Liwei Shi. Hydrodynamic analysis of the spherical underwater robot SUR-II. *International Journal of Advanced Robotic Systems*, 10:1–12, 2013.

[40] Xu Ma, Shuxiang Guo, Liguo Li, Yuehui Ji, and Yunliang Wang. The underwater motion simulation of a spherical amphibious robot. In *Proceedings of the IEEE International Conference on Mechatronics and Automation (ICMA)*, pages 145–149, 2014.

[41] Yaxin Li, Shuxiang Guo, and Yu Wang. Design and characteristics evaluation of a novel spherical underwater robot. *Robotics and Autonomous Systems*, 94:61–74, Aug 2017.

[42] F. Wan, S. Guo, X. Ma, Y. Ji, and Y. Wang. Characteristic analysis on land for an amphibious spherical robot. In *Proceedings of the IEEE International Conference on Mechatronics and Automation, ICMA*, pages 1945–1950, 2014.

[43] Ji-hong Li, Byung-ho Yoon, Seung-sub Oh, Jung-san Cho, Jong-geol Kim, Mun-jik Lee, and Jung-woo Lee. Development of an Intelligent Autonomous Underwater Vehicle , P-SURO. In

Proceedings of the IEEE OCEANS International Conference, Sydney, volume 12, pages 0–4, 2010.

[44] K. Alam, T. Ray, and S. G. Anavatti. Design and construction of an autonomous underwater vehicle. *Neurocomputing*, 142:16–29, 2014.

[45] Stephan Wirth, Pep Lluis Negre Carrasco, and Gabriel Oliver Codina. Visual odometry for autonomous underwater vehicles. In *Proceedings of the IEEE OCEANS International Conference, Bergen*, pages 1–6. Jun 2013.

[46] V M Hung and U. J. Na. Remote control system of a 6 DOF underwater robot. In *Proceedings of the International Conference on Control, Automation and Systems*, pages 2575–2580. Oct 2008.

[47] Gi Hun Yang, Wooseok Choi, Sang Hyo Lee, Kyung Sik Kim, Hyun Jin Lee, Hyeun Seok Choi, and Young Sun Ryuh. Control and design of a 3 DOF fish robot 'Ichtus'. In *Proceedings of the IEEE International Conference on Robotics and Biomimetics, ROBIO*, pages 2108–2113, 2011.

[48] S. Parameswaran and Sera Selvin. Fish model for underwater robots. In *Proceedings of the Annual IEEE India Conference (INDICON), Hyderabad*, 2011.

[49] Shaurya Shriyam, Anuj Agrawal, Laxmidhar Behera, and Anupam Saxena. Robotic Fish Design and Control based on Biomechanics. *IFAC Proceedings Volumes*, 47(1):662–669, jan 2014.

[50] Jagadeesh Kadiyam and Santhakumar Mohan. Conceptual design of a hybrid propulsion underwater robotic vehicle with different propulsion systems for ocean observations. *Ocean Engineering*, 182:112–125, jun 2019.

[51] M. Santhakumar and T. Asokan. Coupled, non-linear control system design for autonomous underwater vehicle (AUV). *2008 10th International Conference on Control, Automation, Robotics and Vision, ICARCV 2008*, pages 2309–2313, 2008.

[52] Abhra Roy Chowdhury, Bhuneshwar Prasad, Vinoth Vishwanathan, Rajesh Kumar, and S. K. Panda. Finding an operating region for a bio-inspired robotic fish underwater vehicle in the Lighthill framework. *2013 IEEE International Conference on Robotics and Biomimetics, ROBIO 2013*, pages 854–860, 2013.

[53] Abhra Roy Chowdhury, Bhuneshwar Prasad, Vinoth Vishwanathan, Rajesh Kumar, and S. K. Panda. Bio-harmonized Dynamic Model of a Biology Inspired Carangiform Robotic Fish Underwater Vehicle. *IFAC Proceedings Volumes*, 47(3):7258–7265, jan 2014.

[54] Abhra Roy Chowdhury, Bhuneshwar Prasad, Vinoth Vishwanathan, Rajesh Kumar, and S. K. Panda. Kinematics study and implementation of a biomimetic robotic-fish underwater vehicle based on Lighthill slender body model. *2012 IEEE/OES Autonomous Underwater Vehicles, AUV 2012*, 2012.

[55] Alissa Ully Ashar, Muhammad Akbar Jamaludin, M. Fadhli Zakiy, and Arief Syaichu-Rohman. Design, kinematic modeling, and implementation of autonomous fish robot for underwater sensing. In *Proceedings of the Joint International Conference on Rural Information and Communication Technology and Electric-Vehicle Technology, RICT and ICEV-T*, 2013.

[56] Tuong Quan Vo, Hyoung Seok Kim, and Byung Ryong Lee. A study on turning motion control of a 3-joint fish robot using sliding mode based controllers. In *Proceedings of the International Conference on Control Automation and Systems (ICCAS), KINTEX, Gyeonggi-do, Korea*, pages 1556–1561, Oct 2010.

[57] Sung Hee Choi and Jangmyung Lee. Robust navigation algorithm of the fishlike robot in the unknown underwater environment. In *Proceedings of the 9th International Conference on Ubiquitous Robots and Ambient Intelligence, URAI*, pages 266–271, 2012.

[58] Madis Listak, Deivid Pugal, and Maarja Kruusmaa. CFD simulations and real world measurements of drag of biologically inspired underwater robot. In *Proceedings of the IEEE/OES US/EU-Baltic International Symposium*, pages 1–4. May 2008.

[59] J. Yu, C. Wang, and G. Xie. Coordination of multiple robotic fish with applications to underwater robot competition. *IEEE Transactions on Industrial Electronics*, 63(2):1280–1288, Feb 2016.

[60] David S. Jung, Peter P. Pott, Taavi Salumae, and Maarja Kruusmaa. Flow-aided path following of an underwater robot. In *Proceedings of the IEEE International Conference on Robotics and Automation*, pages 4602–4607, 2013.

[61] Wei Zhao, Yonghui Hu, Long Wang, and Yingmin Jia. Development of a flipper propelled turtle-

like underwater robot and its CPG-based control algorithm. In *Proceedings of the IEEE Conference on Decision and Control*, pages 5226–5231. 2008.

[62] Hee Joong Kim and Jihong Lee. Designing diving beetle inspired underwater robot(D.BeeBot). In *Proceedings of the 13th International Conference on Control Automation Robotics and Vision (ICARCV)*, volume 2014, pages 1746–1751, Dec 1997.

[63] B. H. Jun, H. Shim, B. Kim, J. Y. Park, H. Baek, P. M. Lee, W. J. Kim, and Y. S. Park. Preliminary design of the multi-legged underwater walking robot CR200. In *Proceedings of the OCEANS MTS IEEE International Conference on The Living Ocean and Coast - Diversity of Resources and Sustainable Activities, Yeosu*, pages 8–11, 2012.

[64] B. H. Jun, H. Shim, B. Kim, J. Y. Park, H. Baek, S. Yoo, and P. M. Lee. Development of seabed walking robot CR200. In *Proceedings of the OCEANS MTS IEEE International Conference, Bergen*, pages 1–5. Jun 2013.

[65] J. I. Kang, S. K. Jeoung, J. Y. Oh, H. S. Choi, Y. H. Kim, J. Y. Kim, S. H. Yu, and H. K. Cho. An analysis of carbon fiber hull structure of a new underwater glider. *International Journal of Modern Physics B*, 32(19):1840065, Jul 2018.

[66] Ngoc-duc Nguyen, Hyeung-sik Choi, Ngoc-Huy Tran, and Seo-Kang Kim. Development of Ray-Type Underwater Glider. In Vo Hoang Duy, Tran Trong Dao, Ivan Zelinka, Sang Bong Kim, and Tran Thanh Phuong, editors, *AETA 2017 - Recent Advances in Electrical Engineering and Related Sciences: Theory and Application*, volume 465 of *Lecture Notes in Electrical Engineering*, pages 677–685. Springer International Publishing, Cham, Jan 2018.

[67] Aiguo Ming, Takahiro Ichikawa, Wenjing Zhao, and Makoto Shimojo. Development of a sea snake-like underwater robot. In *Proceedings of the IEEE International Conference on Robotics and Biomimetics (ROBIO)*, pages 761–766, 2014.

[68] National Institute Of Oceanography(NIO). AUV Technology-MAYA. www.nio.org/index/option/com_subcategory/task/show/title/AUV Technology/tid/2/sid/134/thid/143. Online; accessed 5-March-2020.

[69] Chunya Sun, Baowei Song, Peng Wang, and Xinjing Wang. Shape optimization of blended-wing-

body underwater glider by using gliding range as the optimization target. *International Journal of Naval Architecture and Ocean Engineering*, 9(6):693–704, Nov 2017.

[70] Fathallah Elsayed, Hui Qi, Li Li Tong, and Mahmoud Helal. Optimal Structure Design of Elliptical Deep-Submersible Pressure Hull. *Materials Science Forum*, 813:85–93, Mar 2015.

[71] A. Mitra, J.P. Panda, and H.V. Warrior. The effects of free stream turbulence on the hydrodynamic characteristics of an AUV hull form. *Ocean Engineering*, 174:148–158, Feb 2019.

[72] Benedetto Allotta, Luca Pugi, Fabio Bartolini, Alessandro Ridolfi, Riccardo Costanzi, Niccolò Monni, and Jonathan Gelli. Preliminary design and fast prototyping of an Autonomous Underwater Vehicle propulsion system. *Proceedings of the Institution of Mechanical Engineers, Part M: Journal of Engineering for the Maritime Environment*, 229(3):248–272, Aug 2015.

[73] J C P Liou. AUV hydrodynamics for survivability and controllability. In *Proceedings of the OCEANS IEEE International Conference*, number 2, pages 1–9, 2011.

[74] Lihong Wu. Applying dynamic hybrid grids method to simulate AUV docking with a tube. In *Proceedings of the IEEE International Conference on Information and Automation, ICIA*, pages 1363–1366, 2010.

[75] P Stevenson, D Graham, and C Clayson. The Mechanical Design and Implementation of an Autonomous Submersible. *Underwater Technology*, 23(1):31–41, Jan 1998.

[76] J. Błachut and P. Smith. Buckling of multi-segment underwater pressure hull. *Ocean Engineering*, 35(2):247–260, Feb 2008.

[77] Khairul Izman Abdul Rahim, Abdul Rahim Othman, and Mohd Rizal Arshad. Conceptual design of a pressure hull for an underwater pole inspection robot. *Indian Journal of Marine Sciences*, 38 (3):352–358, 2009.

[78] Jagadeesh Kadiyam, Chaitanya Mehta, Santhakumar Mohan, and D. Deshmukh. Implementation of a robust motion control scheme for an Ostraciiform inspired underwater robot with caudal and pectoral fins. *IFAC-PapersOnLine*, 52(21):283–290, jan 2019.

[79] K. Isa and Mohd Rizal A. Motion simulation for propeller-driven USM underwater glider with controllable wings and rudder. In *Proceedings of the 2nd International Conference on Instrumentation Control and Automation, ICA*, pages 316–321, Nov 2011.

[80] B. Allotta, A. Caiti, L. Chisci, R. Costanzi, F. Di Corato, C. Fantacci, D. Fenucci, E. Meli, and A. Ridolfi. An unscented Kalman filter based navigation algorithm for autonomous underwater vehicles. *Mechatronics*, 39:185–195, Nov 2016.

[81] Eric Guerrero Font, Miquel Massot Campos, Pep Lluis Negre, Francisco Bonin Font, and Gabriel Oliver Codina. An USBL-aided multisensor navigation system for field AUVs. In *Proceedings of the IEEE International Conference on Multisensor Fusion and Integration for Intelligent Systems (MFI)*, pages 430–435. Sep 2016.

[82] General Dynamics Mission Systems. Hovering auv. http://gdmissionsystems.com/bluefinrobotics/vehicles-batteries-and-services/hauv, . Online; accessed 5-March-2020.

[83] Thor I. Fossen. *Guidance and Control of Ocean Vehicles*. John Wiley & Sons Ltd., 1994.

[84] Thor I. Fossen. *Handbook of Marine Craft Hydrodynamics and Motion Control*. John Wiley & Sons Ltd., 2011.

[85] Gianluca Antonelli. *Underwater Robots*, volume 96 of *Springer Tracts in Advanced Robotics*. Springer International Publishing, Cham, 2014.

[86] Thor I Fossen and Ola Erik Fjellstad. Nonlinear modelling of marine vehicles in 6 degrees of freedom. *Mathematical Modelling of Systems*, 1(1):17–27, Jan 1995.

[87] J. D. Weiss and E. D. T. Noel. Real-time dynamic model learning and adaptation for underwater vehicles. In *Proceedings of the Oceans International Conference, San Diego, USA*, Sep 2013.

[88] Chao Shen, Yang Shi, and Brad Buckham. Nonlinear model predictive control for trajectory tracking of an AUV: A distributed implementation. In *Proceedings of the IEEE 55th Conference on Decision and Control (CDC)*, pages 5998–6003. Dec 2016.

[89] Mohammad Khalaj Amir Hosseini, Omid Omidi, Ali Meghdari, and Gholamreza Vossoughi. A Composite Rigid Body Algorithm for Modeling and Simulation of an Underwater Vehicle Equipped With Manipulator Arms. *Journal of Offshore Mechanics and Arctic Engineering*, 128 (2):119–132, May 2006.

[90] C. S. Chin, M. W. S. Lau, E. Low, and G. G. L. Seet. Software for modelling and simulation of a Remotely-Operated Vehicle (ROV). *International Journal of Simulation Modelling*, 5(3): 114–125, 2006.

[91] Ngatini, Erna Apriliani, and Hendro Nurhadi. Ensemble and Fuzzy Kalman Filter for position estimation of an autonomous underwater vehicle based on dynamical system of AUV motion. *Expert Systems with Applications*, 68:29–35, Feb 2017.

[92] Zhe Wang, Shuxiang Guo, Liwei Shi, Shaowu Pan, and Yanlin He. The application of PID control in motion control of the spherical amphibious robot. In *Proceedings of the IEEE International Conference on Mechatronics and Automation, ICMA*, pages 1901–1906, 2014.

[93] Pouria Sarhadi, Abolfazl Ranjbar Noei, and Alireza Khosravi. Model reference adaptive PID control with anti-windup compensator for an autonomous underwater vehicle. *Robotics and Autonomous Systems*, 83:87–93, Sep 2016.

[94] Tao Liu, Yuli Hu, Hui Xu, Qiankun Wang, and Weiqiang Du. A novel vectored thruster based on 3-RPS parallel manipulator for autonomous underwater vehicles. *Mechanism and Machine Theory*, 133:646–672, Mar 2019.

[95] Jangho Bae, Jeongae Bak, Sangrok Jin, TaeWon Seo, and Jongwon Kim. Optimal configuration and parametric design of an underwater vehicle manipulator system for a valve task. *Mechanism and Machine Theory*, 123:76–88, May 2018.

[96] Jorge Silva and Joao Sousa. Models for simulation and control of underwater vehicles. *New Approaches in Automation and Robotics*, pages 197–207, May 2008.

[97] Ayman B. Mahfouz, Mahmoud R. Haddara, and Christopher D. Williams. Prediction of the Hydrodynamic Parameters in the Coupled Heave and Pitch Motion Equations for Underwater Robotic Vehicles Using Measured Responses at Sea. *Journal of Offshore Mechanics and Arctic Engineering*, 123(3):93–102, Aug 2001.

[98] Juan Julca Avila, Kazuo Nishimoto, Claudio Mueller Sampaio, and Julio C. Adamowski. Experimental Investigation of the Hydrodynamic Coefficients of a Remotely Operated Vehicle Using a Planar Motion Mechanism. *Journal of Offshore Mechanics and Arctic Engineering*, 134(2): 021601, May 2012.

[99] Juan S. Cely, Roque Saltaren, Gerardo Portilla, Oz Yakrangi, and Alejandro Rodriguez-Barroso. Experimental and Computational Methodology for the Determination of Hydrodynamic Coeffi-

cients Based on Free Decay Test: Application to Conception and Control of Underwater Robots. *Sensors*, 19(17):3631, Aug 2019.

[100] C. S. Chin, W. P. Lin, and J. Y. Lin. Experimental validation of open-frame ROV model for virtual reality simulation and control. *Journal of Marine Science and Technology (Japan)*, 23(2): 267–287, 2018.

[101] Rui Yang, Benoit Clement, Ali Mansour, Ming Li, and Nailong Wu. Modeling of a Complex-Shaped Underwater Vehicle for Robust Control Scheme. *Journal of Intelligent & Robotic Systems*, 80(3-4):491–506, Dec 2015.

[102] Yang Luo, Qing Xiao, and Guangyu Shi. A Fluid-Structure Interaction Study on a Bionic Fish Fin with Non-Uniform Stiffness Distribution. *Journal of Offshore Mechanics and Arctic Engineering*, 142(5), Oct 2020.

[103] Sh. Mansoorzadeh and E. Javanmard. An investigation of free surface effects on drag and lift coefficients of an autonomous underwater vehicle (AUV) using computational and experimental fluid dynamics methods. *Journal of Fluids and Structures*, 51:161–171, Nov 2014.

[104] F. R. Menter, R. B. Langtry, S. R. Likki, Y. B. Suzen, P. G. Huang, and S. Volker. A Correlation-Based Transition Model Using Local Variables—Part I: Model Formulation. *Journal of Turbomachinery*, 128(3):413, 2006.

[105] You Hong Eng, Cheng Siong Chin, and Michael Wai Shing Lau. Added mass computation for control of an open-frame remotely-operated vehicle: Application using WAMIT and MATLAB. *Journal of Marine Science and Technology (Taiwan)*, 22(4):405–416, 2014.

[106] Chen-wei Chen and Ning-min Yan. Prediction of Added Mass for an Autonomous Underwater Vehicle Moving Near Sea Bottom Using Panel Method. In *2017 4th International Conference on Information Science and Control Engineering (ICISCE)*, pages 1094–1098. Jul 2017.

[107] Mochammad Agoes Moelyadi and Bagus Bambang Riswandi. CFD Based Added Mass Prediction in Cruise Condition of Underwater Vehicle Dynamic. *Journal of Physics: Conference Series*, 1005 (1):012011, Apr 2018.

[108] Josefine Severholt. Generic 6-DOF Added Mass Formulation for Arbitrary Underwater Vehicles based on Existing Semi-Empirical Methods, 2017.

[109] Edward V. Lewis. *Principles of Naval Architecture: Volume III - Motion in Waves*. The Society of Naval Architects and Marine Engineers (SNAME), 1988.

[110] R.G. Dong. Effective mass and damping of submerged structures. Technical Report 4, Lawrence Livermore National Laboratory (LLNL), Livermore, CA, Apr 1978.

[111] J. N. Newman. *Marine Hydrodynamics*. MIT Press, 1977.

[112] S.K. Choi, G.Y. Takashige, and J Yuh. Experimental study on an underwater robotic vehicle: ODIN. In *Proceedings of IEEE Symposium on Autonomous Underwater Vehicle Technology (AUV'94)*, pages 79–84. 1994.

[113] H.H. Wang, S.M. Rock, and M.J. Lees. Experiments in automatic retrieval of underwater objects with an AUV. In *'Challenges of Our Changing Global Environment'. Conference Proceedings. OCEANS '95 MTS/IEEE*, volume 1, pages 366–373. 1995.

[114] D.M. Lane, J.B.C. Davies, G. Casalino, G. Bartolini, G. Cannata, G. Veruggio, M. Canals, C. Smith, D.J. O'Brien, M. Pickett, G. Robinson, D. Jones, E. Scott, A. Ferrara, D. Angelleti, M. Coccoli, R. Bono, P. Virgili, R. Pallas, and E. Gracia. AMADEUS: advanced manipulation for deep underwater sampling. *IEEE Robotics & Automation Magazine*, 4(4):34–45, 1997.

[115] V. Rigaud, E. Coste-Maniere, M.J. Aldon, P. Probert, M. Perrier, P. Rives, D. Simon, D. Lang, J. Kiener, A. Casal, J. Amar, P. Dauchez, and M. Chantler. UNION: underwater intelligent operation and navigation. *IEEE Robotics & Automation Magazine*, 5(1):25–35, Mar 1998.

[116] Jonathan Evans, Paul Redmond, Costas Plakas, Kelvin Hamilton, and David Lane. Autonomous docking for Intervention-AUVs using sonar and video-based real-time 3D pose estimation. In *Oceans 2003. Celebrating the Past ... Teaming Toward the Future (IEEE Cat. No.03CH37492)*, volume 4, pages 2201–2210 Vol.4. 2003.

[117] Jagadeesh Kadiyam, Santhakumar Mohan, Devendra Deshmukh, and Taewon Seo. Simulation-based semi-empirical comparative study of fixed and vectored thruster configurations for an underwater vehicle. *Ocean Engineering*, 234:109231, aug 2021.

[118] Yu Wang, Shuo Wang, Qingping Wei, Min Tan, Chao Zhou, and Junzhi Yu. Development of an Underwater Manipulator and Its Free-Floating Autonomous Operation. *IEEE/ASME Transactions on Mechatronics*, 21(2):815–824, Apr 2016.

[119] Simson T. Wilson, a. P. Sudheer, and Santhakumar Mohan. Dynamic modelling, simulation and spatial control of an underwater robot equipped with a planar manipulator. In *Proceedings of the International Conference on Process Automation, Control and Computing*, pages 1–6, Jul 2011.

[120] Mizuho Shibata, Yuusuke Onishi, and Sadao Kawamura. Experimental evaluation of a flexible joint driven by water pressure for underwater robots. In *Proceedings of the IEEE RSJ International Conference on Intelligent Robots and Systems (IROS)*, pages 4011–4016, 2010.

[121] M. Santhakumar and J. Kim. Modelling, simulation and model reference adaptive control of autonomous underwater vehicle-manipulator systems. In *Proceedings of the 11th International Conference on Control, Automation and Systems (ICCAS)*, pages 643–648, 2011.

[122] Zhou Jie and Shu Zong Wang. Dynamics modeling and maneuverability simulation of the unmanned underwater vehicle hanging torpedoes externally. In *Proceedings of the International Asia Conference on Informatics in Control, Automation, and Robotics, CAR*, pages 207–210, 2009.

[123] I. Schjolberg and O. Egeland. Control of an underwater robot system connected to a ship by a slender marine structure. In *Proceeding of the IEEE International Conference on Control Applications*, pages 43–48. Sep 1996.

[124] Sunghee Choi, Howon Lee, Donghyuk Lee, and Jang Myung Lee. Obstacle avoidance algorithm of the underwater robot in the underwater environment. In *Proceedings of the IEEE ASME International Conference on Advanced Intelligent Mechatronics (AIM)*, pages 369–373. Jul 2012.

[125] Sophia M. Schillai, Stephen R. Turnock, Eric Rogers, and Alexander B. Phillips. Evaluation of terrain collision risks for flight style autonomous underwater vehicles. In *Proceedings of the IEEE/OES International Conference on Autonomous Underwater Vehicles (AUV)*, pages 311–318. Nov 2016.

[126] Dayal R Parhi and Shubhasri Kundu. Review on guidance, control and navigation of autonomous underwater mobile robot. *International Journal of Artificial Intelligence and Computational Research*, 4(1):21–31, 2012.

[127] J. Yuh. Design and control of autonomous underwater robots: A survey. *Autonomous Robots*, 8 (1):7–24, 2000.

[128] Xianbo Xiang, Lionel Lapierre, and Bruno Jouvencel. Smooth transition of AUV motion control: From fully-actuated to under-actuated configuration. *Robotics and Autonomous Systems*, 67:14–22, May 2015.

[129] Caoyang Yu, Xianbo Xiang, Lionel Lapierre, and Qin Zhang. Nonlinear guidance and fuzzy control for three-dimensional path following of an underactuated autonomous underwater vehicle. *Ocean Engineering*, 146:457–467, Dec 2017.

[130] P. S. Londhe and B. M. Patre. Adaptive fuzzy sliding mode control for robust trajectory tracking control of an autonomous underwater vehicle. *Intelligent Service Robotics*, 12(1):87–102, Jan 2019.

[131] Zheping Yan, Man Wang, and Jian Xu. Robust adaptive sliding mode control of underactuated autonomous underwater vehicles with uncertain dynamics. *Ocean Engineering*, 173:802–809, Feb 2019.

[132] Mohammad Hedayati Khodayari and Saeed Balochian. Modeling and control of autonomous underwater vehicle (AUV) in heading and depth attitude via self-adaptive fuzzy PID controller. *Journal of Marine Science and Technology*, 20(3):559–578, Sep 2015.

[133] Ji Hong Li and Pan Mook Lee. A neural network adaptive controller design for free-pitch-angle diving behavior of an autonomous underwater vehicle. *Robotics and Autonomous Systems*, 52 (2-3):132–147, Aug 2005.

[134] Khoshnam Shojaei. Three-dimensional neural network tracking control of a moving target by underactuated autonomous underwater vehicles. *Neural Computing and Applications*, 31(2):509–521, Feb 2019.

[135] Yingkai Xia, Kan Xu, Ye Li, Guohua Xu, and Xianbo Xiang. Improved line-of-sight trajectory tracking control of under-actuated AUV subjects to ocean currents and input saturation. *Ocean Engineering*, 174:14–30, Feb 2019.

[136] Dhrubajit Chowdhury, S. Nandy, R. Ray, and S. N. Shome. Behavior-based control applied to underwater vehicles to achieve local goals. *2015 IEEE Underwater Technology, UT 2015*, may 2015.

[137] Habib Choukri Lamraoui and Zhu Qidan. Path following control of fully-actuated autonomous underwater vehicle in presence of fast-varying disturbances. *Applied Ocean Research*, 86:40–46, May 2019.

[138] Raja Rout and Bidyadhar Subudhi. Design of Line-of-Sight Guidance Law and a Constrained Optimal Controller for an Autonomous Underwater Vehicle. *IEEE Transactions on Circuits and Systems II: Express Briefs*, 68(1):416–420, jan 2021.

[139] Meenakshi Sarkar, Sambhunath Nandy, and Sankar Nath Shome. Energy Efficient Trajectory Tracking Controller for Underwater Applications: ARobust Approach. *Aquatic Procedia*, 4:571–578, jan 2015.

[140] Zheping Yan, Zewen Yang, Lidong Yue, Lu Wang, Heming Jia, and Jiajia Zhou. Discrete-time coordinated control of leader-following multiple AUVs under switching topologies and communication delays. *Ocean Engineering*, 172:361–372, 2019.

[141] Guillaume Allibert, Minh Duc Hua, Szymon Krupínski, and Tarek Hamel. Pipeline following by visual servoing for Autonomous Underwater Vehicles. *Control Engineering Practice*, 82:151–160, Oct 2018.

[142] Subhasish Mahapatra, Bidyadhar Subudhi, Raja Rout, and B. V.S.S.Krishna Kumar. Nonlinear H Control for an Autonomous Underwater Vehicle in the Vertical Plane. *IFAC-PapersOnLine*, 49 (1):391–395, jan 2016.

[143] Shuang Liu, Mete Ozay, Takayuki Okatani, Hongli Xu, Kai Sun, and Yang Lin. Detection and Pose Estimation for Short-Range Vision-Based Underwater Docking. *IEEE Access*, 7:2720–2749, 2019.

[144] Shubhasri Kundu and Dayal R. Parhi. Modified Shuffled Frog Leaping Algorithm based 6DOF Motion for Underwater Mobile Robot. *Procedia Technology*, 10:295–303, jan 2013.

[145] Jagadeesh Kadiyam, Anjali Parashar, Santhakumar Mohan, and Devendra Deshmukh. Actuator fault-tolerant control study of an underwater robot with four rotatable thrusters. *Ocean Engineering*, 197:106929, feb 2020.

[146] Jeongae Bak, Yecheol Moon, Jongwon Kim, Santhakumar Mohan, Tae Won Seo, and Sangrok Jin. Hovering control of an underwater robot with tilting thrusters using the decomposition and

compensation method based on a redundant actuation model. *Robotics and Autonomous Systems*, 150:103995, apr 2022.

[147] Luke Stutters, Honghai Liu, C. Tiltman, and D.J. Brown. Navigation Technologies for Autonomous Underwater Vehicles. *IEEE Transactions on Systems, Man, and Cybernetics, Part C (Applications and Reviews)*, 38(4):581–589, Jul 2008.

[148] Liam Paull, Sajad Saeedi, Mae Seto, and Howard Li. AUV navigation and localization: A review. *IEEE Journal of Oceanic Engineering*, 39(1):131–149, 2014.

[149] Asaf Tal, Itzik Klein, and Reuven Katz. Inertial navigation system/doppler velocity log (ins/dvl) fusion with partial dvl measurements. *Sensors*, 17(2), 2017.

[150] Xiaoping Yun, E.R. Bachmann, and S. Arslan. An inertial navigation system for small autonomous underwater vehicles. In *Proceedings of the IEEE International Conference on Robotics and Automation*, volume 2, pages 1781–1786. 2000.

[151] B. Allotta, R. Costanzi, N. Monni, L. Pugi, A. Ridolfi, and G. Vettori. Design and simulation of an autonomous underwater vehicle. In *Proceedings of the European Congress on Computational Methods in Applied Sciences and Engineering, Vienna, Austria*, number Eccomas, Sep 2012.

[152] H. Choi, S. Chung, H. Park, and J. Seo. Design and control of a convertible ROV. In *Proceedings of the OCEANS IEEE International Conference, Yeosu*, pages 1–7. May 2012.

[153] Xiaokai Mu, Jia Guo, Yan Song, Qixin Sha, Jingtao Jiang, Bo He, and Tianhong Yan. Application of modified EKF algorithm in AUV navigation system. In *Proceedings of the IEEE OCEANS International Conference, Aberdeen*, pages 1–4. Jun 2017.

[154] James C. Kinsey, Qingjun Yang, and Jonathan C. Howland. Nonlinear dynamic model-based state estimators for underwater navigation of remotely operated vehicles. *IEEE Transactions on Control Systems Technology*, 22(5):1845–1854, 2014.

[155] Xinhui Shao, Bo He, Jia Guo, and Tianhong Yan. The application of AUV navigation based on adaptive extended Kalman filter. In *Proceedings of the IEEE OCEANS International Conference, Shanghai*, pages 1–4. Apr 2016.

[156] B. Allotta, A. Caiti, R. Costanzi, F. Fanelli, D. Fenucci, E. Meli, and A. Ridolfi. A new AUV navigation system exploiting unscented Kalman filter. *Ocean Engineering*, 113:121–132, Feb 2016.

[157] Hamid Shariati, Hassan Moosavi, and Mohammad Danesh. Application of particle filter combined with extended Kalman filter in model identification of an autonomous underwater vehicle based on experimental data. *Applied Ocean Research*, 82:32–40, Jan 2018.

[158] Nagamani Modalavalasa, G. Sasi Bhushana Rao, K. Satya Prasad, L. Ganesh, and M. N.V.S.S. Kumar. A new method of target tracking by EKF using bearing and elevation measurements for underwater environment. *Robotics and Autonomous Systems*, 74:221–228, dec 2015.

[159] N. S. Sangu. Investigation of impact behaviour of hybrid frp laminates for armor applications. Master's Thesis, Indian Institute of Technology Guwahati, Jun 2016.

[160] Sonu Sharma and Rajesh Kumar Sharma. CFD investigation to quantify the effect of layered multiple miniature blades on the performance of Savonius rotor. *Energy Conversion and Management*, 144:275–285, jul 2017.

[161] BlueRobotics. T200 trusters with blueesc. https://bluerobotics.com/store/thrusters/t200-thruster-blueesc/. Online; accessed 5-March-2020.

Publications

Patent Published:

- Avilash Sahoo, S. K. Dwivedy, and P. S. Robi,"AN UNDERWATER VEHICLE", Indian Patent App no. 201831046760 A, 12 June 2020.

Journals:

1. A. Sahoo, S. K. Dwivedy, and P. S. Robi,"Advancements in the field of Autonomous Underwater Vehicle," Ocean Engineering, vol. 181, pp. 145-160, June 2019. doi: https://doi.org/10.1016/j.oceaneng.2019.04.011

2. A. Sahoo, S. K. Dwivedy, and P. S. Robi,"Compact Low-Cost Unmanned Underwater Vehicle: Design and Fabrication," Journal of Mechanisms and Robotics. (Revised manuscript under review)

3. A. Sahoo, S. K. Dwivedy, and P. S. Robi,"Dynamic Modelling of a Compact Low-Cost Autonomous Underwater Vehicle," J. Offshore Mech. Arct. Eng., (Manuscript under review)

4. A. Sahoo, S. K. Dwivedy, and P. S. Robi,"Trajectory Tracking Controller for an Autonomous Underwater Vehicle," (Manuscript to be submitted)

5. A. Sahoo, S. K. Dwivedy, and P. S. Robi,"Adaptive Neuro-Fuzzy Control Design for an Compact Autonomous Underwater Vehicle," (Manuscript to be submitted)

Conferences:

1. A. Sahoo, S. K. Dwivedy, and P. S. Robi, "Design of a compact rov for river exploration," in Proceedings of the Advances in Robotics, AIR'17, New Delhi, India, pp. 30:1 – 30:6, ACM Digital Library, 2017.

2. A. Sahoo, S. K. Dwivedy, and P. S. Robi, "Dynamic modelling and control of a compact autonomous underwater vehicle," in Proceedings of the 6th International Conference on Robot Intelligence Technology and Applications, RITA18, Putrajaya, Malaysia, 16-18 Dec, 2018.

3. A. Sahoo, S. K. Dwivedy, and P. S. Robi, "Development of a PID Control Strategy for a Compact autonomous underwater vehicle," in Proceedings of the ASME 2019 38th International Conference on Ocean, Offshore and Arctic Engineering (OMAE2019), June 9-14, 2019, Glasgow, Scotland.

4. A. Sahoo, S. K. Dwivedy, and P. S. Robi, "Adaptive Fuzzy PID Controller for A Compact Autonomous Underwater Vehicle," in Proceedings of the Virtual Global OCEANS 2020: Singapore and U.S. Gulf Coast, Oct 5-14, 2020.

Book Chapter:

- A. Sahoo, S. K. Dwivedy, and P. S. Robi,"Dynamic Modelling and Control of a Compact Autonomous Underwater Vehicle," Lecture Notes in Mechanical Engineering. Springer, Singapore. pp. 303-321, 2019. ISBN: 978-981-13-8323-6. doi: https://doi.org/10.1007/978-981-13-8323-6$_$25